KAZAN SCIENCE WEEK 2025

ABSTRACTS

KAZAN SCIENCE WEEK

ABSTRACTS OF THE
INTERNATIONAL CONFERENCES
“MODERN DEVELOPMENT OF MAGNETIC RESONANCE”

KAZAN, SEPTEMBER 22 – OCTOBER 03, 2025

ORGANIZERS AND SPONSORS

Российская Академия Наук

Federal Research Center
"Kazan Scientific Center of
the Russian Academy of Sciences"

Ministry of Science
and Higher Education
of the Russian Federation

Academy of Sciences
of the Republic of Tatarstan

Government
of the Republic of Tatarstan

Ministry of Education and Science
of the Republic of Tatarstan

Prokhorov General Physics
Institute of RAS (GPI RAS)

Zavoisky Physical-Technical
Institute FRC KazanSC RAS

Lomonosov Moscow
State University

Kazan Federal University

MIPT
MOSCOW INSTITUTE OF PHYSICS AND TECHNOLOGY

MEPhI
National Research
Nuclear University MEPhI

ЭЛЕМЕНТ

AVESTA
LASERS AND OPTICAL SYSTEMS

special
systems
PHOTONICS

"НАУКА"
Центр Технического Сопровождения

SLS
PRIME TECHNOLOGY

Solar
Laser
Systems

LLS

LAOPA

Solar Laser Systems

SOLAR LS Company has been working in the international photonics market for more than 30 years. We are experts in the design and manufacturing of solid-state laser systems and spectral analysis instruments for science, medicine and industry. Currently, the company comprises scientific research laboratories, a design department, a mechanical and assembly production facility, an optical department, and a group for adjustment and service maintenance. Therefore, we complete the entire cycle of work on creating laser and spectral analysis systems - from research and development to the supply of finished products and their service maintenance. Our instruments and systems successfully operate in more than 25 countries all over the world. Being one of the market leaders, we offer our customers the widest range of the cutting-edge solid-state lasers, laser systems and spectral instruments. Reliability and technical perfection of SOLAR LS products are ensured by more than 30 years of manufacturing experience while design and concept incorporates with the latest achievements of the photonics.

Our laser product line includes:

- Nanosecond lasers with lamp and diode pumping with pulse energy up to 2.5 J, pulse repetition rates up to 100 Hz;
- Lasers with kHz pulse repetition rates with average power up to 10 W, pulse repetition rates from 1 to 100 kHz;
- Picosecond and femtosecond lasers with average power up to 8 W, pulse energy up to 1 mJ, pulse duration from 150 fs to 30 ps;
- Tunable nanosecond laser systems with a tuning range from 200 nm to 20 μm.

All lasers are equipped with harmonic generators and nonlinear converters, providing the capability to operate in UV, visible and IR spectral ranges.

Typical spectral products of our company are:

- Monochromators/spectrographs with a focal length from 44 to 522 mm;
- Compact spectrometers in the spectral range from 190 to 2560 nm with high optical sensitivity, low level of stray light and high resolution;
- Tunable light sources based on xenon lamps in the spectral range from 190 to 2500 nm, with high resolution up to 0.1 nm;
- Wavelength meters for lasers and diodes in the spectral range from 190 to 1800 nm with high accuracy and extremely high resolution.

We offer a wide range of detectors and accessories to complete our spectral instrument registration systems, as well as to collect light and input/output it into a fiber or spectral instrument. In addition to standard models of lasers and spectral instruments, our specialists are ready to develop and manufacture absolutely unique systems for your specific requirements and tasks.

Why we are confident in excellent results:

- Extensive experience: over 30 years of designing and producing laser systems and spectral analysis instruments to meet the current User's needs;
- Rapid and high-quality development of custom instruments;
- Established small-scale production process;
- Our team is involved in optimizing optical schemes designs for experiments using our spectral analysis instruments and laser systems;
- We provide stable OEM-supplies of high-quality instruments and systems.

Фемтосекундные твердотельные лазеры


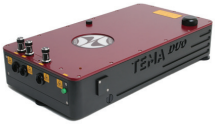


TiF
Ti:S лазер
- λ_{range}: 690-1040 нм
- τ_{pulse}: 6 фс - 30 пс
- P_{av}: до 4 Вт
- PRR: 40...125 МГц

TeMa
иттербиевый лазер
- λ: 1030...1054 / 525 нм
- τ_{pulse}: 15-150 фс
- P_{av}: >20 Вт / >8 Вт
- PRR: 10-80 МГц

CrF
Cr:F лазер
- λ_{range}: 1230-1270 нм
- τ_{pulse}: <70 фс
- P_{av}: до 1 Вт
- PRR: 75...125 МГц

Katyusha
многоканальная система
- λ: 525 / 740-860 / 1050 нм
- τ_{pulse}: <150/<50/<200 фс
- P_{av}: 1.5 Вт на 800 нм
- PRR: 80 МГц

TOPOL
ОПО с накачкой
- λ_{range}: 205-4750 нм
- τ_{pulse}: <150 фс
- P_{av}: >3 Вт
- PRR: 80 МГц

Фемтосекундные волоконные лазеры





YFOA
иттербиевый лазер
- λ: 1030...1064 нм
- τ_{pulse}: <100 фс
- P_{av}: до 50 Вт
- PRR: 40-80 МГц

ANTAUS
микроджоульный
- λ: 1030...1053 нм
- τ_{pulse}: <250 фс
- E_{pulse}: до 60 мкДж
- P_{av}: до 50 Вт

PErL, EFO
эрбиевые лазеры
- λ: 1560 нм
- τ_{pulse}: 50...300 фс; 5 пс
- P_{av}: до 5 Вт
- PRR: 30...100 МГц

EFOA-SH/PErL-PM-SH
эрбиевый лазер
- λ: 1560/780 нм
- τ_{pulse}: <50 фс
- P_{av}: >2 Вт
- PRR: 30...100 МГц

EFO-COMB
комб-генератор
- λ: 200...3390 нм
- F_{rep}: 100-250 МГц
- Стаб.: $1*10^{-17}$ на 1 с

Усилители

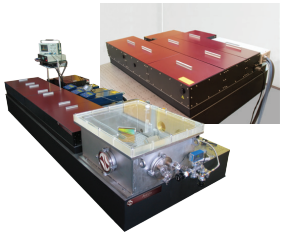


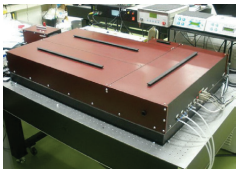


AVET и REUS
титан-сапфировые усилители
- λ: 740...950 нм
- τ_{pulse}: <35 фс (опция <8 фс)
- P_{peak}: до 20 ТВт
- E_{pulse}: >550 мДж@10 Гц

TETA иттербиевый усилитель
- λ: 1030/515/343/257 нм
- τ_{pulse}: <180 фс (опция <30 фс)
- P_{av}: до 30 Вт @ 2 МГц
- E_{pulse}: до 2 мДж

FREGAT хром-форстеритовый усилитель
- λ: 1240 нм
- τ_{pulse}: <100 фс
- E_{pulse}: до 100 мДж
- PRR: 10 Гц...1 кГц

PARUS
параметрический усилитель
- λ_{range}: 190 нм - 15 мкм
- τ_{pulse}: от <30 фс
- Eff. S+I: >10% от накачки

Непрерывные твердотельные лазеры


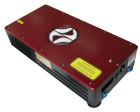

TiC Ti:S лазер
- λ: 690-1040 нм
- P_{av}: до 6 Вт
- <1 МГц ширина линии

TEMA-CW
- λ: 1010-1070 нм
- P_{av}: до 15 Вт
- USB

LF-100 Cr:F лазер
- λ: 1210-1290 нм
- P_{av}: до 1 Вт
- USB

DLS одночастотный диодный лазерный источник
- λ: 400...1670 нм
- P_{av}: до 10 Вт

АВЕСТА
ЛАЗЕРЫ И ОПТИЧЕСКИЕ СИСТЕМЫ

ООО «АВЕСТА», ул. Физическая, 11
Троицк, 108840, Москва, Россия
Тел.: +7 (495) 138-99-56

fs@avesta.ru
www.avesta.ru

Диагностическое оборудование

AA-DD и IRA
сканирующие автокорреляторы
- λ_{range}: 420 нм - 11 мкм
- τ_{pulse}: 10 фс - 250 пс
- Чувствительность: от 100 мВт^2
- USB и ПО для Windows

ASF, ASF-FROG
одноимпульсные автокорреляторы и FROG
- Диапазон длин волн: 400-2200 нм
- Диапазон длительности: 5 фс - 20 пс
- USB, ПО для Windows и LabView

SPIDER
измеритель спектральной фазы
- Input λ: 550-2200 нм
- Input $\tau_{pulse\ range}$: 5-320 фс
- USB и ПО для Windows

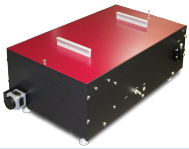

COMET измеритель контраста
- Диапазон длин волн: 700-1500 нм
- Динамический диапазон: 10^{10}
- Временной диапазон: до 10 нс
- USB и ПО для Windows

OD фотоприемники
- Диапазон длин волн: 200-2600 нм
- Полоса до 2500 МГц
- Время нарастания от 0.5 нс
- Со смещением, с усилителем, лавинные, волоконные

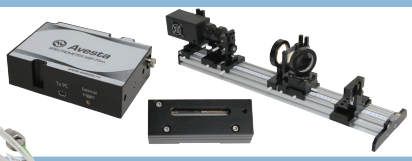

Спектрометры и сенсоры
- λ: 190-3450 нм
- Разрешение: от 0.01 нм
- Волоконный/free-space
- USB и ПО для Windows

Компоненты

OG ЭО и АО селекторы импульсов
- Длины волн: 210...2700 нм
- Выходная частота: до 40 МГц
- Пропускание >90%
- Контраст >2 000:1
- Блок генерации задержек
- USB, ПО для Windows и LabView

ALock. Блок ФАПЧ
- Входной сигнал до 3 ГГц
- Полоса ПИД до 2 МГц
- PZT до 50 Вт
- Синхронизация лазеров
- Стабилизация CEP
- ASOPS, THz-ASOPS

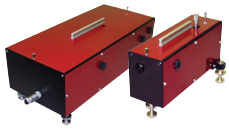

AG генераторы гармоник
- Выход: 195 нм - 5 мкм
- ЧГ на 800 нм = ТГ+основная
- Преобразование: до >50%

APC призменный компенсатор
GVD на 800 нм:
от +16500 фс^2 до -13800 фс^2

Compulse компрессор
- 6 фс, 500 мкДж на 800 нм
- 30 фс, 200 мкДж на 1030 нм

OA оптические аттенюаторы
- Динамический диапазон: 10^2
- λ: 250...2000 нм
- Модели с низкой дисперсией
- Порог пробоя: до 10 Дж/см^2

AF ротаторы и изоляторы
- λ: 400...1250 нм
- Изоляция: >38 dB; >60 dB
- Широкопол. и перестраив.
- Апертура: до 20 мм
- Порог пробоя: до 5 Дж/см^2

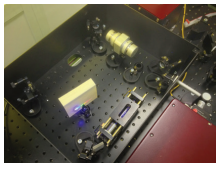

GECON генератор суперконтинуума
- Вх. λ: 800; 1030-1064 нм
- Вых. λ: 200-1200 нм
- Преобразование: >50%

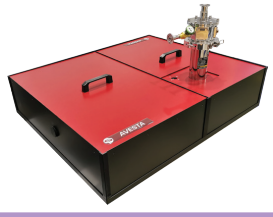

Tera-Ax ТГц генератор
- Центр. частота: 1 ТГц
- Длительность ТГц: <1 пс
- Энергия ТГц: >1 мДж
- ЭО детектор (опция)
- Версия с криостатом

• чопперы • шаттеры • USB контроллеры • оптомеханика • столики • оправы •

ООО «АВЕСТА», ул. Физическая, 11
Троицк, 108840, Москва, Россия
Тел.: +7 (495) 138-99-56

fs@avesta.ru
www.avesta.ru

rev 2507

LASERS & LASER SYSTEMS

PULSED Nd:YAG LASERS

- Pulse energy up to 2.5 J
- Flat top beam profile
- Pulse repetition rate up to 200 Hz
- All harmonics from 1064 to 213 nm
- Adjustable pulsewidth
- Adjustable pulse shape

FEMTO-, PICOSECOND LASERS

- Pulsewidth (FWHM) up to 110 fs
- Output power up to 7 W
- Output energy up to 1 mJ
- Harmonic generators
- Diode pumping
- Pulse selectors

TUNABLE LASERS

- Ti:Sapphire lasers, DFG converters
- Optical parametric oscillators
- Tuning range from 0.2 to 20 μm
- Linewidth up to 0.005 nm
- Pulse energy up to 100 mJ

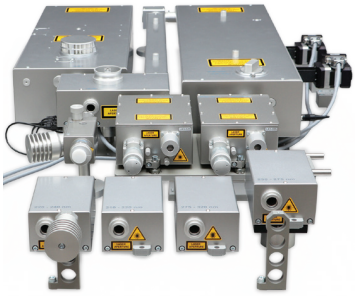

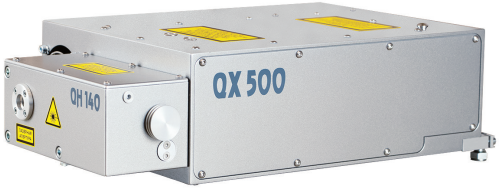

DIODE-PUMPED LASERS

- Compact industrial design
- Built-in or external harmonic generators
- up to 150 mJ per pulse at 20 Hz
- up to 3 W @ 355 nm at 30 kHz

SPECTRAL INSTRUMENTS

MONOCHROMATORS/ SPECTROGRAPHS

- Single and double
- Focal length from 44 to 522 mm
- Wide range of detectors

SPECTROMETERS

- Spectral range from 190 to 2560 nm
- High optical sensitivity
- Fiber input

WAVELENGTH METERS FOR LASERS AND DIODES

- Spectral range from 190 to 1800 nm
- High accuracy ± 3 pm
- FWHM and spectral line monitoring and analysis

TUNABLE LIGHT SOURCES

- Spectral range from 190 to 2500 nm
- Spectral resolution up to 0.1 nm

BUILT WITH ADVANCED TECHNOLOGIES

PULSED Nd:YAG LASERS

- Wavelength 1064, 532, 355, 266 and 213 nm
- Pulse energy up to 4 J
- Repetition rate up to 10 kHz
- Integrated energy meter
- Compact housing
- Manufactured in the Republic of Belarus

Convenient Operation · High Reliability · Guaranteed Service

SLS Prime Technology unites leading experts in lasers and laser systems development and production to bring innovative equipment to domestic markets.

We place special emphasis in engineering diode-pumped lasers, deliberately dissolving the boundaries of their applications between science and industry. We are determined that our products are designed to succeed in both domains.

AZURITE is our first and proven model of diode-pumped lasers generating nanosecond pulses. It delivers **up to 160 mJ** pulse energy at **up to 30 Hz** repetition rates in a completely **"dry" design**.

Its **extended service interval of over 1 billion pulses** makes AZURITE a robust solution not only for a wide range of R&D applications but also for integrating in industrial environments operating 24/7.

We use **exclusively domestically sourced components** for all critical parts, ensuring system maintainability and reliable long-term service support.

Please contact our specialists for more details by e-mail or phone:

SLS Prime Technology | +375 (17) 382-00-55 | sales@sls-prime.com | www.sls-prime.com

SLS
PRIME TECHNOLOGY

PULSED
Nd:YAG LASERS

AZURITE
Compact diode-pumped lasers

- Up to 160 mJ pulse energy at up to 30 Hz repetition rate
- >1 billion shots lifetime
- Completely dry cooling design
-

GRAPHITE
Compact lamp-pumped lasers

- 200 mJ - 750 mJ pulse energy at up to 100 Hz repetition rate
- >30 million shots lifetime
- Water-air cooling

CORUNDUM
Lamp-pumped Joule-class lasers

- Up to 1.5 J pulse energy at up to 20 Hz repetition rate
- >30 million shots lifetime
- Water-air cooling

OBSIDIAN
Picosecond lasers

- Up to 2 mJ pulse energy at up to 1 kHz repetition rate
- 300-500 ps pulse duration
- SLM operation mode

AMETHYST
Tunable laser systems

- Tunable output in the 0.2–20 μm range
- Up to 150 mJ pulse energy
- Customized configurations available

- *All Nd:YAG laser models incorporate replaceable harmonic generators for wavelength selection from IR to UV: 1064 nm, 532 nm, 355 nm, 266 nm, and 213 nm.*
- *Nd:YAG lasers are available with single longitude mode (TEM00) option.*
- *Lasers with pulse energies up to 4 J are available on a custom-order basis.*
- *Tunable wavelength systems are developed to individual specifications based on Nd:YAG lasers enhanced with OPOs and sum- and difference-frequency generators.*

SLS Prime Technology | +375 (17) 382-00-55 | sales@sls-prime.com | www.sls-prime.com

ЭЛЕМЕНТ

Сайт: https://element-msc.ru/

Компания «ЭЛЕМЕНТ» – надежный поставщик аналитического оборудования, запчастей и расходных материалов на российском рынке уже более 20 лет.
Мы не только обеспечиваем лаборатории и научные центры передовой техникой, но и предлагаем полный спектр сервисных услуг, включая гарантийное обслуживание и ремонт приборов.

«ЭЛЕМЕНТ» является официальным дистрибьютором SHIMADZU в России, а также представляет ряд других ведущих производителей аналитического оборудования. Среди наших партнеров:

- **ZHONGTAI (CIQTEK)** – разработчик спектрометров ядерного магнитного резонанса (ЯМР) и электронного парамагнитного резонанса (ЭПР) X и W диапазона, а также уникального оборудования для измерения магнитных свойств веществ, включая NV-магнитометры и квантовые NV-микроскопы.
- **Zhenyi Scientific** – китайский производитель инновационных решений в области ЯМР-анализа, включая **бескриогенные низкопольные ЯМР-анализаторы** для пищевой науки, материаловедения и биомедицины.

ЭЛЕМЕНТ

СПЕКТРОМЕТРЫ ЯДЕРНОГО МАГНИТНОГО РЕЗОНАНСА (ЯМР)

ЯМР-спектрометры Zhenyi на постоянном магните серии HT-PNMR12 (60/90МГц)

Предназначены для проведения рутинных экспериментов. В зависимости от конфигурации они способны регистрировать ЯМР-спектры ядер: ^{1}H, ^{19}F, ^{13}C, ^{31}P. Уникальный постоянный магнит не требует охлаждения криогенными жидкостями. Для уменьшения влияния анизотропии магнитного поля используется система вращения. Все блоки прибора находятся в едином корпусе. Заводская гарантия 24 месяца с момента поставки.

- Две модификации: HT-PNMR12-6 на 60 МГц / HT-PNMR12-9 на 90 МГц
- Магнитное поле: 1,4 Тл / 2,1 Тл
- Разрешение: < 0,8 Гц / < 0,5 Гц
- Соотношение S/N (1% этилбензол): 100:1 / 120:1
- Температурная стабильность: 0,001 К/ч через 4 часа после запуска

Высокопольные ЯМР-спектрометры ZHONGTAI CAN400 и CAN600 (400/600 МГц)

Современные высокочувствительные ЯМР-спектрометры с интеллектуальным управлением и сверхпроводящим магнитом, обеспечивающим исключительную однородность поля. Приборы оснащены автоматизированным зондом и модульной системой, что позволяет проводить точные исследования молекулярной структуры с минимальным вмешательством оператора. ЯМР-спектрометры ZHONGTAI идеально подходят для современных лабораторий, сочетая высокое разрешение, надежность и удобство в эксплуатации.

- Две модели: CAN400 / CAN600
- Рабочая частота на ядрах 1H – 400 МГц / 600 МГц
- Магнитное поле: 9,39 Тл / 14,09 Тл
- Соотношение S/N (0,1% этилбензол): ≥ 500:1 / ≥ 850:1
- Наблюдаемые ядра: ^{1}H, ^{13}C, ^{15}N, ^{31}P, ^{19}F и другие
- Разрешение: < 0,0005 Гц
- Диаметр теплого отверстия: 54 мм
- Опции: температурная приставка (от -150 °C до +150 °C), автосамплер на 72 образца

СПЕКТРОМЕТРЫ ЭЛЕКТРОННОГО ПАРАМАГНИТНОГО РЕЗОНАНСА (ЭПР)

ЭПР -спектрометры X-, Q-, W- диапазона от ZHONGTAI

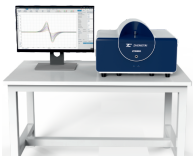

ZT6500

ZT15C

ZT15P

ZT60W

Линейка ЭПР спектрометоров ZHONGTAI включает :

- компактную настольную модель ZT6500
- две высокочувствительные модели ЭПР X-диапазона. Модель ZT15C для работы в CW-режиме и модель ZT15P с возможностью работы в импульсном +CW режиме. Обе модели можно модернизировать для работы в Q-диапазоне (с магнитом 1,8Т).
- Вершина линейки - высокочастотный ЭПР-спектрометр W-диапазона ZT60W.

Кроме этого, производитель предлагает большой набор опций: резонаторы, азотные и гелиевые температурные приставки, системы облучения, ячейки для разных приложений, в том числе для модернизации ЭПР-спектрометров сторонних производителей.

8 (800) 250-34-64
element-msc.ru
info@element-msc.ru

ЭЛЕМЕНТ

"НАУКА"

Центр Технического Сопровождения

Адрес: 129626, Россия, Москва,
ул. Маломосковская, 22, стр. 1, «Технопарк»
Телефон: +7 (499) 322 06 62
Моб.: +7 915 404 65 97
E-mail: d.naberezhnyi@cts-nauka.ru

ЦЕНТР ТЕХНИЧЕСКОГО СОПРОВОЖДЕНИЯ «НАУКА» ЗАНИМАЕТСЯ ПОСТАВКОЙ И ОБСЛУЖИВАНИЕМ НАУЧНОГО ОБОРУДОВАНИЯ ДЛЯ ЛАБОРАТОРИЙ, РЕШАЯ СЛЕДУЮЩИЕ ЗАДАЧИ:

- разработка комплексного решения под задачи пользователя, в том числе поставка оборудования, разработанного по индивидуальным проектам
- поставка, запуск и обслуживание оборудования
- объединение приборов от разных производителей в единый комплекс
- поставка всех необходимых расходных материалов
- гарантийное и постгарантийное обслуживание

ЛАБОРАТОРНОЕ ОБОРУДОВАНИЕ | РАСХОДНЫЕ МАТЕРИАЛЫ | СЕРВИС

КОМПАНИЯ ОБРАЗОВАНА В 2013 ГОДУ И ЗАРЕКОМЕНДОВАЛА СЕБЯ КАК НАДЕЖНЫХ ПОСТАВЩИК ПРИБОРОВ ДЛЯ ИССЛЕДОВАНИЙ В ОБЛАСТИ ФИЗИКИ И ХИМИИ.

www.scientific-technology.ru | www.nauka-shop.ru | www.lgrinc.ru | www.cryoindustries.ru

ЦТС «НАУКА» ПРЕДЛАГАЕТ ШИРОКИЙ ПЕРЕЧЕНЬ УНИКАЛЬНОГО ОБОРУДОВАНИЯ ДЛЯ НАУЧНЫХ ИЗЫСКАНИЙ:

КРИОГЕННОЕ ОБОРУДОВАНИЕ:

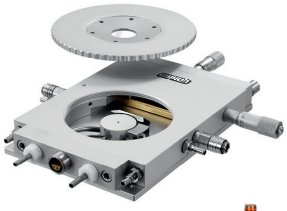

+ Столики для микроскопии с задаваемой температурой / давлением от **Linkam Scientific Instruments**.

+ **Advanced Research Systems:** оптические криостаты замкнутого цикла, проточные, сверхвысоковакуумные, исследовательские станции с зондом и иные аксессуары.

+ **Cryo Industries of America:** оптические безжидкостные криостаты, поточные гели евые криостаты, гелиевые и безжидкостные сверхпроводящие магниты, системы охлаждения газового потока, системы для криомикроскопии, генераторы жидкого азота, криостаты He-3, трансферные линии и сосуды Дьюара.

+ **SHI Cryogenic Group (Sumitomo):** криокулеры (криогенные рефрижераторы), крионасосы, гелиевые компрессоры.

+ **Quantum Design:** безжидкостные оптические криостаты, ожижители гелия, системы квантовой микроскопии, системы наноосаждения PVD/CVD, SQUID магнетометры, безжидкостные станции для исследования материалов и криомикроскопии.

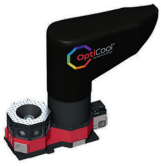

+ **Cryogenic Limited:** безжидкостные измерительные системы 18 Тл и криокулеры, криостаты замкнутого цикла, магниты высокого разрешения для ЯМР, SQUID магнетометры.

ВАКУУМНОЕ ОБОРУДОВАНИЕ:

PFEIFFER VACUUM

EDWARDS

Leybold

+ пластинчато-роторные насосы, спиральные насосы, турбомолекулярные насосы от **Pfeiffer Vacuum, Edwards Vacuum, Leybold GmbH.**

EVP®

+ вакуумные насосы и крионасосы от **EVP** и других производителей

YUNMU VAC TECH

+ вакуумные камеры, вакуумная арматура от **Yunmu** и иных производителей.

СОПУТСТВУЮЩИЕ АКСЕССУАРЫ:

SMC

+ Чиллеры, сосуды Дьюара, трансферные линии и многое другое.

"НАУКА"

Центр Технического Сопровождения

Адрес: 129626, Россия, Москва,
ул. Маломосковская, 22, стр. 1, «Технопарк»
Телефон: +7 (499) 322 06 62
E-mail: info@nauka-shop.ru
www.nauka-shop.ru

ИЗМЕРИТЕЛЬНОЕ ОБОРУДОВАНИЕ:

Zurich Instruments

+ синхронные усилители от **Zurich instruments**

KEITHLEY
A Tektronix Company

+ генераторы и измерители электронных сигналов от **Keithley Instruments**

ABB

+ портативные газовые анализаторы от **ABB**

ThermoFisher SCIENTIFIC

+ спектрометры от **Thermo Fisher Scientific**

EDINBURGH INSTRUMENTS

+ спектрометры от **Edinburgh Instruments**

HORIBA

+ спектрометры от **Horiba**

[L G R]

+ изотопные анализаторы от **Los Gatos Research**

NETZSCH

+ термические анализаторы от **Netzsch.**

ЛАБОРАТОРНОЕ ОБОРУДОВАНИЕ | РАСХОДНЫЕ МАТЕРИАЛЫ | СЕРВИС

АО «ЛЛС» — ВАШ ПРОВОДНИК В МИРЕ ОПТИКИ И ФОТОНИКИ!

Нам доверяют эксперты отрасли, а мы обеспечиваем интеграцию оборудования под ключ — от поставки до пусконаладки

10 лет мы лидеры рынка оптики и фотоники — отбираем лучших производителей и предлагаем альтернативные решения без компромиссов по качеству.

Представим оборудование, доступное в АО «ЛЛС» (более 300 производителей):

- **Оптический анализ материалов: микроскопия, спектроскопия и терагерцовые технологии:**
  Apex Photon, Optosky, Oceanoptics, CIQTEK, YSL Photonics, B-THz,Toptica, CNI Laser
- **Производство и тестирование ФИС:**
  CUMEC, OMTools, Moji Nano, Santec, Quantifi photonics, Anritsu, Yokogawa, Toptica
- **Комплектующие и системы для микрообработки материалов:**
  NordLase, Grace Laser, Moji Nano, Huaray, ScanLab
- **Оптомеханика от ведущих мировых производителей:**
  LBTEK, OMTools, Thorlabs, Newport, Coremorrow, Luminous
- **Волоконно-оптические компоненты и оборудование для работы с волокном:**
  LightComm, Shinho, CSRazer, XLG, AFR, Optizone
- **Охлаждение атомов и квантовые технологии:**
  Faraday, CasColdAtom, Tuptek, Connet, KeyangPhotonics, Vision Datum, QUBIG, Zurich Instruments
- **Оборудование для измерения характеристик лазерного пучка:**
  Cai Huang Thermoelectricity, Ophir, Lightcomm, Dataray

+ многое другое оборудование на выставке

На стенде АО «ЛЛС» вас будут ждать подарки

ЛЛС

info@lenlasers.ru

+7 (812) 507 81 00

lenlasers.ru

специальные системы
ФОТОНИКА

О КОМПАНИИ

ООО «Специальные Системы. Фотоника» является специализированным поставщиком и интегратором лазерно-оптических и волоконно-оптических компонентов, измерительного, спектрального и технологического оборудования, источников излучения и лазерных систем различного назначения.

Специалисты компании обеспечивают высококвалифицированную техническую и информационную поддержку по продукции и оборудованию от ведущих мировых производителей для заказчиков из России и ЕАЭС.

Миссия компании - это внедрение передовых лазерно-оптических технологий и продукции в текущие и перспективные разработки российских научных и производственных центров. Активное участие в развитии фотоники в России, как наиболее перспективного направления науки и технологий.

НАПРАВЛЕНИЯ ДЕЯТЕЛЬНОСТИ И УСЛУГИ

- Дистрибуция лазерно-оптических и волоконно-оптических компонентов
  и оборудования.
- Комплексное оснащение лабораторий и производств.
- Разработка и производство волоконно-оптических модулей и систем (ВОЛС, радиофотоника).
- Собственная лаборатория с передовым измерительным и технологическим оборудованием.
- Технический консалтинг, инженерный сервис и обучение специалистов
  заказчика.
- Подготовка документации для закупочных процедур на электронных торговых площадках (ФЗ 223 и ФЗ 44).
- Логистические услуги, таможенное оформление лабораторного оборудования и лазерных компонентов.

ЛАКОПА
ПРОВОДНИК ИННОВАЦИЙ

Компания Лакопа – проводник инновационных решений, которая обеспечивает доступ к экспертным знаниям и перспективным технологиям, способствует повышению уровня научных исследований, подготовке квалифицированных кадров, способных работать с прорывными идеями и творчески мыслить.

Наша компания является официальным дистрибьютером Suzhou Niumag Analytical Instrument - ведущего производителя, специализирующееся на разработке и применении технологии «низкопольного ядерного магнитного резонанса». Компания отличается мощным научно-исследовательским потенциалом, осуществляет полный цикл производства. Благодаря постоянному накоплению технологий, новаторским решениям и разработкам в различных областях применения оборудования, Niumag быстро стало высокотехнологичным предприятием, ориентированным на привлечение в команду ведущих специалистов в отрасли, инновации и развитие.

纽迈 NIUMAG

НАСТОЛЬНЫЙ ТВЕРДОТЕЛЬНЫЙ ЯМР-СПЕКТРОМЕТР С ВРАЩЕНИЕМ ОБРАЗЦА ПОД МАГИЧЕСКИМ УГЛОМ (MAS)

Настольный твердотельный ЯМР-спектрометр MAS20 использует вращение под магическим углом для достижения высокоточного измерения химического сдвига в твердых телах или гетерогенных системах, что позволяет анализировать структурное и молекулярное движение, а также анализировать компонентный состав.

ТЕХНИЧЕСКИЕ ХАРАКТЕРИСТИКИ:

- Тип магнита: постоянный магнит, не требует охлаждения и обеспечивает крайне низкие затраты на обслуживание
- Индукция магнитного поля: 0,5 Тл
- Диаметр ротора: 3,5 мм
- Максимальная скорость: 20 кГц
- Детектируемые ядра: доступны в исполнениях 1H, 7Li, 19F и 31P
- Безопасность: магнитное поле <2 Гс на корпусе прибора
- Температура окружающей среды: 20–26 °C, температурный дрейф <2 °C/ч
- Влажность окружающей среды: менее 80%
- Питание: 220 В, 50/60 Гц
- Пользовательский интерфейс: английский

ОБЛАСТИ ПРИМЕНЕНИЯ:

MAS20 применяется для научных исследований, обучения, предварительного анализа образцов и рутинного контроля качества, особенно для изучения парамагнитных материалов. Прибор позволяет устранить значительные боковые полосы вращения (spinning sidebands) парамагнитных материалов в традиционных магнитно-резонансных системах с высоким полем, которые влияют на качественный и количественный анализ.

- Материалы для литиевых аккумуляторов: анализ дефектов, идентификация информации о связях Li-O-TM (TM = Co, Cr, Mn,Fe, Ni) и анализ искажений
- Фосфорсодержащие материалы: анализ распределения Fe^{2+}/Mn^{2+} в парамагнитных фосфатных соединениях и кислотности катализаторов
- Парамагнитные комплексы: определение структуры и дифференциация кристаллических и аморфных структур
- Фторсодержащие материалы: определение содержания фтора, участия фтора в реакциях и структурный анализ
- Анализ жидкостей: определение содержания масла, воды и каучука в сложных системах

Специалисты компании имеют большой опыт работы в области перспективных разработок и знают, как сложно прокладывать путь первопроходцам. Сотрудничая со многими ведущими экспертами, мы развиваем междисциплинарные коммуникации для обмена опытом, подбираем правильные технологии, адаптируем их для решения самых сложных задач.

НАШ САЙТ

ПОДПИСЫВАЙТЕСЬ НА НАШ ТЕЛЕГРАММ КАНАЛ

Дополнительную информацию о продуктах и решениях компании можно получить, отправив запросы на электронную почту **marketing@lacopa.group**

MODERN DEVELOPMENT OF MAGNETIC RESONANCE

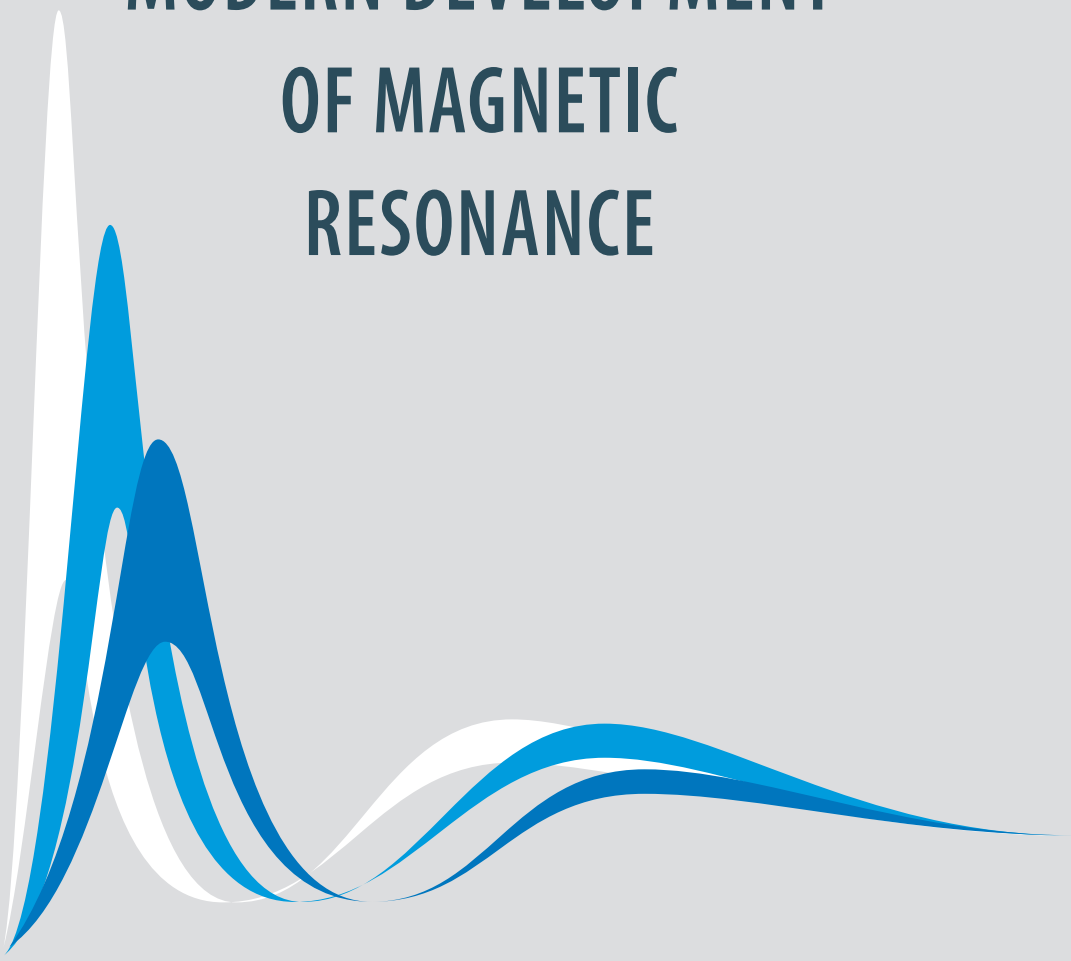

KAZAN, SEPTEMBER 29 – OCTOBER 03, 2025

Published by Zavoisky Physical-Technical Institute, FRC Kazan Scientific Center of RAS, Kazan
www.kfti.knc.ru

COMMITTEE

Kev SALIKHOV (Russia), chairman
Vadim ATSARKIN (Russia)
Elena BAGRYANSKAYA (Russia)
Pavel BARANOV (Russia)
Michael BOWMAN (USA)
Sergei DEMISHEV (Russia)
Rushana EREMINA (Russia)
Matvey FEDIN (Russia)
Marat GAFUROV (Russia)
Daniella GOLDFARB (Israel)
Hitoshi OHTA (Japan)
Alexander SMIRNOV (Russia)
Valery TARASOV (Russia)
Violeta VORONKOVA (Russia)
Roman YUSUPOV (Russia)

SCIENTIFIC SECRETARIAT

Tatiana GAVRILOVA
(t.gavrilova@knc.ru)

Anna MOROZOVA
(morozova_anna_s@mail.ru)

LOCAL COMMITTEE CHAIRMAN

Sergey KHANTIMEROV

SECTIONS

- ADVANCES IN MAGNETIC RESONANCE THEORY AND INSTRUMENTATION
- MODERN METHODS OF MAGNETIC RESONANCE
- LOW-DIMENSIONAL SYSTEMS, NANO-SYSTEMS AND MOLECULAR MAGNETS
- SPIN-BASED INFORMATION PROCESSING AND OPTICAL QUANTUM TECHNOLOGIES
- STRONGLY CORRELATED ELECTRON SYSTEMS
- CHEMICAL AND BIOLOGICAL SYSTEMS
- DEFECTS AND SPIN QUBITS
- MAGNETIC RESONANCE IMAGING AND APPLICATIONS IN MEDICAL PHYSICS
- RELATED PHENOMENA

SECTION COLOR SCHEME

ADVANCES IN MAGNETIC RESONANCE THEORY AND INSTRUMENTATION

MODERN METHODS OF MAGNETIC RESONANCE

LOW-DIMENSIONAL SYSTEMS, NANO-SYSTEMS AND MOLECULAR MAGNETS

SPIN-BASED INFORMATION PROCESSING AND OPTICAL QUANTUM TECHNOLOGIES

STRONGLY CORRELATED ELECTRON SYSTEMS

CHEMICAL AND BIOLOGICAL SYSTEMS

DEFECTS AND SPIN QUBITS

MAGNETIC RESONANCE IMAGING AND APPLICATIONS IN MEDICAL PHYSICS SYSTEMS

RELATED PHENOMENA

CONTENTS

SECTION 1
ADVANCES IN MAGNETIC RESONANCE THEORY AND INSTRUMENTATION

SECTION 2.
MODERN METHODS OF MAGNETIC RESONANCE

ZAVOISKY AWARD LECTURE

Electron spin resonance from spin ensemble to single spin

Jiangfeng Du

University of Science and Technology of China, Hefei 230026, China & Zhejiang University, Hangzhou 310058, China
e-mail: qcmr@ustc.edu.cn

Electron Spin Resonance (ESR) is a powerful scientific technique widely used in cutting-edge research and industry. While traditional ESR primarily relies on spin ensembles, recent advances have extended its reach to the single-spin level. This lecture presents our research progress in both spin ensemble and single-spin ESR technologies.

(I) Spin Ensemble ESR: We have successfully developed a suite of ESR spectrometers covering frequency from X-band to W-band, including both pulsed and continuous-wave operation. These instruments provide researchers with powerful tools for scientific discovery across diverse fields.

(II) Single-Spin ESR: We have developed single-spin ESR techniques utilizing Nitrogen-Vacancy (NV) centers in diamond. This breakthrough has enabled the detection and manipulation of individual electron spins, finding applications in basic physics, information science, and life sciences. Significant research outcomes have been achieved, including probing exotic spin interactions beyond the Standard Model, studying non-Hermitian quantum physics, advancing single-spin quantum computing, and performing single-molecule scale magnetic resonance spectroscopy.

We anticipate that continued technological advancement will ensure ESR remains a vital tool in future scientific research, leading to further innovative discoveries and applications.

PLENARY LECTURES

EPR in living cells using spin labels based on triarylmethyl and nitroxide radicals

E.G. Bagryanskaya[1], V.M. Tormyshev[1], A.E. Raizvikh[1,2], D.A. Kuznetsov[1,2], S.S. Ovcherenko[1], O.A. Chinak[3]

[1] N.N. Vorozhtsov Novosibirsk Institute of Organic Chemistry SB RAS, Novosibirsk 630090, Russia
[2] Novosibirsk State University, Novosibirsk 630090, Russia
[3] Institute of Chemical Biology and Fundamental Medicine SB RAS, Novosibirsk 630090, Russia

This presentation overview our last papers concerning application of spin labels based on triarylmethyl (TAM) and nitroxide radicals to study biopolymers in living systems [1–4]. Being a low-toxic and hydrophilic representative of TAM, OX063 has shown its suitability for *in-vivo* EPR experiments and design of spin labels [1]. Using ^{13}C labeling, we investigated the oxidative degradation of OX063 into quinone-methide (QM) under the influence of superoxide as well as further thiol-promoted reduction of QM into TAM radical, which formally corresponds to substitution of a carboxyl function by a hydroxyl group. We found these transformations being quantitative in model reactions mimicking specific features of biological media and confirmed the presence of these reactions in the blood and liver homogenate of mice *in vitro*. [3] The emergence of the trityl with the hydroxyl group can be masked by an initial TAM in EPR spectra and may introduce distortions into EPR-derived oximetry data if they have been obtained for objects under hypoxia. ^{13}C labeling allows one to detect its presence, considering its different hyperfine splitting constant on $^{13}C_1$ (2.04 mT) as compared to OX063 (2.30 mT). The potential involvement of these reactions should be considered in the application of TAM in experiments *in vivo* and *in cell*. We also investigated the redox transformations of the ^{13}C-enriched triarylmethyl radical OX063 in human cancer cells [4]. The conjugation of OX063 to the cell-penetrating peptide RL2 enabled the tracking of the OX063 transformations under aerobic conditions in living cancer cells. It was demonstrated that OX063 undergoes oxidation to QM by reactive oxygen species in both cell lines. Subsequent reduction of QM by thiols results in the formation of the pH-sensitive radical OX063-OH. The analysis of EPR spectra revealed an average intracellular pH (5.64-5.86) and a 45.6% conversion of QM to OX063-OH. The generation of OX063-OH radicals was observed for both OX063 and QM, opening up the possibility of quantifying the redox status of cells by means of the TAM-OH radicals. The results support the applicability of ^{13}C-OX063-OH as a probe for monitoring of pH in tumors, which could improve personalized diagnosis and therapy.

Acknowledgement. This work was supported by RSF grant N 25-13-00327.

1. Tormyshev V.M., Bagryanskaya E.G.: Trityl Radicals: Synthesis, Properties, and Applications. Russian Chemical Bulletin **70**(12), 2278–2297 (2021)
2. Ovcherenko S.S., Chinak O.A., Chechushkov A.V., Dobrynin S.A., Kirilyuk I.A., Krumkacheva O.A., Richter V.A., Bagryanskaya E.G.: Molecules **26**(18), 5442 (**2021)**
3. Ovcherenko S.S.; Raizvich A.E.; Rogozhnikova O.Y.; Tormyshev V. M., Trukhin D.V., Koval V.V., Salnikov G.E., Genaev A.M., Shernyukov A.V., Bagryanskaya E.: Chemistry–A European Journal **30** (52), e202400718 **(2024)**
4. Raizvich A.E., Ovcherenko S.S., Chinak O.A., Trukhin D., Rogozhnikova O.A., Tormyshev V.M., Koval V.V., Bagryanskaya E.G., **2025**, submitted.

New type of Griffiths phase with enhanced ferromagnetic interaction. The breaking of the universal paradigm

S.V. Demishev

Vereshchagin High Pressure Physics Institute of Russian Academy of Sciences, Troitsk, Moscow, Russia

The modification of the magnetic properties of ferromagnets induced by doping and disorder may be understood in the universal paradigm of formation of a Griffiths phase [1, 2]. This theoretical scenario got numerous experimental confirmations for either the materials with pure ferromagnetic (FM) interactions [6–12], or the MnSi-based spiral magnets [3], where magnetic order at $T_C \sim 29$ K results from the combination of dominating FM exchange and more weak Dzyaloshinskii-Moriya interaction. When Griffiths phase is formed, the randomness in FM system leads to suppression of Curie temperature T_C with the dopant concentration increase [1–3]. This universal, expected in theory, behavior holds for Fe and Co impurities substituting Mn [4]. The effect of doping for $Mn_{1-x}Fe_xSi$ and $Mn_{1-x}Co_xSi$ is strong and, according to [4] for $x > 0.1$ (Co) or $x > 0.2$ (Fe) any FM type magnetic transition is completely suppressed.

In the present report we discuss breaking of the universal paradigm in the novel solid solution system $Mn_{1-x}Rh_xSi$ synthesized in high pressure (~8 GPa) and high temperature (1500–1700 K) conditions [5]. In the rhodium concentration interval $x = 0.05$–0.8 the material maintains the B20 structure observed in the parent compound MnSi. Analysis of the magnetization field dependencies measured in the magnetic field up to 9 T shows that $Mn_{1-x}Rh_xSi$ demonstrates anomalous power laws $M = A(T) \times H^{1-\xi(T)}$ in the wide temperature range 2–400 K, which is in contradiction to any ferromagnet driven by an ordinary equation of state [6]. This result poses two fundamental problems, namely the explanation of the observed anomaly and finding the order parameter and determination of Curie temperature. We developed the model for a Griffiths-like disordered cluster ferromagnetic phase [5, 7], in which magnetic disorder is determined by random local magnetic fields H_l with a power-law distribution function $w \sim |H_l|^{-\xi}$ ($\xi < 1$). This approach is entirely different from the standard one, as long as typically the Griffiths phase is characterized by dispersion of the local magnetic transition temperatures in spin clusters [1, 2]. Our theory allows describing analytically the experimentally known magnetic properties of Griffiths ferromagnetic phases [8] from a unified point of view, including the transition from the Curie-Weiss law for magnetic susceptibility $\chi \sim 1/(T - T_C)$ to an anomalous power-law dependence $\chi \sim 1/(T - T_C)^{\xi}$ in the range of temperature T exceeding the Curie temperature T_C. The developed approach makes it possible for the first time to explain the appearance of a power-law dependence of magnetization M on the magnetic field H, $M = A(T) \times H^{1-\xi(T)}$, in the ferromagnetic region $T < T_C$ and to propose a method for experimental determination of the order parameter, which may be reasonably approximated by coefficient $A(T)$. Comparison with experimental data leads to conclusion that it is precisely the disorder of this type playing the main role in ferromagnetic Griffiths systems, and the division into magnetic clusters should be valid for temperatures both above and below the Curie point. It is shown that the peculiarities of the magnetic properties of the Griffiths cluster system are not associ-

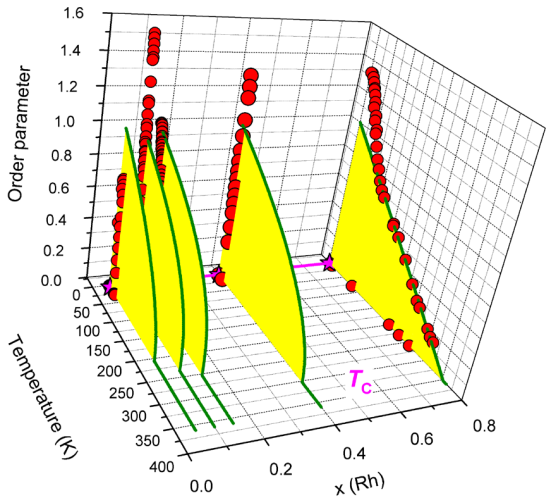

Fig. 1. Order parameters in FM Griffiths phase for $Mn_{1-x}Fe_xSi$ solid solutions with various rhodium content.

ated with the anomalous behavior of the magnetization of an individual cluster, but arise as a result of the disorder-induced modification of the integral characteristics of a disordered ferromagnet. The electron spin resonance and nuclear magnetic resonance measurements support the formation of the Griffiths-type phase with strong dispersion of the local magnetic fields in $Mn_{1-x}Rh_xSi$.

The analysis of the temperature dependence of the order parameter in FM Griffiths phase $Mn_{1-x}Rh_xSi$ demonstrate effect of strong enhancement of Curie temperature by a factor 8–12 with respect to the parent compound MnSi (Fig. 1). This parameter reaches T_C ~350 K for $x = 0.8$ thus breaking the expected in [1–3] universal suppression of the magnetic transition temperature. We argue that the observed increase in Curie temperature is a direct result of the Griffiths phase formation and may be due to the spin-fluctuation mechanism of enhancement of the magnetic interaction.

Author is grateful to V.V. Brazhkin for stimulating discussions and wishes to thank A.V. Tsvyashchenko, V.N. Krasnorussky, A.V. Bokov, D.A. Salamatin, O.S. Volkova, I.K. Shamova, A.V. Semeno, I.V. Yatsyk and R.M. Eremina for providing experimental data. My special thanks to A.E. Os'kin for his help in data procession. Support from RSF project 22-12-00008-П is acknowledged.

1. Griffiths R.B.: Phys. Rev. Lett. **23**, 17–19 (1969)
2. Bray A.J.: Phys. Rev. Lett. **59**, 586–589 (1987)
3. Demishev S.V. et al.:Physics-Uspekhi **59**, 559–563 (2016)
4. Bauer A. et al.: Phys. Rev. B **82**, 064404 (2010)
5. Demishev S.V. et al.: JETP Letters **121**, 111–118 (2025)
6. Vonsovskii S.V.: Magnetism, New York: J. Wiley, 1974.
7. Demishev S.V.: Doklady Rossiskoi Academii Nauk. Fizika, Tehnicheskie Nauki **521**, 31–38 (2025) (in Russian)
8. Eremina R.M.: Appl. Mag. Reson. **56**, 559–579 (2025)

EPR of nanoporous materials: New applications

M.V. Fedin, Y.N. Albrekht, A.A. Yazikova, A.S. Poryvaev

International Tomography Center SB RAS, Novosibirsk, Russia

Porous materials with nanoscale pores attract great attention in modern chemistry and materials science. In particular, they are employed to solve various problems of sorption, separation of mixtures, catalysis, photocatalysis, etc.; therefore optimization of functional properties of these materials for target applications is a topical task.

Electron paramagnetic resonance (EPR) spectroscopy is a highly informative method for studying and optimizing magnetic, structural, and functional properties of nanostructures and nanomaterials. In our recent series of studies, we have developed a number of new EPR approaches to study micro/nanoporous media [1], including metal-organic frameworks (MOFs) [2–5], porous organosilica materials [6–8], and type-III porous liquids based on MOF nano/microparticles dispersed in ionic liquids and their aqueous mixtures. In particular, we have studied the mechanisms of paramagnetic gas sorption into the pores of MOFs and organosilicas, optimized sorbents of toxic nitrogen oxides (NO, NO_2) and methods for their regeneration, and demonstrated the potential for using paramagnetic molecules grafted or adsorbed into porosity for quantum computing applications. In addition, using a spin probe encapsulated in MOFs, we have studied the stability of a series of porous liquids involving ZIF-8 MOF. The report will overview the key results of recent years and discuss the prospects for the application of EPR spectroscopy in the study and design of functional nanoporous media.

This work was supported by the Russian Science Foundation (No. 24-13-00119).

1. Fedin M.V.: Russ. Chem. Bull. **72**, 312 (2023)
2. Poryvaev A.S. et al.: Chem. Sci. **15**, 5268 (2024)
3. Tomilov A.S. et al.: Russ. J. Coord. Chem. **50**, 646 (2024)
4. Yazikova A.A. et al.: J. Phys. Chem. C **129**, 8455 (2025)
5. Albrekht Y.N. et al.: Small, **21**, 2503196 (2025)
6. Poryvaev A.S. et al.: Angew. Chem. Int. Ed. **60**, 8683 (2021)
7. Poryvaev A.S. et al.: ACS Appl. Mater. Interf. **15**, 5191 (2023)
8. Yazikova A.A. et al.: J. Haz. Mat. **478**, 135520 (2024)

Comparison of electron spin relaxation and pulse turning angles of lanthanide complexes with differing coordination numbers

G.R. Eaton, S.S. Eaton

Department of Chemistry and Biochemistry, University of Denver, Denver, CO 80210 USA

Field-swept spin-echo detection permits observation of wide lanthanide spectra that extend over thousands of gauss. EPR spin-lattice relaxation times were measured for seven lanthanide(III) ions bound to a phosphine oxide ligand (tris-(3,5-dimethoxyphenyl) phosphine oxide) that forms meridional pseudo-octahedral 6-coordinate complexes [1]. EPR spectra and relaxation times are compared with previously reported results for lanthanides in aqueous solution, bound to the protein lanmodulin, and bound to the bio-inspired small-molecule chelator 3,4,3-LI-(1,2-HOPO) [2]. The emphasis in this discussion will be on the *g* value and energy level information provided by the electron spin turning angle in pulsed EPR measurements of lanthanides. For example, samarium(III) requires about 20 dB (100 times) as much incident microwave power to create a 90º pulse as do terbium(III) and erbium(III). The turning angles provide insight into the J values for the ground states.

The EPR spectra and relaxation times are sensitive to the coordination environment and are emerging tools for characterization of both small-molecule and biomolecule interactions with lanthanide ions. Both Kramers and non-Kramers ions will be discussed.

1. These complexes were provided by Prof. Thomas Albrecht and Jacob Brannon, Colorado School of Mines, Golden, Colorado, USA.
2. Larringa W.B., Cotruvo J.A., Worrell B.T., Eaton S.S., Eaton G.R.: Chemistry – A European Journal **29** (2023) e202303215.

Antiferromagnetic spintronics and magnonics

S.A. Nikitov[1,2], D.V. Kalyabin[1,2], A.R. Safin[1,2]

[1] Kotel'nikov Radioengineering and Electronics Institute of the Russian Academy of Sciences, Moscow, Russia
[2] Moscow Institute of Physics and Technology (National Research University), Dolgoprudny, Russia

In the current work we present the review of the recent results obtained in our group in the field of antiferromagnetic (AFM) spintronics and magnonics. We begin with theoretical results describing the dynamic of the magnetic excitations in two sub-lattice AFM based on the Landau-Lifshits-Gilbert-Slonczewski equations of magnetizations motion supported by the Neel formalism. These equations include losses, exchange, dipole (anisotropy) interactions and spin current. In contrast with ferromagnets spin torque moment in AFM for easy axis polarization compensates the losses in one sub-lattice while increases them in another sub-lattice. In particular this model permits to describe basic results in a number of recent papers published on our studies. For example, as a first result we suggested temperature controlled generator of terahertz (THz) frequencies based on heterostructure ortho-ferrite (HoFeO) – heavy metal (HM-Pt) generating frequencies in the range 0.2–0.8 THz [1]. On the other hand a frequency controlled THz detector on the AFM-HM structure is proposed in [2]. We also have studied direct and inverse spin Hall effects in AFM resonator, in particular, in the hetestructure $FeBO_3$/Pt [3,4]. In same works we have studied microwave spin pumping from α-Fe_2O_3, while at the frequency 1.1 THz spin pumping from thin film NiO was studied in [5]. Continuing THz studies in AFM we have performed experiments on the influence of elastic deformations on the ferromagnetic and antiferromagnetic modes in various AFM materials. This was done using both Brillouin light scattering experimental setup and microwave setup [6]. All this leads to formation of the THz component base using AFM materials [1–11].

This work was supported by the Russian Foundation for Basic Research (grant 24-19-00250).

1. Mescheryakov A. et al.: J Phys. D Appl. Phys. **54**, 195001 (2021)
2. Safin A. et al.: MDPI Magnetochemistry **8**(2), P.26 (2022)
3. Gabrielyan D. et al.: J. Appl. Phys. **136**, 083902 (2024)
4. Gabrielyan D. et al.: J. Phys. D Appl. Phys. **57**, 305003 (2024)
5. Stremoukhov S.P. et al.: Res. Phys. **57**, 107377 (2024)
6. Bogdanova T.V. et al.: Appl. Phys. Lett., V. 124, 092410 (2024)
7. Safin A. et al.: Ultrasonics **119**, 106588 (2022)
8. Popov P. et al.: Phys. Rev. Appl. **13**, 044080 (2020)
9. Consolo G. et al.: Phys. Rev. B: **103**, 134431 (2021)
10. Mitrofanova A. et al.: Appl. Phys. Lett. **120**, 072402 (2022)
11. Mitrofanova A. et al.: IEEE Transactions on Nanotechnology, V. 22, P. 620–627 (2023)

Magnetic resonance and integrative structural biology, outside and inside mammalian cells

T. Polenova[1,2,3], A.M. Gronenborn[1,2,3], C.M. Quinn[1], K.T. Movellan[1,2], C. Guo[1,2], S. Zeinalilathori[1,2], J. Struppe[4], D. Banks[4], J. Kempf[4]

[1] Department of Chemistry and Biochemistry, University of Delaware, Newark, DE 19716, United States
[2] Pittsburgh Center for HIV Protein Interactions, University of Pittsburgh School of Medicine, Pittsburgh, PA 15261, United States
[3] Department of Structural Biology, University of Pittsburgh School of Medicine, Pittsburgh, PA 15261, United States
[4] Bruker Biospin Corporation, 15 Fortune Drive, Billerica, MA 01821, United States

I will present our advancements in next-generation magnetic resonance techniques for atomic-level analysis of large biological complexes and proteins in their natural settings. I will illustrate how we integrate magic angle spinning (MAS) NMR with medium-resolution cryo-EM and data-driven molecular dynamics simulations to enhance our understanding of the structure and dynamics of HIV-1 protein assemblies and their functions. I will also present the use of ^{19}F dynamic nuclear polarization (DNP)-enhanced MAS NMR in studying protein assemblies and proteins within mammalian cells. Achieving over 35-fold signal enhancements, we can capture high signal-to-noise ratio MAS NMR spectra from nanomole amounts of proteins in mere minutes, producing two-dimensional dipolar correlation spectra with exceptional resolution. This research opens avenues for utilizing ^{19}F DNP-enhanced MAS NMR in cellular contexts to investigate protein structure, dynamics, and ligand interactions. I will address the challenges and opportunities presented by magnetic resonance in integrative structural biology.

Nuclear hyperpolarization in electron transfer in chiral systems

T.V. Leshina[1], I.M. Magin[1], N.E. Polyakov[1], K.M. Salikhov[2]

[1] Voevodsky Institute of Chemical Kinetics and Combustion of the Siberian Branch of RAS
[2] Zavoisky Physical-Technical Institute, FRC Kazan Scientific Center of Russian Academy of Sciences, Kazan, Russia
e-mail: salikhov@kfti.knc.ru

Electron transfer (ET) is an elementary chemical act that has been widely studied due to its involvement in many chemical, biological and physical processes. A new direction of interest in ET is related to the search for ways to control the state of electron spins with the aim of using spins as qubits in spintronics, quantum computing and quantum information science. Over the past decades, the use of chirality as a way to control the dynamics of electron spins has been actively discussed. The phenomenon of chiral-induced electron spin selectivity (CISS) is currently being intensively studied as it concerns the use of electron spins in quantum technologies. At present, considerable attention is also paid to photoinduced ET in chiral donor-acceptor dyads recommended as models for studying the mechanism of influence of a chiral medium on the spin dynamics of electrons. At the same time, using the method of chemically induced dynamic nuclear polarization (CIDNP), it was shown that photoinduced ET in chiral systems exhibits nuclear spin selectivity (the so-called NSS effect). In the present review, we have summarized the current data on NSS effect, and have attempted to build bridge between NSS and CISS phenomena. The presented data may support the conclusion that NSS and CISS have a common origin due to the processes occurring during the passage of electrons through a chain of chiral atoms.

1. Ageeva A.A., Doktorov A.B., Polyakov N.E., Leshina T.V.: Mol. Sci. **23**, 3060 (2022)

Spin excitations in ordered XXZ-chain system Cs_2CoCl_4

A.I. Smirnov, T.A. Soldatov

P. L. Kapitza Institute for Physical Problems RAS, Moscow, Russia

Cs_2CoCl_4 is a unique quasi 1D antiferromagnet with a high degree of one-dimensionality and a very good correspondence to an important quantum many-body model of the XXZ antiferromagnetic S=1/2 chain. The high degree of one dimensionality is provided by a large ratio of intrachain–to–interchain exchange about 20. The main (intrachain) exchange between S = 3/2 Co^{2+} ions is J = 0.74 K. The XXZ anisotropy arises due to the single ion anisotropy of the easy plane type which is parametrized by the DS_z^2 term of the spin Hamiltonian with D = 7 K [1]. At low temperatures $T << D$ an effective spin (pseudospin) value s = 1/2 is valid because the upper spin doublet S_z = +/–3/2 is not populated. In the pseudospin representation the effective exchange anisotropy arises instead of the single ion anisotropy, the relative exchange anisotropy reaches 25% in the limit $D >> J$ [1]. The S = 1/2 XXZ chain model shows remarkable ground states – a spin liquid at absolute zero and 1D weakly ordered antiferromagnet in a transverse field. Excitations are of the spinon-type, as found in DMRG simulations of [2]. In the long wavelength limit there is a maximum in the spectral density of S = 1 excitations shifted down with respect to the frequency of the quasi-Larmor mode. This shift was recently detected experimentally [3] by the observations of ESR signals in the temperature range between the Néel temperature and exchange temperature $J/k_{B.}$. Below the Néel temperature T_N = 0.22 K the 3D long range antiferromagnetic order with 8 magnetic sublattices occurs [4] instead of the specific quasi one dimensional spin liquid.

In the present research we study the transformation of the ESR spectrum from a single mode ESR of the spin liquid to the multimode antiferromagnetic resonance of an 8-sublattice antiferromagnetic structure. The challenge for this study appears from controversy expectations. One the one hand, we expect a strong transformation of the excitation spectrum due to appearance of a multisublattice magnetic structure, one the other hand, this transformation occurs due to a very weak interchain interaction and should be therefore also weak.

The observed temperature evolution of the ESR spectrum is shown in Fig. 1. Below the Néel temperature we observe the main resonance line remains in the same resonance field, i.e. at the frequency of an intracorrelated XXZ chain. At the same time a change of the spectrum arises due to the appearance of numerous weak satellites. The sum of integral intensities of all satellites consists only about 10 % of the total integral intensity. The frequency-field dependence of the main ESR line M is presented in Fig. 2 by closed symbols, and of weak satellites – by open symbols. The calculated frequency of the XXZ chain model [2] is shown by a solid line. Thus, our experiment shows appearing of new weak spectral components with strongly deviating frequencies, but the most part of spectral weight remains at the same frequency, in a correspondence with the contradictory expectations. This scenario realizes in the frequency range near or above the exchange frequency J/h ~50 GHz, i.e for the ener-

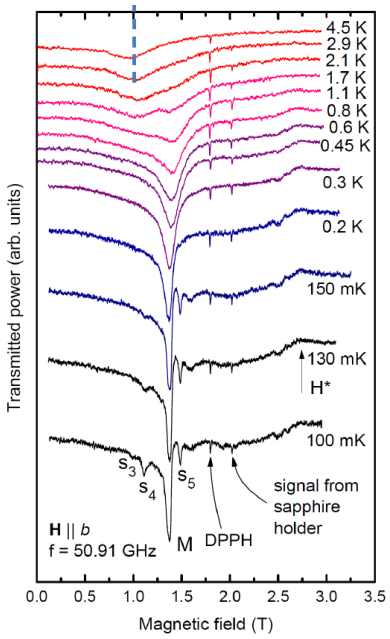

Fig. 1. Temperature evolution of the ESR.

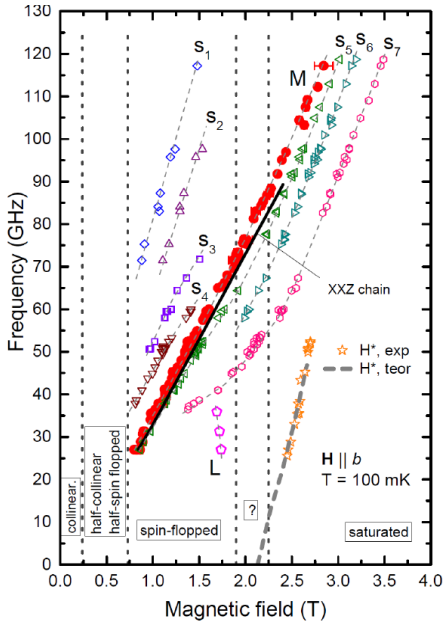

Fig. 2. Frequency-field dependencies for the main ESR line M(closed symbols) and weak satellites (open symbols). Solid line represents calculated resonance frequency for a separate XXZ chain.

gies of excitations exceeding the energy of interchain interaction. At the same time, for frequencies below 50 GHz the spectrum of the ordered phase is much more complicated and can't be described as a main resonance line surrounded by satellites. Nevertheless, for frequencies above 60 GHz the concept of the weak interchain interaction gives a good approximation for the most part of the spectral weight. Thus, we conclude that, due to a weak interchain interaction, the dynamics of a complicated spin structure of Cs_2CoCl_4 may be approximately presented as that of 1D XXZ chain.

The work is supported by Russian Science Foundation Grant № 22-12-00259.

1. Breunig O. et al.: Phys. Rev. Lett. **111**, 187202 (2013)
2. Laurell P. et al.: Phys. Rev. Lett. **127**, 037201 (2021)
3. Soldatov T.A., Edelman V.S., Smirnov A.I.: Applied Magnetic Resonance **55**, 1137 (2024)
4. Kenzelman M. et al.: Phys. Rev. B **65**, 144432 (2002)

High resolution NMR and nuclear spin hyperpolarization with fast field cycling

A.S. Kiryutin, I.V. Zhukov, O.B. Morozova, N.N. Fishman, D.A. Markelov, N.N. Lukzen, M.P. Geniman, A.V. Yurkovskaya

International Tomography Center, SB RAS, Novosibirsk, Russia

In this presentation, the fundamentals of spin chemistry and nuclear hyperpolarisation will be outlined concisely. Furthermore, a brief overview of the results from the past decade of research conducted within our Novosibirsk groups will be provided. The prevailing theoretical approach for the description of different types of spin hyperpolarisation has been re-formulated in terms of level crossings (LC) and level anti-crossings (LAC) of interacting spin states [1].

In order to explore the full potential of the unified approach, which addresses different types of LACs through magnetic field variation, a fully automatic, low-cost field cycling add-on was built in Novosibirsk [2]. This add-on covers the ultra-wide magnetic field range from 10 nT to 19.4 T. The shuttling device is characterised by its compact design and compatibility with commercial high-resolution NMR spectrometers. The apparatus under discussion enables the undertaking of variable heteronuclear two-dimensional nuclear magnetic resonance (2D NMR) and nuclear relaxation measurement with high resolution and high-throughput. This apparatus facilitates para-hydrogen-induced nuclear spin hyperpolarisation (PHIP) and signal amplification via reversible exchange (SABRE), as well as proton and heteronuclear photo-CIDNP and photo-SABRE [3]. It was demonstrated that the most efficient polarization transfer occurs at LACs, and that such transfer is of a coherent nature. It is evident that the utilisation of magnetic field dependence has led to the formulation of highly efficient experimental protocols for the hyperpolarisation of ^{13}C, ^{15}N, ^{19}F, ^{31}P and ^{77}Se nuclei via the implementation of adiabatic magnetic field modulation at LACs [4, 5]. The proposed approach has the potential to enhance the efficiency of hyperpolarization processes at zero and ultralow magnetic fields (ZULF), as well as at weak and strong magnetic fields through the application of shaped pulses of oscillating magnetic fields.

In the domain of spin chemistry, the magnetic interactions between electrons and nuclei are encoded in the field dependence of CIDNP (Chemically Induced Dynamic Nuclear Polarisation). This process is modulated by nuclear relaxation dispersion, which plays a crucial role in the dynamics of the system. The combination of studies conducted over an ultra-wide magnetic field range facilitates the disentangling of contributions from distinct mechanisms to singlet-triplet conversion, thereby unveiling the occurrence of polarization transfer among nuclei. Photochemically active, covalently linked electron donor–bridge–acceptor triads have long been the focus of solar energy storage, due to their resemblance to photosynthetic reaction centres. A series of donor-acceptor dyads were examined through ^{13}C, ^{15}N and ^{1}H field-dependent and ^{1}H time-resolved photo-CIDNP, with theoretical calculations providing a contemporary framework. This comprehensive approach elucidated the LACs in magnetic field dependence and ascertained the sign and

values of the electronic exchange interaction and detailed map of ^{13}C and ^{1}H hyperfine interactions in transient, short-lived biradicals [6].

The phenomenon of photoinduced intramolecular electron transfer (ET) is of paramount importance in the realm of charge transport in biological and synthetic systems. In the recent study, the ET was examined in peptide His-Glu-Tyr-Gly (1) and the conjugate His-Gln(BP)-Tyr-Gly (2) with benzophenone (BP) as a photoactive electron acceptor and His or Tyr as donors [7]. Time-resolved and field-dependent chemically induced dynamic nuclear polarization (CIDNP) techniques were employed to investigate electron transfer (ET) mechanisms and kinetics. Peptide 1, with benzophenone as photosensitiser, initially forms two types of radical, with a radical centre at either His or Tyr residue. Consequent to this, electron transfer (ET) occurs from Tyr residue to the His radical, both intra- and intermolecularly. Conjugate 2 forms two types of biradicals under irradiation: with radical centres at Tyr and BP across the entire pH range, and with radical centres at His and BP at slightly basic pH. Field-dependent CIDNP revealed nonzero electronic exchange interaction ($2J(ex) = –8.78$ mT) at acidic pH, indicating proximity between BP and Tyr radicals. Low-field CIDNP spectra exhibited pronounced emissive polarization patterns, accompanied by pH-dependent exchange interactions in transient biradicals.

The CIDNP work was supported by Russian Science Foundation (grant No. 23-73-10103) and SABRE experiments were supported by the Russian Science Foundation (Grant No. 25-23-00607).

1. Ivanov K.L., Pravdivtsev A.N., Yurkovskaya A.V., Vieth H.-M., Kaptein R.: Progress in Nuclear Magnetic Resonance Spectroscopy **81**, 1–36 (2014)
2. Kiryutin A.S., Pravdivtsev A.N., Ivanov K.L., Grishin Y.A., Vieth H.-M., Yurkovskaya A.V.: Journal of Magnetic Resonance **263**, 79–91(2016)
3. Kozienko V.P., Kiryutin A.S., Yurkovskaya A.V.: J. Chem. Phys. **157**, 174201 (2022)
4. Kozinenko V. P., Kiryutin A. S., Yurkovskaya A.V. Chemistry–Methods. e202400060 (2025)
5. Kiryutin A.S., Markelov D.A., Matsulevich Z.V., Kosenko I.D., Kireev N.V., Godovikov I.A., Yurkovskaya A.V.: Journal of the American Chemical Society 10.1021/jacs.5c06450 (2025)
6. Zhukov I., Fishman N., Kiryutin A., Lukzen N., Steiner U.E., Vieth H.-M., Schäfer J., Lambert C.A.E., Yurkovskaya A.V.: Journal of Chemical Physics 155, 224201 (2021)
7. Fishman N.N., Herr K., Morozova O.B., Zhukov I.V., Geniman M.P., Brodrecht M., Wissel T., Buntkowsky G., Yurkovskaya A.V.: Scientific Reports **15**, 1, 20135 (2025)

SECTION 1

ADVANCES IN MAGNETIC RESONANCE THEORY AND INSTRUMENTATION

oral

A new type of MCA pulses combining constant and offset-independent adiabaticity for magnetic resonance

A.V. Snadin[1,2], A.S. Kiryutin[1,2], N.N. Fishman[1], N.N. Lukzen[1,2]

[1] International Tomography Center Siberian Branch RAS, Novosibisrks, Russia
[2] Novosibirsk State University, Novosibisrk, Russia

Adiabatic pulses are widely used in magnetic resonance techniques, and their development and refinement remain very relevant. Adiabatic inverting pulses are highly robust for radiofrequency or microwave magnetic field inhomogeneities and enable manipulation of spins over a large frequency range. We proposed the new inverting pulses for spin 1/2 which combine the adiabaticity remaining constant for the single isochromat throughout the pulse and the same adiabaticity for all isochromats in a given bandwidth, but only at the single instant of time when the frequency of the pulse coincides with the frequency of the isochromat. The dependence of inversion performance of these pulses on peak amplitude of RF field, while preserving the pulse shape, is studied. These pulses may be useful for a number of MRI techniques where inverting pulses are an integral part. A comparison with other widely used adiabatic inverting pulses reveals performance improvements, achieving up to 30–40% enhancement in inversion efficiency.

oral

Recombination operator model construction

I.A. Frolov[1,2], **P.A. Purtov**[1,2]

[1] Voevodsky Institute of Chemical Kinetics and Combustion, Siberian Branch, Russian Academy of Sciences, Novosibirsk, Russia
[2] Novosibirsk State University, Novosibirsk, Russia

It is a well-known fact that spin density matrix evolution should be described in terms of spin evolution, diffusion, and recombination operators. Several phenomenological alternatives to the classical recombination operator were proposed in recent years. This work (as with previous [1-3]) is intended to eliminate the phenomenology. We start with a simple enough physical model that leads exactly to the classical recombination operator and then generalise it in order to obtain physically more realistic characteristics of the model.

Let $\hat{H} = \hat{H}_0 + \hat{V}$ — Hamiltonian of system, $\hat{V}$ — perturbation, eigenstates of $\hat{H}_0$ are as follows:

- $\hat{H}_0|s\rangle = E_s|s\rangle$ (singlet radical pair)
- $\hat{H}_0|t\rangle = E_t|t\rangle$ (triplet radical pair)
- $\hat{H}_0|i\rangle = E_i|i\rangle$ (singlet reservoir, i ranges over values)
- $\hat{H}_0|k\rangle = E_k|k\rangle$ (triplet reservoir, k ranges over values)

Furthermore, we construct $\hat{V}$ with non-zero elements only for transitions $\langle i|\hat{V}|s\rangle$, $\langle s|\hat{V}|t\rangle$, $\langle t|\hat{V}|k\rangle$. Assuming the reservoirs are dense, we treat them as continuous recombination spectra. All the spectra information we need to describe radical pair spin state evolution is contained in $\rho(E)|V(E)|^2$ (for each reservoir), where $\rho(E)$ is the density of states. The case in which these functions are constant (E ranges from $-\infty$ to ∞) corresponds to the classical recombination operator. The following generalisations are considered in this work:

- $\rho(E)|V(E)|^2 = const$ if $E_{min} \le E \le E_{max}$; 0, otherwise (bounded uniform distribution); we will set $\rho \equiv \frac{1}{E_{max} - E_{min}}$
- $\rho(E)|V(E)|^2$ is given by Lorentz distribution

1. Purtov P.A.: Chem. Phys. Lett. **496**, 335 (2010)
2. Sosnovsky D.V., P.A. Purtov: Chem. Phys. Lett. **608**, 136 (2014)
3. Purtov P.A.: Zeitschrift für Physikalische Chemie **231**, 225 (2017)

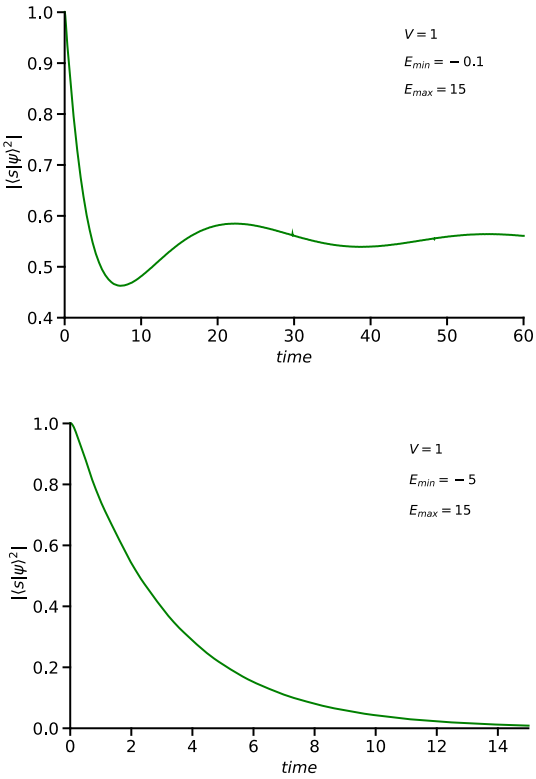

Fig. 1. The time-dependence of being in a radical pair state for a bounded uniform distribution. The unit of energy E (arbitrary) corresponds to the unit of time $\hbar/E$. $E_s = 0$, $\langle s|\hat{V}|t\rangle = 0$, initial state is |s⟩. It is easily noticed that recombination can be either reversible or irreversible depending on the spectrum.

oral

Quasi-stable structures in liquid antimony: DFT analysis

A.A. Tsygankov[1,2], B.N. Galimzyanov[1,2], A.V. Mokshin[1,2]

[1] Kazan Federal University, Institute of Physics, Kazan, Russia
[2] Udmurt Federal Research Center of the Ural Branch of the RAS, Izhevsk, Russia

Nuclear magnetic resonance method is frequently used for local structure analysis of liquids [1]. Liquids are often characterized by the presence of a homogeneous distribution of atoms at large distances and short-range order at small distances. However, liquid antimony is an unusual system due to its structure, which exhibits anomalies in the form of shoulders in the radial distribution function and static structure factor [2–4]. The reason for the existence of this anomaly is not yet fully understood [4, 5]. The precence of bonded structures was confirmed by various methods, in particular, with nuclear magnetic resonance. The radial distribution function is a characteristic of the probability of finding a particle at a certain distance from another particle. Therefore, we can conclude that this feature can only occur if atoms form at least quasi-stable structures [5–7]. To reproduce the structural features of liquid antimony, ab-initio molecular dynamics simulations were performed in the VASP package [8] using density functional theory (DFT) methods at temperature $T = 923$ K and pressure $P = 1.0$ atm.

To determine the possibility of the existence of stable structures in liquid antimony, the distribution of particles by neighbourhood times was calculated from the obtained results of ab-initio molecular dynamics simulations. In the framework of the Williams-Landel-Ferry model, it was shown that in the regions bounded by a sphere of radius 5 Å there are stable formations with a lifetime greater than 1.6 ps [9]. In order to identify such structures, the order parameters q_4 and q_6 were estimated and the structures were characterized. The results demonstrated the formation of triangular structures with lengths $a = 3.07$ Å, $b = 4.7$ Å and angles $\alpha = 45°$ and $\beta = 90°$ in liquid antimony (Fig. 1). Furthermore, the quasi-stable formations were observed to exert a

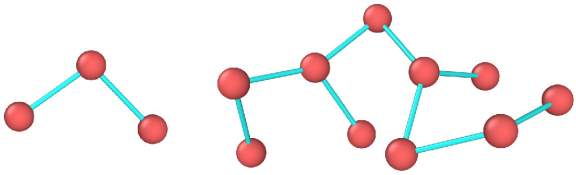

Fig. 1. Example of triangular structure and chain formed by antimony atoms.

direct influence on the presence of a shoulder in the radial distribution function and the static structure factor.

The work was carried out on the basis of the grant provided by the Academy of Sciences of the Republic of Tatarstan in 2024 for the implementation of fundamental and applied research work in scientific and educational organizations, enterprises and organizations of the real sector of the economy of the Republic of Tatarstan.

1. Raugei S., Klein M.L.: J. Chem. Phys. **116**, 7087–7093 (2002)
2. Yang M., Trizio E., Parinello M.: Chem. Sci. **15**, 3382–3392 (2024)
3. Greenberg Y., Yahel E., Caspi E.N., Beuneu B., Dariel M.P., Makov G.: J. Chem. Phys. **133**, 094506 (2010)
4. Waseda Y., Suzuki K.: Phys. Stat. Sol. (b) **49**, 339–347 (1972)
5. Jones R.O., Ahlstedt O., Akola J., Ropo M.: J. Chem. Phys. **146**, 194502 (2017)
6. Mokshin A.V., Khusnutdinoff R.M., Galimzyanov B.N., Brazhkin V.V.: Phys. Chem. Chem. Phys. **22**, 4122–4129 (2020)
7. Tsygankov A.A., Galimzyanov B.N., Mokshin A.V.: J. Mol. Liq. **418**, 126699 (2025)
8. Kresse G., Hafner J.: Phys. Rev. B. **47**, 558 (1993)
9. Williams M.L., Landel F.R., Ferry J.D.: J. Am. Chem. Soc. **77**, 3701–3707 (1955)

oral

Spin-crossover in Cu_2MnBO_5:Cr ludwigite

D.V. Popov[1], R.G. Batulin[2], M.A. Cherosov[2], I.V. Yatsyk[1], R.M. Eremina[1]

[1] Zavoisky Physical-Technical Institute, FRC Kazan Scientific Center of RAS, Kazan, Russia
[2] Kazan (Volga Region) Federal University, Kazan, Russia

Oxyborates with formula $M_2M'BO_5$, where M is a divalent and M' is a trivalent metal ion, are classified as ludwigites. These compounds have four non-equivalent crystallographic positions per unit cell for aforementioned metal ions to occupy, resulting in the random distribution of magnetic ions, mixed valence of ions, strong electron correlations and unusual charge ordering. This feature leads to observation of unconventional magnetic properties in ludwigites [1, 2].

Ludwigite Cu_2MnBO_5, doped by Cr ions at a concentration of 0.08 per unit cell was studied via the magnetization, XPS, EPR and the temperature dependence of the specific heat measurements. The compound undergoes two phase transitions at T_1 = 52 and T_2 = 59 K into a canonical spin-glass state. Studies reveal that the effective magnetic moment decrease from 5.33 up to 4.38 μB with an increase of the external magnetic field up to the magnetic field 3T, as well as the Curie-Weiss constant (Fig. 1). This reduction is attributed to the transition from a high-spin state to a low-spin state for manganese ions. This is further confirmed by the specific heat studies exhibits, as the Einstein temperatures change with the magnetic field.

This work was supported by the Russian Science Foundation (project no. 23-72-00047).

1. Popov D.V. et al.: Journal of Physics and Chemistry of Solids **148**, 109695 (2021)
2. Popov D.V. et al.: Journal of Alloys and Compounds **976**, 173143 (2024)

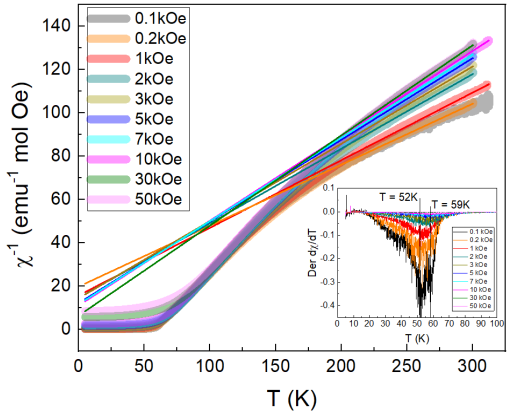

Fig. 1. Temperature dependence of the inverse magnetic susceptibility in Cu_2MnBO_5:Cr. Inset: derivative for the magnetic susceptibility with established transition temperatures.

oral

Calculation of interaction parameters of Pu^{3+} ions with spins of fluorine nuclei in CaF_2

R. Ziatdinov, M.V. Eremin

Kazan Federal University, Kazan, Russia
razik.ziat@gmail.com

Experimental data obtained by ENDOR method [1] revealed that the interaction of Pu^{3+} 5f-electrons with fluorine nuclei in CaF_2 crystal differs significantly from the classical dipole-dipole interaction. There is a large isotropic electron-nucleus interaction with the A_s parameter, which was found to be negative. The reason for this anomalous phenomenon has not yet been explained.

In this work, we consider the effect of mixing the 5f-electron wave functions of the Pu^{3+} ion with the 2s- and 2p- wave functions of fluorine on the values of the electron-nuclear double resonance (ENDOR) parameters A_s and A_p. Using the technique of irreducible tensor operators, we derive expressions for the spin Hamiltonian parameters of A_s and A_p via the hybridization parameters $\lambda_{f\sigma} = s_{f\sigma} + \gamma_{f\sigma}$, $\lambda_{f\pi} = s_{f\pi} + \gamma_{f\pi}$ and $\lambda_{fs} = s_{fs} + \gamma_{fs}$. In addition to this generally accepted covalent approach, the virtual transfer processes of 2s- and 2p- electrons of fluorine into the empty 6d-shell of plutonium have been taken into account. All overlap integrals were calculated on the Hartree-Fock wave functions of plutonium taken from [2], which were previously approximated by Gaussian-type orbital expansions. In the numerical evaluations of A_s and A_p, the covalency parameters $\gamma_{f5\sigma}$, $\gamma_{5f\pi}$, $\gamma_{6d\sigma}$, $\gamma_{6d\pi}$ were assumed to be proportional to the overlap integrals $s_{f\sigma}$, $s_{f\pi}$, $s_{\sigma s}$ interaction with the A_s parameter, which was found to be negative. As it could be expected on the basis of transferred hyperfine interaction analysis, for rare-earth compounds (see, for example, [3]), the magnitude and sign of A_s for the Pu^{3+} ion in CaF_2 can be explained by virtual processes of transfer of 2s- and 2p- electrons of fluorine to the empty 6d-shell of plutonium. Moreover, using the experimental data of [1] we obtained the covalence parameters of 5f- and 6d-electrons of Pu^{3+} in CaF_2.

1. KolbeW., Edelstain N.: Electron-Nuclear Double Resonance of Pu^{3+} in CaF_2 // Phys. Rev. B **4**. no. 9. P. 2869–2875 (1971)
2. Schreckenbach G., Hay P.J., Martin R.L.: Density Functional Calculations on Actinide Compounds: Survey of Recent Progress and Application to $[UO_2]^{2+}$ // J. Comput. Chem. - 1999. - Vol. 20. - P. 70-90
3. Falin M.L., Eremin M.V., Bill H., Lovy D.: ENDOR and transferred hyperfine interaction of impurity rare-earth ions with nearest diamagnetic ions in crystals // Appl. Magn. Reson. - 1995. - Vol. 9. - P. 329-354.

poster

A new approach to finding an analytical solution to the Bloch equations for magnetization components under modulation conditions of a constant magnetic field

A.A. Gol'dberg[1], S.A. Klimova[1], R.V. Davydov[1], D.S. Provodin[1], V.V. Davydov[1,2]

[1] Peter the Great St.Petersburg Polytechnic University, Saint-Petersburg, Russia
[2] Saint-Petersburg Electrotechnical University "LETI", Saint-Petersburg, Russia

In recent years, nuclear magnetic resonance (NMR) technology has been implemented in various rapid monitoring devices, flow meters, fluid state analyzers, and flowing liquid NMR magnetometers for solving scientific and industrial problems [1, 2]. A key challenge in using such devices involves describing NMR signals recorded using modulation techniques. The modulation-based NMR signal detection method offers significant advantages for operation in weak magnetic fields or with fluid flows, as in NMR flow-relaxometers and NMR magnetometers.

Currently, only approximate solutions of the Bloch equations exist for describing NMR signals under modulation conditions, or numerical solutions are employed. This creates difficulties in certain research and technical applications, particularly when determining longitudinal relaxation times T_1 [3]. This is especially important for compact NMR relaxometers used in rapid monitoring of condensed media and flow conditions [1]. This work presents an exact analytical solution of the Bloch equations without approximations.

Consider the Bloch equations in a rotating coordinate system [3], incorporating dispersion and absorption signals through magnetization components M_x and M_y:

$$\begin{cases} \dfrac{du(t)}{dt} + \dfrac{v(t)}{T_1} + (W + \gamma H_m \sin(\omega_m t))v(t) = 0 \\ \dfrac{dv(t)}{dt} + \dfrac{v(t)}{T_2} - (W + \gamma H_m \sin(\omega_m t))u(t) + \gamma H_1 M_z(t) = 0 \\ \dfrac{dM_z(t)}{dt} + \dfrac{M_z(t)}{T_1} - \dfrac{M_0}{T_1} - \gamma H_1 v(t) = 0 \end{cases}$$

Rewritten in alternative form:

$$\begin{cases} \dot{u}(t) + \dfrac{v(t)}{T_2} + (W + \gamma H_m \sin(\omega_m t))v(t) = 0 \\ \dot{v}(t) - (W + \gamma H_m \sin(\omega_m t))u(t) + \dfrac{v(t)}{T_2} + \gamma H_1 M_z(t) = 0 \\ \dot{M}_z(t) - \gamma H_1 v(t) + \dfrac{M_z(t)}{T_1} = \dfrac{M_0}{T_1} \end{cases}$$

Introducing the notation:

$$x(t)=\begin{pmatrix} u(t) \\ v(t) \\ M_z(t) \end{pmatrix},\quad A(t)=\begin{pmatrix} -\frac{1}{T_2} & -W-\gamma H_m \sin(\omega_m t) & 0 \\ W+\gamma H_m \sin(\omega_m t) & -\frac{1}{T_2} & -\gamma H_1 \\ 0 & \gamma H_1 & -\frac{1}{T_1} \end{pmatrix},\quad f(t)=\begin{pmatrix} 0 \\ 0 \\ \frac{M_0}{T_1} \end{pmatrix}$$

The system with initial conditions becomes:

$$\dot{x}(t)+A(t)x(t)=f(t),\ x(0)=x_0=\begin{pmatrix} 0 \\ 0 \\ M_H \end{pmatrix}$$

The general solution of the system is:

$$x(t)=\exp\left(-\int_0^t A(s)ds\right)x_0+\int_0^t \exp\left(\int_t^s A(k)dk\right)f(s)ds$$

The computed integrals are:

$$B(t)=-\int_0^t A(s)ds=\begin{pmatrix} \frac{t}{T_2} & \frac{\gamma H_m}{\omega_m}(\cos(\omega_m t)-1)-Wt & 0 \\ -\frac{\gamma H_m}{\omega_m}(\cos(\omega_m t)-1)+Wt & \frac{t}{T_2} & -\gamma H_1 t \\ 0 & \gamma H_1 t & \frac{t}{T_1} \end{pmatrix}$$

$$C(s,t)=\int_t^s A(k)dk=\begin{pmatrix} \frac{s-t}{T_1} & -\frac{2H_m}{\omega_m}(\cos(\omega_m s))-\cos(\omega_m t) & 0 \\ -\frac{2H_m}{\omega_m}(\cos(\omega_m s))-\cos(\omega_m t) & 0 & -\frac{s-t}{T_1} \\ 0 & 0 & \gamma H_1(s-t) \end{pmatrix}$$

For matrix exponential calculations, we note that the studied matrices can be expressed as:

$$D=\begin{pmatrix} a & b & 0 \\ -b & a & -c \\ 0 & c & d \end{pmatrix}$$

poster

The final solution is obtained by determining the Jordan form of the matrix, yielding the solution functions:

$$u(t) = (A_3)_B M_H + \frac{M_0}{T_1}\int_0^t (A_3)_C ds$$

$$v(t) = (A_6)_B M_H + \frac{M_0}{T_1}\int_0^t (A_6)_C ds$$

$$M_z(t) = (A_9)_B M_H + \frac{M_0}{T_1}\int_0^t (A_9)_C ds$$

The coefficients $(A_i)_B, (A_i)_C$ are calculated according to the considered cases depending on parameter values.

The proposed new approach enables analytical solutions for dispersion and absorption signals, as well as the magnetization component M_z. Analysis shows that $u(t)$, $v(t)$, and $M\_z(t)$ depend solely on H_1, H_0, H_m, ω_m, and the relaxation times T_1 and T_2. This significantly expands potential NMR applications in various fields using the described instruments.

1. Davydov V.V., Dudkin V.I., Vysoczky M.G., Myazin N.S.: Appl. Magn. Reson. **51** 653–666 (2020)
2. Eremina R., Gippius A., Gafurov M.: Appl. Magn. Reson.e **54(4-5)**, 435 (2023)
3. Leshe A.: Nuclear induction. Veb Deustscher Verlag Der Wissenschaften, Berlin, 1963.

SECTION 2

MODERN METHODS OF MAGNETIC RESONANCE

oral

^{77}Se SABRE via tandem scalar coupling: First parahydrogen-induced hyperpolarization of selenium

A.S. Kiryutin[1], D.A. Markelov[1], Zh.V. Matsulevich[2], I.D. Kosenko[3], N.V. Kireev[3], I.A. Godovikov[3], A.V. Yurkovskaya[1]

[1] International Tomography Center, SB RAS, Novosibirsk, Russia
[2] Nizhni Novgorod State Technical University, Nizhni Novgorod, Russia
[3] Nesmeyanov Institute of Organoelement Compounds of RAS, Moscow, Russia

We demonstrate the first successful hyperpolarization of ^{77}Se nuclei using Signal Amplification By Reversible Exchange (SABRE), applied to a biologically relevant selenium–nitrogen heterocycle, 3-methyl-[1,2,4]-selenadiazolo-[4,5-a]-pyridine-4-ium chloride (SDAP)[1]. The polarization transfer was carried out at ultralow magnetic fields (0.1 μT to 5 μT), using parahydrogen as the polarization source. Remarkably, high levels of nuclear spin polarization were obtained simultaneously for both ^{77}Se and ^{15}N nuclei at their natural isotopic abundances, reaching 7.0% and 5.6%, respectively. These results enable direct detection of ^{15}N and ^{77}Se signals at micromolar concentrations, using a single scan at 9.4 T, without isotopic enrichment.

Mechanistic analysis revealed a tandem polarization transfer pathway, in which ^{77}Se polarization is relayed through scalar coupling with ^{15}N nuclei in the SABRE polarization transfer complex. This cooperative polarization mechanism enables efficient hyperpolarization of low-γ, low-abundance heteronuclei such as ^{77}Se. Our findings establish microtesla SABRE as a powerful, low-cost alternative to d-DNP for enhancing multinuclear NMR sensitivity in spin systems involving multiple heteronuclei. The demonstrated method opens new avenues for studying selenium-containing compounds in organic synthesis, catalysis, and biomedical research via heteronuclear NMR.

This work was supported by the Russian Science Foundation (No. 25-23-00607).

1. Kiryutin A.S., Markelov D.A., Matsulevich Zh.V., Kosenko I.D., Kireev N.V., Godovikov I.A., Yurkovskaya A.V.: J. Am. Chem. Soc. (2025) accepted paper 09.06.2025. DOI: 10.1021/jacs.5c064501. Kiryutin A.S., Markelov D.A., Matsulevich Zh.V., Kosenko I.D., Kireev N.V., Godovikov I.A., Yurkovskaya A.V.: J. Am. Chem. Soc. (2025) accepted paper 09.06.2025. DOI: 10.1021/jacs.5c06450

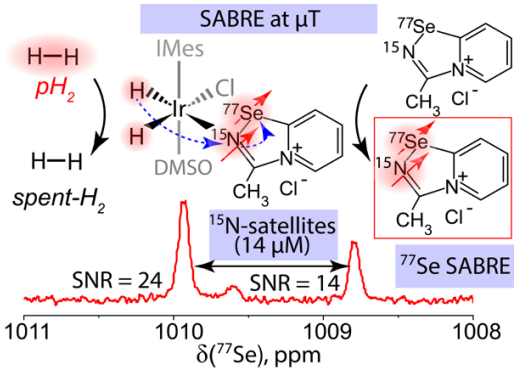

Fig. 1. Polarization of ^{77}Se nuclei via scalar interactions with parahydrogen-derived protons and ^{15}N nuclei. ^{77}Se NMR spectrum of hyperpolarized 3-methyl-[1,2,4]-selenadiazolo-[4,5-a]-pyridine-4-ium chloride (SDAP), acquired using the SABRE method at a magnetic field of 0.4 μT and room temperature. The spectrum was obtained at natural isotopic abundance of both ^{15}N and ^{77}Se. The experiment was performed in methanol-d$_4$ solution under 5 bar parahydrogen pressure.

oral

Echo phenomena in spin spectroscopy

N.M. Suleimanov[1], **S.A. Moiseev**[1,2]

[1] Zavoisky Physical-Technical Institute, FRC Kazan Scientific Center of RAS, Kazan, Russia
[2] Kazan Quantum Center, Kazan National Research Technical University n.a. A.N. Tupolev, Kazan, Russia

75 years ago, in 1950, Erwin Hahn discovered [1] that the nuclear spins precessing with different phases in non-uniform magnetic fields created by the local environment of these spins, can be brought back into phase by the application of a certain sequence of radio frequency (RF) pulses, leading to the generation of responding signal pulse. He appropriately called this response the *spin echo*.

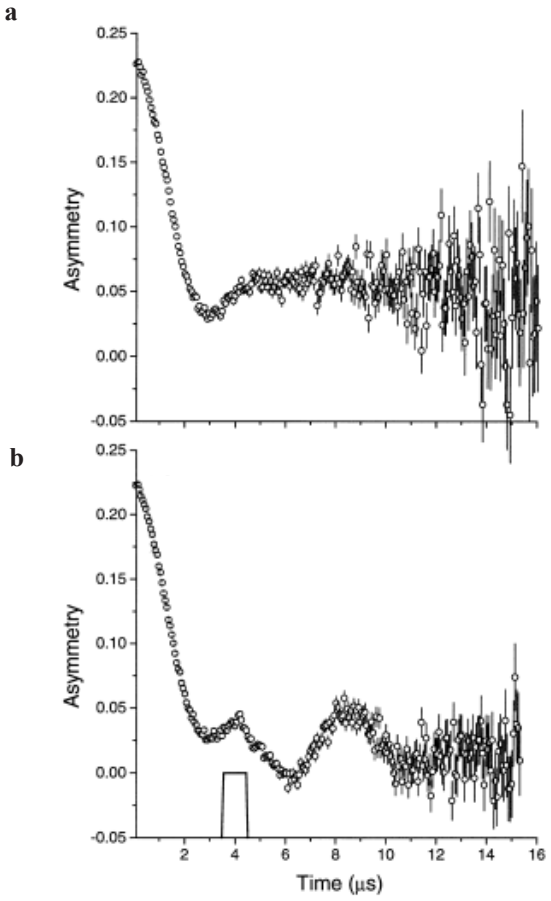

Fig. 1. The time dependence of the muon polarization in boron at room temperature in zero external magnetic field befor (**a**) and after (**b**) applying the signal pulse of non-oscillatory magnetic field with the time delay τ = 3.5 μs.

oral

In this report the development of spin echo phenomena firstly observed on protons and its impact on spin spectroscopy in other ranges of particle physics will be given.

The fundamental parameters of a spin system are the relaxation times, which are determined by interactions within the spin system (spin-spin relaxation) and the interaction of the spin system with the environment in which it is located (spin-lattice relaxation). When we talk *spin echo*, it means a direct method for determining spin correlation, that is crucial for the spin coherence and her stability (resistance) in such areas as magnetic resonance imaging, quantum computing and spintronics. In this report the features of *spin echo* formation in nuclear magnetic spins: protons, muons and neutrons, experimental facilities for its measurements, and their application in studies of the processes of destruction and maintenance of spin coherence will be mainly considered. Along with the classical echo [2], the first observation of the muon spin echo generation in zero external magnetic field [3] and the time-of-flight neutron spin echo [4] will be described. The use of nuclear particles, muons and neutrons, which can be implanted at any materials allows to investigate the quantum dynamics of charged states in semiconductors, superconductors and individual ions. On Figure the first observation of the muon spin echo signal generated in zero external magnetic field after applying the single pulse of non-oscillatory magnetic field is presented.

1. Hahn E.L.: Phys. Rev. **80**, 580 (1950)
2. Kreitzman S.R., Williams D.L., Kaplan N., Kempton J.R., Brewer J.H.: Phys. Rev. Lett. **61**, 2890 (1988)
3. Suleimanov N.M., Moiseev S.A., Clark-Gayther M.A., Cottrell S.P., Cox S.F.J.: Physica B: Condensed Matter 676–680 (2000)
4. Mezei F., ed. (1980). Neutron Spin Echo. Lecture Notes in Physics, Vol. 128. Berlin, Heidelberg, New York: Springer.

poster

Time resolved EPR study of CNI tempo

M.M. Bakirov[1], A.A. Sukhanov[1], H. Zhang[2], J. Zhao[2], Yu.E. Kandrashkin[1]

[1] Zavoisky Physical-Technical Institute, FRC Kazan Scientific Center of RAS, Kazan, Russia
[2] State Key Laboratory of Fine Chemicals, Frontiers Science Center for Smart Materials, School of Chemical Engineering, Dalian 116024, China

Photoexcited molecules with multiple spins are promising components for diverse technologies, including light-emitting and energy-storage devices and elements of quantum information processing. The spin-involved photo-induced proposes in these molecules are of particular interest. Here, we present the results of the study of the CNI Tempo dyads (6-(TEMPO)-1-oxo-1H-phenalene-2,3-dicarbonitrile) by time resolved electron paramagnetic resonance (TREPR) spectroscopy. The molecular structure is shown in Fig. 1. This chromophore-stable radical dyad can form several metastable excited states under photo-illumination.

TREPR investigations of CNI Tempo dyads were conducted at 80 K and at room temperature. The sample was dissolved in the mixture Toluene+2-Methyltetrahydrofuran, (10^{-4} M/L).

The results of the experiments are presented in Fig. 2. The low-temperature signal comes from the ground state of the molecule, i.e. from the radical TEMPO. The decay time of this spin-polarized signal exceeds 10 μs. The room temperature spectrum consists of three well-resolved hyperfine lines, corresponding to the projection of the nuclear spin of the nitrogen. There is also the additional signal centered approximately at 342.5 mT. This resonance field is consistent with the transition of the excited quartet

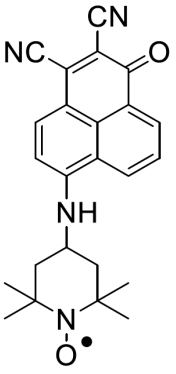

Fig. 1. Structure of 6-(TEMPO)-1-oxo-1H-phenalene-2,3-dicarbonitrile.

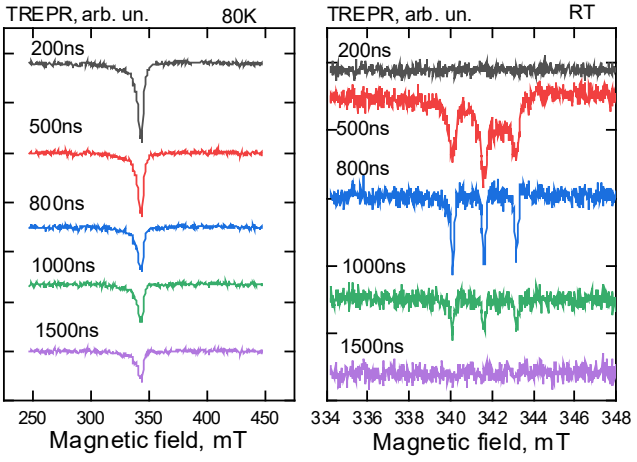

Fig. 2. TREPR of 6-(TEMPO)-1-oxo-1H-phenalene-2,3-dicarbonitrile at 80 K (left) and at room temperature (right).

poster

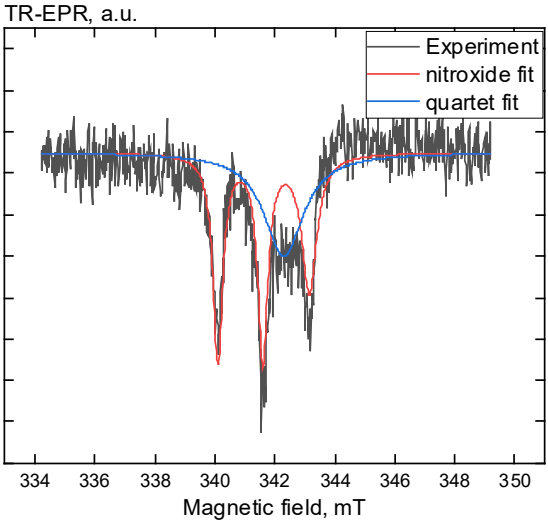

Fig. 3. Structure of 6-(TEMPO)-1-oxo-1H-phenalene-2,3-dicarbonitrile . TR EPR spectra of 6-(TEMPO)-1-oxo-1H-phenalene-2,3-dicarbonitrile for fluid solution at DAF = 500 ns.

state, formed by the interaction between the excited triplet state of the chromophore and the doublet state of the stable radical. Figure 3 shows a comparison of the room temperature spectrum with the expected spectra of the ground and excited quartet states of the dyad. This figure illustrates the formation of the CNI-Tempo quartet state under light excitation.

poster

Antisite defects in cathode materials of lithium (sodium)-ion batteries. EPR study

R.R. Fatykhov

Zavoisky Physical-Technical Institute, FRC Kazan Scientific Center of RAS, Kazan, Russia

In lithium-ion batteries, the electron and ion transport that occurs during the charge/discharge process is associated with the movement of electrons and ions within the crystal lattice structure of cathode materials. In the process of obtaining cathode materials, so-called antisite defects arise, which are associated with the fact that some of the transition element ions fill the alkali metal positions, and the alkali metal is localized in the transition element positions. Such antisite defects create an obstacle to the mobility of the alkali metal ion and electrons, which in turn worsens the characteristics of lithium-ion batteries, such as cyclability, specific capacity. Therefore, understanding the mechanisms of the occurrence of such defects and their evolution in the process of intercalation/deintercalation of sodium or lithium plays an important role in the properties of cathode materials.

Because antisite defects represent the point defects to detect their requires the use of complex structural techniques [1].

The paper will consider the application of EPR methods for studying antisite defects of their modifications arising in cathode materials. In our article, EPR measurements were carried out in non-stoichiometric cobaltite Na_xCoO_2, in the range of sodium concentrations x = 0.53; 0.58; 0.64; 0.75; 0.76; 0.79, and the influence of degradation processes on the properties of the Na_xCoO_2 system was studied [1]. It is known that in stoichiometric $NaCoO_2$, cobalt ions have the valence of Co^{3+} and are in the low-spin configuration t^6_{2g}. This state corresponds to a completely filled 3d orbital. This configuration has zero spin and is characterized by the absence of an EPR signal. An EPR signal was detected in a non-stoichiometric sample of sodium $Na_{0.79}CoO_2$ (Fig. 1). The analysis of the obtained EPR results allows us to say that the observed resonance signal is caused by magnetic Co^{4+} ions, the appearance of which in the studied system is associated with sodium non-stoichiometry and the presence of antisite defects caused by the localization of cobalt ions in sodium positions. In the low temperature region $T < 50$ K, a sharp decrease in the EPR line width, g-factor and integral intensity of the EPR signal is observed. This means that in the specified temperature range, there is a significant decrease in the magnetization of the sample. Sodium non-stoichiometry in Na_xCoO_2 samples leads to the appearance of cobalt ions in the proportion Co^{3+}_x /Co^{4+}_{1-x} depending on the sodium ion content, at which magnetic Co^{4+} ions and non-magnetic Co^{3+} ions are randomly distributed in the crystal lattice. In this case, the dominant interaction between the magnetic cobalt ions will be short-range magnetic correlations between nearby magnetic ions, which typically leads to a spin glass-type magnetic state where the magnetic moments are "frozen" in random orientations.

In another work, $LiCoO_2$ samples with excess Li of 0%, 1.0%, 2.0%, 3.0%, 4.1%, 5.1%, 6.2%, 7.3%, 8.3% and 12.8% were synthesized and the effect of excess Li on its microstructure and electrical properties was studied [2]. According to their model, the defect in $LiCoO_2$ is most likely a pair of antiimpurity Li and an oxygen vacancy. $LiCoO_2$ is a p-type semiconductor, and Co^{4+}, which has unpaired electrons in d-orbitals, apparently

poster

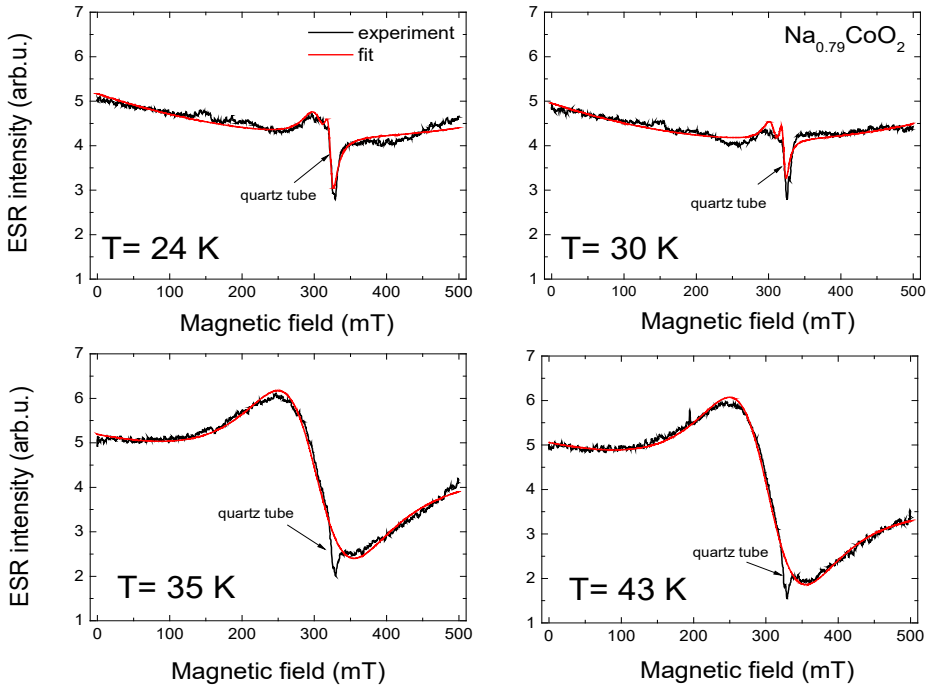

Fig. 1. EPR spectra of $Na_{0.79}CoO_2$ at different temperatures: 24, 30, 35 and 43K. Red lines are the results of spectral approximation using the Lorentzian shape of the absorption line.

contains charge carriers. Therefore, it is believed that the electronic conductivity of LCO depends on the amount of Co^{4+}. The authors of this work carried out EPR measurements on $LiCoO_2$ samples with excess Li of 1.0%, 4.1% and 7.3% to estimate the Co^{4+} content in LCO. The peak appears at $g \approx 2.13$ for all spectra, and the electron conductivity is strongly dependent on Imax. Compared with 1.0% Li excess, the maximum value of the EPR peak with 4.1% Li excess was larger. It was shown that the increase in Co^{4+} was due to the charge compensation by the excess Li. On the other hand, in the case of 7.3% Li excess with antiimpurity Li, the maximum value of the peak was lower than that with 4.1% Li excess without antiimpurity Li. These results indicate that the Li antilayer was compensated not only by Co^{4+} but also by the oxygen vacancy, which resulted in the decrease in the electron conductivity upon the formation of the Li antilayer.

Thus, the EPR method began to be used predominantly to determine and describe the mechanisms of occurrence of antistructural defects that arise during the synthesis process.

1. Quang D.T., Murukanahally K D., Takaaki T.H. et al.: Direct Observation of Antisite Defects in $LiCoPO_4$ Cathode Materials by Annular Dark- and Bright-Field Electron Microscopy. ACS Appl. Mater. Interfaces, **5**, 9926−9932 (2013)
2. Fatukhov R.R., Khantimerov S.M., Suleimanov N.M. et al.: Electron Paramagnetic Resonance in non-stoichiometric cobaltite Na_xCoO_2 and study of the influence of degradation processes on properties of Na_xCoO_2. Phys. Solid State **6**, 894–901 (2024)
3. Shinichi T., Taiki S., Ryusei K. et al.: New insight into designing a thick-sintered cathode for Li-ion batteries: the impact of excess lithium in $LiCoO_2$ on its electrode performance. J. Mater. Chem. A **13**, 2943–2949 (2025)

poster

Inversion of ensemble of frequency-distributed spins using a chirp pulse sequences

I.T. Khairutdinov, R.B. Zaripov

Zavoisky Physical-Technical Institute, Russian Academy of Sciences, Kazan, Russia, semak-olic@mail.ru

In EPR experiment usually one has to cope up with challenge of increased spectral width with limited rf power. A simple hard pulse provides excitation or inversion over a limited range of resonance offsets that cannot be increased due to pulse power constraints. One solution to cope with this problem of bandwidth is use of adiabatic pulses. Adiabatic pulses are known to have increased bandwidths and high tolerance to spatial variations in RF field intensity.

Because of the importance of low-power, broadband heteronuclear decoupling at high magnetic fields, much of the work has focused on the inversion properties of adiabatic full-passage (AFP) pulses. However an AFP pulse is not an ideal rotation pulse or a universal rotation pulse. While it transfers the magnetization from z to $-z$, it doesn't rotate x to $-x$ and y to y. This would be an ideal π rotation pulse around y axis. Therefore, an AFP pulse is not a suitable refocusing element in spin-echo sequences, since the pulse produces an undesirable phase roll across the spectrum as a function of chemical shifts. Ideal broadband π rotation pulses can find application in broadband spin echo sequences.

Propagator (rotation) for an AFP pulse is

$$P = Exp[\pi R_y] Exp[R_z \omega_{eff}(t) dt], \quad (1)$$

where $\omega_{eff} = \sqrt{(\omega_0 - \omega(t))^2 + {\omega_1}^2}$, $\omega(t) = -C + at$, w_0 is spins frequency distribution, w_1 – adiabatic pulse amplitude, $w(t)$ – pulse carrier frequency, a – sweep rate, $R_{x,y,z}$ – π angle rotation matrices around x, y, z axis [5].

Adiabaticity condition is satisfied when

$$\frac{a\omega_1}{{\omega_{eff}}^2} \ll \omega_{eff} \text{ or } a \ll {\omega_1}^2 .$$

Propagator (1) has such a simple form under adiabatic conditions. It is the basis for constructing various chirp π pulse sequences. In this work analysis of signals after the action of pulses with different degrees of adiabaticity was carried out.

The reported study was funded by RSF according to the research project № 22-72-10063.

1. Baum J., Tycko R., Pines A.: Broadband and adiabatic inversion of a two level system by phase modulated pulses, Phys. rev. A. **32**, 3435–3447 (1985)
2. Böhlen J.-M., Rey M., Bodenhausen G.: Refocusing with chirped pulses for broadband excitation without phase dispersion, J. Magn. Reson. **84**, 191–197 (1989)
3. Power J.E., Foroozandeh M., Adams R.W., Nilsson M., Coombes S.R., Phillips A.R., Morris G.A.: Chem. Commun. **52**, 2916–2919 (2016)
4. Hwang T.L., van Zijl P.C.M., Garwood M.: Broadband adiabatic refocusing without phase distortion, J. Magn. Reson. **124**, 250–254 (1997)
5. Sarkar S., Purusottam R.N., Kumar A., Khaneja N.: Chirp pulse sequences for broadband π rotation: J. Magn. Reson. **328**, 107002 (2021)

poster

Spin-Hall effects in epitaxial $Pd_{1-x}Fe_x$/Pt and $Pd_{1-x}Fe_x$/W thin film structures

Zh.Kh. Pulotov[1], A.Kh. Kadikova[1], B.F. Gabbasov[1], I.V. Yanilkin[1], A.I. Gumarov[1], A.G. Kiiamov[1], L.R. Tagirov[1,2], R.V. Yusupov[1]

[1] Kazan Federal University, Kazan, Russia
[2] Zavoisky Physical-Technical Institute, Kazan, Russian Federation

Spin-Hall Effects (SHE) are phenomena arising from the interplay between charge and spin currents in materials with strong spin-orbit coupling. SHE consists in the occurrence of a spin current during the flow of a charge current, which leads to a spatial redistribution of charge carriers (electrons) with oppositely directed spins. The efficiency of spin-to-charge conversion is characterized by the spin-Hall angle. Spin-Hall effects hold promise for superconducting spintronics as a fast mechanism for magnetization switching in a switchable ferromagnetic layer within superconducting spin valves, eliminating the need for an external magnetic field. However, superconducting elements can only function at cryogenic temperatures, making palladium-iron (Pd-Fe) solid solutions one of the most promising materials for ferromagnetic layers in superconducting spin valves. Magnetic ordering in the $Pd_{1-x}Fe_x$ alloy (with iron content x = 1–12 at.%) occurs at temperatures well below room temperature [1, 2]. In heavy normal metals such as Pt and W, which exhibit strong spin-orbit coupling, spatial redistribution of oppositely oriented spins occurs. The focus of this study is the direct and inverse spin-Hall effects in thin-film heterostructures $Pd_{0.90}Fe_{0.10}$/Pt, $Pd_{0.88}Fe_{0.12}$/Pt, and $Pd_{0.94}Fe_{0.06}$/W, as well as their magnetodynamic properties investigated with ferromagnetic resonance (FMR).

Thin-film structures $Pd_{0.90}Fe_{0.10}$/Pt and $Pd_{0.88}Fe_{0.12}$/Pt, along with the ferromagnetic layer $Pd_{0.94}Fe_{0.06}$, were synthesized using molecular beam epitaxy, while the tungsten (W) layer was deposited via electron-beam evaporation. Structural characterization by low-energy electron diffraction (LEED) and X-ray diffraction (XRD) confirmed the epitaxial growth of all heterostructures and the presence of an α-phase tungsten layer. XRD analysis revealed complete intermixing of Pt and Pd-Fe layers in the $Pd_{0.90}Fe_{0.10}$/Pt bilayer heterostructure after ex-situ annealing at 800°C for 1 hour, which was not observed in the as-deposited $Pd_{0.90}Fe_{0.10}$/Pt sample. Additionally, the annealed $Pd_{0.90}Fe_{0.10}$/Pt sample exhibited a weak in-plane uniaxial anisotropy. This is reflected in FMR spectra line broadening and a resonance shift toward higher magnetic fields compared to the as-deposited heteroepitaxial $Pd_{0.90}Fe_{0.10}$/Pt structure. FMR studies of the $Pd_{0.88}Fe_{0.12}$/Pt sample revealed absorption line broadening relative to the resonance line of a single $Pd_{0.88}Fe_{0.12}$ thin film, attributed to losses caused by charge current generation in the normal metal under spin pumping conditions due to the inverse spin-Hall effect.

Orientation-dependent FMR studies of $Pd_{0.90}Fe_{0.10}$ and $Pd_{0.88}Fe_{0.12}$ samples confirmed a tendency of cubic magnetocrystalline anisotropy constants decrease, consistent with our previous findings for Pd-Fe alloys with iron concentrations up to 8% [1]. The $Pd_{0.88}Fe_{0.12}$ thin film exhibits weak uniaxial magnetocrystalline anisotropy (K_u = –6.3×10³ erg/cm³), typical for thin ferromagnetic films, with no in-plane anisotropy. In contrast, the $Pd_{0.90}Fe_{0.10}$ sample demonstrates uniaxial anisotropy (K_u = –6.5×10³ erg/cm³) and

poster

small in-plane anisotropy constants, with cubic (K_1 = 1.7×10³ erg/cm³) and tetragonal (K_2 = −1.4×10⁴ erg/cm³) contributions.

In heavy normal metals Pt and W with strong spin-orbit coupling, spatial spin separation occurs. Experiments were conducted to observe SHE and inverse SHE (ISHE) in $Pd_{0.88}Fe_{0.12}$/Pt and $Pd_{0.94}Fe_{0.06}$/W heteroepitaxial structures. SHE was detected via FMR spectra observation when an alternating electric current passed through the sample instead of modulating the magnetic field. Under these conditions, the direct SHE modulates the magnetization of the ferromagnetic layer, leading to a resonance line shift. In the $Pd_{0.88}Fe_{0.12}$/Pt heterostructure, an effective modulation field of 50 mG was estimated at an AC current amplitude of 5 mA, while in $Pd_{0.94}Fe_{0.06}$/W, the corresponding values were 40 mG at 2.5 mA. However, charge current passage through the heterostructure also induces an alternating magnetic field due to electromagnetic induction (Oersted field). To confirm the SHE contribution, the spatial distribution of the current-induced magnetic field in the $Pd_{0.88}Fe_{0.12}$ and $Pd_{0.94}Fe_{0.06}$ layers was calculated. Comparison with the effective modulation field demonstrated that at least 70% of the effective modulation field is due to the SHE.

The inverse spin-Hall effect manifests itself in a voltage generated by spin-dependent electron scattering under spin pumping. In experiments with a sample of the heteroepitaxial $Pd_{0.88}Fe_{0.12}$/Pt structure, a voltage signal of ~1 μV was detected below the Curie temperature of the ferromagnetic layer, between 20 and 150 K [4]. A weak dependence of the voltage amplitude on the sample temperature is observed. This, in our opinion, is due, on the one hand, to a decrease in magnetization with increasing temperature, thus reducing the spin current under spin pumping conditions, and on the other hand, the sample is a metal, whose resistance increases with increasing temperature. Thus, the two effects cancel each other in a given temperature range. The Hall angle for platinum was calculated, which at a temperature of 20 K was: α_{SHE} = (0.35±0.02)%. No ISHE signal was detected in $Pd_{0.94}Fe_{0.06}$/W due to its low magnetization, resulting in insufficient spin current under spin pumping.

1. Yanilkin I.V., Yusupov R.V. et al.: Epitaxial thin-film $Pd_{1-x}Fe_x$ alloy: a tunable ferromagnet for superconducting spintronics. Science China Materials **63**, 1–10 (2020)
2. Pulotov Zh.Kh., Yusupov R.V. et al.: Magnetoresonant properties and spin-Hall effects in epitaxial $Pd_{1-x}Fe_x$ and $Pd_{1-x}Fe_x$/Pt thin film structures. Magnetic Resonance – Current State and Future Perspective (EPR-80). Book of abstracts, p. 142–143 (2024)
3. Sinova J. et al.: Spin Hall effect. Reviews of Modern Physics **87**, 1213–1260 (2015)
4. Pulotov Zh.Kh., Yusupov R.V.: Spin Hall effects in the heteroepitaxial structure Pd0.88Fe0.12/Pt. Competition for the best scientific work of KFU students, 89–92 (2024) (In Russian)

poster

EPR experiments in $LiDyF_4$ at subterahertz frequencies

A.D. Shishkin[1], G.S. Shakurov[1], I.V. Romanova[2], V.V. Semashko[1], O.A.Morozov[1], S.L. Korableva[2]

[1] Zavoisky Physical-Technical Institute, FRC Kazan Scientific Center of RAS, Kazan, Russia
[2] Kazan Federal University, Kazan, Russia

Recently, much attention has been paid to temperature sensors based on measurements of the luminescence spectra of rare earth ions in nanocrystals. The high sensitivity of such sensors is proposed to be used to create terahertz range detectors and visualizers. In this case, high luminescent characteristics should be combined with high absorption capacity in the terahertz range. Promising compounds for these purposes are high-level doped rare earth fluoride crystals. We have studied a crystal $LiDyF_4$ in which the room temperature strong absorption of terahertz waves by the crystalline matrix is supplemented by resonant absorption between the Stark components of the ground-state multiplet $^6H_{15/2}$.

Since this crystal has not been studied in the terahertz range before, we performed spectroscopic studies in the range of 50–600 GHz in magnetic fields up to 0.9 T at $T = 4.2$ K. Previously, we studied the crystal $LiYF_4$:Dy (0.05%) and found that the energy interval between the ground and first excited doublet is 14.4 cm^{-1} [1]. When registering resonant transitions between doublets, *g*-factors and polarization dependences of EPR spectra in a magnetic field were measured. The results obtained for the concentrated crystal ($LiDyF_4$) differed sharply from the diluted one ($LiYF_4$:Dy). By studying the angular dependences of the EPR spectra, we found that when the crystal rotated along the axis of symmetry, when the magnetic field was perpendicular, the interdoublet transitions changed their intensity depending on the mutual orientation of B and a, and the lines of the intradoublet transition changed their position in the magnetic field. Stark splitting decreased to ~10 cm^{-1}, but at the same time the effective g-factors observed for the intra and interdoublet transition lines increased significantly. This circumstance is favorable for creating detectors whose sensitivity is controlled by a magnetic field. Indeed, a large *g*-factor allows changing the crystal's absorption capacity in a wide frequency range using small magnetic fields. However, the physics of such sharp changes in spectroscopic characteristics is not yet clear. The report discusses possible causes of the observed phenomena.

1. Shakurov G.S., Malkin B.Z., Vanyunin M.V., Korableva S.L.: Phys. of the Solid St. **50**, 1619–1624 (2008)

poster

Influence of magnetic correlations on scattering of current carriers in iron arsenides

D.E. Zhelezniakova, I.I. Gimazov, Y.I. Talanov

Zavoisky Physical-Technical Institute, FRC Kazan Scientific Center of RAS, Kazan, Russia

This report presents the results of transport measurements of $Ba(Fe_{1-x}Co_x)_2As_2$ and $Ca(Fe_{1-x}Co_x)_2As_2$ crystals with varying concentrations of cobalt impurities. The data were obtained through transport study with direct current method (Fig.1) and high frequency measurements (microwave absorption at 9.5 GHz). The contributions of different mechanisms to current carriers scattering, including phonon, electron-electron interaction, spin fluctuation, and others, were analyzed. The influence of nematic fluctuations (anisotropic scattering due to magnetic fluctuations) on temperature dependence of resistivity was estimated.

Figure 1 shows the temperature dependence of the resistivity of $Ba(Fe_{1-x}Co_x)_2As_2$ crystals with different values of x. These dependencies reflect all phase transitions occurring in the crystal with decreasing temperature: structural transition from tetragonal to orthorhombic crystal lattice, antiferromagnetic ordering in the form of spin density waves, and superconducting transition.

According to theoretical calculations [1], at high temperatures resistivity has linear dependence due to two-dimensional scattering of current carriers on spin fluctuations. With decreasing temperature, fluctuations become three-dimensional, and the dependence becomes of form $\rho(T) \propto T^{3/2}$. This change in dimensionality is due to increase in correlation length of magnetic interactions and formation of exchange coupling between FeAs conducting planes.

1. Fernandes R.M., Abrahams E., Schmalian J.: Phys. Rev. Lett. **107**, 217002 (2011)

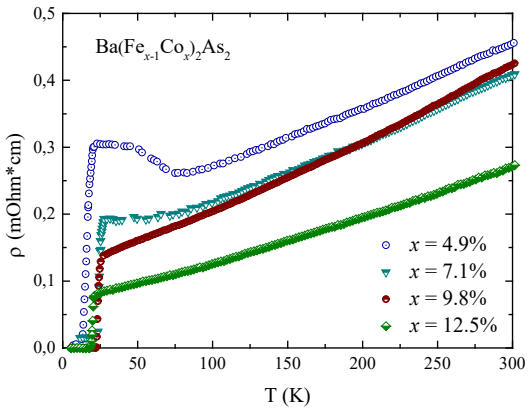

Fig. 1. Temperature dependences of the resistivity of $Ba(Fe_{1-x}Co_x)_2As_2$ crystals with different values of x.

SECTION 3

LOW-DIMENSIONAL SYSTEMS, NANO-SYSTEMS AND MOLECULAR MAGNETS

oral

Synthesis, self-assembly and magnetic properties study of rare-earth ions trifluoride

E.M. Alakshin, E.I. Boltenkova, A.M. Garaeva, B.M. Mukhamadullin, A.V. Bogaychuk

Institute of Physics, Kazan Federal University, Kazan, Russia
e-mail: alakshin@gmail.com

Nanoscale materials are of interest not only from a scientific point of view, opening up new insights into the study of physics, chemistry, biology, and fundamental processes, but also from the point of view of practical application.

ReF_3 nanoparticles activated with rare earth ions have proven to be highly sensitive temperature sensors, scintillators, and MRI and CT contrast agents, which is increasingly being used in fundamental biology to study cellular processes. The process of targeted delivery of such nanoparticles is associated with their agglomeration by organic functional groups (antibodies, photosensitizers, other molecular complexes) and the creation of organic-inorganic complexes. The effectiveness of the action and stability of existing complexes in physiological fluids is far from perfect. Therefore, the development of new approaches, the selection of relevant materials (for example, organic coatings such as PEG, PEI, chlorine, etc.), as well as the modeling of certain processes (self-assembly and chemical reaction kinetics), is an urgent task. One of the main goals of this work is to study the kinetics of a chemical reaction and the formation of nanoparticles in real time using nuclear magnetic resonance methods, with a further attempt to build a physical model for the synthesis of rare earth fluorides.

This work introduces real-time ^{1}H NMR monitoring of fluoride nanoparticle formation directly within a capillary system, in different magnetic field. The selection of analytical methods for in-process monitoring (TEM, FRET, DLS, XRD, NMR, UV spectroscopy) should account for their limitations, tailored to specific goals, material properties, and process dynamics – especially critical for magnetic nanoparticles susceptible to agglomeration and self-assembly.

Focusing on DyF_3 nanoparticles, we examined how hydrothermal synthesis (classical autoclave vs. microwave irradiation) influences their r_2 transverse relaxivity in colloidal solutions. T_2 relaxation times were measured via ^{1}H NMR for various nanoparticle concentrations at 0.6, 3.65, and 9.4 T. Critically, autoclave processing yielded the maximum relaxation rate enhancement, outperforming both microwave-treated and untreated samples. From this data, we determined the field-dependent optimal sizes for DyF_3 nanoparticles to function effectively as MRI contrast agents.

This work was financially supported by the Russian Science Foundation (Project No. 23-72-10039).

oral

Complementarity of EPR and neutron scattering techniques in the study of long-period chiral magnets

E.V. Altynbaev[1,2]

[1] Saint Petersburg State University, 199034, Russia, St. Petersburg
[2] NRC "Kurchatov InstituteX – PNPI, 188300, Gatchina, Russia
e-mail: e.altynbaev@spbu.ru

The complementarity of electron paramagnetic resonance (EPR) and neutron scattering techniques in the study of long-period chiral magnets is presented. EPR provides local information about spin dynamics and magnetic anisotropy, while neutron scattering reveals long-range magnetic order and collective excitations. Their combination is particularly powerful for studying complex chiral structures like skyrmions and helical spirals.

We demonstrate how this synergy allows to characterize the Dzyaloshinskii-Moriya interaction and its role in forming topological spin textures. Example of experimental results on model chiral magnets for local (EPR) and global (neutron) probes is presented in Fig. 1, revealing complete picture of magnetic behavior. This approach is crucial for developing new spintronic materials with tailored properties and providing complete information on magnetic structures of studied objects.

1. Demishev S.V. et al.: JETP Lett **115**, 11, 717–723 (2022)
2. Grigoriev S.V. et al.: Phys. Rev. B, **74**, 214414 (2006)

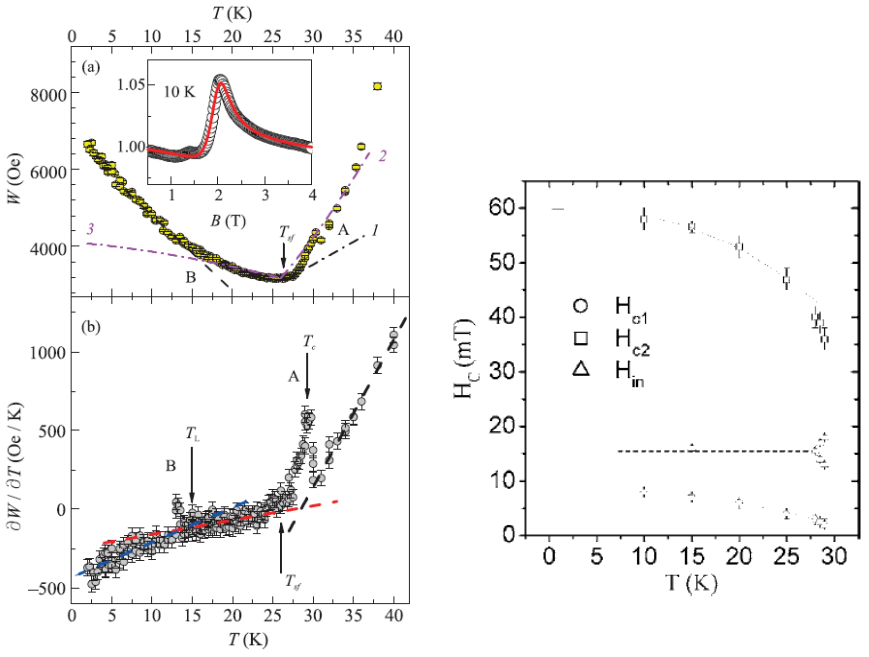

Fig. 1. Complementary information from EPR [1] (left, local scales) and neutron scattering (right [2], long-range order) in chiral magnet MnSi.

oral

Ethanol inside graphene oxide membranes – spin probe technique investigation

D.A. Astvatsaturov[1,2], K.E. Gurianov[2], N.A. Chumakova[1,2]

[1] N.N. Semenov Federal Research Center for Chemical Physics, Moscow, Russia
[2] Lomonosov Moscow State University, Moscow, Russia

Graphene oxide membranes (GOMs) are partially ordered layered materials with a complex inner structure. Membranes attract a lot of attention because they demonstrate selective permeability for gases and liquids [1]. Materials are also capable of separating ions [2], desalinating water [3], and are promising species for use as drug delivery platforms [4]. By now, it has been established that a dry membrane is impermeable to gases and a number of polar liquids, but is highly permeable to water [1]. It has been shown that water penetrates through the membrane with a rate of 5 orders of magnitude higher than ethanol [1]. At present, there is no evident answer to the question of what is the mechanism of a liquid transport through a graphene oxide membrane, and what is the phase state of an intercalated substance in the inter-plane space of GO membranes.

The present work is devoted to the study of ethanol sorption by graphene oxide membranes and the determination of the mobility of the intercalated substance in the inter-plane space using the spin probe technique. Earlier, we showed that polar liquids can coexist inside powder graphite oxide as three fractions with different molecular mobility (microviscosity). Ethanol demonstrates a significantly greater contribution of a highly mobile liquid-like fraction compared to water and acetonitrile [5].

The experiments were carried out using the membrane made of graphene oxide synthesized by Hummers' method. Ethanol was inserted into the membrane as blowing the membrane from both sides under conditions of the controlled ethanol vapor content in the gas flow (*in situ*) and in the mode of the ethanol penetration through the membrane (*in operando*). The mobile liquid-like fraction is formed inside the membrane *in situ,* but was not formed *in operando*. Thus, the molecular mechanism of the movement of alcohol molecules through the membrane is not connected with the formation of a condensed liquid phase.

This study was carried out as part of the state assignment on the topic "Interdisciplinary approaches to the creation and study of micro-/nanostructured systems" (registration no. 125012200595-8).

1. Nair R.R., Wu H.A., Jayaram P.N., Grigorieva I.V., Geim A.K.: Science, **335**, 442–444 (2012)
2. Abraham J., Vasu K.S., Williams C.D., Gopinadhan K., Su Y., Cherian C.T., Dix J., Prestat E., Haigh S.J., Grigorieva I.V., Carbone P., Geim A.K., Nair R.R.: Nat. Nanotechnol. **12**, 546–550 (2017)
3. Ge R., Huo T., Gao Z., Li J., Zhan X.: Membranes (Basel) **13**, 1–27 (2023)
4. Oliveira A.M.L., Machado M., Silva G.A., Bitoque D.B., Ferreira J.T., Pinto L.A., Ferreira Q.: Nanomaterials **12**, 1–20 (2022)
5. Astvatsaturov D.A., Yankova T.S., Kokorin A.I., Melnikov M.Y., Chumakova N.A.: J. Phys. Chem. C **128**, 17940–17952 (2024)

oral

Full 180° magnetization reversal of planar Ni microparticles without magnetic field

A. A. Bukharaev[1,2], D.A. Bizyaev[1], N.I. Nurgazizov[1], A.P. Chuklanov[1]

[1] Zavoisky Physical-Technical Institute, FRC Kazan Scientific Center of RAS, Kazan, Russia
[2] Academy of Sciences of the Republic of Tatarstan, Kazan, 420111 Russia

One of the methods for recording information on magnetic media is based on changing the magnetization direction of a single magnetic particle. It is convenient for data processing if under standard conditions such a particle has 2 possible directions of magnetization differing by 180°. Then, one of these states can be assigned as 1, the other as 0. The simplest way to achieve such magnetization behavior is to elongate the particles along a specific, pre-selected direction and perform the recording by magnetic field [1]. For stable information storage over time, a high coercive force is required, and therefore rewriting requires comparatively large energy. This energy can be reduced by using the magnetoelastic effect that occurs during uniaxial deformation [1]. The effect can be created by using as a substrate: (1) single crystals with an anisotropic coefficient of thermal expansion [1, 2]; (2) ferroelectric crystals [1, 3]. When the temperature changes, the substrate of the first type expands or contracts unevenly along its axes, which leads to anisotropic deformation in the particle. As a result, uniaxial magnetic anisotropy is induced, and if it is not collinear with the magnetization, the latter can change direction. A similar case occurs on substrates of 2nd type when an electric potential is applied. However, due to symmetry reasons, the magnetization direction cannot be rotated by more than 90° using this approach. A 180° rotation can be achieved either by using an additional external magnetic field or by 2 successive rotations at angles close to 90°.

In the latter case, it is necessary to use particles with more than two stable magnetization states, between which successive switching is performed. In [4], using a four-petal planar Ni particle on a ferroelectric substrate, the possibility of rotating the magnetization direction by 180° through two successive rotations by 90° was demonstrated.

In this work, the rotation of the magnetization direction by 180° in planar Ni particles solely by the thermally induced magnetoelastic effect was investigated. A single-crystal lithium triborate (LiB_3O_5, LBO) with different thermal expansion coefficients ($\alpha_x = 10.8\times10^{-5}$ °C^{-1}, $\alpha_z = 3.4\times10^{-5}$ °C^{-1}) was used as the substrate. Ni polycrystalline square particles with shape anisotropy in the form of concave sides and rounded corners were formed on the substrate (Fig. 1a). The concavity of the sides (the ratio of the particle size in the narrowest part to its lateral size, i.e., the length of the side of the square into which it could be inscribed) was 32%. The particles had a polycrystalline structure, a thermal expansion coefficient $\alpha_{Ni} = 1.3\times10^{-5}$ °C^{-1}, and a Young's modulus of 310 GPa, so for every degree of increase or decrease temperature, uniaxial tension or compression equivalent to 15.5 MPa was induced. The lateral size of the particle was varied from 0.4 to 5 μm with a step of 0.1 μm, the height was 30 nm. The angle between the deformation axis and the nearest particle easy magnetization axis (EA) was fixed at 15° (Fig. 1a). The particle sizes were sought at which serial tension and compression of 310 MPa (corresponding to heating and cooling by 20 °C, respectively)

oral

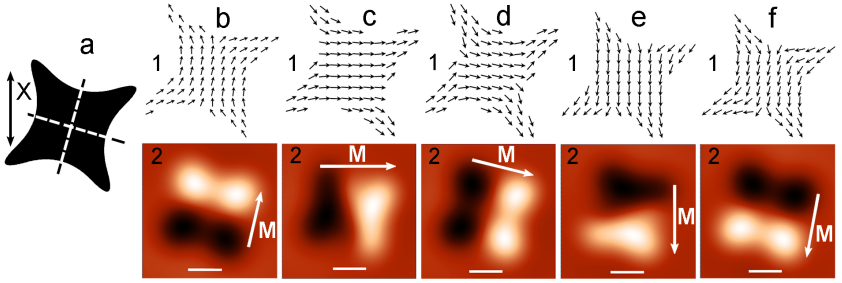

Fig. 1. a particle used for modeling, dashed lines denotes the EA. Sequential changes in the magnetic structure of a Ni particle on LBO with changing sample temperature: initial state at 30 °C (**b**), after heating to 50 °C (**c**), after cooling to 30 °C (d), after cooling to 10 °C (**e**), after heating to 30 °C (**f**). 1 – magnetization distributions modeled in OOMMF, 2 – corresponding virtual MFM images. *X* is the axis of deformation. The scale bar is 0.5 μm. **M** denotes the total magnetization vector.

lead to magnetization reversal. The OOMMF software package was used for simulation [5]. It has the following stages. For each particle size, the equilibrium distribution of magnetization in the absence of deformation (K_1 = 0 J/m^3) was simulated (Fig. 1b). This magnetization distribution was taken as the initial one; the average magnetization direction (*M*) with respect to the *X* axis was 15°, and it coincided with the EA. Then, the equilibrium distribution of magnetization under uniaxial tension of 310 MPa (K_1 = 16 kJ/m^3) was calculated (Fig. 1c), which corresponded to heating by 20 °C. The results showed that vector M rotated by 75°, and the angle between M and the *X* axis became 90°. Then, cooling the system to the initial temperature (K_1 = 0) was simulated. In this case, M rotated by another 15°, and thus, the angle between *M* and the *X* axis became 105° (Fig. 1d). Next, particle compression due to cooling by 20 °C was simulated (K_1 = –16 kJ/m^3), which led to *M* rotating by another 75° (Fig. 1e). Successive heating of the sample to the initial temperature (K_1 = 0) led to *M* rotating by another 15°, i.e., the direction of the particle magnetization became opposite to the initial one. For the studied particles, rotation was observed in the range of lateral sizes from 0.33 to 0.94 μm.

Thus, the possibility of reversal the direction of quasi-uniform magnetization of a particle solely due to the thermally induced magnetoelastic effect was demonstrated. The reversal process is feasible in planar particles of a certain size range, with shape anisotropy and EA rotated relative to the extension/compression axis. Four successive stages are required: heating above the initial temperature, cooling to the initial temperature, further cooling below the initial temperature, and heating back to the initial temperature. Each of these stages leads to a rotation of the average magnetization of the particle by an angle less than 90° in the same direction. The result of this process is a stable distribution of magnetic moments, rotated by 180° relative to the original.

1. Bukharaev A.A., Zvezdin A. K., Pyatakov A.P., Fetisov K.: Phys. Usp. **61**, 1175 (2018)
2. Bizyaev D.A. et al.: PSS - RRL, 2000256 (2020)
3. Morosov A.I.: Physics of the Solid State **56**, 865 (2014)
4. Wang Z. et al.: ACSNano **8**, 7793 (2014)
5. Donahue M.J., Porter D.G., OOMMF User's Guide, Version 1.0 (Natl. Inst. Standards Technol., Gaithersburg, MD, 1999)

oral

Magnetic properties of Ca_2CoNbO_6

D.I. Fazlizhanova[1], R.G. Batulin[2], Y.A. Deeva[3], T.I. Chupakhina[3], I.V. Yatsyk[1], R.M. Eremina[1]

[1] Zavoisky Physical-Technical Institute, FRC Kazan Scientific Center of RAS, Kazan, Russia
[2] Kazan (Volga Region) Federal University, Kazan, Russia
[3] Institute of Solid State Chemistry of the Russian Academy of Sciences (UB), Ekaterinburg, Russia

In the last decade, there has been an active search for stable thermoelectrics operating at high temperatures (in the region near 600 K). As it has been shown, the properties of thermoelectrics are inuenced not only by the processes of diffusion of charge carriers and phonons, but also by the spin components. The great interest in double perovskites has been attracted by the possibility of their use as thermoelectrics. The Seebeck coefficient S = 4–6.5 V/K was measured for Ba_2CoNbO_6 double perovskites at various temperatures [1].

The double perovskite Ca_2CoNbO_6 was synthesized using the pyrolysis method of nitrate-organic mixtures of the corresponding components with a diffraction pattern indexed based on the space group $P12_1/c1$. Using DFT calculations for two different distributions of Co/Nb we found that Co is in the high-spin state in the double perovskite Ca_2CoNbO_6. The experimental magnetic moment is calculated as $\mu_{eff} = 5.52\mu_B$. For the Co^{3+} in the high-spin state with a g-factor of 2.1, the theoretical magnetic moment is 5.14 μ_B. The temperature dependence of conductivity was described by the model of small polaron hoping with the band gap is 0.25 eV.

ESR measurements were performed using a Bruker ELEXSYS E500-CW spectrometer equipped with continuous-ow He and N2 cryostats.

Measurements were performed in the X-band with a frequency of 9.4 GHz, a temperature range of 5–340 K, and a magnetic field range of 0–1.4 T. The view of ESR spectra is shown in Fig. 1. Two ESR lines were observed below 110K with g-factors are approximately 2.3 and 4.33.

1. Popov D.V., Batulin R.G., Cherosov M.A. et al.: Journal of Alloys and Compounds, **1009**, 176900 (2024).

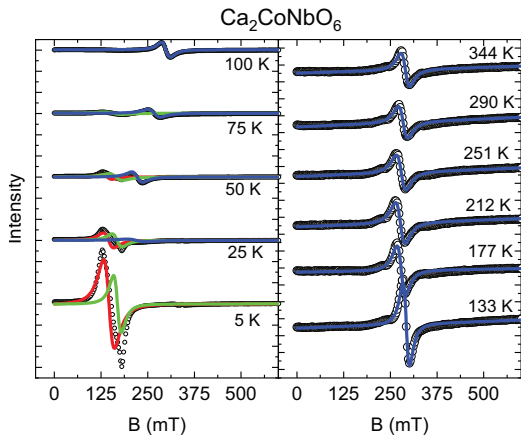

Fig. 1. Temperature dependencies of ESR spectra in Ca_2CoNbO_6.

oral

Ab initio magnetic properties simulation of nanoparticles based on ReF_3 and $LiReF_4$ (Re = Tb, Dy, Ho)

A.I. Faskhutdinova, I.V. Romanova, O.V. Nedopekin

Institute of Physics, Kazan Federal University, Kazan, Russian Federation
e-mail: vukhuholl@gmail.com

Owing to their diverse magnetic properties, rare earth-lithium tetrafluoride and rare earth trifluorides ReF_3 and $LiReF_4$, (Re = Tb, Dy, Ho) have attracted considerable research interest in recent years. Nanoparticles of these compounds demonstrate tunable ionic conductivity along with functional magnetic properties, which opens significant application prospects in biotechnology and medicine [1]. A major limitation stems from their inherent fluoride toxicity, necessitating protective polymer coatings. The formation of such coatings depends critically on the spatial distribution of magnetic moments at particle surfaces. Experimental studies reveal heterogeneous moment distributions that adversely affect coating quality. Consequently, investigating the size-dependent magnetic properties of nanoparticles has emerged as a pressing research objective. Existing data on this issue remain insufficient and inconclusive, while experimental characterization is impeded by the technical challenges of magnetic calculations. Computational modeling approaches offer a viable alternative.

In this work, using the VASP package and density functional theory, calculations of the magnetic moments of $LiTbF_4$, $LiDyF_4$, $LiHoF_4$ and TbF_3, DyF_3, HoF_3 were performed for nanoclusters sizes 0.7–1.0 nm and slabs thickness 2–6.2 nm. An inhomogeneous distribution of magnetic moments and different magnetic arrangements were observed and analyzed depending on the nanocluster's size and slab thickness.

1. González-Mancebo D. et al: Particle & Particle Systems Characterization **34** (2001)

oral

Magnetic properties of microsized and nanosized PrF_3 powders

A.M. Garaeva, A.S. Makarchenko, G.A. Dolgorukov, I.V. Romanova, B.M. Mukhamadullin, E.I. Boltenkova, E.M. Alakshin

Kazan Federal University, Kazan, Russia

The PrF_3 is a dielectric Van Vleck paramagnet. The Pr^{3+} ion has the electron structure $4f^{12}$. Due to the low symmetry of the PrF_3 crystal field, the ground multiplet $^3H_4$ is split into 9 singlets. The nucleus of the rare earth element has a non-zero nuclear spin 5/2 and this element compounds have nuclear magnetism. PrF_3 can be used for the dynamic polarization of ^{3}He nuclear spins [1]. The polarized system of nuclear spins of gaseous ^{3}He is widely used in medicine for NMR tomography of the lungs [2, 3].

Micro-sized PrF_3 powder particles were obtained by crushing a single crystal and then sifting through a 45 μm sieve. Nanoparticles of PrF_3 with a size of 56×34 nm were obtained by hydrothermal synthesis using a nitrate reaction [4]. Control of the chemical composition and confirmation of crystallinity was carried out by X-ray phase analysis on a Bruker D8 Advance Cu Kα diffractometer, λ = 1.5418 Å. Based on photographs taken by transmission electron microscopy on a HitachiHT Exalens microscope, the shape and characteristic size of particles in the resulting powders were determined.

In this work, magnetizations of micro- and nano-sized PrF_3 powders were investigated. Magnetic field (0–9 T) and temperature (5–300 K) dependences of magnetization were measured using the multifunctional system for measuring physical properties with a superconducting magnet PPMS-9. A change in the magnetization of PrF_3 nanopowder is observed compared to a microsized sample. An explanation for this phenomenon is proposed.

Also, ^{3}He NMR in contact with nanosized PrF_3 particles were studied. The measurements were carried out on the home-built NMR spectrometry [5]. The effect of a powder of magnetic PrF_3 particles on the rate of longitudinal and transverse relaxation of helium-3 nuclei in the adsorbed layer, gas and liquid, and with adsorbed helium-4 was studied. The measurements were carried out at a temperature of 1.5 K in fields up to 800 mT. The mechanisms of magnetic nuclear relaxation are considered. A model that describing the nuclear magnetic relaxation of helium-3 in contact with PrF_3 nanoparticles is proposed.

This work was financially supported by the Russian Science Foundation (Project No. 23-72-10039).

1. Tagirov M.S.: JETP Letters **61**, 652 (1995)
2. Moller H.E., Chen X.J., Chawla M.S. et al.: J. Magn. Res. **135**, 133 (1998)
3. Nacher P.J.: Poincaré Seminar **159** (2007)
4. Alakshin E.M., Gabidullin B.M., Gubaidullin A.T. et al.: arXiv preprint arXiv:1104.0208 (2011)
5. Dolgorukov G.A., Kuzmin V.V., Bogaychuk A.V. et al.: Magn. Reson. Solids **20**, 18206 (2018)

oral

Magnetic ordering in the decorated square kagomé lattice magnets

V.N. Glazkov[1,*], Ya.V. Rebrov[1,2], M.M. Markina[3], A.F. Murtazoev[3], P.S. Berdonosov[3], A.N. Vasiliev[3]

[1] P. Kapitza Institute for Physical Problems, Kosygin str. 2, 119334 Moscow, Russia
[2] Faculty of Physics, HSE University, Myasnitskaya str. 20, 101000 Moscow, Russia
[3] Lomonosov Moscow State University, Leninskie gory 1, 119991, Moscow, Russia
*glazkov@kapitza.ras.ru

Nabokoite family compounds $ACu_7(TeO_4)(SO_4)_5B$ (A=Na, K, Cs, Rb; B=Cl, Br) are the example of decorated square kagomé lattice (SKL): six copper ions form 2D SKL layers, while seventh ion takes inter-layer position [1]. Both intra-layer and inter-layer exchange bonds are highly frustrated. As a result, all compounds of this family orders around 3–5 K, while Curie-Weiss temperature is about 150–200 K.

We have performed accurate absolute calibration of the ESR absorption in the paramagnetic phase (10 K < T < 200 K) which revealed that broad ($\Delta B \approx 2$ T) paramagnetic absorption corresponds to approximately 1/7 of all copper ions present. This observation can be interpreted as ESR response of the decorating inter-layer copper ions.

Transformation of this paramagnetic absorption into antiferromagnetic resonance below the Neél temperature possibly reveals partial ordering of inter-layer copper ions, while SKL layers remain in the disordered spin-liquid state.

Antiferromagnetic resonance frequency-field dependences and temperature dependences of spin-wave gaps below the Neél temperature are qualitatively different for nabokoite compounds with light (Na, K) and heavy (Cs, Rb) alkali ions. Compounds with light alkali ions demonstrate a two-step magnetic ordering into a non-collinear phase, while their heavy-alkali-ions counterparts demonstrate convenient easy-axis collinear ordering. Presumably, this qualitative difference in the choice of the ordering pattern is a result of partial lifting of the exchange bonds frustration due to minute structure modification at (anti)segnetorelectric transition, observed earlier in light-alkali-ions compounds only [2].

The work was supported by RSF grant 22-12-00259-П.

1. Murtazoev A.F., Lyssenko K.A., Markina M.M. et al.: ChemPhysChem **24**, e202300111 (2023); Markina M.M., Berdonosov P.S., Vasilchikova T.M. et al.: Mat. Chem. Phys. **319**, 129348 (2024)
2. Rebrov Ya.V., Glazkov V.N., Murtazoev A.F. et al.: JMMM **592**, 171786 (2024)

oral

Spin dynamics of disordered structures and one-dimensional chains

E.I. Kovycheva, K.B. Tsiberkin, V.K. Henner

Perm State University, Perm, Russia

Different modifications of carbon, such as fullerene arrays, have electrical, optical and mechanical properties that are valuable for practical applications. Also, there are additional possibilities to modify their parameters and stabilize various configurations [1]. In particular, they are potentially applicable for creating electrodes with a high specific surface area in energy storage devices (capacitors, batteries). The properties of these materials can be controlled by introducing metal cores into the shells or by depositing magnetic ions on the carbon surface. In addition, the described materials can find applications in the development of new systems for storing, processing and transmitting information using spin magnetic moments [2].

The numerical method used in our previous works is modified to perform calculations in a rotating coordinate system and supplemented by the construction of Fourier spectra of the obtained magnetization signals. Calculations were performed for ordered (chain, square lattice) and disordered (magnetic particles randomly located on the surface of a nanosphere and nanotube) structures.

Spectra of an ordered rectangular structure of 9 spins in a rotating coordinate system (RCS) at different parameters of dipole interaction (pd):

We can note that in an ordered planar structure in a rotating magnetic field, an increase in the dipole interaction parameter leads to the division of the main peak into several peaks (Fig. 1).

Now let us consider the spectra of disordered spherical and cylindrical structures of 9 spins in a rotating coordinate system (Fig. 2):

At these graphs of the spectra of spherical and cylindrical structures (Fig. 2) additional peaks are observed close to zero. It is noticeable that these peaks appear only

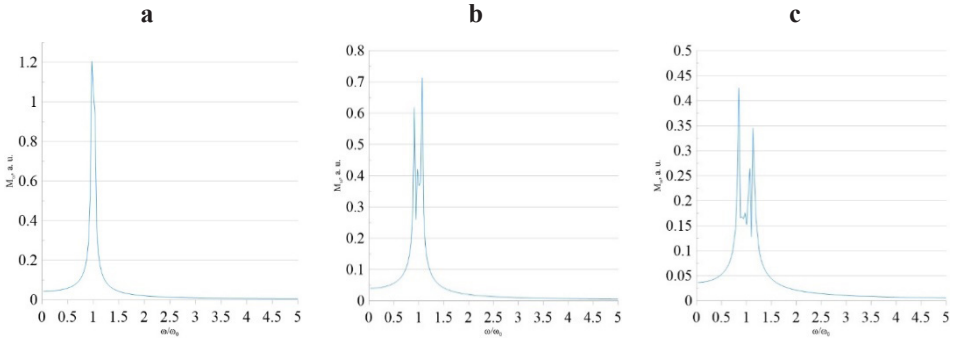

Fig. 1. Spectrum of an ordered rectangular lattice of 9 spins in the RCS, **a** pd = 0.01, **b** pd = 0.025, **c** pd = 0.05.

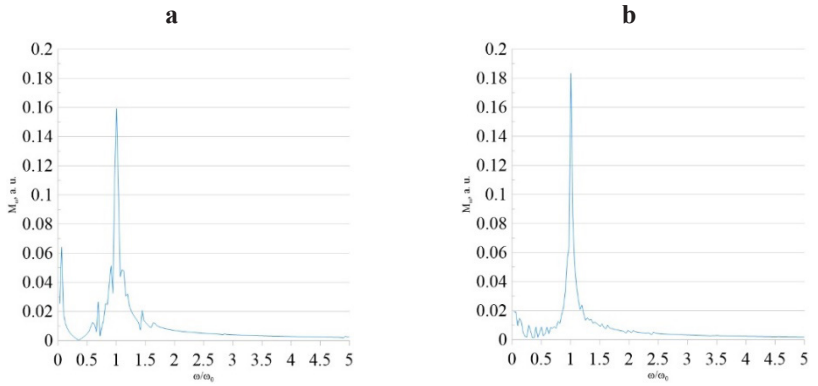

Fig. 2. Spectrum of disordered random structure in the RCS for 9 spins, number of realizations 20, pd = 0.025. **a** spherical structure; **b** cylindrical structure.

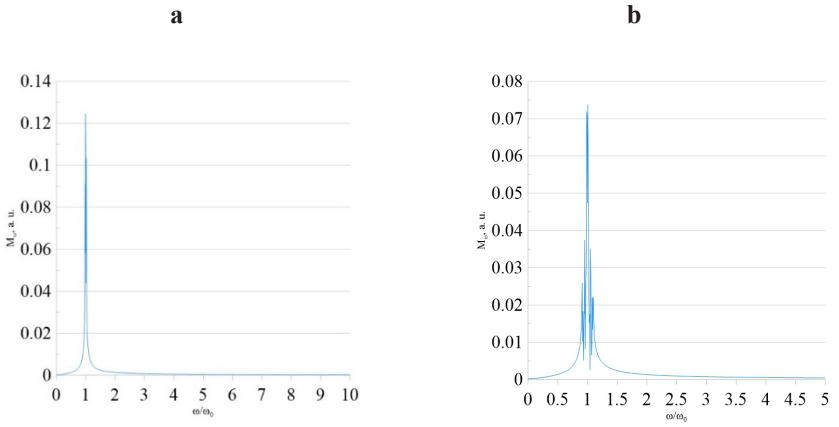

Fig. 3. a spectrum of a disordered stationary chain of 9 spins with a spread of 0,01, pd = 0.025, number of realizations 50; **b** spectrum for a chain of 9 spins with a spread of 0.15. pd = 0.025, number of realizations 100.

in the RCS spectra, and only for disordered structures (in the spectrum of a rectangular ordered structure we cannot see the same thing (Fig. 1)). Also there is no strong division of the main peak into several, as was the case with the ordered rectangular structure (Fig. 1).

In the second part of the work, one-dimensional chains of spins were studied. These chains were oriented at different angles to the external field. The influence on signals and spectra was also considered. The influence of random deviations in the chain structure on signals and spectra is also considered (Fig. 3).

1. Sosunov A.V., Tsiberkin K.B., Henner V.K.: The effect of functionalization of carbon nanoshells on their elec-trical properties. Bulletin of Perm University. Physics, no. 2, 63–68 (2019)
2. Tsiberkin K.B.: Wave Dynamics of Magnetization of a Ferromagnetic Impurity in a Paramagnetic Matrix. Phys. Metals Metallogr. **122**, 358–361 (2021)

oral

NMR of LIQUID ^{129}Xe in porous media near triple point

K.O. Sannikov, P. R. Mampouya, A.V. Klochkov

Institute of Physics, Kazan Federal University, Kazan, Russia

The study of new nanostructured and nanoporous materials requires various characterization techniques. ^{129}Xe nuclear magnetic resonance (NMR) provides a unique and comprehensive characterization of multiscale porous materials using the adsorption and diffusion of xenon atoms. ^{129}Xe is particularly interesting due to its relatively high natural abundance (26.4%) and its nuclear spin (1/2). In addition to that, xenon atom has a very large electron cloud. Thanks to these combined features, this nucleus is very suitable for NMR spectroscopy: any change in its electron cloud is reflected in its NMR characteristics [1].

A large number of works are devoted to the study of hyperpolarized xenon in various media. However, there are few works that study xenon with a natural abundance composition and natural polarization in a liquid state.

The small gyromagnetic ratio (11.78 MHz/T) and the use of a resistive magnet (up to 1 T) impose limitations on signal magnitude. To achieve maximum sensitivity, a low-temperature high-Q NMR probe with the ability to change and adjust the frequency was developed and assembled. In addition, the xenon phase diagram is quite "capricious": when condensing xenon gas into the experimental cell and maintaining it in a stable liquid phase, a number of problems may arise. To ensure proper condensation and control of the xenon phase transition, heaters were added to the NMR probe: one is wound on the condensation capillary, the other is installed under the experimental cell. Several thermometers (PT1000) are also added to monitor the temperature gradient along the NMR probe. Additional corresponding radio frequency noise is eliminated.

In this work we present preliminary results of ^{129}Xe NMR studies in porous media (inverse opal with cavities of about 200 nm was chosen as test sample) in liquid and solid phases.

1. Boventi M., Mauri M., Simonutti R.: Appl. Sci. **12**, 3152 (2022)

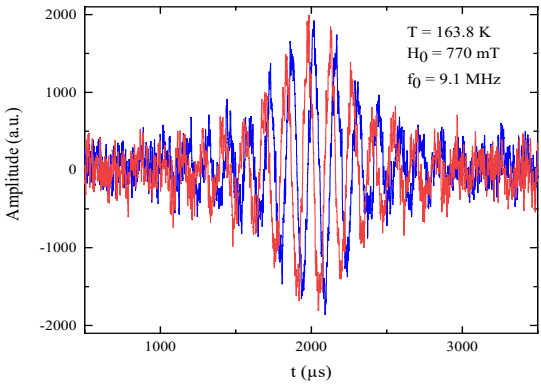

Fig. 1. ^{129}Xe spin echo of liquid xenon in inverse opal sample obtained by a single scan. Xenon gas with natural content of the ^{129}Xe isotope is used.

oral

Analysis of EPR spectra of NASICON:Fe^{3+} considering the distribution of fine structure parameters

D.A. Saritsky, D.N. Grishchenko, M.A. Medkov, A.M. Ziatdinov

Institute of Chemistry, Far Eastern Branch of the RAS, Vladivostok 690022, Russia
denissaricki@mail.ru

This work discusses the results of EPR studies on NASICON powder doped with iron ions ($Na_{3+x}Fe_xZr_{2-x}Si_2PO_{12}$, x = 0.1). Magnetically nonequivalent states of impurity ions and the types of crystal fields acting on them were identified. The EPR spectra were recorded using a JES-X330 spectrometer (JEOL, Japan) equipped with a variable temperature unit ES-13060 DVT5 (JEOL, Japan). The EPR spectra analysis was performed using the EasySpin software package implemented in MATLAB.

For the quantitative description of the Fe^{3+} EPR spectrum in the powder particle, the following spin Hamiltonian was chosen:

$$\hat{H} = g\beta(\boldsymbol{B}, \hat{\boldsymbol{S}}) + D\left(\hat{S}_z^2 - \frac{S(S+1)}{3} + \lambda\left(\hat{S}_x^2 - \hat{S}_y^2\right)\right),$$

where $\lambda = E/D$, and other parameters have their conventional meanings.

The EPR spectrum of NASICON:Fe^{3+} powder was calculated assuming distributions in the fine structure parameters D and λ. The weight w of each individual spectrum $F(B, D, \lambda)$ was modeled by a double normal distribution:

$$w(D,\lambda) = \frac{1}{2\pi\sigma_D\sigma_\lambda} e^{-\left[\frac{(D-D_0)^2}{2\sigma_D^2} + \frac{(\lambda-\lambda_0)^2}{2\sigma_\lambda^2}\right]}$$

where σ_D and σ_λ are the standard deviations of parameters D and λ, D_0 and λ_0 are the mean values of parameters D и λ in the distribution. The approximation of the

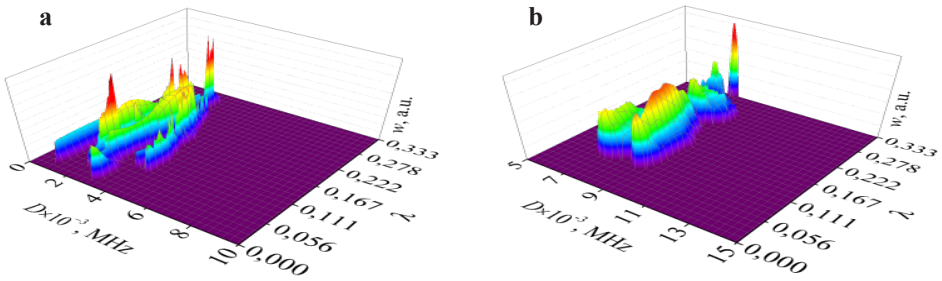

Fig. 1. Distributions of the fine structure parameters D and λ of the NASICON:Fe^{3+}, EPR spectrum obtained by approximating spectrum components in weak (**a**) and strong (**b**) crystal fields. T = –160 °C.

oral

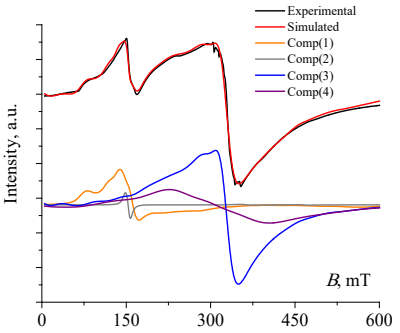

Fig. 2. Experimental (black) and theoretical (red) EPR spectra of NASICON:Fe^{3+} powder. Comp(i) (i = 1, 2, 3, 4) denote components of the theoretical spectrum. T = –160 °C.

experimental EPR spectrum, accounting for the parameter distributions D and λ, was performed using the expression

$$F(B) = \int_{\lambda}\int_{D} f(B, D, \lambda) \cdot w(D, \lambda)\mathrm{d}D\mathrm{d}\lambda \ .$$

Improvement of the Fe^{3+} EPR spectrum fit in the studied powder was achieved by varying the weights w using a gradient descent method. The results of these calculations, accounting for distributions of D and λ, shown in Fig. 1, are presented in Fig. 2.

Computer modeling of the NASICON:Fe^{3+} powder EPR spectrum shows it is a superposition of four types of Fe^{3+} ion spectra (Fig. 2). According to EPR data on $NaZr_2(PO_4)_3$, single crystals doped with Fe^{3+} ions [1], the impurity iron ions substitute for Zr^{4+} ions with local charge compensation and reduced positional symmetry. This information allows components 3 and 4 of the powder EPR spectrum to be attributed to Fe^{3+} ions substituting Zr^{4+} in a weak crystal field with rhombic distortion. These distributed spectra differ in the mean fine structure parameters D_0 and λ_0, their standard deviations σ_D and σ_λ, line widths, and effective spectroscopic splitting factors, determined by the magnetic field at the zero-line crossing by resonance. The resonance with a narrower linewidth can be assigned to Fe^{3+} ion clusters coupled via averaging spin-exchange interaction. The broader resonance likely belongs to isolated Fe^{3+} ions interacting via dipole-dipole interactions that broaden the line.

Spectra types 1 and 2 correspond to Fe^{3+} ions in a strong crystal field with a significant rhombic component. Spectrum type 1 corresponds to Fe^{3+} ions with λ varying from 0.07 to 0.29, and type 2 corresponds to Fe^{3+}, ions with $\lambda \approx 1/3$. In literature [2], EPR spectra of types 1 and 2 are attributed to Fe^{3+} ions located on or near particle surfaces where structural disorder is likely. They may also belong to Fe^{3+} ions in the glassy phase of the sample [3].

Quantitative analysis of the integrated intensities of the NASICON:Fe^{3+} powder EPR spectrum components at –160 °C indicates that the total intensities of Fe^{3+} resonances in strong and weak crystal fields relate approximately as 1:3.

This work was supported by the state assignment to the Institute of Chemistry of the Far Eastern Branch of the RAS (project FWFN-2025-0005).

1. Bulka G.R., Vinokurov V.M., Galeev A.A. et al.: Crystallogr. Rep. **50**, 827–835 (2005)
2. Stosser R., Scholz G.: Appl. Magn. Reson. **15**, 449–468 (1998)
3. Rao M.V.S., Kumar A.S., Ram G.C. et al.: Phase Transitions. **91**, 92–107 (2017)

oral

Crossover spin-3/–pseudospin-1/2 in spin-chain antiferromagnet Cs_2CoCl_4

T.A. Soldatov, A.I. Smirnov

P.L. Kapitza Institute for Physical Problems RAS, Moscow, Russia

Cs_2CoCl_4 is a quasi-1D antiferromagnet with magnetic Co^{2+} ions carrying spin S = 3/2. The main exchange J = 0.74 K acts along the chains directed parallel to b-axis. The interchain exchange integral J' is an order of magnitude weaker [1, 2]. Remarkable feature of this material is strong single-ion anisotropy D = 7 K of the easy-plane type. This anisotropy results in separation of the upper spin doublet of Co^{2+} ion from the lower one and makes possible the use of a pseudospin s = 1/2 representation at low temperatures. As a result, strong easy-plane anisotropy of the effective exchange interaction and the renormalization of the g-factor should arise [3]. Thus spin system of Cs_2CoCl_4 should be equivalent to the set of weakly interacting strongly anisotropic chains of pseudospins s = 1/2 (the so-called XXZ chains). The quantum model of s = 1/2 XXZ antiferromagnetic chain is known to demonstrate remarkable collective ground states and excitations. There is a quantum critical spin liquid in zero field, long-range 1D-antiferromagnetic order in transverse field and restored spin liquid state before saturation. Collective excitations are of spinon-type [4]. Some of these features were detected experimentally [1, 3, 5].

The aim of this work is to check whether the crossover between spin-3/2 and pseudospin-1/2 really occurs. We plan to observe the characteristic spectrum of spin-3/2 at the easy-plane crystal field anisotropy and follow the transformation of this spectrum into the spectrum of spin s = 1/2 with renormalized g-factor. We studied the spin dynamics at temperatures from 3 to 250 K in the wide frequency range 25-120 GHz and in the magnetic field applied along the b-axis. This magnetic field is transverse to the anisotropy axis. $\mathbf{H} \parallel b$ is the only direction at which magnetic field lies within easy planes for all Co^{2+} ions. Local anisotropy axes of Co^{2+} ions have the same direction within each spin chain but alternates from one spin chain to another. Temperature evolution of 102 GHz ESR is shown in Fig. 1a. It exhibits two modes M and M'. The mode M' is obviously thermally activated. This confirms the population of the upper spin doublet with heating. Energy levels calculated for single spin S = 3/2 with easy-plane anisotropy and corresponding frequency-field dependencies are shown by solid and dashed lines in Fig. 1c and Fig. 1b [6]. We notice good accordance of theory with experiment at T = 15 K with fitting parameters D = 7 K and g = 2.0. This correspondence and thermally activated intensity of M' approve that at high-temperatures ($T \gtrsim D$) we deal with the system of paramagnetic spins S = 3/2 in a crystal field. At temperatures $T \lesssim 3$ K we observe g-factor of M mode g_M = 3.3. This value is in a good accordance with the theoretical expectation of pseudospin s = 1/2 g-factor $g_{1/2}$ = 4(1–3J/2D) [3]. We also observe a small temperature shift of the resonance field of mode M' towards lower fields (see Fig. 1a) presumably associated with the exchange interaction.

oral

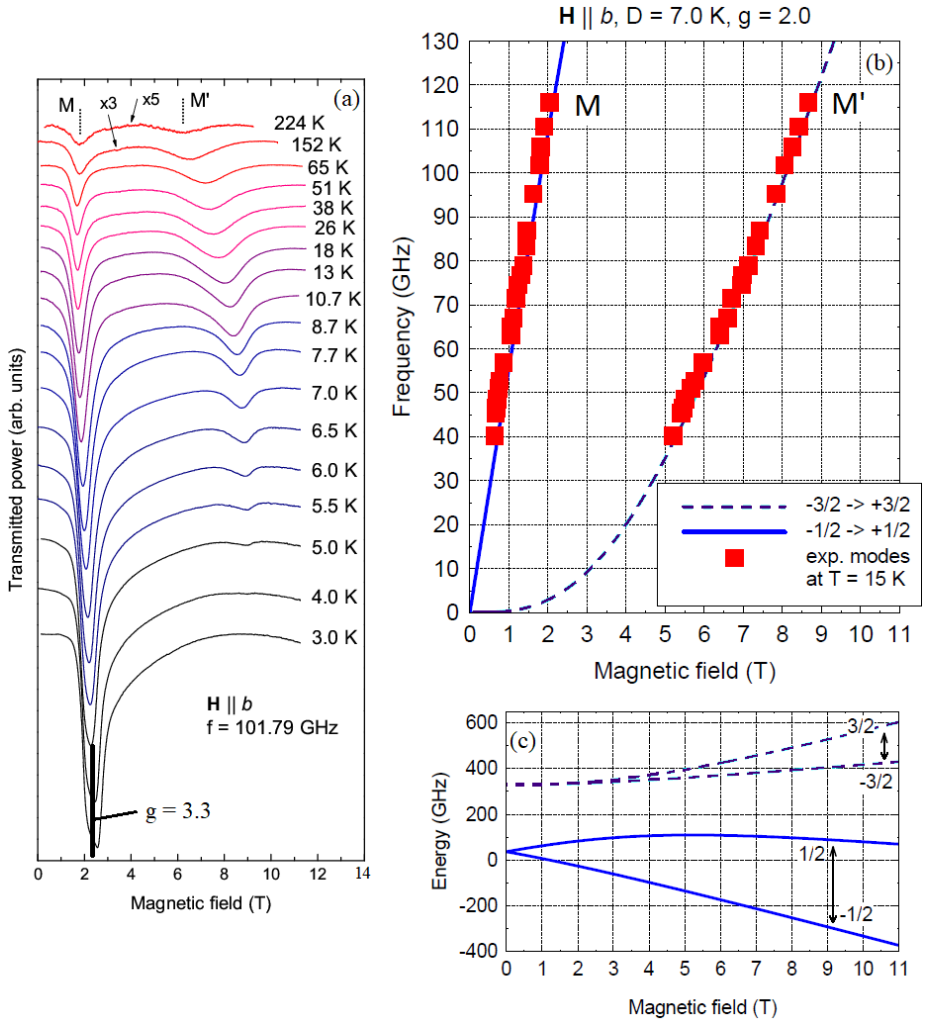

Fig. 1. **a** f = 101.79 GHz ESR records at different temperatures. **b** Frequency-field diagram taken for T = 15 K compared to the theory (solid and dashed lines) with g = 2.0 and D = 7 K. **c** Energy levels of single spin-3/2 with g = 2.0 and D = 7 K.

Thus we conclude that at lowering the temperature below 15 K a crossover from spin-3/2 to pseudospin-1/2 occurs in Cs_2CoCl_4.

The work is supported by Russian Science Foundation Grant № 22-12-00259-П.

1. Kenzelmann M. et al.: Phys Rev. B **65**, 144432 (2002)
2. Yoshizawa H. et al.: Phys Rev. B **28**, 3904 (1983)
3. Breunig O. et al.: Phys. Rev. Lett. **111**, 187202 (2013)
4. Laurell P. et al.: Phys. Rev. Lett. **127**, 037201 (2021)
5. Soldatov T. el al.: Appl. Magn. Reson. **55**, 1137 (2024)
6. Abragam A., Bleaney B.: Clarendon Press, Oxford (1970)

oral

Dynamics of classical magnetic moments after a few T_2: manifestation of collective modes

K.B. Tsiberkin

Institute of Physics and Mathematics, Perm State University, Perm, Russia

The realization of collective spin dynamics in dipole-coupled systems has been considered in nuclear spins under adiabatic demagnetization [1, 2] or in coupled electron-nuclear spin dynamics [3]. Theory of ultracold NMR was developed earlier [4]. Recent data about some rare-earth compounds, e.g. $ErBr_3$, show there is a weak exchange interaction, therefore the dipole coupling produces spin waves temperatures up to mK and even units of K, when the sample is under a strong constant magnetic field; these spin waves were directly observed [5]. Similar systems are known as low-temperature paramagnets [6].

A finite ensemble of classical magnetic dipoles is considered. All the particles are located in a uniform cubic lattice (Fig. 1) and interact each other by the dipole forces. An external field is strong enough to produce the state close to the magnetic saturation. The relative magnitude of dipole interaction is assumed to be $p_d = 0.01$ of Zeeman energy. The direct numerical simulation of system dynamics is realized. At the initial time interval, a short pulse of transverse field occurs. It has the magnitude H_x and duration τ. After the pulse ends, the system oscillates freely. We have considered two kinds of the initial perturbations: "weak" has a "pulse area" $H_x\tau = 10$, and "strong" has $H_x\tau = 100$, in dimensionless units. The field H_x here is referred to H_0 units, and the time is measured in periods of Larmor frequency.

A "weak" perturbation with a "pulse area" 10 does not produce a huge deviation of the total magnetization from the initial state in systems of 15^3, 20^3, 35^3 and 40^3 particles (Fig. 2a). After the Gaussian-like decay, magnetization exhibits slow damping, which is between $t^{-1/2}$ and t^{-1}. The first dependence corresponds the long-range part

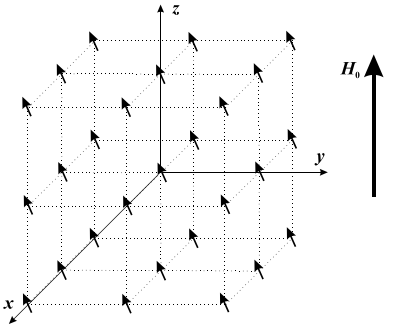

Fig. 1. Schematic structure of finite dipole ensemble at cubic lattice and orientation of the longitudinal magnetic field.

oral

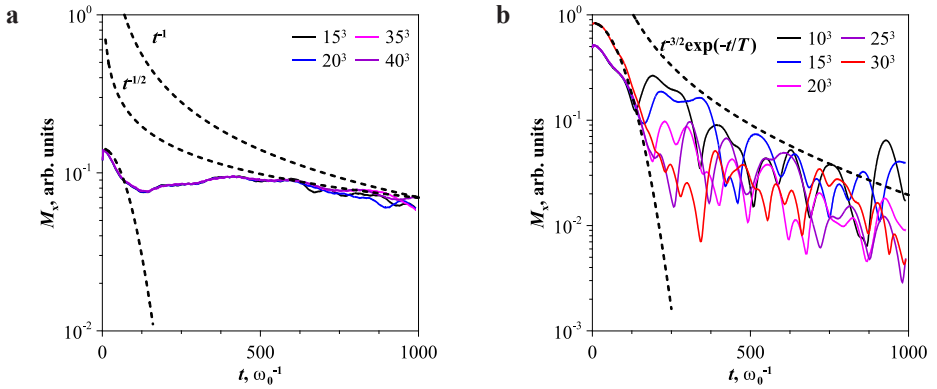

Fig. 2. Simulated envelopes of transverse magnetization after: **a** "weak" and **b** "strong" initial perturbation.

of the dipole interaction, and there is no significant contribution from the short-wave collective modes. This indicates that the magnetic moments in the system turn only at small angles close to each other after the "weak" short transverse pulse.

A "strong" perturbations with a "pulse area" 100 and durations between (0.1÷10) ω_0^{-1} give significant deviation angles of the magnetization, and M_x tends towards the saturation value during the initial pulse. The envelope of the magnetization signal is also Gaussian before T_2, while in the time interval of few T_2, the signal is limited by law $t^{-3/2}\exp(-t/T)$ which can be obtained under assumption that the collective modes (spin waves) of all the possible lengths are excited in lattice, and the inelastic scattering of spin waves realized. That matches a general features of spin wave approach [4, 7].

We assume that an experimental realization of the dipole spin-waves can be based on the effective magnetic moments induced at the doped carbon surface because the adatoms of H, F or N induce effective moments on the order of μ_B [8]. If the characteristic distance between the magnetic centers is of order 1 nm, the typical dipole energy is 10^{-7} eV. Considered p_d = 0.01 corresponds to the longitudinal field $H_0 \approx 1.6 \cdot 10^3$ Oe and Larmor frequency ~4.8 GHz. Thus, a pulse with τ = 1.0 and dimensionless H_x = 100 corresponds to a duration of 0.2 ns and field strength of $1.6 \cdot 10^5$ Oe (16 T). Under the given H_0, the collective excitations will remain stable at temperatures near 1 mK. These estimates correspond the rarefied system; at high concentration of the adatoms the necessary temperature are mitigated, but the external field and pulse field must be enforced.

1. Jacquinot J.F., Weckenbach W.T., Chapellier M. et al.: C. R. Acad. Sci. B Phys. **278**, 93–96 (1974)
2. Ehnholm G.J., Ekström J.P., Jacquinot J.F. et al.: J. Low Temp. Phys. **39**, 417–450 (1980)
3. Andrienko A.V., Ozhogin B.I., Safonov V.L. et al.: Sov. Phys. Usp. **34**, 843–861 (1991)
4. Feldman E.B., Khitrin A.K.: Phys. Letters A **153**, 60–62 (1991)
5. Wessler Ch., Roessli B., Kramer K.W. et al.: Comm. Phys. **5**, 185 (2022)
6. Glazkov V.N.: Phys. Usp. **67**, 1248–1253 (2024)
7. Akhiezer A.I., Baryakhtar V.G., Peletminskii S.V.: Spin Waves. New-York: North-Holland (1968), 372 p
8. Yazyev O.V., Helm L.: Phys. Rev. B **75**, 125408 (2007)

oral

Very strong concentration dependence of Mn^{2+} and Gd^{3+} EPR spectra parameters in $Pb_{0.995}Cu_{0.003}$ Gd_xMn_yS semiconductors

V.A. Ulanov[1,2], I.V. Yatzyk[1], R.R. Zainullin[2]

[1] Zavoisky Physical-Technical Institute, FRC Kazan Scientific Center of RAS, Kazan, Russia
[2] Kazan State Power Engineering University, Kazan, Russia

The mixed $Pb_{0,996}Cu_{0,003}Mn_xGd_yS$ crystals under study were synthesized on the basis of a galena (PbS), a member of the group of lead chalcogenides (PbS, PbTe, PbSe) [1]. The PbTe and PbSe semiconductors have long been the focus of attention of many researchers due to new possibilities of using them as effective materials for creating new nanoelectronic and spintronic devices. Unlike the PbTe and PbSe semiconductors, the physical properties of galena remain poorly studied.

It must be noted, the galena crystals typically have an electronic type conductivity. But, during their growth process there is a high probability of the formation of sulfur vacancies (donor defects). Therefore, it was interesting to study the possibilities of control the concentration and type of free charge carriers by an additional doping the synthesized material with copper or sulfur. Such method was used in this study.

The crystal studied in present work was grown using the vertical Bridgman method. Conical quartz crucible was used. Copper impurity was introduced into the furnace charge using a Cu_2S compound. Gadolinium and manganese impurities were introduced in the form of fine powders of the corresponding metals. Some amount of sulfur required to ensure stoichiometry was also included in the furnace charge. All components of the furnace charge were chemically pure. The prepared furnace charge was loaded into a quartz crucible, and annealed for 3 h at $T = 250°C$, and evacuated with a vacuum pump. The crucible was sealed and placed in the growth chamber of the Donets-2 setup, where it was moved downward vertically in a thermal field with a temperature gradient of 250 deg/cm. The rate at which the crucible was lowered was 1.2 cm/h. The EPR experiment was performed on an ER200SRC spectrometer (EMX/plus, Bruker) with an ITC503S temperature controller (Oxford instruments) in the *X* range.

EPR spectra of two $Pb_{0,996}Cu_{0,003}Gd_xMn_yS$ ($x_1 \approx y_1 \approx 5\cdot10^{-4}$, $x_2 \approx 8\cdot10^{-4}$, $y_2 \approx 2\cdot10^{-4}$) semiconductor crystals are represented in Fig. 1. These spectra were recorded at $T = 5$ K and 100 K, orientation $H_0 \| <001>$ and microwave power $P = 10$ mW.

Fig. 1a represents the EPR spectra of the sample 1 ($Pb_{0,996}Cu_{0,003}Gd_xMn_yS$ with $x_1 \approx y_1 \approx 5\cdot10^{-4}$).

Fig. 1b represents the EPR spectra of the sample 2 ($x_2 \approx 8\cdot10^{-4}$, $y_2 \approx 2\cdot10^{-4}$).

As it can be seen in Fig.1*a* and Fig.1*b*, the observed spectra of Gd^{3+} centers ($S_{Gd} = 7/2$) consist of seven lines with relative characteristic intensities corresponding approximately to the series 7:15:12:16:12:15:7. Relative positions and intensities of the seven lines of Gd^{3+} centers clearly indicate their cubic symmetry. In addition to the lines of Gd^{3+} centers, the EPR spectra in Fig. 1 contain six lines of the same intensity which belong to Mn^{2+} centers of cubic symmetry with $S = 5/2$ and $I = 5/2$. The angular dependences of positions of the EPR lines confirm the cubic symmetry of the Gd^{3+} and Mn^{2+}centers in samples 1 and 2.

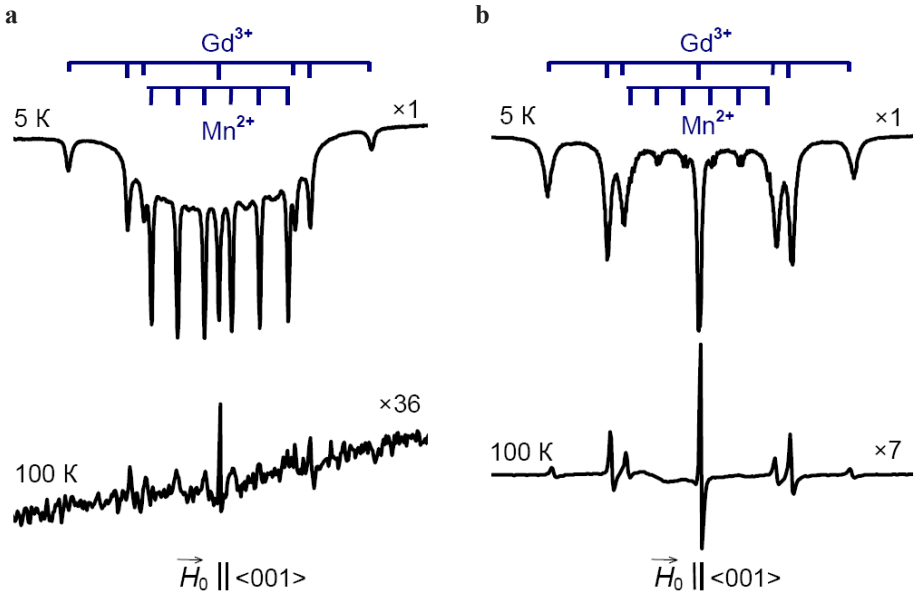

Fig. 1. Concentration and temperature-related changes in the intensities and shapes of EPR spectra lines of Gd^{3+} and Mn^{2+} centers in the $Pb_{0,996}Cu_{0,003}Gd_xMn_yS$ crystals ($\vec{H}\|<110>$, f_{mw} = 9,415 GHz).

In Fig. 1a, one can see that the amplitudes of Gd^{3+} and Mn^{2+} EPR lines with inverted-bell shapes decrease unusually rapidly to almost zero in a fairly narrow temperature range (5 K–100 K).

Fig. 1b represents complex line shapes for Mn^{2+} centers and rapid decrease of amplitudes of Mn^{2+} EPR lines with temperature. As it can be seen here, the EPR lines of Mn^{2+} can be represented as a superposition of two lines with inverted-bell shape and Dysonian-type shape. In contradistinction to Fig. 1a, here it can be seen that the EPR lines of Gd^{3+} centers are observed nicely in the more wide temperature region.

Obviously, the unusual shapes of the EPR lines of the Mn^{2+} and Gd^{3+} centers and the unusual temperature-related changes in the shapes of these lines demonstrate the very strong dependence of dynamic properties of the Mn^{2+} and Gd^{3+} centers on their relative concentrations.

The experimental facts got in the present study will be discussed.

1. Kaidanov V.I., Ravich Yu.I.: Sov. Phys. Usp. **145**, 51–86 (1985)

oral

Diverse magnetic chains in inorganic compounds

A. Vasiliev

Lomonosov Moscow State University

oral

WBr_5: A novel layered ferromagnet for future spintronic applications

O. Volkova[1]

[1] Lomonosov Moscow State University, 119991 Moscow, Russia

Ferromagnetic polymorph of tungsten bromide WBr_5 has been obtained by direct bromination of tungsten. It crystalizes in a triclinic space group $P\bar{1}$ with a = 9.798(6) Å, b = 10.644(7) Å, c = 11.783(9) Å, α = 68.39(6)°, β = 68.90(5)°, γ = 89.48(6)°. It consists of W_2Br_{10} dimers coupled into a three-dimensional framework by halogen bonds shown in the inset to Fig. 1. The average g-factor of W^{5+} ($5d^1$) ions, g_{av} = 1.86(48), has been established by the X-band electron spin resonance spectroscopy. The formation of a ferromagnetically ordered state at T_C = 34 K was confirmed in magnetization M, shown in Fig. 1, and specific heat C_p measurements. The magnetization loop taken at 2 K is characterized by the saturation moment of 0.15 μ_B/f.u., the remnant magnetization of 0.1 μ_B/f.u. and a coercive field of 1.5 T. A slow relaxation dynamics of ferromagnetic domain walls below T_C has been revealed in measurements of ac - magnetic susceptibility. First-principles calculations unveil the one intra- and two inter-dimer exchange interactions: J_1 = 18 K, J_2 = 13 K and J_3 = 8 K, respectively. The ferromagnetic nature of the system is confirmed by band structure and density of states calculations, with W-*d* and Br-*p* states contributing significantly near the Fermi level [1].

Layered morphology of this system makes it attractive for numerous energy – effective spintronic applications. Similar to the other ferromagnetic insulators among van der Waals systems it can be checked for voltage-tunable magnetism, colossal magnetoresistance and energy-efficient spin orbit torque switching. These were observed in $Cr_2Ge_2Te_6$, but new-generation materials for low-power magnetic memory storage and sensors are needed [2].

1. Vorobyova A.A., Boltalin A.I., Morozov I.V. et al.: 2D Materials, submitted (2025)
2. Wang Z. et al.: Nat. Nanotechnol. **13**, 554–559 (2018)

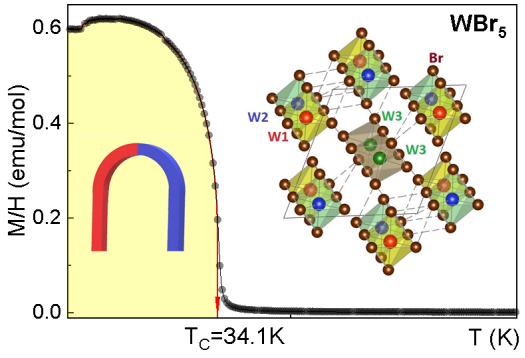

Fig. 1. The temperature dependence of reduced magnetization in crystal structure of WBr_5.

oral

Polarized neutron reflectometry with oscillating magnetic field

V.D. Zhaketov[1,2,3,*], E.D. Kolupaev[1,4], A.N. Chernikov[1], Yu.V. Nikitenko[1]

[1] Joint Institute for Nuclear Research, Dubna, Russia
[2] Moscow Institute of Physics and Technology, Dolgoprudny, Russia
[3] Dubna State University, Dubna, Russia
[4] Lomonosov Moscow State University, Moscow, Russia
[*] zhaketov@nf.jinr.ru

Polarized neutron reflectometry (PNR) is a powerful method for studying magnetic and superconducting multilayer thin films and superlattices [1]. PNR is used, for example, to study proximity effects in ferromagnet/superconductor systems [2] or to study systems with nontrivial magnetic ordering [3, 4]. Recently, it has been proposed to study Fibonacci systems along with superlattices and three-layer neutron resonator systems.

The resonance method associated with spin neutron resonance is described in [5–7]. It's found evidence for neutron spin resonance in the film and observed a spatial beam-splitting. The beam-splitting finds its origin in the exchange of an energy quantum $h\omega$ between the oscillating field and the neutron. The development of this method is also promising for the study of other resonance phenomena using reflectometry with polarized neutrons: Josephson resonance, ferromagnetic resonance, inverse Faraday effect, nuclear magnetic resonance, etc.

At present, a working prototype for neutron reflectometric studies in an oscillating magnetic field has been developed. The field frequency is 10–30 MHz, the amplitude is 1–10 Oe. A low-temperature system for working with an oscillating magnetic field is being developed. The thermostatic system with 4He pumping will be placed in a highly uniform magnetic field created by a polar magnet with warm coils.

1. Nikitenko Yu.V. et al.: Physics of Particles and Nuclei **53**, 6, 1089–1125 (2022)
2. Khaydukov Yu.N. et al.: Phys. Rev. B **99**, pp. 140503(R) (2019)
3. Devyaterikov D.I. et al.: Journal of Surface Investigation **16**, 5, 839–842 (2022)
4. Zhaketov V.D. et al.: Physics of the Solid State **65**, 7 (2023)
5. Kozhevnikov S.V.: Journal of Physics: Conference Series, **340**, 01284 (2012)
6. Ignatovich V.K. et al.: NIM A **620**, 410–413 (2010)
7. Kozhevnikov S.V.: Journal of Surface Investigation **6**, 5, 784–795 (2012)

poster

Features of solid-phase synthesis of $Gd_{2-x}Dy_xTi_2O_7$ and $Gd_{1-x}Dy_xTiO_3$ titanates

V.A. Achintseva, R.G. Batulin, M.A. Cherosov, A.L. Zinnatullin, I.V. Romanova

Kazan (Volga Region) Federal University, Institute of Physics, Kazan, Russia

Perovskite-like rare-earth metal oxides attract significant attention due to their unique physical properties, including magnetic ordering and a pronounced magnetocaloric effect [1]. One of these materials is gadolinium titanate ($GdTiO_3$), which contains titanium in the 3^+ oxidation state, as well as $Gd_2Ti_2O_7$ with a pyrochlore structure. These compounds are considered promising candidates for use in solid-state magnetic refrigeration systems [2].

As part of the study, experiments were conducted on the solid-phase synthesis of titanates with the general formula $Gd_{2-x}Dy_xTi_2O_7$ and $Gd_{1-x}Dy_xTiO_3$. The aim of the work was to investigate the synthesis features of these compounds and determine the optimal conditions for obtaining single-phase products. Various starting materials were used for the synthesis, including titanium metal, titanium (IV) oxide, and rare-earth oxides of Gd and Dy. The synthesis reactions were carried out in an argon atmosphere or a mixture of argon and hydrogen at various temperatures (1200–1400°C) and durations (10–20 hours).

XRD patterns, along with Rietveld analysis, were performed to confirm the formation of a single crystalline phase with a pyrochlore structure, independent of the initial conditions and starting titanium reagents.

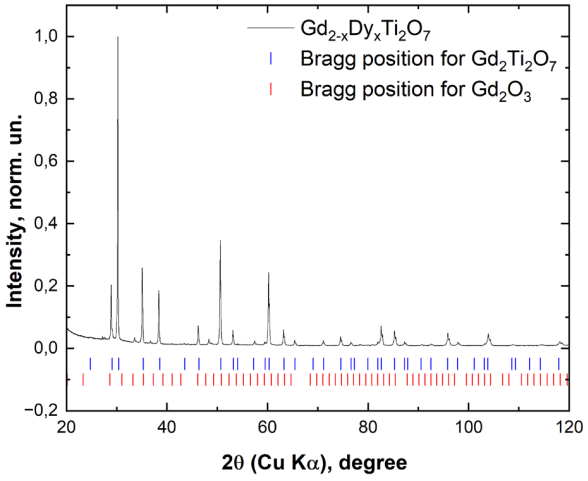

poster

The experiments demonstrated that the solid-phase synthesis of $Gd_{2-x}Dy_xTi_2O_7$ and $Gd_{1-x}Dy_xTiO_3$ titanates is a complex process that requires careful selection of starting materials, synthesis conditions, and firing parameters. The optimal synthesis conditions depend on the specific formula of the compound and can only be determined experimentally. The results obtained can be useful for further studies of the properties of these compounds and their applications in various fields.

The research was carried out with funding from the Russian Science Foundation grant No. #25-22-00324

1. Omote H., Watanabe S., Matsumoto K., Gilmutdinov I., Kiiamov A., Tayurskii D.: Cryogenics **101**, 58–62 (2019)
2. Zhou H.D., Goodenough J.B.: J. Phys Cond.Matter **17**, 7395 (2005)

poster

Magnetic resonance in nanogranular composites: observation of “double-quantum” excitations in ferromagnetic nanoparticles

M.Yu. Dmitrieva[1,2], A.B. Drovosekov[1], A.V. Sitnikov[3,4], S.N. Nikolaev[4], V.V. Rylkov[4,5,6]

[1] Kapitza Institute for Physical Problems, RAS, 119334, Moscow, Russia
[2] National Research University Higher School of Economics, 101000, Moscow, Russia
[3] Voronezh State Technical University, 394026, Voronezh, Russia
[4] National Research Centre “Kurchatov Institute”, 123182, Moscow, Russia
[5] Institute of Theoretical and Applied Electrodynamics, RAS, 125412, Moscow, Russia
[6] Fryazino branch of the Kotelnikov Institute of Radio Engineering and Electronics, RAS, 141190, Fryazino, Russia

Films of metal-insulator nanogranular composites M_xD_{100-x} with different compositions and percentage of metallic and dielectric phases (M = Ni, CoFeB; D = Al_2O_3, ZrO_2; $x \approx 10-80$ at.%) were studied by magnetic resonance technique. Each of the studied samples (thickness ~ 1 μm) was an ensemble of ferromagnetic (FM) metal nanogranules (size of 2–8 nm), randomly located inside of an amorphous oxide dielectric matrix. The experiments were carried out in a wide range of frequencies (f = 7−37 GHz) and temperatures (T = 4.2−300 K) at different orientations of the magnetic field (up to 17 kOe) with respect to the film plane.

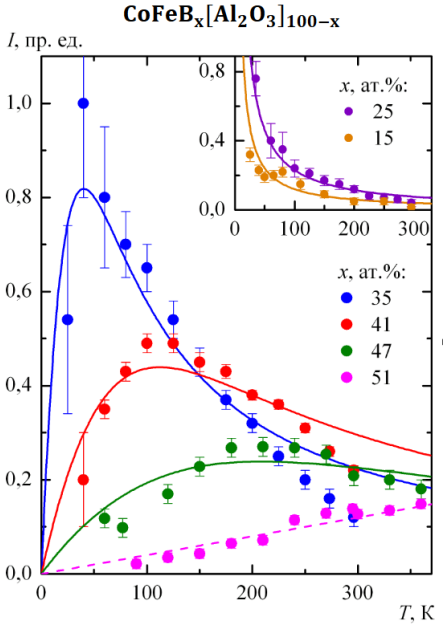

Fig. 1. Temperature dependences of the integral intensity of the additional absorption peak for different concentrations of the FM phase in films from the series of samples $(CoFeB)_x(Al_2O_3)_{100-x}$ (different colors indicate different x values). Round signs correspond to experimental data, and lines — to the “giant spin” model.

poster

It was found that at concentrations of the metallic FM phase below the percolation threshold, the experimental spectra, besides the usual signal of the ferromagnetic resonance (FMR), contain an additional absorption peak characterized by a double effective g-factor $g_{\text{eff}} \approx 4$. Furthermore, the observed peak demonstrates a number of other unusual properties:

• It is better manifested in the longitudinal geometry of the resonance excitation.

• The temperature dependence of the peak intensity has a non-monotonic character with a maximum in temperature. This maximum shifts to higher temperatures with an increase of the FM phase content (Fig. 1).

The appearance of such a peak in the resonance spectra can be explained within the framework of the "giant spin" model [1] by excitation of "forbidden" ("double-quantum") transitions inside the FM nanogranules with a change in the spin projection $\Delta m = \pm 2$. Within this approach, it is possible to explain the better manifestation of the $g_{\text{eff}} \approx 4$ peak in the longitudinal geometry of the resonance excitation, as well as the anomalous temperature dependence of its intensity [1−3].

Work was supportred by RSF grant 22-12-00259-П (M.Yu. Dmitrieva, EPR experiments).

1. Noginova N., Weaver T., Giannelis E.P. et al.: Phys. Rev. B **77**, 014403 (2008)
2. Fittipaldi M., Mercatelli R. et al.: Phys. Chem. Chem. Phys. **18**, 3591 (2016)
3. Drovosekov A.B., Dmitrieva M.Yu. et al.: JETP **166**, 383 (2024)

poster

EPR of cubic center of Gd^{3+} in Rb_2NaF_6 single crystal before phase transition at T = 300 K

M.L. Falin[1], V.A. Latypov[1], S.L. Korableva[2]

[1] Zavoisky Physical-Technical Institute, FRC Kazan Scientific Center of RAS, Kazan, Russia
[2] Kazan Federal University, Kazan, Russia

A family of crystals with the structure of cryolite-elpasolite A_2BCX_6 (A^+, B^+, C^{3+} are mono- and trivalent metal cations, X is the halogen anion: F^-, Cl^-, Br^-) is one of attracting types of crystals. Such compounds doped with rare-earth elements are promising materials for the practical usage in scintillators for X-rays, broadband tunable lasers etc. It is known that such crystals at room temperature have the cubic elpasolite structure with the space group O_h^5. It was established experimentally that many of them, e.g., Cs_2NaYF_6, Cs_2NaScF_6 etc. keep this structure to low temperatures. It was assumed in many works that the symmetry of the Rb_2NaYF_6 crystal also remains cubic in a wide temperature interval (4.2–300 K). However our study of paramagnetic defects in Rb_2NaYF_6 using electron paramagnetic resonance (EPR) and optical spectroscopy showed that a phase transition takes place in this crystal at the temperature of 150 K [1–3]. It was found that cubic paramagnetic centers of Yb^{3+} ions transform into centers of tetragonal symmetry. Simultaneously and independent of us the authors [4] studied the undoped Rb_2NaYF_6 crystal by Raman spectroscopy and hydrostatic pressure, and established that the phase transition from the cubic into the distorted phase accompanied by the recovery of the soft mode occurs in it at T = 154 K.

This report is concerned with investigation of the impurity paramagnetic centers formed by Gd^{3+} ions in Rb_2NaYF_6 single crystal.

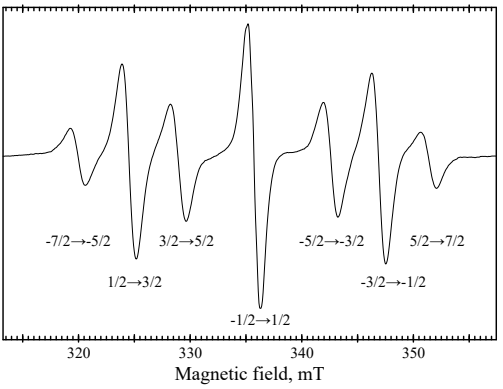

Fig. 1. EPR spectrum of the Gd^{3+} ion in Rb_2NaYF_6. T = 300 K. ν = 9.335 GHz.

poster

Single crystals Rb_2NaYF_6 doped with Gd^{3+} ions were grown by the Bridgman method. Experimental studies of EPR spectra (Fig. 1) were performed on a modified ERS-231 spectrometer (Germany) in the X-band at temperature of 300 K.

The parameters of the corresponding spin Hamiltonians, the ground states and their wave functions were determined. Structural model of the observed complex was proposed. The experimental results were analyzed in comparison with those for the same paramagnetic ion in other hosts.

1. Falin M.L., Gerasimov K.I., Latypov V.A., Leushin A.M., Khaidukov N.M.: Phys. Rev. **B 87**, 115145 (2013)
2. Leushin A.M.: Phys. Sol. State **35**, 2558 (2013)
3. Falin M.L., Latypov V.A., Leushin A.M., Korableva S.L.: J. Alloys and Compounds **688**, 295 (2016)
4. Krylov A.S., Vtyurin A.N., Oreshonkov A.S., Voronov V.N., Krylova S.N.: J. Raman Spectrosc. **44**, 763 (2013)

poster

Morphology of the surface of the implanted silicon to increase the efficiency of light absorption formed by pulsed light heating

B.F. Farrakhov, Ya.V. Fattakhov

Zavoisky Physical-Technical Institute, FRC Kazan Scientific Center of RAS, Kazan, Russia

One of the most promising directions in increasing the absorption capacity of the semiconductor surface is to create directional scattering and increase the surface area, which is equivalent to reducing the reflection coefficient of the surface or increasing the absorption capacity of solar cells. The increase in surface area is achieved through texturing, i.e. the formation of unique relief structures on the surface of solar cells, differing in various shapes, sizes and densities [1].

The aim of the work was to determine the effect of ion implantation (II) with B^+, He^+, and He^{++} ions and pulsed light heating (PLH) on the mechanism of formation of recrystallized relief periodic microstructures from the molten phase on the surface of a c-Si plate for their use in solar energy.

C-Si plates of the KDB-1 brand with a crystallographic surface orientation of (111)+4° and KEF (111)+4° were used as samples for the study. II was performed with B^+ ions with energy E = 40 keV and doses $D = 3.12 \cdot 10^{15}$ cm^{-2} and $D = 6.25 \cdot 10^{15}$ cm^{-2}, He^+ ions with energy E = 40 keV and dose $D = 3 \cdot 10^{16}$ cm^{-2}, He^{++} ions with energy E = 80 keV and a dose of $D = 2 \cdot 10^{16}$ cm^{-2}.

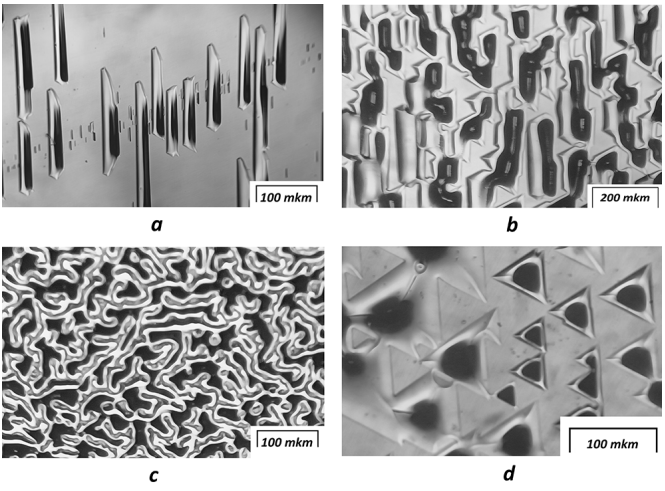

Fig. 1. Micrographs of the surface of ion-implanted Si(111)+4° (**a** – with B^+ ions with energy E = 40 keV and dose $D = 3.1 \cdot 10^{15}$ cm^{-2}, **b** – with He^+ ions with energy E = 40 keV and dose $D = 3 \cdot 10^{16}$ cm^{-2}, **c** – with He^{++} ions with an energy of E = 80 keV and a dose of $D = 2 \cdot 10^{16}$ cm^{-2}, and **d** – with B^+ ions with an energy of E = 40 keV and a dose of $D = 6.25 \cdot 10^{15}$ cm^{-2} after PLH duration of t = 3.5 s.

The samples were PLH with pulses of second durations from halogen incandescent lamps on a Pulse-6 installation with a radiation power density of one lamp $W = 10$ $W \cdot cm^{-2}$ with a pulse duration of 3.5 s (there are 22 lamps in total). The modified surfaces of the Si samples were analyzed using an MBS-9 optical microscope. The formed structures were recorded on a digital camera.

Figure 1 shows micrographs of structures on the surface of Si samples obtained after 3.5 s exposure time. It can be seen that powerful light pulses from halogen lamps lead to the formation of relief surfaces of various shapes and densities.

1. Farrakhov B.F., Fattakhov Ya.V., Stepanov A.L.:Bulletin of the Russian Academy of Sciences: Physics **88**, 1122–1125 (2024)

poster

Effect of Bi^{3+} co-doping on Yb^{3+} local structure in CeO_2 nanoparticles

A.K. Ginkel[1], O.A. Morozov[1,2], S.L. Korableva[1], M.S. Pudovkin[1], R.M. Rakhmatullin[1], V.V. Semashko, A.A. Rodionov[1]

[1] Kazan Federal University, Institute of Physics, Kazan, Russia
[2] Zavoisky Physical-Technical Institute, FRC Kazan Scientific Center of RAS, Kazan, Russia

Cerium dioxide (CeO_2) nanoparticles doped with rare-earth ions are erspective materials for various applications such as catalysis, medicine, bio-imaging, photoenergy, and temperature sensing [1]. The oxygen vacancies play a crucial role in many applications of ceria nanoparticles in the pure and doped form. In this work, we report about EPR and optical study of the CeO_2: 0.1%Yb^{3+} nanoparticles and the CeO_2: 0.1%Yb^{3+} nanoparticles co-doped with 0.5%Bi^{3+} ions, annealed at 600°C and 1000°C. EPR spectra of Yb^{3+} ions show the significant change in the local structure of these ions upon doping with Bi^{3+} and annealing of NPs from 600°C to 1000°C. The EPR linewidth of the sample co-doped with 0.5%Bi^{3+} is significantly larger as compared with the sample without Bi^{3+} (58 G vs 28 G). This can be explained by more imperfections in the local environment of Yb^{3+} ions introduced by Bi^{3+} ions. The ratio of the cubic centers with $g \sim 3.43$ of Yb^{3+} ions to trigonal centers with $g \sim 3.06$ is considerably decreased for the sample co-doped with Bi^{3+} ions. The appearance of the trigonal center with $g \sim 2.75$ upon annealing of NPs at 1000°C indicates the formation of more oxygen vacancies in the local environment of Yb^{3+} ions in CeO_2 NPs in this sample (Fig. 1a) [2].

Luminescence spectra of Yb^{3+} ions also show significant change upon annealing of NPs from 600°C to 1000°C and revealed increased the intensity in the sample co- doped with Bi^{3+} (Fig. 1b). The luminescence spectra evolution with annealing temperature corresponds to the EPR spectral changes.

In conclusion, co-doping with Bi^{3+} ions leads to the increase of a number of the oxygen vacancies in CeO_2 nanoparticles which improves the functional properties of ceria-based materials.

1. Montini T., Melchionna M., Monai M., Fornasiero P.: Chem. Rev. **116**, 5987−6041 (2016)
2. Abraham M.M., Weeks R.A., Clark G.W., Finch C.B.: Phys. Rev. **148**, 350–352 (1966)

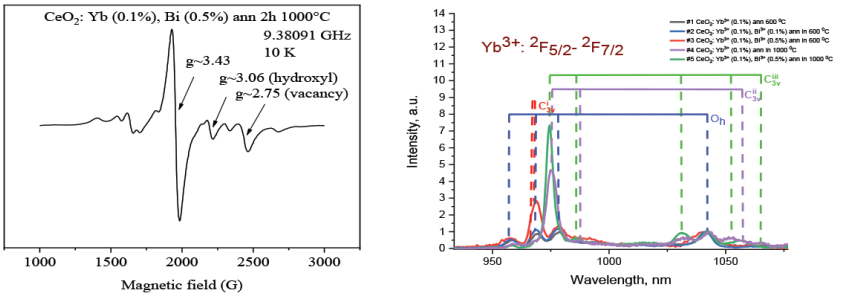

Fig. 1. EPR spectra of CeO_2: 0.1%Yb^{3+} NPs co-doped with 0.5%Bi^{3+} ion; annealed **a** 1000°C, **b** normalized room-temperature luminescence spectrum of #1 - #5 NPs samples under excitation at λ_{ex} = 350 nm (absorption band CT Ce^{4+}).

poster

Cross-relaxation of nitrogen-related centers in diamond

A.S. Gurin[1], D.D. Kramushchenko[1], A.M. Skomorokhov[1], P.G. Baranov[1], S.Ya. Kilin[2], R.A. Babunts[1]

[1] Ioffe Institute RAS, Saint Petersburg, Russia
[2] National Research Nuclear University "MEPhI", 31, Kashirskoe Highway, Moscow, 115409 Russia

The unique properties of nitrogen vacancy centers (NV-centers) in diamond allow optical detection of magnetic resonance and level anticrossing at room temperature in zero and weak magnetic fields [1–3]. NV-centers are actively used as magnetic field and temperature sensors. They can serve as a source of single photons and can also be considered as a material platform for quantum spintronics [4].

In low magnetic fields in synthetic diamonds with high nitrogen concentrations, a number of signals associated with the cross-relaxation (CR) process are registered (Fig. 1a, b)). CR occurs when the transition frequency of two spin species, each having different spin polarization, coincide.

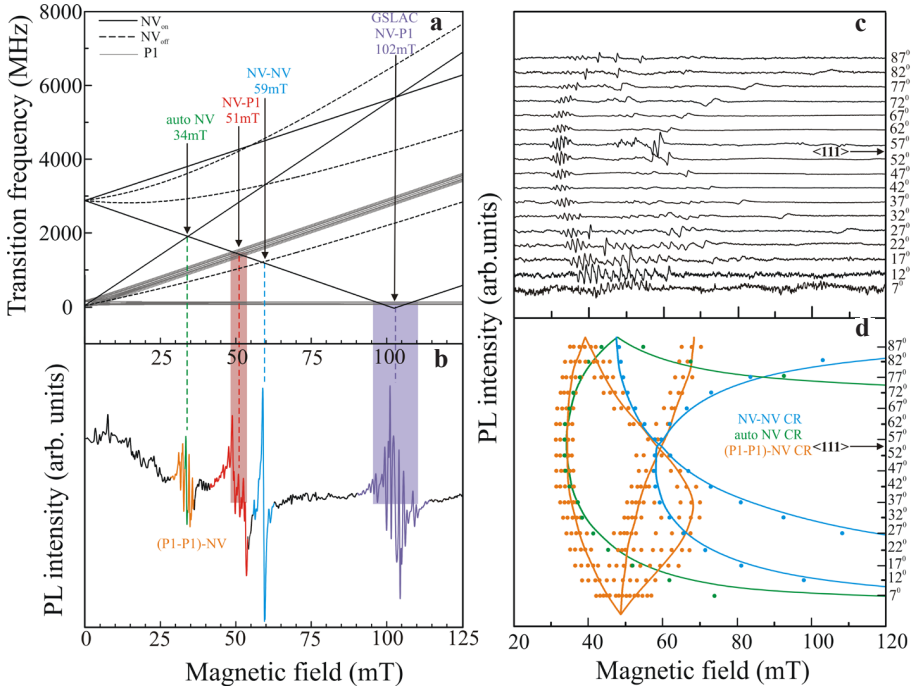

Fig. 1. Transition frequencies of NV and nitrogen centers (**a**) and photoluminescence (**b**) as function of magnetic field along <111> crystallographic direction. Angular dependences of the nitrogen-related defects CR lines for (110) rotation plane (**c**). Experimental data include autocrossing for NV centers (green lines), CR between NV-NV centers (blue lines) and between NV and NOC4 centers (orange lines) (d). Dots are experimental data of cross-relaxation and draw curves are the calculated angular dependencies.

poster

The group of lines with a peak at 51 mT arises because of cross-relaxation between NV centers co-aligned with magnetic field and the nitrogen centers (P1). At 59 mT the transition frequencies between the two differently orientated NV centers coincide [5]. The feature at 102 mT can be assigned to the ground state level anti-crossing of aligned NV centers. A number of CR signals at 34 mT with magnetic field orientation along <111> crystallographic direction signals have been observed earlier. The authors of Ref. [6] ascribed these signals with autocrossing for NV centers (autoNV).

Angular dependences of the nitrogen-related centers CR lines in the magnetic field are plotted in Fig. 1c, d. It should be noted that we have not yet found such detailed angular dependences of the NV-P1 and NV-NV cross resonances over a wide range of angles in the literature. From angular dependencies it was found that number of CR signals at 34 mT consists of not only early assigned autoNV CR line, but also of CR lines identified with nitrogen pair and NV center.

Observation of nitrogen pairs by cross-resonance can be used in quantum magnetometry. The advantages of such magnetometers are that microwave radiation is not required, and the applied magnetic field is weaker and not necessarily precisely aligned compared to magnetometers operating on the basis of anticrossing.

This research was supported by a grant from the Ministry of Science and Higher Education of the Russian Federation No. 075-15-2024-556.

1. Gruber A. et al.: Scanning confocal optical microscopy and magnetic resonance on single defect centers // Science **276**, no. 5321, 2012–2014 (1997)
2. Jelezko F. et al.: Single spin states in a defect center resolved by optical spectroscopy // Applied physics letters **81**, no. 12, 2160–2162 (2002)
3. Nizovtsev A.P. et al.: NV centers in diamond: spin-selective photokinetics, optical ground-state spin alignment and hole burning // Physica B: Condensed Matter **340**, 106–110 (2003)
4. Awschalom D. D., Epstein R., Hanson R. The diamond age of spintronics // Scientific American **297**, no. 4. 84–91 (2007)
5. Jarmola A. et al. Temperature-and magnetic-field-dependent longitudinal spin relaxation in nitrogen-vacancy ensembles in diamond // Physical Review Letters **108**, no. 19, 197601 (2012)
6. Wunderlich R. et al.: Magnetic field and angle-dependent photoluminescence of a fiber-coupled nitrogen vacancy rich diamond // Journal of Applied Physics. – 2021. – Т. 130. – №. 12.

poster

Inverse spin-hall effect and structural phase transitions in $Ni_{80}Fe_{20}/Mn_xPt_{1-x}$ bilayers

A.Kh. Kadikova[1], I.V. Yanilkin[1], A.I. Gumarov[1], B.F. Gabbasov[1], D.G. Zverev[1], L.R. Tagirov[1,2], R.V. Yusupov[1]

[1] Zavoisky Physical-Technical Institute, FRC Kazan Scientific Center of RAS, Kazan, Russia
[2] Institute of Physics, Kazan Federal University, Kazan, Russia

MnMe-class antiferromagnets, where Me = Pd, Ir, Pt, remain a promising research subject for a long time due to the spin-charge conversion effects discovered in them. For example, in equiatomic configurations, MnIr and MnPt systems exhibit significant exchange bias effects and classical spin Hall effects (SHE) [1], while Mn_3Pt and Mn_3Ir systems are promising for switching the magnetization direction of ferromagnets with perpendicular magnetic anisotropy (PMA) via the magnetic spin Hall effect [2]. In this regard, studying spin Hall effects in systems containing a Mn_xPt_{1-x} layer remains a relevant research task today. In this work, the inverse spin-Hall effect (ISHE) was investigated in bilayer heteroepitaxial $Ni_{80}Fe_{20}/Mn_xPt_{1-x}$ systems. The Hall angles for Mn_xPt_{1-x} layers with $x = 0.49…0.61$ were estimated. Additionally, the dependence of the ISHE signal contribution on the crystallinity of the heterostructure was demonstrated. The structural phase transition of the Mn_xPt_{1-x} layer from the cubic A2 phase → tetragonal $L1_0$ phase, accompanied by a magnetic phase transition from paramagnet to the antiferromagnet, was also studied. It was found that depositing Mn_xPt_{1-x} via molecular beam epitaxy in ultrahigh vacuum at 300°C does not lead to the formation of a homogeneous $L1_0$ phase in all heterostructures. Mn_xPt_{1-x} layers grown on $Ni_{80}Fe_{20}$ tend to form a complex low-symmetry epitaxy type. Under prolonged annealing, such low-symmetry structural domains relax into higher symmetry configurations. In particular, domains with (100) orientations were found to emerge, which can provide a significant exchange bias effect in the heterostructure.

1. van den Brink A., Vermijs G., Solignac A. et al.: Nat. com. **7**, 1, 10854 (2016)
2. Pu Y., Shi G., Yang Q. et al.: Adv. Func. Mat. **34**, 33, 2400143 (2024)

poster

VSM, MFM and FMR studies of rutile TiO_2 implanted with doubly positively charged cobalt ions

R.I. Khaibullin[1], E.M. Begishev[1], D.A. Bizyaev[1], V.V. Bazarov[1], I.R. Vakhitov[2], A.A. Sukhanov[1]

[1] Zavoisky Physical-Technical Institute, FRC Kazan Scientific Center of RAS, Kazan, Russia
[2] Institute of Physics, Kazan Federal University, Kazan, Russia

Oxide semiconductor TiO_2 implanted with 3d-ions reveals room temperature ferromagnetism [1–3], and ones is perspective materials for spintronics applications [4]. In the given work, we have implanted Co^{2+} ions with energy of 80 keV into thin (001)-face oriented plate of single-crystalline rutile (TiO_2) to a high fluence of 1.0×10^{17} ions/cm^2 at substrate temperature of 900 K by using an ion-beam implanter ILU-3. The magnetic properties of the Co-ions implanted TiO_2 rutile plate have been studied in detail by vibrating sample magnetometry (VSM), magnetic force microscopy (MFM) and ferromagnetic resonance (FMR) methods at different orientation of applied magnetics field with respect to the surface of rutile plate in the temperature range of 4–300 K. For the first time, we observed strong perpendicular magnetic anisotropy in ferromagnetic behavior of Co-ions implanted rutile plate, as well the contribution of doubly positively charged magnetic ions of cobalt (Co^{2+}) to the formation of long-range magnetic order in the implanted rutile.

Thin rutile plate implanted with cobalt ions exhibits ferromagnetism at room temperature (Fig. 1). The high value of residual magnetization in out-of-plane geometry and the detailed studies of the angular dependence of residual magnetization (Fig. 1b) indicate on strong perpendicular anisotropy in Co-ions implanted rutile. The equilibrium position of the magnetization vector of the sample corresponds to the polar angle $\theta \cong 60^o$. Moreover, a stripe magnetic domain structure have been observed in MFM images that is typical for thin magnetic films with strong perpendicular magnetic anisotropy.

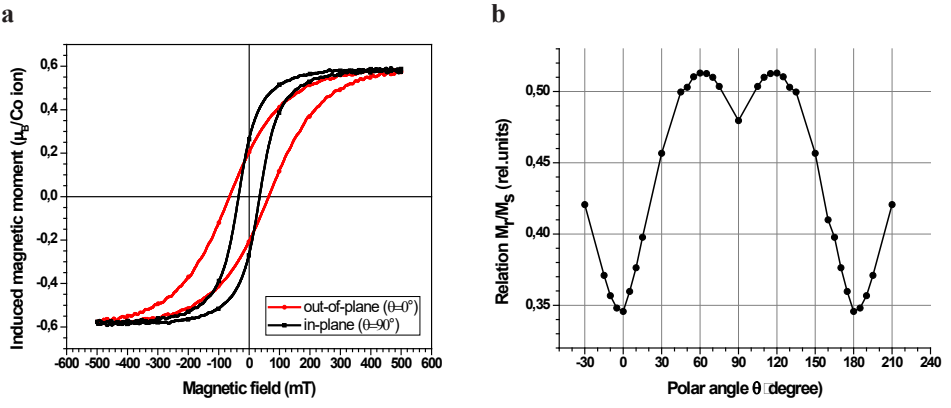

Fig. 1. a Room-temperature magnetic hysteresis loops of Co-ions implanted (001) TiO_2 plate for in-plane and out-of-plane orientation of the applied magnetic field; **b** The angular dependence of residual magnetization on the polar angle (θ) at room temperature.

poster

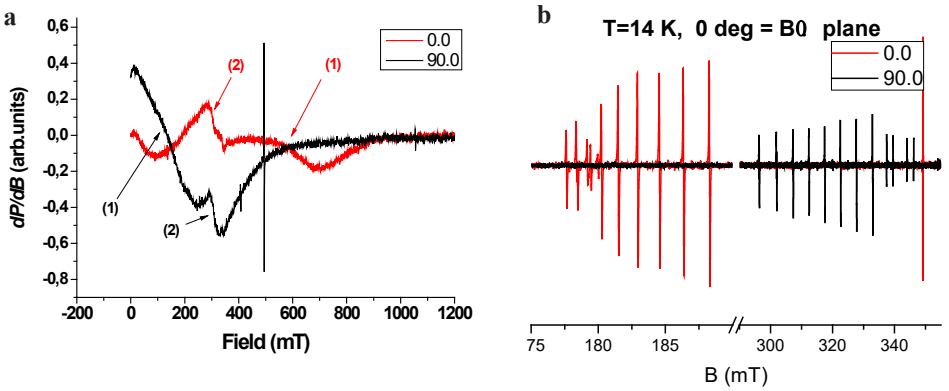

Fig. 2. a FMR spectra of Co-ions implanted (001) TiO_2 plate at room temperature; **b** EPR spectra of Co^{2+} ions with hyperfine structure at a low temperature of 14 K for out-of-plane ($\theta = 0^o$) and in-plane ($\theta = 90^o$) orientations of the applied magnetic field.

Two types of FMR signals were observed in the magnetic resonance spectra recorded at room temperature in cobalt-implanted rutile (Fig. 2a). The first signal with a strong angular dependence of the resonance field on the polar angle was attributed to magnetic cobalt nanoparticles located in a thin surface layer of the rutile plate. The second isotropic signal is associated with the formation of a ferromagnetic solid solution of cobalt ions Co^{2+} bound by indirect exchange interaction through electrons captured by oxygen vacancies in the crystalline matrix of rutile. Such divalent cobalt ions were first observed by us at low measurement temperatures, as shown in Fig. 2b. Note that at low measurement temperatures, below 50 K, both FMR signals disappear.

1. Khaibullin R.I., Tagirov L.R., Rameev B.Z. et al.: J. Phys. Cond. Matter **16**, L443-L449 (2004)
2. Vakhitov I.R., Shemukhin A.A., Gumarov A.I. et al.: Mater. Res. Express. **6**, 116103 (2019)
3. Vakhitov I.R., Lyadov N.M., Vdovin V.I. et al.: Crystals. **13**, 355 (2023)
4. Bhardwaj P., Singh J., Verma V., Kumar R.: Physica B **696**, 416596 (2025)

poster

^{35}Cl NQR relaxation study of fine powders

I. Mershiev, G. Kupriyanova

Institute of Physical and Mathematical Sciences and Information Technology,
Immanuel Kant Baltic Federal University, Kaliningrad, Russia

Relaxation processes in small particles are strongly influenced by the spin diffusion, which depends on particle size [1]. Relaxation rate on the surface of the powder is much shorter, but it shows a degree of sensitivity to the environment [2]. The topic of the study is influence of size and diffusion effects on relaxation in powders.

The $KClO_3$ polycrystalline samples were prepared by grinding in hand mortar and sifting through a set of laboratory sieves with 75 to 63, 63 to 52, and 52 to 39 mcm mesh sizes. CPMG experiments were made at 28.09MHz at 25°C with the results of inverse integral transform presented at Fig.1.

Distribution of spin-spin relaxation time shows that relaxation rates at the surface and the bulk of powder crystallites have ratio about 1:4 for the larger sizes of the powder particles. It increases with decrease of the average particle size, as the relative change of relaxation rate on the surface is more prominent, where spins are affected by increased density of impurities. The study shows that the relaxation rate in the surface of the powder particles is more sensitive to the change of the average size of particles, than the relaxation rate in the particle bulk.

1. Rabbani S.R., Edmonds D.T.: Nuclear spin-lattice relaxation-time reduction in small particles. Phys. Rev. B **50**, no. 9 (1994)
2. Sinyavsky N.Y., Mershiev I.G., Kupriyanova G.S.: Application of nuclear quadrupole resonance relaxometry to study the influence of the environment on the surface of the crystallites of powder // Zeitschrift für Naturforsch. A. **70**, no 6 (2015)

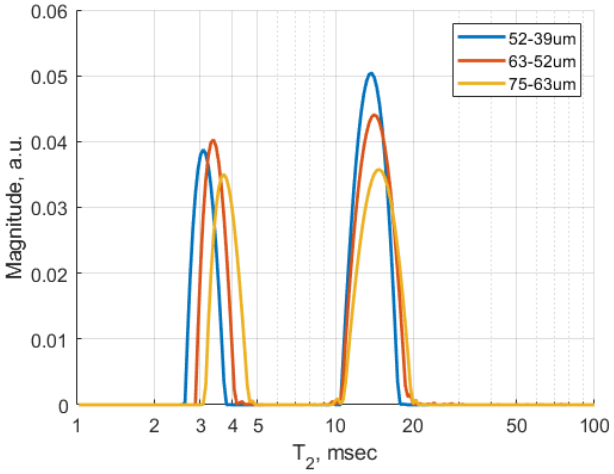

Fig. 1. T_2 relaxation time distributions for the $KClO_3$ powders with different ranges of particle sizes.

poster

Monitoring of nanoparticles nucleation in capillary system using ^{1}H NMR

B.M. Mukhamadullin, E.I. Boltenkova, A.M. Garaeva, A.V. Bogaychuk, E.M. Alakshin

Institute of Physics, Kazan Federal University, Kazan 420008, Russian Federation
e-mail: bulatm4635@gmail.com

The real-time monitoring of the formation of fluoride nanoparticles in capillary system using ^{1}H NMR up to 9.4 T will be presented.

To obtain nanoparticles with predefined parameters requires precise real-time control over synthesis parameters. Common analytical methods for in-process monitoring include transmission electron microscopy (TEM), fluorescence resonance energy transfer (FRET), dynamic light scattering (DLS), X-ray diffraction (XRD), nuclear magnetic resonance (NMR), and ultraviolet (UV) spectroscopy. However, each technique has inherent limitations, necessitating careful selection based on experimental goals, material properties, and process conditions.

Previous research has largely examined slow chemical transformations and nanoparticle nucleation dynamics [1, 2]. Traditional approaches, such as reagent drip-feed systems or microfluidic reactors, present difficulties in NMR data collection due to rapid signal decay. In contrast, coprecipitation in colloidal solutions proceeds nearly instantaneously, making NMR relaxometry challenging for studying nucleation, growth, and colloidal stability – primarily due to ultrashort relaxation times. To mitigate this, viscous environments are employed to decelerate reaction kinetics [3].

The development of simple and universal methods for monitoring nanoparticle formation processes remains an important scientific task, since this is crucial for obtaining new nanostructures with the desired morphology and functionality. In this paper, an *in situ* method is proposed for quantifying in real time the processes of nucleation and growth of nanocrystals, determining their concentration and kinetics of reagent consumption. Using the example of the formation of dysprosium fluoride (DyF_3) nanoparticles in a capillary system, it is shown that ^{1}H NMR spectroscopy makes it possible to track these processes without disrupting the reaction. The analysis of chemical shifts of water protons provides detailed information on the formation of nanoparticles under controlled diffusion conditions. The proposed method makes it possible to study in detail the course of chemical reactions and processes affecting the formation of nanoparticles.

This work was financially supported by the Russian Science Foundation (Project No. 23-72-10039).

1. Chae Y. et al.: Analytical chemistry **93**(4), 2106–2113 (2021)
2. Mashiach R. et al.: Nature Communications **12**(1), 229 (2021)
3. Gholami T. et al.: Materials Science and Engineering: B **304**, 117370 (2024)

poster

Using atomic force microscopy to fabricate test structures from upconversion luminescent particles for confocal microscopy

N.I. Nurgazizov, A P. Chuklanov, Ye.O. Mityushkin, V.G. Nikiforov

Zavoisky Physical-Technical Institute, FRC Kazan Scientific Center of RAS, Kazan, Russia

To investigate intracellular dynamics in living systems, methodologies combining high temporal resolution and, crucially, high spatial resolution are essential. Confocal microscopy (CM) exemplifies such a technique. CM has been widely adopted for non-destructive imaging of living tissues, enabling detailed visualization of both surface topography and internal structures. When measuring specific intracellular parameters, such as temperature, upconversion luminescent particles (ULPs) at nanoscale or microscale sizes offer a promising approach. This technique leverages pairs of rare-earth ions (e.g., Yb^{3+} and Er^{+3}), where the first ion absorbs low-energy photons in the near-infrared range (corresponding to the optical transparency window of biological tissues). Subsequent nonradiative energy transfers enable the second ion to emit higher-energy photons in the visible spectrum. The emission spectra of these systems exhibit temperature-dependent behavior due to the strong thermal sensitivity of energy levels governing nonradiative transitions. This property enables their application in addressing the aforementioned challenge. However, the random intracellular distribution of ULPs introduces complexity in interpreting CM signals. Consequently, developing test structures is critical for refining data-processing algorithms and minimizing imaging artifacts. Here, we propose a method to fabricate CM-compatible test structures. This approach relies on precise manipulation of ULPs and their agglomerates on surfaces.

Atomic force microscopy (AFM) was employed to fabricate test structures. This technique was selected for its dual capability to characterize physicochemical properties of micro- and nano-objects with nanoscale precision and to perform controlled manipulations. We utilized sodium yttrium fluoride particles ($NaYF_4$) co-doped with Yb^{3+} and Er^{3+} ions. These particles were synthesized via hydrothermal methods [1, 2], yielding cylindrical ULPs with dimensions of approximately 1 × 0.1 μm. Under λ = 974 nm laser excitation, the ULPs exhibited bright upconversion luminescence in the visible spectrum, consistent with Er^{3+} ion emission characteristics [2]. Manipulations were performed using an AFM Solver-Bio (NT-MDT) integrated with a Biolam P2-1 inverted optical microscope. The AFM probe achieved coarse positioning accuracy of 5 μm, while the 100 × 100 μm^2 scanning field – combined with substrate large-scale markers – enabled repeated nanometer-precise repositioning. Silicon cantilevers (Tap150Al-G, BudgetSensors) with a resonance frequency of ~150 kHz and a spring constant of ~5 N/m were used for all experiments.

Test-structure fabrication involved AFM tip-mediated imprinting of ULPs and their agglomerates onto clear substrates. Synthesized ULPs were first deposited from a solution onto a “donor substrate”, positioned adjacent to a clean “target substrate” patterned with large-scale markers. This configuration enabled coarse alignment prior to nanoscale deposition. Test-structure fabrication was carried out in several stages. Initially, the AFM probe was brought into contact mode with the donor substrate, and

poster

a large-area scan was performed to facilitate the transfer of ULPs onto the probe tip. Successful transfer was confirmed both visually, by observing film thinning in the scanned region under an optical microscope, and instrumentally, by detecting a shift in the probe's resonance frequency, which indicated the attachment of ULPs. The ULP-loaded probe was then positioned over a pre-selected area of the target substrate using large-scale markers for precise alignment. Areas chosen for deposition were required to be free of contaminants with morphology similar to ULPs and to be located near markers to allow for repeated, nanometer-scale positioning. The AFM probe was precisely positioned at the desired location on the target substrate and manually pressed against the surface. The system was then switched to forced oscillation mode, with the probe pulled along the excitation generator frequency at maximum voltage amplitude, resulting in a sharp and substantial increase in the amplitude of AFM probe oscillations. This abrupt rise in oscillation amplitude facilitated the release of ULPs from the probe tip onto the substrate surface. Following each deposition, the procedure was repeated at subsequent locations, enabling "drawing" of points. Through this approach, ULP marks were arranged in various geometric patterns, including triangles, squares, crosses, and hexagons, providing versatile calibration structures for subsequent imaging analysis. Mathematical algorithms developed for processing CM-images were applied to these prepared structures, demonstrating a significant reduction in artifacts related to the discrete nature of the observed objects. The results confirm that the use of well-defined test patterns enhances the reliability and accuracy of image analysis by minimizing the influence of object discreteness on the quantitative evaluation of experimental data.

1. Ren G., Zeng S., Hao J.: J. Phys. Chem. C **115**, 20141 (2011)
2. Mityushkin E.O., Zharkov D.K., Leontyev A.V., Nurtdinova L.A., Shmelev A.G., Nikiforov V.G.: Bull. RAS: Phys. **87**, 1806–1811 (2023)

poster

ESR of nanoparticles powder of europium metaphosphate $Eu(PO_3)_3$ doped by Eu^{2+} ions

N.S. Saenko, N.I. Steblevskaya, M.V. Belobeletskaya, A.M. Ziatdinov

Institute of Chemistry, Far Eastern Branch of the RAS, Vladivostok, Russia
saenko@ich.dvo.ru

The Eu^{3+} is a non-Kramers ion, while the ground state of the Eu^{2+} ion is characterized by spin $S = 7/2$. Both natural europium isotopes ^{151}Eu (47.82%) and ^{153}Eu (52.18%) have a nuclear spin $I = 5/2$, but they are differ in the values of the nuclear spectroscopic splitting factor. The EPR spectrum of a single-crystal sample containing Eu^{2+} of both isotopes is a superposition of two spectra with fine and hyperfine structure and with effective values of the spectroscopic splitting factor g^* near the value of the g-factor of a free electron g_e [1]. The Eu^{2+} ions are located at crystal lattice sites with different crystal field symmetries in many europium compounds and they exhibit so-called U-spectrum (U stands for ubiquity) [2]. The typical U-spectrum contains a set of lines with effective values of the spectroscopic splitting factor $g^* \sim 6.0$; 4.5; 2.8 and 2.0 [2–5]. The line with $g^* \sim 2.0$ in this spectrum is usually attributed to both single Eu^{2+} centers and defects in the crystal structure [3, 6]. In $Eu(PO_3)_3 : Eu^{2+}$, defects can be imperfections of the metaphosphate structure such as PO_2^-, PO_3^{2-}, PO_4^{4-}, as well as holes in the oxygen-phosphorus system, which appear as asymmetric lines in the EPR spectra of metaphosphates [7, 8]. The fine and hyperfine structure Eu^{2+} lines is averaged in polycrystalline samples, which leads to complex spectra containing many components with comparable widths and intensities [3, 9]. It is obvious from the above, that the interpretation of the EPR spectra of powder compounds containing the Eu^{2+} ions becomes non-trivial task.

This paper reports the results of EPR studies of nanosized powder particles of trivalent europium metaphosphate $Eu(PO_3)_3$, doped with divalent europium ions. The compound under study was prepared by low-temperature pyrolysis of europium and tributyl phosphate [10]. All EPR spectra of this compound were recorded on a JEOL-X330 spectrometer (Japan, JEOL) equipped with a DVT5 variable temperature unit (ES-13060). EPR spectra analysis was performed using computer modeling.

Three components can be distinguished in the EPR spectrum of the $Eu(PO_3)_3 : Eu^{2+}$ powder, they differ significantly in peak-to-peak width and peak intensity (Fig. 1). The widest of them ($\Delta B = 149$ mT) at room temperature is characterized by $g^* = 2.139$ (Fig. 1b), and can be attributed to the averaged lines of the fine and hyperfine structure of the Eu^{2+} ions. As the temperature decreases, this line narrows simultaneously with the decrease in the integrated intensity; its g^* value slightly increases and then decreases to the value that less than its value at room temperature (Fig. 1b). The other two components of the spectrum have g^* values close to the g_e value (Fig. 1c, d). The first of them has a width of 10.2 mT at room temperature (Fig. 1c) and may belong to the Eu^{2+} ions with a strong dipole-dipole interaction. When the temperature is reduced to –80 °C, it broadens, and then, by –160 °C, it narrows by ≈18%. The second component has an asymmetric shape and narrows with a decrease in temperature with a simultaneous increase in the integral in-

poster

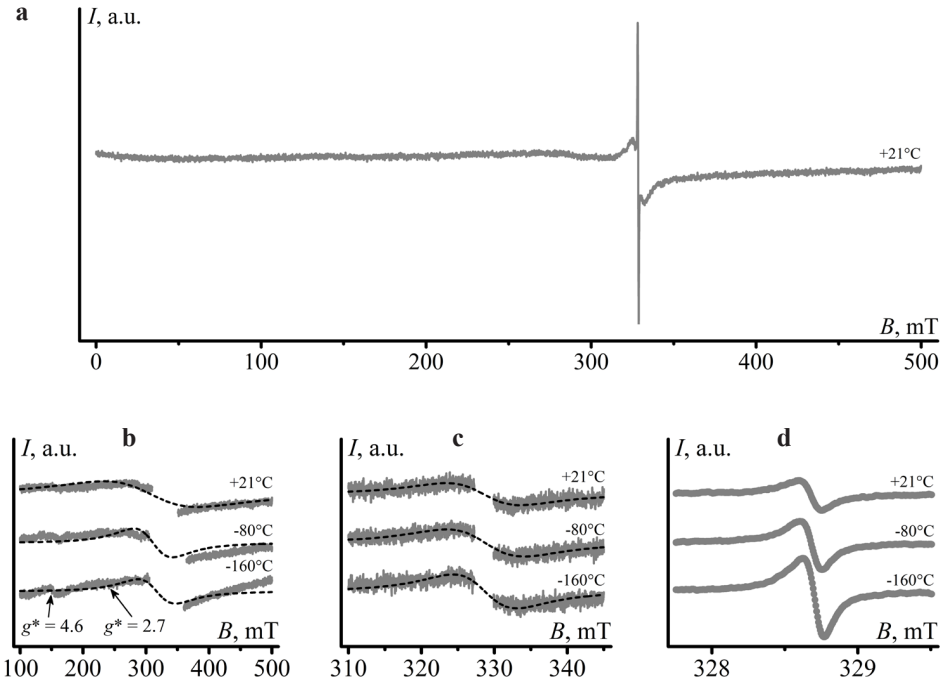

Fig. 1. EPR spectrum of $Eu(PO_3)_3$:Eu^{2+} powder: at 21 °C (**a**); at 21, –80 and –160 °C in the range from 100 to 500 mT with omitted central part of the spectrum (**b**), in the range from 310 to 345 mT with omitted central part of the spectrum (**c**); in the range from 327.75 to 329.50 mT (**d**). Gray lines and dots are the experimental data, dashed lines are the approximations.

tensity (Fig. 1d). This component may belong to defects of the metaphosphate structure, significantly distant from the phosphorus atom, since it does not exhibit a doublet hyperfine structure caused by the interaction of the electron spin of the defect ($S = 1/2$) with the nuclear spin of phosphorus ^{31}P ($I = 1/2$). It worth to note that in the EPR spectrum of the powder under study at low temperatures, a low-intensity resonance with $g^* \approx 2.7$ is also recorded (Fig. 1b), which according to literature might be considered as the component of the U-spectrum of Eu^{2+} ions [2, 4]. The spectrum component with $g^* \approx 4.3$ (Fig. 1b) may belong to impurity Fe^{3+} ions entering the sample from precursors during synthesis.

This work was carried out within the framework of the state assignment to the Institute of Chemistry FEB RAS (project FWFN-2025-0005).

1. Zyuzin A.M., Salkin D.A.: Phys. Solid State **61**, no. 10, 1849 (2019)
2. Brodbeck C.M., Iton L.E.: J. Chem. Phys. **83**, no. 9, 4285–4299 (1985)
3. Iton L.E. et al.: J. Chem. Phys. **79**, no. 3, 1185–1196 (1983)
4. Shlyakhtina A.V. et al.: Ceram. Int. **47**, no. 19, 26898–26906 (2021)
5. Vasin A.A. et al.: Russ. J. Phys. Chem. A **94**, 2467–2473 (2020)
6. Secu M. et al.: Ceram. Int. **47**, no. 24, 35089–35095 (2021)
7. Griscom D.L. et al.: J. Appl. Phys. **54**, no. 7, 3743–3762 (1983)
8. Ebeling P., Ehrt D., Friedrich M.: Opt. Mater. (Amst) **20**, no. 2, 101–111 (2002)
9. Secu C., Rostas A.-M., Secu M.: Nanomaterials **12**, no. 17, 3016 (2022)
10. Steblevskaya N.I. et al.: Russ J. Inorg. Chem. **64**, N. 2. P. 179–184 (2019)

poster

Analysis and modeling of EPR spectra of $Na_2Ti_6O_{13}:Fe^{3+}$ considering the distribution of fine structure parameters

D.A. Saritsky, V.V. Zheleznov, A.M. Ziatdinov

Institute of Chemistry, Far Eastern Branch of the RAS, Vladivostok 690022, Russia,
denissaricki@mail.ru

This work discusses the results of EPR studies on $Na_2Ti_6O_{13}$ powder doped with iron ions. Magnetically nonequivalent states of impurity ions and the types of crystal fields acting on them were identified. The EPR spectra were recorded using a JES-X330 spectrometer (JEOL, Japan) equipped with a variable temperature unit ES-13060 DVT5 (JEOL, Japan). The EPR spectra analysis was performed using the EasySpin software package implemented in MATLAB.

The EPR spectrum of $Na_2Ti_6O_{13}:Fe^{3+}$ powder contains resonances corresponding to different positions of iron ions in the structure. Several narrow resonances are observed in the low-field region of the spectrum (Fig. 1). According to literature [1], the resonance with an effective spectroscopic splitting factor g^* ≈4.3 is attributed to the high-spin configuration of Fe^{3+} ions in a crystal field with strong rhombic distortion. The resonance at g^* ≈5.6 is characteristic of ions in crystal fields with a strong axial component [2]. The origin of features at g^* ≈8.4 and ≈17 remains unclear and is debated in the literature.

In the high-field region, a broad intense resonance is observed, whose g^* value depends on temperature, changing from 2.25 at 20 °C to 2.05 at –160 °C. However, its intensity changes only slightly. The temperature dependence of g^* is a typical sign of superparamagnetic resonance; however, in such cases, the sign of the change should be opposite to what is observed. Moreover, the resonance intensity should decrease [3]. This anomaly may be explained if the resonance represents a sum of paramagnetic and superparamagnetic resonances. The superparamagnetic resonance may arise from clusters or nanoparticles of iron oxide, while isolated Fe^{3+} ions in a weakly distorted octahedral crystal field, for example in the substitution positions of Ti^{4+} ions, are responsible for paramagnetic resonance.

The analysis of $Na_2Ti_6O_{13}:Fe^{3+}$ powder EPR spectra was performed using the spin Hamiltonian:

$$\hat{H} = g\beta(\boldsymbol{B}, \hat{\boldsymbol{S}}) + D\left(\hat{S}_z^2 - \frac{S(S+1)}{3} + \lambda\left(\hat{S}_x^2 - \hat{S}_y^2\right)\right),$$

where β is the Bohr magneton, $\boldsymbol{B}$ is the magnetic field vector, g is the spectroscopic splitting factor, assumed isotropic in the studied samples, $\hat{\boldsymbol{S}}$ is the spin angular momentum operator vector, $\hat{S}_x$, $\hat{S}_y$, $\hat{S}_z$ are spin operators along the x, y and z axes respectively, S is the spin quantum number of the electron system, D is the axial component of the crystal field, and $\lambda = E/D$, where E is the rhombic component of the crystal field.

poster

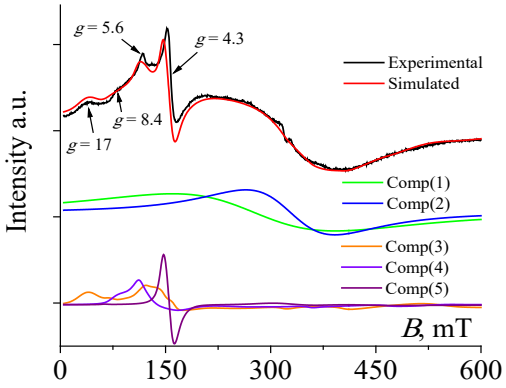

Fig. 1. Experimental (black) and theoretical (red) EPR spectra of $Na_2Ti_6O_{13}$ powder doped with iron. Comp(*i*) (*i* = 1–5) denote components of the theoretical spectrum. *T* = –160 °C.

To account for the spread of crystal field parameters in simulating low-field maxima, a double normal distribution over *D* and λ was used:

$$w(D,\ \lambda) = \frac{1}{2\pi\sigma_D\sigma_\lambda} e^{-\left[\frac{(D-D_0)^2}{2\sigma_D^2}+\frac{(\lambda-\lambda_0)^2}{2\sigma_\lambda^2}\right]},$$

where σ_D and σ_λ are the standard deviations of *D* and λ, D_0 and λ_0 are their mean values in the distribution.

The maxima at *g** ≈17, ≈5.6 and ≈4.3 correspond to different Fe^{3+} centers (positions) in the structure; accordingly, their simulations were performed using separate lines, each with its own set of parameters and distributions (Fig. 1, Comp(3)-(5)). The main resonance was approximated by two broad lorentzians (Fig. 1, Comp(1) and (2)). Analysis of temperature-dependent changes in the parameters of the main resonance components confirms the superparamagnetic origin of one of them.

1. Castner T., Newell G.S., Holton W.C., Slichter C.P.J.: Chem. Phys. **32**, 668–673 (1960)
2. Jahagirdar A.A., Dhananjaya N., Monika D.L. et al.: Spectrochim. Acta A. **104**, 512–518 (2013)
3. Berger R., Bissey J.-C., Kliava J. et al.: J. Magn. Magn. Mat. **234**, 535–544 (2001)

poster

Magnetoelectric properties of skyrmions

T.S. Shaposhnikova, R.F. Mamin

Zavoisky Physical-Technical Institute, FRC Kazan Scientific Center of RAS, Kazan, Russia

Magnetic skyrmions are particle-like nanometer-sized spin textures found in several magnetic materials and heterostructures, and are characterized by a long lifetime [1–3]. The emergent electromagnetism associated in them with the non-coplanar spin structure of skyrmions. One of the possible microscopic mechanisms of the emergence of the magnetoelectric effect in skyrmions is due to the presence of the Dzyaloshinskii-Moriya interaction [1, 2]. Since magnetic skyrmions are now established in insulating materials, where the magnetoelectric multipoles govern the linear magnetoelectric response, one can manipulate electrical properties of skyrmions using applied magnetic fields.

The work examines the magnetoelectric effect of separate skyrmion within the framework of the phenomenological approach. We apply our formalism to skyrmions of different helicities (Neel skyrmion and Bloch skyrmion types). The direction of the local magnetization vector of skyrmion depends on the distance ρ from the skyrmion's center and the polar angle φ. Inhomogeneous distribution of magnetization leads to an inhomogeneous electric polarization [4]. An analytical expression for the polarization has been obtained for skyrmions of different helicities. The action of the magnetic field on the magnetic subsystem causes changes in the inhomogeneous distribution of electric polarization, and consequently, a magnetoelectric response arises [4, 5]. The local and total magnetoelectric responses has been found for the external magnetic field applied in the skyrmion's plane. It has been shown that the response of skyrmion depends on its helicity. Calculations have been carried out for different ansatzes describing the skyrmion's shape.

The study was performed with the financial support from the government assignment for FRC Kazan Scientific Center of RAS.

1. Nagaosa N., Tokura Y.: Nat. Nano. **8**, 899–911 (2013)
2. Bhowal S., Spaldin N.A.: Phys. Rev. Lett. **128**, 227204 (2022)
3. Zhang H., Zhang Y., Hou Z., Qin M., Gao X., Liu J.: Mater. Futures **2**, 032201 (2023)
4. Mostovoy M.: Phys. Rev. Lett. **96**, 067601 (2006)
5. Gareeva Z.V., Shul'ga N.V., Sharafullin I.F., Doroshenko R.A., Zvezdin A.K.: J. Exp. Theor. Phys. **136**, 53–58 (2023)

poster

Effect of counterions in Fe(III) complexes with β-enaminones on their magnetic properties

A.R. Sharipova, E.N. Frolova, O.A. Turanova, L.V. Bazan, A.N. Turanov

Zavoisky Physical-Technical Institute, FRC Kazan Scientific Center of RAS, Kazan, Russia

The presence of a counterion and its nature (geometry and ability to intermolecular interactions) in Fe(III) complexes in most cases significantly alter the crystal lattice, thereby influencing the magnetic properties of the compounds.

Therefore, the study of changes in the magnetic properties of complexes in a series of different counterions is of particular interest, opening up possibilities for fine regulation of the spin state of the Fe(III) ion: LS (S = 1/2), HS (S = 5/2), bistable state (LS + HS), spin-crossover, SCO (mutual transition LS ↔ HS).

The synthesis, identification, and results of magnetic properties study of a new Fe(III) complexes with tridentate NNO donors β-enaminone of the composition $[FeL_2]X$ (L = 1-phenyl-3-(quinolin-8-ylamino)prop-2-en-1-onato), X = SCN (**1**), NO_3 (**2**), Cl (**3**), ClO_4 (**4**) are presented. Fe(III) ion is octahedrally coordinated by four nitrogen atoms and two oxygen atoms from two ligands in the donor environment of N_4O_2 in each complex molecule. The synthesis of the complexes was carried out by the layer-by-layer diffusion method, which eliminates the influence of elevated temperatures during the synthesis process and thereby reduces the likelihood of the formation of chains, oxides and other undesirable structures.

The analysis of the EPR spectra at 4–340 K allowed us to establish that complex **1** exhibits a bistable state. In samples **2** and **3**, smooth incomplete spin cross-overs (SCO) are observed. For sample **4**, almost complete SCO is registered.

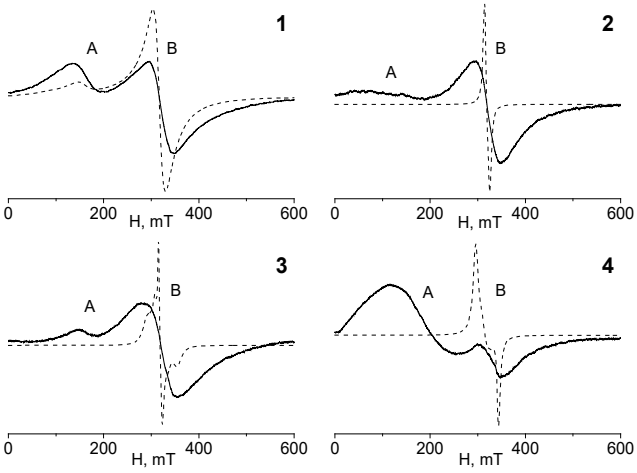

Fig. 1. The shape of the EPR lines of complexes **1**–**4** at 4K (dashed line) and 340K (solid line). A and B indicate the position of lines for HS and LS complexes Fe(III), respectively.

poster

Study of spin-orbit torques induced by current in magnetic tunnel junctions

N.Kh. Useinov

Institute of Physics, Kazan Federal University, Kazan 420008, Russian Federation

The exploration of spin-orbit torque (SOT), which correlates the momentum of the electron with its spin, has given rise to a new field known as spin orbitronics. This field focuses on the manipulation of nonequilibrium material properties via spin-orbit interaction (SOI) [1, 2]. Spin orbitronics has garnered particular attention in metallic and semiconducting systems due to its role in the reciprocal conversion of spin and charge currents. SOI arises from both extrinsic and intrinsic sources. Extrinsic contributions stem from spin-orbit-coupled impurities and interfaces, while intrinsic effects result from spin-orbit interactions in the material's band structure. In low-dimensional multilayered structures, the intrinsic effect, referred to as Rashba SOT, emerges from the breaking of structural inversion symmetry.

In the framework of the quasiclassical Green's function formalism and the nearly free electron approximation, we study the spin-orbit torque induced by the Rashba effect and the tunneling anisotropic magnetoresistance (TAMR) in magnetic tunnel junctions (MTJs) with a single barrier. Our research focuses on a heterostructure with one insulator and ferromagnetic metals: ferromagnetic metal (FM)/insulator (I)/ferromagnetic metal (FM). This heterostructure includes an asymmetric Rashba interface spin-orbit interaction.

The work intends to show that the angular dependence of the tunnel anisotropic magnetoresistance is significantly enhanced by almost an order of magnitude when the Rashba spin-orbit torque is taken into account. This enhancement is retained even at moderate exchange splittings of the spin subbands, which indicates that such MTJs are promising for highly efficient spintronic applications.

Our objective is to develop spin orbitronics: to derive analytical expressions and numerical calculations that cover the key characteristics of the phenomena caused by the Rashba SOI, in particular, the spin-orbit torques (SOT) and TAMR under conditions of applied voltage. For this purpose, the work uses the formalism of quasiclassical Green's functions and the quantum-mechanical derivation of the transmission coefficients of conduction electrons through the MTJ [3]. These methods allow a self-consistent treatment of interfacial SOT, bias voltage effects in realistic electronic band structures.

This work was supported by the Kazan Federal University Strategic Academic Leadership Program.

1. Manchon A., Železný J., Miron I., Jungwirth T., Sinova J., Thiaville A., Garello K., Gambardella P.: Rev. Mod. Phys. **91**, 035004-80 (2019)
2. Fert A., Ramesh R., Garcia V., Casanova F., Bibes M.: Rev. Mod. Phys. **96**, 015005-78 (2024)
3. Useinov N., Zaitsev N., Tagirov L.: Magn. Reson. Solids. EJ **26**, 24112-7 (2024)

poster

Observation of transient nutation on a two-quantum transition

R.B. Zaripov, R.T. Galeev

Zavoisky Physical-Technical Institute, FRC Kazan Scientific Center of RAS, Kazan, Russia

The features of the stationary and echo-detected EPR spectra of the endofullerene triplet state are analyzed. At high amplitudes of the alternating microwave field ω_1, a two-quantum transition is observed in a center of EPR spectrum. The results of the experiment on transient nutation in this area are discussed. It is established that one of the contributions to the nutation oscillates at a frequency of ω_1. This one is associated with the simultaneous excitation of the two transitions of the triplet state (similar to that presented in [1]). The other contribution has a significantly lower frequency them ω_1. It arises due to the excitation of the two-quantum transition.

Endofullerene $Y_3N@C_{80}$ was chosen as the object of study [2, 3]. Transient nutation was realized in the version of a 3-pulse sequence with photoexcitation of the sample by continuous laser irradiation (532 nm, 90 mW).

1. Uvarov M.N., Kulik L.V., Pichugina T.I., Dzuba S.A.: Spectrochimica Acta Part A: Molecular and Biomolecular Spectroscopy (2011)
2. Zalibera M., Krylov D.S., Karagiannis D., Will P.-A., Ziegs F., Schiemenz S., Lubitz W., Reineke S., Savitsky A., Popov A.: Angew.Chem. Int. Ed. **57**, 277–281 (2018)
3. Zalibera M., Ziegs F., Schiemenz S., Dubrovin V., Lubitz W., Savitsky A., Deng Sh.H.M., Wang X.-B., Avdoshenko S.M., Popov A.A.: Chem. Sc. **12**, 7818–7838 (2021)

SECTION 4

SPIN-BASED INFORMATION PROCESSING AND OPTICAL QUANTUM TECHNOLOGIES

oral

Coherent spectroscopy on NV center on invisible transition

S.M. Drofa[1,2,3], V.V. Soshenko[3,4], I.S. Cojocaru[1,3,4], S.V. Bolshedvorskii[3,4], P.G. Vilyuzhanina[1,3,5], E.A. Primak[1,2,3], A.M. Kozodaev[1,3,5], A. Chernyavskiy[1,2,3], V.G. Vins[6], V.N. Sorokin[1,2], A.N. Smolyaninov[4], S.Ya. Kilin[5,7], A.V. Akimov[1,3,4]

[1] Russian Quantum Center, Moscow, 143025, Russia
[2] Moscow Institute of Physics and Technology, Dolgoprudny, Moscow Region, 141701, Russia
[3] P.N. Lebedev Institute RAS, Moscow, 119991, Russia
[4] LLC Sensor Spin Technologies, Moscow, Russia
[5] National Research Nuclear University "MEPhI", Moscow, 115409 Russia
[6] LLC Velman, Novosibirsk, 630060, Russia
[7] B.I. Stepanov Institute of Physics NASB, Minsk, 220072 Belarus

NV center in diamond are popular defects for sensing applications. In particular our group developed rotation sensor utilizing the nuclear spins of nitrogen-vacancy color centers in diamond have been demonstrated. However, such a device consumes significant power which is mainly due to use of RF antenna, controlling nuclear spins of NV centers. Similar porblems appear in other sensors, utilizing nuclear spin in NV centers – either rather strong RF field or strong magnetic field is required. To address this issue, the coherent manipulation of nuclear spins via coherent population trapping at moderate magnetic fields using microwave fields has been successfully demonstrated in isotopically pure diamond.

In this work, we demonstrate that a similar technique can be applied to a diamond plate with a natural abundance of carbon-13, which holds significant potential for practical sensing applications. Although the forbidden resonances required for coherent control were only partially observed, coherent population trapping was successfully demonstrated at both visible and invisible transitions, with an apparent contrast of up to 98±11% and a true contrast of approximately 35±7%. This finding confirms the feasibility of coherent nuclear spin control even in diamond plates with naturally occurring carbon-13.

oral

New mechanism of coherent photons emission

Yu. Bunkov

Russian Quantum Center, 30 Bolshoy Boulevard, Skolkovo, Moscow

In this paper, we propose an original mechanism for generating coherent radiofrequency photons based on Bose–Einstein condensation of magnons.

Coherent photons used in lasers and masers are caused by the quantum-mechanical phenomenon of stimulated (induced) electromagnetic radiation. Excited atoms emit photons with the same quantum state as the stimulated photons. The density of already existing photon states in the resonator is multiplied. We have discovered and demonstrated another method for obtaining coherent photons. It is based on the electromagnetic radiation emitted by magnon from a Bose-Einstein condensate (mBEC). In the case of usual magnetic resonance with a small concentration of magnons, the latter emit photons corresponding to the local frequency of magnons. The resonance line is broadened by both homogeneous and inhomogeneous broadening. In a large number of investigations, we found that as the magnon density increases above the critical value corresponding to the theory of BEC formation for particles and quasiparticles, the magnetic resonance line narrows. Both homogeneous and inhomogeneous line broadening disappears. A magnon, annihilating, emits a photon in the same quantum state as the existing magnon. Therefore, in the case of the formation of a coherent state of magnons in BEC state, they emit coherent photons.

The existence of the magnon Bose condensate was first discovered in superfluid 3He-B [1]. At the same time, the related phenomenon of magnon (spin) superfluidity was discovered [2]. Then mBEC was discovered in superfluid 3He-A [3]. It was then discovered in solid-state antiferromagnets [4]. Finally, magnon Bose condensation was discovered at room temperature in an Yttrium Iron Garnet (YIG) film magnetized perpendicular to its surface. It has been shown theoretically [5] that the mBEC in YIG at room temperature should occur in the conditions when the angles of deflection of magnetization precession exceed of about $\theta = 2.5°$. Experimental studies have shown that the phase transition from magnon gas to mBEC occurs in the range of deflection angles about $\theta = 3°$ [6–8].

In this case, there is no need for a resonator. The role of the resonator is played by magnetic resonance, the frequency of which can be tuned by changing the magnetic field. To achieve the required concentration of magnons, we can use the gain in the feedback line. That is, the emitted photons are amplified by a radio-frequency amplifier. This signal is fed back to the sample. With a sufficient gain, the magnon density is sufficient to form mBEC. That is, the principle of self-generation is realized and at the same time we enter the region of coherent radiation of radio-frequency photons.

We proposed to create a self-generator of coherent radiation based on the following principle. Electromagnetic radiation of the mBEC is picked up by an antenna and fed to the amplification cascade. The signal from this cascade is fed to the emitter, which excites magnons in the same sample. The emitter and antenna are oriented at an angle

of 90° to minimize their direct interaction The presence of feedback with amplification leads to self-generation of radiation.

An important feature of this device is the use of the Bose amplification principle, first proposed by R. Feynman. According to this principle, in the presence of a Bose condensate, new particles can only appear in the quantum state of already existing particles of the ground state. Therefore, even if after the amplification cascade, spectrum of electromagnetic radiation of the emitter broadens due to thermal fluctuations and external noise, these changes will not affect the quantum state of the Bose condensate after the amplification cycle. To accumulate radio frequency photons, one can use a radio engineering resonator and emit this coherent radiation outward using an antenna. Further research into this new method of producing coherent radiation may find mani application in the future.

In this way we have realized the state of a continuously living Bose-Einstein condensate.

This work is supported by Russian science foundation. Grant No. 22-12-00322

1. Borovik-Romanov A.S. et al.: JETP Lett. **40**, 1033 (1984)
2. Borovik-Romanov A.S. et al.: Phys. Rev. Lett. **62**, 1631 (1989)
3. SatoT. et al.: Phys. Rev. Lett. **101**, 055301 (2008)
4. Bunkov Yu.M., Konstantinov D.: JETP Lett., 1**12**, 95 (2020)
5. Bunkov Y.M., Safonov V.L.: Journal of Magnetism and Magnetic Materials **452**, 30–34 (2020)
6. Knyazev G.A. et al.: Optics Express **32**, 8, 13761 (2024)
7. Petrov P.E. et al.: JETP Letters **119**, 118 (2024)
8. Bunkov Yu.M. et al.: Scientific Reports **11**, 7673 (2021)

oral

Influence of nuclear spin on the Rabi frequency of erbium ions doped in a $YLiF_4$ single crystal

Yu.E. Kandrashkin, R.B. Zaripov

Zavoisky Physical-Technical Institute, FRC Kazan Scientific Center of RAS, Kazan, Russia

Rabi oscillations are commonly used to investigate quantum coherence in qubits. Recently, we predicted that the Rabi frequency would depend on the projection of the nuclear spin of the ion when there is a strong hyperfine interaction (HFI) [1]. Strong HFI in rare-earth ions is known to lead to anti-crossing of spin sublevels. This occurs when the HFI is comparable to the Zeeman interaction, resulting in a nonlinear dependence of the electron spin sublevels on the magnetic field. The HFI flip-flop term promotes the mixing of electron-nuclear wavefunctions, described by the ladder operators of electron (S) and nuclear (I) spins: $S_+I_- + S_-I_+$. This term preserves the total magnetic moment of the two spins but alters their projections. For an electron spin of $S = 1/2$, the state with an electron spin projection of $m_S = +1/2$ borrows some contribution from the state with a projection of $m_S = -1/2$. Consequently, the ion's interaction with local fields decreases. It has been shown that strong HFI reduces electron spin interactions in other directions as well, particularly in the plane perpendicular to the direction of the external field [1]. Thus, the ion's reduced magnetic moment affects its interactions with the microwave field.

Here, we report the experimental evidence of this phenomenon. Significant changes in the Rabi frequencies were observed in nutation experiments on the isotopically pure $YLiF_4$ single crystal doped with ^{167}Er ($I = 7/2$) ions (see Fig. 1). The nutation frequencies were measured at several magnetic fields corresponding to nuclear spin-allowed EPR transitions. The obtained experimental data are in good agreement with the results of the theory. Changes in nutation frequencies result from the difference in the mixing of spin wavefunctions, which is caused by changes in the ratio of the strengths of the hyperfine and Zeeman interactions.

1. Kandrashkin Yu.E., Journal of Magnetic Resonance **365**, 107728 (2024)

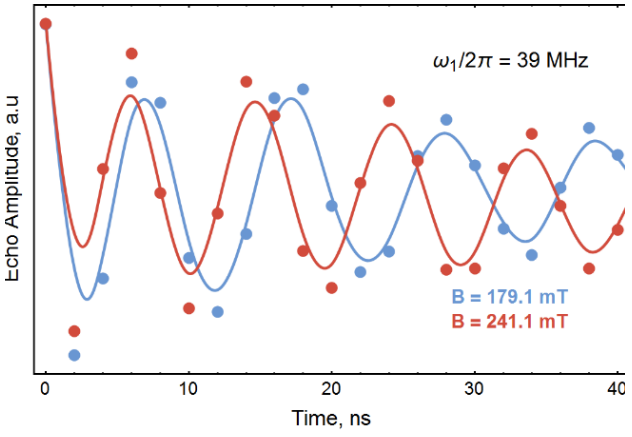

Fig. 1. Three pulse nutation data are shown as a function of the first microwave pulse length at two erbium ion EPR transitions, with a fixed microwave irradiation amplitude of $\omega_1/2\pi$ = 39 MHz. The points represent the experimental data and the curves represent the basis spline function of the data.

oral

Collective modes approach for simulating the shape of EPR lines

S.O. Travin[1], K.M. Salikhov[2]

[1] N.N. Semenov Federal Research Center for Chemical Physics Russian Academy of Sciences, Moscow
[2] Zavoisky Physical-Technical Institute, FRC Kazan Scientific Center of RAS, Kazan, Russia

The shape of the EPR spectrum in conditions when spin exchange is an essential feature of the spin system contains peculiar information about . The mathematical model of such systems used in our work was the paradigm of collective modes developed by Kev Salikhov in the last ten or more years [1]. Our task was to extract the quantitative parameters of this model and correlate them with the physical characteristics of the environment in which the measurements were taken. Thus, our idea, if successfully developed, can be used to determine the characteristics of molecular dynamics in a wide variety of objects, such as membranes, glasses, colloidal systems, semiconductors, superconductors etc.

At present, the most widespread approach for simulating and analyzing the EPR spectra in the presence of the coherence and dephasing transfer is usage of pseudo-Voigt individual line shape for each individual resonance. Despite the fact that this method most often gives an excellent fit of experimental spectra, it suffers from a very serious inherent drawback: an excessive number of tuning parameters. And the inevitable consequence of this vice is that it is extremely difficult to give any physical meaning to these parameters, especially to compare them with theoretical forecasts.

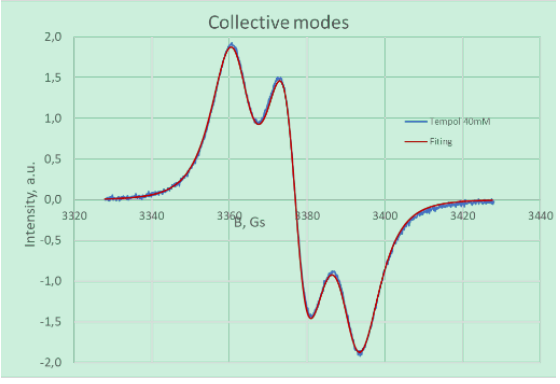

Fig. 1. Typical fitting of EPR line with collective mode eigen resonances, including absorption and dispersion. Note, that regression function includes only three adjustable parameters.

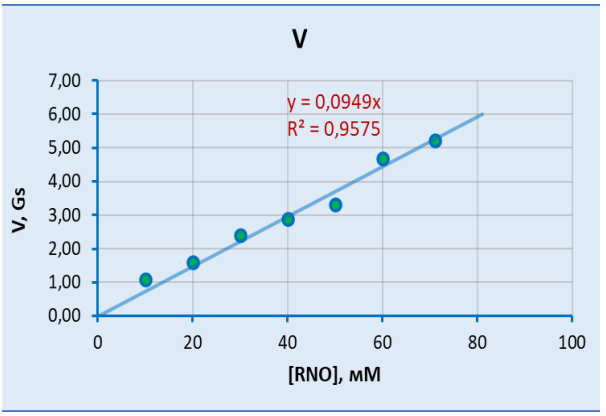

Fig. 2. Linear dependence of empirically determined coherence transfer rate on the concentration of radical. The slope of the straight line allows to determine the diffusion coefficient in the medium and the collision radius for the exchange interaction.

The alternative approach is to numerically simulate spectra and to fit the spectrum observed in a real experiment by varying the coherence transfer rates using eigenvectors of spin-Hamiltonian.

New approach [2] is based on finding the collective coherence modes. It makes possible to describe on a common platform the transformations of spectra at any coherences transfer rates: from the very slow coherence transfer rate which leads to line broadening, then to the rate which gives the coalescence (or association) of the spectral lines and further to the very fast rate which leads to exchange narrowed spectra.

In this case the number of adjustable parameters in the model is minimal. For example the spin exchange for triplet spectra of TEMPOL in the wide range of concentrations can be fitted with collective mode with only three parameters (Fig. 1), instead of 12 parameters for pseudo-Voigt approach.

Moreover, all these three parameters (namely hyperfine splitting a, own line width $\Gamma = 1/T_2$ and coherence transfer rate $V = k_{ex}C$) has very clear sense and can be quantitively estimated theoretically.

On the Fig. 2 there is plot of concentration dependence of V, from which one can readily estimate the mobility of the radical in the medium (it's diffusion coefficient) and the collision radius for the exchange interaction.

1. Salikhov K.M.: Fundamentals of spin exchange. story of a paradigm shift. © Springer Nature Switzerland AG 2019
2. Salikhov K.M.: Consistent paradigm of the spectra decomposition into independent resonance lines. Appl. Magn. Reson. **47**, 1207–1227 (2016)

poster

Implemenetation of quantum computing on high-spin ions of paramagnetic complexes using phase-modulated microwave pulses

M.R. Arifullin, V.L. Berdinskiy

Orenburg State University, Orenburg, Russia

Quantum computing is becoming a groundbreaking technology that has attracted widespread attention around the world. In the race to develop quantum computers over the past three decades, the leading platform has changed from one system to another over time. It is possible that a completely new type of qubit, which has not yet been proposed or implemented, could lead to significant breakthroughs in quantum computing. Therefore, it is essential to properly design and develop physical qubits in order to build scalable quantum computers [1].

The use of high-spin ions embedded in crystal matrices as a new qubit platform would avoid the technical difficulties associated with other qubit platforms, such as high vacuum, strong magnetic fields, and laser radiation. This would simplify the management of qubits and scale systems, increasing the stability and reliability of their operation.

One of the unique advantages of this approach based on microwave manipulation of high-spin ions allows the use of multi-spin paramagnetic ions to manipulate individual qubits, for example, a high-spin paramagnetic center with spin $S = 2$ in a zero magnetic field that is rich in energy levels. To describe the implementation of quantum computing algorithms, it is necessary to have a consistent theory of pulsed spin evolution for high-spin ion systems.

The vast majority of modern magnetic resonance theories focus on describing spin dynamics and relaxation in strong magnetic fields. In order to construct control pulse sequences for implementing quantum computing on high-spin systems in zero magnetic fields, we need a rigorous and consistent theory for their spin evolution.

As a first step in studying the possibilities of high-spin ions, it is necessary to study the spin dynamics of particles whose state is described by the zero-field splitting Hamiltonian without taking anisotropy into account. The spin states of paramagnetic ions in zero magnetic fields do not produce the observed magnetization; they correspond to states that are described in optical spectroscopy by the term “alignment”. These states are entangled states of the types $T_+ + T_-$ and $T_+ - T_-$. Therefore, the proposed theory must describe microwave control of the “alignment” of ion spin states and its transformation into “orientation”, or magnetization [2–3].

Resonant microwave pulses are also capable of creating magnetization of high-spin ($S \geq 1$) metal ions, even in the absence of an external magnetic field. This transformation of the spin states of ions is similar to the alignment-orientation transition in atomic spectroscopy, which allows the use of universal quantum gates in a single operation.

The phase jump of the high-frequency component of the microwave pulse is equivalent to a change in the direction of the vector of the effective magnetic field in a

rotating coordinate system. If the frequency of the microwave pulse coincides with the Larmor precession frequency, then a change in orientation of the vector in the rotating frame will change the trajectory of evolution of electron spin in multi-spin systems. These trajectories allow changing spin states of the system. However, the results of the action of microwave pulses with a phase jump strongly depend on both the initial state of electron spins and their "inclusion" in entangled multispin states.

1. Nielsen M.A., Chuang I.L. Quantum Computation and Quantum Information. Maidenhead: Cambridge University Press (2000). 700 p.
2. Arifullin M.R., Berdinskiy V.L.: Physics of the Solid State **62**, 3 (2020)
3. Arifullin M.R., Berdinskiy V.L.: Russ. Phys. J. **63**, 5 (2020)

poster

Magnetic memristor based on cobalt-implanted rutile (TiO_{2-x}): VSM, MOKE and FMR studies

E.M. Begishev, N.M. Lyadov, V.V. Bazarov, A.A. Sukhanov, R.I. Khaibullin

Zavoisky Physical-Technical Institute, FRC Kazan Scientific Center of RAS, Kazan, Russia

It is well known that non-stoichiometric rutile (TiO_{2-x}) exhibits a memristive effect caused by the migration of positive charged oxygen vacancies under an applied electric field [1]. Additionally, oxygen vacancies may act as mediators of long-range magnetic order in magnetically diluted (3d-ions doped) oxide semiconductors such as TiO_{2-x} and SnO_{2-x} [2, 3]. For the first time, we propose combining the memristive properties of non-stoichiometric cobalt-ions doped titanium dioxide with its ferromagnetic properties to form novel non-volatile memory cells – magnetic memristors for semiconductor spintronic.

The 40 keV cobalt ions were implanted into the single crystalline (001)-rutile plates TiO_2 at the fixed fluence of 1.5×10^{17} ions/cm^2 and substrate temperature of 900 K but at different ion currents density (j) in the range of 3–10 μA/cm^2. Then strip-type memory cells (Fig. 1) with dimensions ranging from 100 to 800 μm were fabricated on Co-ions implanted rutile samples by using electron-beam lithography and ion-beam deposition of gold contacts.

The lithographic samples of magnetic memristors were characterized using ferromagnetic resonance technique (FMR), vibrating sample magnetometry (VSM) and magneto-optic Kerr effect (MOKE) measurements at room temperature.

The analysis of FMR spectra taken in out-of-plane geometry of the applied magnetic field shows the presence of two ferromagnetic phases in the Co-ions implanted rutiles. The first anisotropic phase is metallic cobalt nanoparticles exhibiting high-field resonance, and second ones is an isotropic solid solution of magnetically coupled Co^{2+} ions exhibiting low-field resonance. It was established that the cobalt nanoparticles phase dominates in the rutile samples implanted at high value j of 8–10 μA/cm^2. On the other side, the diluted

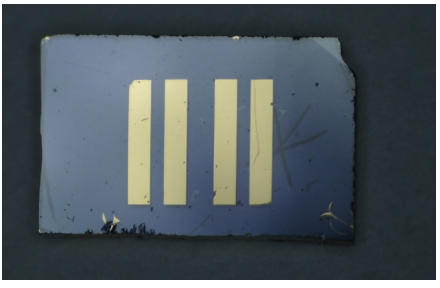

Fig. 1. An example of lithographic structure formed on a rutile plate TiO_{2-x} implanted with cobalt ions.

poster

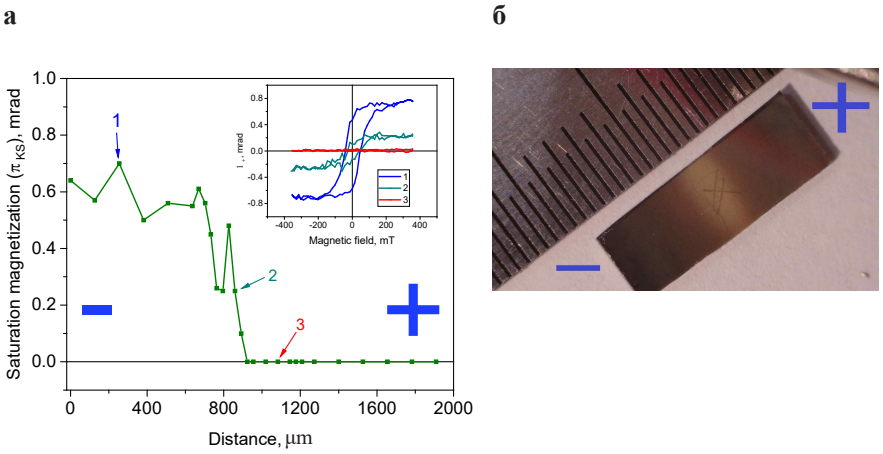

Fig. 2. Effect of spatial distribution of oxygen vacancy concentration on the magneto-optical response in the rutile implanted with cobalt ions at the fluence of 1.5×10^{17} ions/cm^2 and $j \sim 3$–4 μA/cm^2. (**a**) Saturation magnetization (expressed in Kerr angle Θ_K units) distribution along the oxygen vacancy migration path. (**b**) Photo of the sample after oxygen vacancy migration procedure. The places of application of electrical potentials are indicated by the symbols "+" and "–".

magnetic phase of Co^{2+} ions is mainly formed in the samples implanted at low j of 3–4 μA/cm^2.

Both VSM and MOKE measurements show a strong influence of oxygen vacancies content on magnetization and magneto-optical response (MOKE) (Fig. 2). Namely after electromigration of positively charged oxygen vacancies in lithographic cells of Co^{2+} diluted magnetic sample, the MOKE signal became 2–3 times stronger in vacancy-rich regions of cell compared to the initial state or drop nearly to zero in vacancy-depleted regions of cell. In contrast, no such effect was detected in nanocomposite rutile samples with magnetic nanoparticles of cobalt.

Moreover, for the first time we demonstrate the fundamental possibility of writing and rewriting information bits in the fabricated lithographic structures by applying voltage pulses to memory cells while simultaneously reading data via the registration of magneto-optical response in cells.

1. Lee J.S., Lee S., Noh T.W.: Appl. Phys. Rev. **2**, 031303 (2015)
2. Begishev E.M., Shmelev A.G., Zharkov D.K. et al.: Bull. Russ. Acad. Sci.: Phys. **88**, 2034–2041 (2024)
3. Khaibullin R.I., Gumarov A.I., Vakhitov I.R. et al.: Condens. Matter. **9**, 27 (2024)

SECTION 5

STRONGLY CORRELATED ELECTRON SYSTEMS

oral

Low-frequency dynamics of $LiCu_3O_3$ – a strongly depleted antiferromagnet

S.K. Gotovko[1], A.G. Ivanova[2], P.S. Kudimkina[1], M. Hemmida[3], H.-A. Krug von Nidda[3], L.E. Svistov[1]

[1] P.L. Kapitza Institute for Physical Problems RAS, Moscow, Russia
[2] Shubnikov Institute of Crystallography, Kurchatov Complex Crystallography and Photonics of NRC "Kurchatov Institute", Moscow, Russia
[3] Experimental Physics V, Center for Electronic Correlations and Magnetism, Institute of Physics, University of Augsburg, Augsburg, Germany

$LiCu_3O_3$ is a novel representative of cuprates with mixed valence with spin $S = 1/2$ on a depleted square lattice. It is a unique example of such systems not only because of the high dilution rate but also because the crystal structure of this compound exhibits two types of square lattices with different $Li^+ \rightarrow Cu^{2+}$ substitution ratios simultaneously: 20% in some planes and 40% in other planes (Fig. 1, left panel). These features are an inherent characteristic of the $LiCu_3O_3$ crystal structure. Due to the configuration of exchange interactions, it is natural to expect that planes with different Li^+/Cu^{2+} ratios are magnetically separated. The substitution ratio of 40% in some of the planes is extremely close to the percolation threshold of a 2D square lattice, $x_p \approx 41\%$, which makes the establishment of the long-range order in separate planes problematic.

The previous studies of this unique compound with nuclear magnetic resonance (NMR), magnetization measurements [1] and neutron scattering [2] revealed the occurrence of antiferromagnetic order at $T_{c1} = 123$ K with the wave vector $\mathbf{k} = (1/2,0,1/2)$

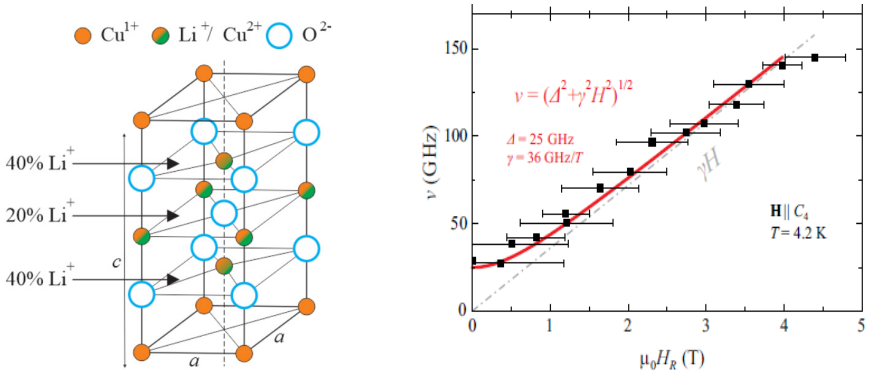

Fig. 1. Left panel: Crystallographic structure of $LiCu_3O_3$. Orange-green circles mark the positions occupied with randomly distributed magnetic Cu^{2+} ions and non-magnetic Li^+ ions, orange circles – non-magnetic Cu^+ ions, blue circles – O^{2-} ions. Right panel: The frequency-field diagram measured at $\mathbf{H} \parallel C_4$, $T = 4.2$ K. The ESR resonances are marked by solid symbols. Segments at each point indicate HWHM of corresponding absorption lines. The red line shows the result of quasilinear approximation with parameters given in Figure. The dash-dotted line is the paramagnetic $\upsilon(H)$ with $\gamma = 36$ GHz/T.

oral

and the change of the magnetic state at $T_{c2} \approx 30$ K. At the same time, broad continuous NMR spectra below T_{c1} reflect that the situation in the crystal is far more complicated than simple collinear antiferromagnetic ordering.

.In recent EPR experiments, only one branch of magnetic resonance was obtained (Fig. 1, right panel) with the temperature behavior not characteristic for ordered magnets. The intensity of the absorption line also demonstrates a decrease at $T \approx T_N$, which is why we suggest that a) two different magnetic subsystems indeed are present in the crystal and b) the signal we observed at low temperatures is the quasi-paramagnetic signal from the disordered highly-depleted subsystem. No additional branches at $\upsilon < 140$ GHz or traces of AFM resonance in ordered subsystem were observed probably due to the high values of the frequency gap in AFM subsystem or a small intensity.

The behavior of the gap of the observed magnetic resonance spectra indicates that this gap is, in fact, not a gap of relativistic nature but a pseudogap of exchange nature associated with finite-sized clusters of magnetic ions. The results were published in [3].

The work was supported by Russian Science Foundation (grant № 22-12-0259-P).

1. Bush A.A., Gotovko S.K., Ivanov V.Yu., Kozlov V.I., Nikolaev E.G., Svistov L.E.: Physical Review B **109**, 115151 (2024)
2. Consiglio A. et al.: Physical Review Letters **132**, 126502 (2024), Supplemental materials
3. Gotovko S.K., Ivanova A.G., Kudimkina P.S., Bush A.A., Kozlov V.I., Hemmida M., Krug von Nidda H.-A., Svistov L.E.: Physical Review B **111**, 064430 (2025)

oral

Current-induced g-factor tuning in zinc oxide-based heterostructures

G.A. Nikolaev[1,2], T.M. Kurbanov[1,2], O.V. Orlov[1,2], S.A. Andreeva[3,1], A.V. Shchepetilnikov[1], I.V. Kukushkin[1]

[1] Institute of Solid State Physics, Russian Academy of Science, Chernogolovka, Russia
[2] Moscow Institute of Physics and Technology (National Research Institute), Dolgoprudnyi, Russia
[3] HSE University, Moscow, Russia

The work studies electron spin resonance (EPR) in a strongly correlated electron system of a ZnO/MgZnO heterostructure. Recently, unexplained additional resonance lines in such structures have been discovered in the range of small magnetic fields. To understand the nature of the phenomena, we successfully adapted the method from [1]: in two-dimensional electronic systems with Bychkov-Rashba (BR) spin-orbit interaction the *g*-factor changes with changes in DC current density (Fig. 1a). The conditions of the experiment are shown in the inset to the Fig. 1a. For the effect to be observed, the effective BR magnetic field δB must be aligned with the external magnetic field *B*, so the current must be applied perpendicular to B. Otherwise, the position of the EPR line will not change significantly with current density. (Fig. 1b). The method will

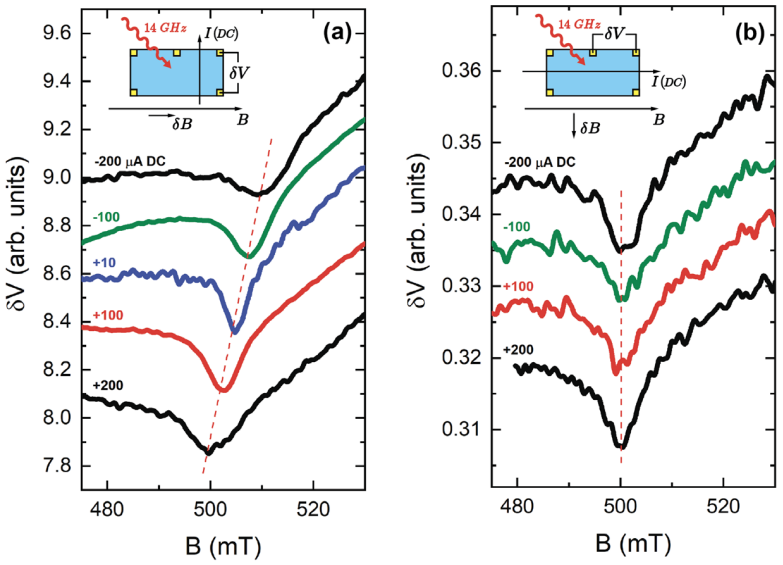

Fig. 1. EPR lines for different orientations of current and measured photovoltage signal. **a** Effective Bychkov-Rashba magnetic field **δB** is oriented along magnetic field **B**. A change in current density changes **δB** magnitude, so changes the *g*-factor. **b δB** is perpendicular to **B**, so *g*-factor is constant within the current range under investigation. Resonance frequency is 14 GHz.

allow separating EPR associated with conduction electrons from the EPR of Zn ions and oxygen vacancies [2].

The experiment was conducted in a He3 cryostat at a temperature of 0.5 K with the ability to change the magnetic field up to 15 T. Indium contacts were formed on the sample in the van der Pauw geometry. Electromagnetic radiation with a frequency from 1 to 40 GHz was used to excite the electron spin resonance. It was generated by a microwave generator and fed to the sample via a coaxial cable. EPR was detected in photovoltage signal using lock-in amplifier.

1. Wilamowski Z., Malissa H., Schäffler F., Jantsch W.: *g*-Factor tuning and manipulation of spins by an electric current: Phys. Rev. Letters **98**(18), 187203 (2007)
2. Bera A., Basak D.: Manifestation of spin-spin interaction between oxygen vacancy and magnesium in ZnMgO nanorods by electron paramagnetic resonance studies.: Applied Physics Letters **99**(19) (2011)

oral

Scaling behavior of superconductors

V.R. Shaginyan

Petersburg Nuclear Physics Institute of NRC "Kurchatov Institute"

In our report, we analyze the scaling of the condensation energy $E\Delta$ divided by γ, $E\Delta/\gamma \sim N(0)\Delta/\gamma$, and quasiparticles of both conventional and unconventional superconductors, where N(0) is the density of states at zero temperature $T = 0$, $\Delta 1$ is the maximum value of the superconducting gap, and γ is the Sommerfeld coefficient. It is shown that Bogoliubov quasiparticles act in superconducting states of unconventional and conventional superconductors. At the same time, quasiparticles are also present in the normal state of unconventional superconductors. We briefly describe the difference between unconventional superconductors and conventional ones, such as the resistivity in normal states and the difference in superfluid density in superconducting states. For the first time, we theoretically show that the universal scaling of $E\Delta/\gamma \sim T2c$ applies equally to both conventional and unconventional superconductors. Our consideration is based on two experimental facts: Bogoliubov quasiparticles act in conventional and non-conventional superconductors and the corresponding flat band is deformed by the non-conventional superconducting state. As a result, our theoretical observations based on the theory of fermion condensation agree well with the experimental facts [1]. We also consider the Homes' law and explain its application to superconductors.

1. Shaginyan V.R., Msezane A.Z., Artamonov S.A.: General Properties of Conventional and High-Temperature Superconductors. Crystals **14**(9), 826 (2024)

oral

ESR evidence of high-temperature magnetic transitions in noncentrosymmetric ternary carbide $GdCoC_2$

S.V. Demishev[1,2,3], A.V. Shestakov[3], I.I. Fazlizhanov[4], I.V. Yatsyk[4], R.M. Eremina[4], A.V. Bokov[1], D.A. Salamatin[1], A.V. Semeno[1,3], A.V. Tsvyashchenko[1]

[1] Vereshchagin High Pressure Physics Institute, RAS, 108840, Troitsk, Moscow, Russia
[2] HSE University, 101000, Moscow, Russia
[3] Prokhorov General Physics Institute, RAS, 119991, Moscow, Russia
[4] Zavoisky Physical-Technical Institute, FRC Kazan Scientific Center of RAS, Kazan, Russia

The compound $GdCoC_2$, a unique ternary carbide with a noncentrosymmetric orthorhombic structure, attracts attention due to its complex phase transitions, including a PM–FM transition and a commensurate–incommensurate transformation, as well as a pronounced magnetocaloric effect [1–3]. The presence of non-collinear magnetic states and formation of spin textures at low temperatures $T \sim 15$ K caused by interplay of ferromagnetic and Dzyaloshinskii–Moriya interactions results in an anomalously large topological Hall effect [1]. The above interesting physics is based on the consideration of the magnetism of Gd magnetic ions. The present study aims at investigation of the magnetic properties of $GdCoC_2$ over a wide temperature range 5-600 K using ESR spectroscopy, providing comprehensive insight into its phase transformations and spin dynamics. The sample was synthesized under high-pressure conditions (8 GPa, 1500–1700 K) using a toroidal chamber at HPPI RAS.

The ESR measurements were carried out in two temperature ranges (5–120, 154–623 K) at microwave frequency ~9.4 GHz (X-band) using Bruker EMX/plus and Varian E12 spectrometers.

The ESR spectra recorded at different temperatures consist of one to four distinct resonance lines (Fig. 1).

Line “L1” (shown in black) emerges at ~15 K in the low-field region and persists up to 450 K. Below room temperature, its integrated intensity remains relatively stable; however, above room temperature, the intensity drops sharply, accompanied by a decrease in linewidth.

Line “L2” (red) is observed throughout the entire temperature range. At low temperatures ($T < 7$ K), it exhibits ferromagnetic characteristics, transitioning to a paramagnetic response above ~30 K ($g \approx 2$). As temperature increases, the line narrows and its integrated intensity gradually decreases up to ~500 K, after which the intensity and linewidth begin to increase.

Line “L3” (blue) is registered similarly to L1, starting from ~15 K. Its intensity reaches a minimum at ~350 K, after which it broadens significantly and grows in intensity. The corresponding g-factor varies within the range of ~3 to ~4.4.

oral

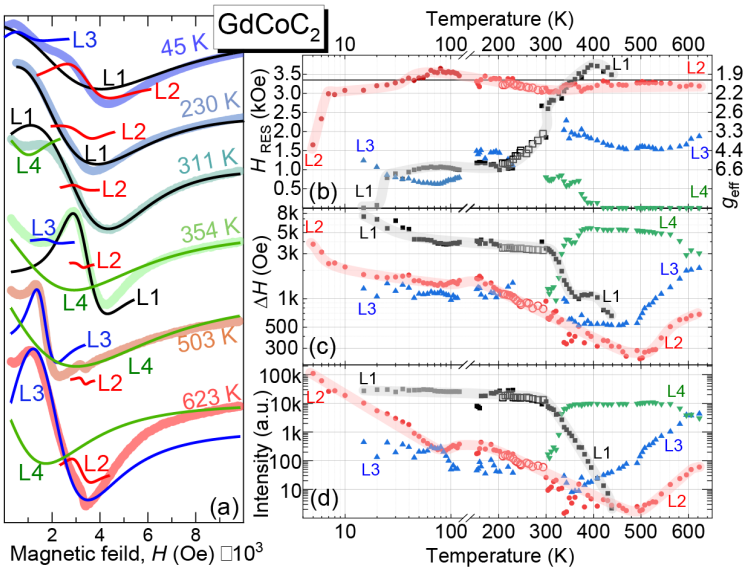

Fig. 1. Temperature evolution of the ESR spectrum of $GdCoC_2$ (**a**); Temperature dependence of the ESR resonance field (**b**), linewidth (**c**) and intensity (**d**).

Line "L4" (green) becomes detectable at ~300 K, with its intensity peaking around 340 K. As the temperature increases further, the resonance field of L4 shifts toward zero, and its parameters subsequently remain nearly unchanged.

These observations indicate several characteristic temperature regions with notable changes in the ESR spectra:

Low-temperature region ($T < 30$ K): presence of ferromagnetic resonance.

Near and above room temperature ($T \gtrapprox 300$ K): emergence of lines L3 and L4.

High-temperature region ($T > 500$ K): growth in the intensity of line L2.

The restructuring of the high-temperature ESR spectra suggests the occurrence of additional magnetic transitions around $T \approx 350$ K and $T \approx 500$ K. This effect constitutes new high temperature magnetic transitions, which may be attributed to the filling of excited states of the Co magnetic ion with increasing temperature.

Support from RSF grant 22-12-00008-П is acknowledged.

1. Xu Y., Ren W. Ma S. et al.: Appl. Phys. Lett. **123**, 072402 (2023)
2. Matsuo S., Onodera H., Kosaka M. et al.: JMMM **161**, 255–264 (1996)
3. Meng L., Xu C., Yuan Y. et al.: RSC Adv. **6**, 74765–74768 (2016)

oral

Critical temperature and order parameter modulation in superconducting heterostructures with domain-structured ferromagnets

V.A. Tumanov, Yu.N. Proshin

Kazan Federal University, Kazan, Russia

Superconductor/ferromagnet (S/F) heterostructures exhibit unique phenomena due to the interplay between superconducting correlations and magnetic ordering [1]. This study focuses on the impact of magnetic domain structures on proximity effects. We also take into account the nonzero electron-electron coupling constant λ_f in ferromagnetic layers [2]. More specifically, we consider S/F/S and F/S/F systems, in which one or both ferromagnetic layers are divided into a periodic system of strip domains (see Fig.1).

.To describe such systems in the dirty limit, we used the Usadel equations taking into account the heterogeneity of the effective exchange field [3]. The boundary conditions include the Kupriyanov-Lukichev conditions [4] at the S/F interfaces and zero current at the external boundaries. The boundary value problem is supplemented by a self-consistency equation that connects the order parameter and the Usadel function. To find the critical temperature in heterostructures with complex magnetic textures, we have developed an iterative approach [5]. In this approach, the normalized spatial distribution of the superconducting order parameter and the critical temperature are refined at each step.

The presence of magnetic inhomogeneities, such as domain walls, leads to an increase in the critical temperature compared to a monodomain case. In the S/F/S systems, the domain structures shift and suppress the T_c minimum versus the F-layer thickness d_f compared to monodomain F-layers. In the F/S/F systems, T_c strongly depends on the mutual orientation of magnetizations in the F-layers and the domain period l_d. If l_d is less than or equal to the superconducting coherence length ξ_s, domain effects dominate; for large l_d the mutual orientation dominates. The order parameter is suppressed within ferromagnetic domains but enhanced near domain walls due to weakened pair-breaking.

In a bulk ferromagnet, an electron-electron coupling does not manifest itself due to the suppression of pairing by ferromagnetic ordering. In the S/F structures the nonzero

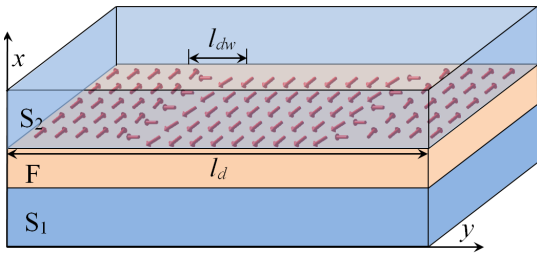

Fig. 1. Schematic image of the $S_1/F/S_2$ system, where ferromagnetic layer is divided into strip domains by the Néel domain walls. The arrows symbolize the local directions of magnetization. l_{dw} is the domain wall thickness.

oral

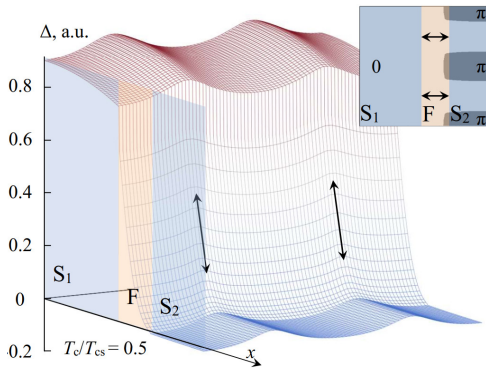

Fig. 2. Distribution of the superconducting order parameter in the S_1(140 Å)/F(57 Å)/S_2(100 Å) system. The inset shows the distribution of the order parameter phase in the plane of this system. Key layers parameters: ξ_s = 125 Å, effective exchange field I = 200 K, characteristic attenuation length (F-layer) ξ_1 = 20.4 Å, coherence length (F-layer) ξ_f = 70 Å, λ_f = 0.179, l_d = 5000 Å, l_{dw}/l_d = 0.015. T_{cs} is the critical temperature of bulk superconductor. See work [6] for more details.

λ_f noticeably increases T_c in both S/F/S and F/S/F systems, broadening parameter ranges for observing phenomena like isolated reentrant superconductivity [2] in asymmetric F/S/F structures.

Periodic magnetic domains enable spatial alternation of the superconducting order parameter phase (0 and π states), forming superconducting phase domains with a specially selected thickness of the ferromagnetic layer. This state was previously proposed for special design of the Josephson junction [7]. In the cited work, the S-F/N-sIS system was considered, where the normal metal area and the homogeneous ferromagnetic region serve as the domain wall and the domain itself, respectively. For the S/F/S system geometry considered in our research there is a set of π-contacts in the plane of the boundary, and alternating 0- and π- contacts perpendicular to the boundary (see Fig. 2). Such system can be used as a controllable 0-π Josephson junction [8], by adding small superconducting contacts separated from the system by a nonmagnetic barrier. The contacts can be placed either on the S layers separated by the ferromagnetic layer or both on a thinner S_2 layer. The F/S/F system can be used in a similar way if a small superconducting contact is placed on the surface of the polydomain ferromagnetic layer. Phase control can be achieved by manipulating domain wall positions via an external magnetic field or switching magnetization in adjacent layers [9]. The predicted phase domains in the S/F/S and F/S/F systems can be useful for superconducting spintronics and memory elements.

1. Buzdin A.I.: Rev. Mod. Phys. **77**, 935–976 (2005)
2. Khusainov M.G., Khusainov M.M., Ivanov N.M., Proshin Yu.N.: JETP Lett. **89**, 626–631 (2009)
3. Bergeret F.S., Volkov A.F., Efetov K.B.: Rev. Mod. Phys. **77**, 1321–1373 (2005)
4. Kupriyanov M., Lukichev V.: Sov. Phys. JETP **67**, 1163–1168 (1988)
5. Tumanov V.A., Proshin Y.N.: JETP Lett. **120**, 608–615 (2024)
6. Tumanov V.A., Proshin Y.N.: Phys. Metals Metallogr. **125**, 237–244 (2024)
7. Bakurskiy S.V., Klenov N.V., Soloviev I.I., Kupriyanov M.Yu., Golubov A.A.: App. Phys. Lett. **108**, 042602 (2016)
8. Gingrich E.C., Niedzielski B.M., Glick J.A., Wang Y., Miller D.L., Loloee R., Pratt W.P. Jr., Birge N.O.: Nat. Phys. **12**, 564-567 (2016)
9. McGilly L.J., Yudin P., Feigl L., Tagantsev A.K., Setter N.: Nat. Nanotechnol. **10**, 145–150 (2015)

oral

Spin chains with non-magnetic defects: NMR studies

E.L. Vavilova

Zavoisky Physical-Technical Institute, FRC Kazan Scientific Center of RAS, Kazan, Russia

Spin chains are a special case of one-dimensional spin systems, i.e. systems where spin interactions along one of the spatial directions are significantly bigger than along the other two. The ground state and temperature behavior of the magnetism of such chains are nontrivial and depend on a number of factors, primarily on the type of the spin and the type and magnitude of the spin interaction(s). The presence of defects introduces an additional degree of freedom into the spin system and can significantly affect its properties. Nuclear magnetic resonance (NMR), being a local dynamic method, has proven itself in studies of low-dimensional and frustrated systems, as well as compounds with defects in spin and crystal structure. This report will consider the effect of spinless inclusions on the properties of chains with different spin values and combinations of interactions. We will discuss the classical Heisenberg chain, the Haldane chain, the chain with alternating interactions, and the chain with frustration of interactions between nearest and next-nearest neighbors.

oral

EPR and optical spectra, and double-loop magnetic hysteresis of SrY_2O_4:Dy crystals

R.V. Yusupov, S.I. Nikitin, B.F. Gabbasov, R.G. Batulin, A.G. Kiiamov, B.Z. Malkin

Institute of Physics, Kazan Federal University, Kazan, Russia

Complex oxides SrR_2O_4 (where R is Y or a rare-earth metal) possess a specific quasi-one-dimensional structure of orthorhombic symmetry with the space group Pnam. The unit cell contains 4 formula units, the lattice constant c = 0.341 nm is about three times less than the lattice constants a =1.007 nm and b =1.191 nm, and each of 28 sublattices is formed by ionic chains running along the c-axis. The impurity Dy^{3+} ions substitute for Y^{3+} ions at two nonequivalent crystallographic sites Y1 and Y2 with the point symmetry group C_s. Magnetically concentrated crystals $SrDy_2O_4$ manifest a classic spin-liquid behavior that is undoubtedly related to the specific single-ion spectral and kinetic properties of the dysprosium subsystem.

The reported study includes the synthesis of single-crystal samples of SrY_2O_4 compound doped with 0.01 at.% and 0.5 at.% of the Dy^{3+} ions. Investigations of the oriented samples with EPR spectroscopy provided an information on the g-factor principal values and principal directions with respect to crystallographic axes and thus on the ground Kramers doublet wavefunctions. Hyperfine coupling constants for odd ^{161}Dy and ^{163}Dy isotopes were also determined.

Thorough measurements of the optical luminescence and excitation spectra with site-selective laser spectroscopy allowed to determine energy level structures of the ground $^4F_{9/2}$ as well as excited ^6H_J (J = 5/2, 7/2, 9/2, 11/2, 13/2, 15/2) and ^6F_J (J = 11/2, 9/2) multiplets of the two nonequivalent Dy^{3+} centers in the SrY_2O_4:Dy (0.5 at.%) single crystal.

Bestfit of energy level pattern within the exchange charge model have given the sets of fifteen crystal field parameters for each of the of the Dy1 and Dy2 centers.

Probably, the brightest result of our study was obtained with the quasi-static vibrating-sample magnetometry: if the magnetic field was applied along the crystallographic b-axis and the sample temperature was below 10 K, a peculiar double-loop hysteresis was observed. The shape of the hysteresis curve depended on temperature, field sweep rate and concentration of the Dy^{3+} impurity in the sample. We show that the observed hysteresis originates from very slow magnetic relaxation of the Dy2 centers: the measured with magnetometer lifetime achieved 1444 seconds at T = 2 K and B = 0.07 T.

Hysteresis curves were successfully reproduced within a model based on the numerical solution of generalized master equations with time-dependent transition probabilities induced by the electron-phonon interaction, quantum tunneling, and cross relaxation [4].

1. Malkin B.Z.: Crystal field and Electron–Phonon Interaction in Rare-Earth Ionic Paramagnets, in: Spectroscopy of solids containing rare-earth ions, ed. by A.A. Kaplyanskii and R.M. Macfarlane, Elsevier Science Publishers, Amsterdam (1987), ch. 2, p. 13-49.
2. Malkin B.Z. et al: Phys. Rev. B **109**, 054434 (2024)

poster

Investigation of the oxidation processes of cobalt thin films by the FMR method

D.A. Arbuzov, A.A. Validov, N.N. Garyf'yanov, A.A. Kamashev, I.A. Garifullin

Zavoisky Physical-Technical Institute, FRC Kazan Scientific Center of RAS, Kazan, Russia

One of the elements of the superconducting spin valve of the F1/F2/S design is the antiferromagnetic layer lying under the F1 layer, which serves to fix the direction of magnetization of the F1 layer. In our previous works, we used a 3 nm cobalt layer deposited by electron beam evaporation and oxidized in an oxygen atmosphere at a pressure of 100 mbar for two hours in a loading chamber [1].

In this work, we investigated the rate of oxidation processes of different thicknesses of cobalt metal films in air, as well as the possibility of preparing cobalt oxide by oxidation with heating to 600 K in air.

For this purpose, a series of samples with thicknesses of 3, 5 and 10 nm were prepared on MgO substrates. In each series, one sample was protected with Si_3Ni_4, one was oxidized by the "standard method" and one sample was an unprotected cobalt film. In addition, we annealed one film in air at $T = 600$ K for 20 minutes, and another one in several stages, the first for 5 minutes, the second for 20 minutes, and the third for 8 hours. FMR was chosen as the research method, since it can be very effective in studying the ferromagnetic component of samples.

As is known, metallic cobalt is a strong ferromagnet, but when oxidized, it transforms into an antiferromagnetic state with a Neel temperature of ~293 K. We hoped to see from the FMR signal intensity how ferromagnetic cobalt transforms into an antiferromagnetic state during its stay in air.

All films showed a good FMR signal with a strong angular dependence when changing the direction of the external magnetic field H from the in-plane to the out-of-plane orientation due to the demagnetizing factor. However, we were unable to observe the time dependence of the decrease in the FMR signal intensity. We also did not see a paramagnetic signal from cobalt oxide at $g \sim 2$ [2], since it was against the background of the signal from the substrate, but significantly weaker. The film annealed in air for 20 minutes was completely oxidized to the entire depth. The film annealed in air for 5 minutes was oxidized to a depth of about 1 nm, further annealing did not give any results.

1. Kamashev A., Validov A., Garif'yanov N., Garifullin I.: Physica C **618**, 1354461 (2024)
2. Busetto C., Neri C., Palladino N., Perrotti E.: Inorganica Chimica Acta **5**, 129–132 (1971)

poster

Magnetic properties of $GdCoC_2$: ESR, static magnetization and magnetocaloric study

S.V. Demishev[1, 2], R.R. Tagirov[3], A.V. Semeno[3], A.V. Shestakov[3], I.I. Fazlizhanov[4], R.M. Eremina[4], A.V. Bokov[1], D.A. Salamatin[1], A.V. Semeno[1,3], A.V. Tsvyashchenko[1]

[1] Vereshchagin Institute for High Pressure Physics, RAS, 108840, Troitsk, Moscow, Russia
[2] HSE University, 101000, Moscow, Russia
[3] Prokhorov General Physics Institute, RAS, 119991, Moscow, Russia
[4] Zavoisky Physical-Technical Institute, FRC Kazan Scientific Center of RAS, Kazan, Russia

$GdCoC_2$ is a ternary rare-earth carbide with an orthorhombic noncentrosymmetric crystal structure, known for its non-collinear magnetic ordering and intriguing topological transport phenomena, including a distinct topological Hall effect at low temperatures [1]. It undergoes a complex sequence of magnetic phase transitions, including a paramagnetic–ferromagnetic transition followed by a commensurate–incommensurate transformation [1]. Earlier studies have shown that $GdCoC_2$ was an antiferromagnet below T_N = 15.6 K with an order-order transition at 14.0 K [2]. The material also exhibits a pronounced magnetocaloric effect, indicating strong field and temperature sensitivity of its magnetic properties [3]. Investigating $GdCoC_2$ by ESR across multiple frequency ranges is of particular interest, as it enables the identification of frequency-dependent contributions to spin dynamics and leads to a deeper understanding of the magnetic

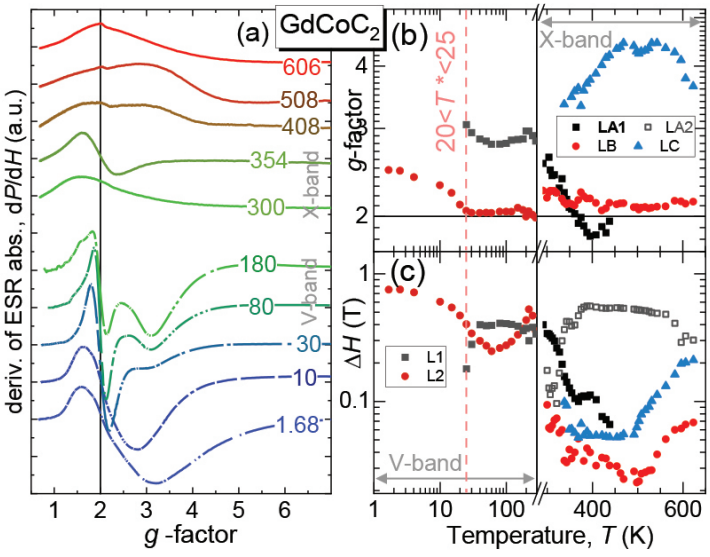

Fig. 1. a Temperature evolution of the EPR spectrum of $GdCoC_2$, temperature dependence of *g*-factor (**b**), linewidth (**c**).

poster

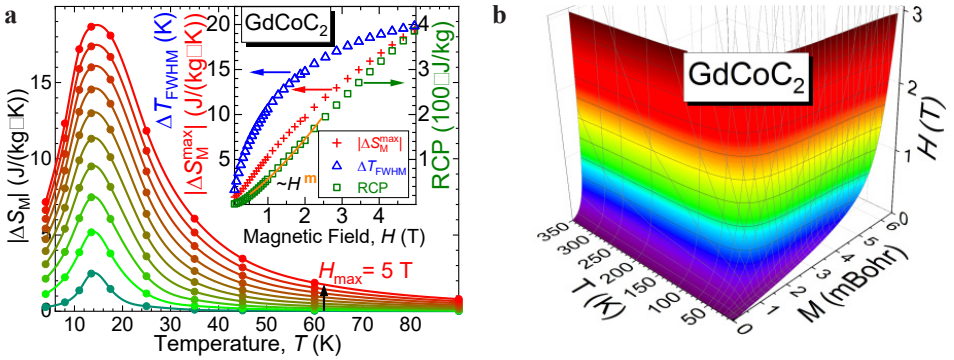

Fig. 2. a Field evolution of the temperature dependence of the change in magnetic entropy and field dependences of ΔT_{FWHM} $|\Delta S_M^{max}|$ and RCP (insert). **b** *H*-*M*-*T*-plot.

properties and relaxation processes in the system. The sample was synthesized under high-pressure conditions (8 GPa, 1500–1700 K) using a toroidal chamber at HPPI RAS. ESR measurements were performed over two wide temperature ranges: 1.6–300 K (V-band, ~60 GHz, magnetooptical spectrometer at GPI RAS) and 300–620 K (X-band, ~9.4 GHz, using a Varian E-12 ESR spectrometer) (Fig. 1).

From one to four ESR lines are observed in the spectrum of the $GdCoC_2$, depending on the temperature. At a frequency of 60 GHz, two prominent lines are detected. Line "L1" emerges around 20 K and exhibits ferromagnetic characteristics up to 350 K, after which it transitions to a paramagnetic response. Above ~300 K, line "LA1" narrows and decreases in intensity, eventually disappearing entirely by 450 K.

Notably, the spectral parameters of lines "L1" and "LA1" at 300 K show excellent agreement at the junction of the two frequency ranges. Additionally, line "LA2", arises between 300 K and 380 K, broadens up to 0.6 T and then shifts toward lower magnetic fields.

The second line "L2" exhibits ferromagnetic behavior up to ~30 K. At higher temperatures, its position stabilizes near $g \approx 2$. In the temperature range above 30 K, the linewidth shows two distinct minima: a shallow one near 60 K and a deeper one around 500 K (see line "LB"). At higher temperatures, the line broadens again, while the integrated intensity increases.

Above room temperature, additional lines "LC" appear, with $3 < g < 4.5$, displays a minimum linewidth in the 350–500 K range, followed by broadening and an increase in intensity with further heating.

The restructuring of the high-temperature ESR spectra suggests the occurrence of additional magnetic transitions around $T \approx 350$ K and $T \approx 500$ K. This effect constitutes new high temperature magnetic transitions, which may be attributed to the filling of excited states of the Co magnetic ion with increasing temperature.

The magnetization study at fields from 0 to 5 T and temperature from 2 to 350 K was performed on Quantum Design SQUID magnetometer MPMS XL5. The field evolution of the temperature dependence of the change in magnetic entropy (ΔS_M) was obtained, where the maximum is observed at temperatures of 15–16 K, and in the field range of 0.5 – 2.5 T the RCP parameter is well described by a power dependence on

poster

the field $m \approx 1.36$ (Fig. 2a). The critical properties of the sample were investigated by analysis of the magnetization measurements in the vicinity of their critical temperature (Fig. 2b). The critical exponents β, γ and δ were evaluated using modified Arrott plots [4] and are most likely close to those predicted by the X-Y Heisenberg model.

Support from RSF grant 22-12-00008-П is acknowledged.

1. Xu Y., Ren W. Ma S. et al.: Appl. Phys. Lett. **123**, 072402 (2023)
2. Matsuo S., Onodera H., Kosaka M. et al.: JMMM **161**, 255–264 (1996)
3. Meng L., Xu C., Yuan Y. et al.: RSC Adv. **6**, 74765–74768 (2016)
4. Arrott A., Noakes J.E. Phys. Rev. Lett. **19**, 786 (1967)

poster

Non-resonant microwave absorption study of anisotropic transport properties in $Bi_{1.06}Sn_{0.04}Sb_{0.9}Te_2S$

T.N. Enderova, V.O. Sakhin, I.I. Gimazov, E.F. Kukovitsky, Yu.I. Talanov

Zavoisky Physical-Technical Institute, FRC Kazan Scientific Center of RAS, Kazan, Russia

Topological insulators (TIs) are quantum materials characterized by an insulating bulk and conducting surface states. Among the most studied TIs are bismuth chalcogenides. However, these materials typically possess a high density of bulk charge carriers, which complicates the study of surface transport properties. Bulk carrier suppression can be achieved through atomic substitution and chemical doping. One of such engineered compounds is $Bi_{1.06}Sn_{0.04}Sb_{0.9}Te_2S$ (BSSTS) [1]. In this system, the dominant contribution to DC transport depends on temperature: bulk conduction dominates above 100 K, while surface conduction becomes decisive below 100 K.

In this study, we employed both DC and AC measurements to investigate the transport properties of BSSTS crystals. Non-resonant microwave absorption at 9.4 GHz was used as the AC technique, it was performed using the Bruker BER 418S X-band EPR spectrometer. We measured the temperature dependence of the non-resonant microwave absorption amplitude, $A_{MWA}(T)$, for two orientations of the BSSTS flakes relative to the magnet component of microwave field. Depending on the sample orientation, the induced current flows either parallel or perpendicular to the flake surface. We have observed significant differences in transport behavior between these configurations.

In the standard configuration with current flowing in the *ab*-plane, we observed the expected competition between semiconducting bulk behavior and metallic surface conduction. In contrast, when the current flowed perpendicular to the ab-plane, the temperature dependence became more complex. In particular, in the temperature range where bulk conduction dominates, a local maximum appeared in the $A_{MWA}(T)$ curve. This may indicate a transition in the prevailing scattering mechanism – from impurity scattering to phonon scattering. While in-plane transport (when current flows in the *ab*-plane) is governed only by phonon scattering at temperatures above 100 K.

Complementary DC measurements of resistance $R(T)$ revealed qualitatively similar results. However, a notable difference emerged: in the AC measurements, the temperature corresponding to the resistance maximum was shifted to higher values. The origin of this shifted becomes from influence of high frequency on transport properties for disordered materials [3].

This research was supported by the Russian Science Foundation, project No. 21-72-20153-P.

1. Kushwaha S.K. et al.: Nature Comm. **7**, 11456 (2016)
2. Abdullaevs N.A.: FTT **63**, no. 8, p. 1062–1067 (2021)
3. Dyre J.C.: Phys. Lett. **108A**, 39, 457–461 (1985)

poster

$CeMnB_5O_{10}$ – new member of a pentaborate family: ESR measurements

T.P. Gavrilova[1], I.V. Yatsyk[1], A.I. Zaitsev[2], A.V. Cherepakhin[2], E.M. Moshkina[2]

[1] Zavoisky Physical-Technical Institute, FRC Kazan Scientific Center of RAS, Kazan, Russia
[2] L Kirensky Institute of Physics, FRC KSC SB RAS, Krasnoyarsk, Russia

Borates of various compositions represent a broad class of compounds, including materials containing rare earth and transition metals and having various structural types. Due to the presence of the complex $[BO_n]^{-}_{(2n-3)}$ anion and cationic polyhedra, as well as the tendency to form chains and planes from these structural elements, many borates have the quasi-low-dimensional magnetic structure. Here we present the electron spin investigations of a new material – $CeMnB_5O_{10}$ pentaborate containing two types of magnetic cations. This compound was studied in two modifications – crystalline and amorphous.

Electron spin resonance (ESR) spectra of the $CeMnB_5O_{10}$ samples were measured using ER 200 SRC (EMX/plus) spectrometer (Bruker, Germany) at the frequency of 9.4 GHz in the temperature range from 115 K to room temperature in steps of 3 K. In all temperature range the ESR absorption spectra of $CeMnB_5O_{10}$ glass sample can be described by one exchange-narrowed resonance line (Fig. 1).

It is suggested that the broad line in ESR spectra of $CeMnB_5O_{10}$ glass sample can appear due to Mn^{2+} magnetic ions ($3d^5$, $S = 5/2$, $I = 5/2$) and Ce^{3+} magnetic ions ($4f^1$, $J = 5/2$), which form the crystal structure of the investigated compound. One can expect that ESR absorption line in $CeMnB_5O_{10}$ glass sample refers to Mn^{2+} magnetic

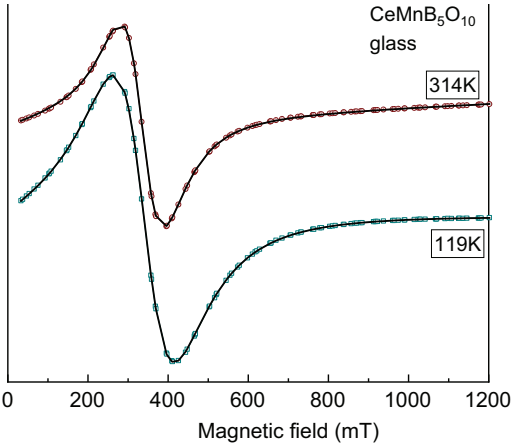

Fig. 1. Typical electron spin resonance spectra in $CeMnB_5O_{10}$ glass sample. Symbols – experimental data, solid line – fitting.

ions, which interact with Ce^{3+} magnetic ions; and the resonance field position is shifted from the values typical for divalent manganese ions at room temperature to the values typical for trivalent cerium ions with decreasing the temperature.

The ESR line is much broader in $CeMnB_5O_{10}$ polycrystalline sample in comparison with glass sample suggesting the lower values of exchange interactions between magnetic ions in this sample. The ESR linewidth and integral intensity in $CeMnB_5O_{10}$ glass sample increase with decreasing the temperature suggesting the observed absorption line is the signal from paramagnetic phase, because the inverse integral intensity demonstrates the linear behavior.

The observed ESR absorption of $CeMnB_5O_{10}$ polycrystalline sample has the more complicated line shape and can be well fitted by the sum of two field derivatives. Similar to the $CeMnB_5O_{10}$ glass sample, one can suggest that the first line is the signal from Mn^{2+} ions which interact with Ce^{3+} ions. The low-field temperature independent ESR signal appears only in $CeMnB_5O_{10}$ polycrystalline sample; it is characterized by *g*-factor values which are not typical for Mn^{2+} and Ce^{3+} ions and has intensity 20 times less than the main signal. This signal suggested the presence of the crystal structure defects or magnetically correlated regions due to mix-valence magnetic ions or other types of magnetic inhomogeneity, which is in agreement with the EDX data.

poster

Nuclear magnetic moments in the 3D Dirac semimetal Cd_3As_2: Suhl-Nakamura interaction approach

Yu. Goryunov[1], A. Nateprov[2]

[1] Zavoisky Physical-Technical Institute, FRC Kazan Scientific Center of RAS, Kazan, Russia
[2] Institute of Applied Physics, Moldova State University, Chisinau, Moldova

Main feature of topological materials are a strong coupling of the spin and orbital degrees of freedom of Dirac electrons. It leads to that the direction of their spins is strongly related to the direction of their motion. This at the first refers to the parent electrons of the topological material. However, the interaction of donor and parent electrons in localized and band states takes of particular importance in the case the modification of the electronic properties such materials by introducing into the material impurity centers with orbital moments. In the case of hybridization spin and orbital states valence zone, it is possible also the mutual influence of Dirac electrons and nuclear magnetic moments, which appears in hyperfine structure of EPR spectra.

Comparison of the quantity of conduction electrons in pure stoichiometric Cd_3As_2 with the number of electrons in the s-shells of metal atoms, electrons from the outer s-shells almost completely enter the valence band. It is impotant to memory that bottom of conduction band in semimetals at the determined wave vectors may be lower

The EPR experiments were carried out on magnetic impurities of d-metals Fe, Cr. These elements, having ionic radii somewhat smaller than the divalent cadmium ion, quite easily enter the crystal structure of cadmium arsenide. This is supported by X-ray diffraction and EDX data. Thus, in the case of doping with iron, despite its noticeable concentration in the sample, the EPR signal from Fe^{2+} is not observed. In the experiment, only a weak signal is observed from the Fe^{3+} ion with a g-factor slightly higher than the *g*-factor of a free electron, which is characteristic of an ion in a pure spin state $3d^5$ with $S = 5/2$, $L = 0$ $g = 2.0036$ versus $g = 2.0023$ for a free electron. Due to this nature of the entry of a magnetic ion into a topological semimetal, the weak anti-localization regime, which is evidenced by a positive magnetoresistance, is preserved at achievable doping levels.

When doped with chromium ions, the EPR signal from divalent chromium ions is also not observed in the X-band. There is a noticeable presence of Cr^{3+} ions, which have a $3d^3$ state with S = 3/2 and L=3. For this state, signals with anisotropic *g*-factors in the range of 1.95–1.98 are usually observed. In the case of Cd3As2, a signal with an anisotropic and anomalously large g factor in the range of 2.13–2.18 is observed in the powder sample. The anomalous value of the g factor is associated with the influence of band electrons, which have giant values of g factors, through the orbital angular momenta of the localized magnetic states of the Cr^{3+} ion.

Isotopes ^{57}Fe and ^{53}Cr have nuclear spins $I_{Fe} = 1/2$ and $I_{Cr} = 3/2$, consequently.

The nuclei of impurities, entering into hyperfine interactions with the electrons of the topological material, can enter into indirect interactions with each other through these electrons. This interaction can be through magnetic quasiparticles magnons, similar to the Suhl-Nakamura interaction in magnets. Also, continuing this analogy, it may be

poster

through long-range interactions by means quasiparticles formed by Dirac electrons, whose states in these materials are topologically protected and can be transmitted over large distances if they have orbital angular momenta. It can be expected that quasiparticles with an integer orbital quantum number will behave similarly to bosons and lead to the emergence of collective modes in the system of nuclear magnetic moments. It may be take place in EPR experiment on Cd_3As_2 doped by Cr. The behavior of the hyperfine structure of the spectrum for Cr^{3+}, which has a large orbital momentum and an antiferromagnetic sign of interaction with band electrons, differs significantly from the behavior of that for Fe^{3+}, which has a zero orbital momentum and a ferromagnetic sign of exchange interaction with band electrons.

1. Goryunov Yu.V., Nateprov A.N.: Phys. Sol. St. **62**,100 (2020)
2. Goryunov Yu.V., Nateprov A.N.: Phys. Sol. St. **66**, 1771 (2024)
3. Suhl H.: Phys. Rev. **109**, 606 (1958)
4. Nakamura T.: Progr. Theor. Phys. **20**, 542 (1958)
5. de Gennes P.G.: Phes. Rev. **129**, 1105 (1963)
6. Turtur C., Bayrewther G.: Phys. Rev. Lett. **72**,1557 (1994)

poster

Influence of cooling conditions on magnetic resonance spectra of $FeCr_2O_4$ multiferroic spinel

M.I. Nasyrova, B.F. Gabbasov, M.A. Cherosov, R.G. Batulin, R.V. Yusupov

Institute of Physics, Kazan Federal University, Kazan, Russia

Multiferroics are solid crystalline materials in which polar and magnetic orderings coexist and interact with each other. Electrical and magnetic properties arise in the material due to its composition and crystal structure. Recently, a strong magneto-optical effect, manifested in a significant rotation of light polarization plane with a change in magnetization, was reported for $FeCr_2O_4$ and $CoCr_2O_4$ spinels which make them interesting for both scientific and applied research [1].

One of the ways to realize a complex magnetic structure is the spiral-modulated ferrimagnetic oredring found in cobalt chromium $CoCr_2O_4$ [2]. The ferrimagnetic transition in this compound occurs at T_C = 93 K, and with a further decrease in temperature, the compound undergoes a transition to a state with a conical magnetic spiral at T_s ~ 28 K. Yamasaki's work demonstrated the critical behavior of both magnetization and electric polarization on cooling in both the magnetic and electric fields. To date, no experiments have been conducted on single crystal $FeCr_2O_4$ samples similar to those performed on $CoCr_2O_4$. The $FeCr_2O_4$ compound exhibits phase transitions to states with long-range orbital ordering within the iron sublattice at 138 K, to a collinear ferrimagnetic state at ~65 K, and to a state with spiral modulation of the magnetic structure at 38 K. It is known that $FeCr_2O_4$ single crystals reveals a magnetic resonance spectrum at temperatures below 65 K [3]. The magnetometry data shows anomalies in the region of ~ 20 K.

The report will present the results of experimental studies of the temperature dependence of the magnetic resonance spectra of a $FeCr_2O_4$ spinel single crystal after cooling down to 10 K under different conditions: in a magnetic and electric field, only in a magnetic field, only in an electric field, in the absence of a magnetic and electric field. It will be shown that the spectra for different types of cooling differ from each other, which indicates a significant effect of the electric charge on the magnetic structure of spinel $FeCr_2O_4$. Therefore, it can be argued that iron chromium spinel has multiferroic properties.

1. Kocsis V., Bordács S., Deisenhofer J. et al.: Strong magneto-optical effects in ACr_2O_4 (A = Fe, Co) spinel oxides generated by tetrahedrally coordinated transition metal ions / et al.] // Phys. Rev. B. **97**. – Art. 125140 (8 p.) (2018)
2. Yamasaki Y., Miyasaka S., Kaneko Y., He J.-P., Arima T., Tokura Y.: Magnetic reversal of the ferroelectric polarization in a multiferroic spinel oxide // Phys. Rev. Lett. **53**. – Art. 207204 (4 p.) (1996)
3. Юсупов Р.В., Черосов М.А., Габбасов Б.Ф.: Магнитные необратимости и невзаимность микроволнового поглощения шпинели $FeCr_2O_4$ и др. // П. в ЖЭТФ. **115**, 190–196 (2022)

poster

Quantitative EPR line shape analysis in a metal based on the semiclassical magnetization dynamics

A.E. Os'kin[1,2], A.V. Popov[1,2], I.V. Yatsyk[3], R.M. Eremina[3], S.V. Demishev[1,2]

[1] Vereshchagin High Pressure Physics Institute of RAS, Troitsk, Moscow, Russia
[2]HSE University, Moscow, Russia
[3]Zavoisky Physical-Technical Institute, FRC Kazan Scientific Center of RAS, Kazan, Russia

EPR line shape in metals is asymmetric and often considered as a *per se* manifestation of Dyson-Feher-Kip theory accounting strong spin diffusion in a skin layer [1]. However, this is not the case, and asymmetry may appear for oscillating localized magnetic moments in metals [2, 3]. The latter situation occurs in various strongly correlated metals and quantum critical systems [3], but the evaluation of EPR line is not simple from the mathematical point of view. For that reason, the empirical asymmetric Lorentz functions are introduced for the data analysis [4]. Despite simplicity, this ansatz may face difficulties with the decomposition of the EPR line into spectral components and with interpretation of the obtained parameters [5].

In the present work, we introduce EPR line shape description in a metal based on the semiclassical magnetization dynamics and related program solution for the experimental data analysis. As long as recent investigation showed that Landau-Lifshitz (LL) and Gilbert (G) relaxation describes different physical mechanisms which may be met in experimental system [6], the general master equation for magnetization dynamics is considered

$$\frac{d\mathbf{M}}{dt} = \gamma \cdot \mathbf{M} \times \mathbf{H} - \delta\lambda \cdot \mathbf{M} \times \mathbf{M} \times \mathbf{H} - (1-\delta)\gamma\eta \cdot \mathbf{M} \times \frac{d\mathbf{M}}{dt}, \tag{1}$$

where γ is the hyromagnetic ratio, λ and η are LL and G relaxation constants respectively, and δ denotes mixing parameter. Assuming Faraday geometry for EPR and linear link between oscillating magnetization **m** and oscillating magnetic field **h**, it is possible obtaining dynamic susceptibility matrix

$$\hat{\chi} = \begin{pmatrix} \chi & \chi_\alpha \\ -\chi_\alpha & \chi \end{pmatrix},$$

$$\chi = \frac{\delta\lambda M_0{}^2(\delta\lambda M_0 H_0 - i\omega) + \gamma M_0(\gamma H_0 - (1-\delta)i\omega\gamma\eta M_0)}{(\delta\lambda M_0 H_0 - i\omega)^2 + (\gamma H_0 - (1-\delta)i\omega\gamma\eta M_0)^2}, \tag{2}$$

$$\chi_\alpha = \frac{\gamma M_0(\delta\lambda M_0 H_0 - i\omega) - \delta\lambda M_0{}^2(\gamma H_0 - (1-\delta)i\omega\gamma\eta M_0)}{(\delta\lambda M_0 H_0 - i\omega)^2 + (\gamma H_0 - (1-\delta)i\omega\gamma\eta M_0)^2}.$$

poster

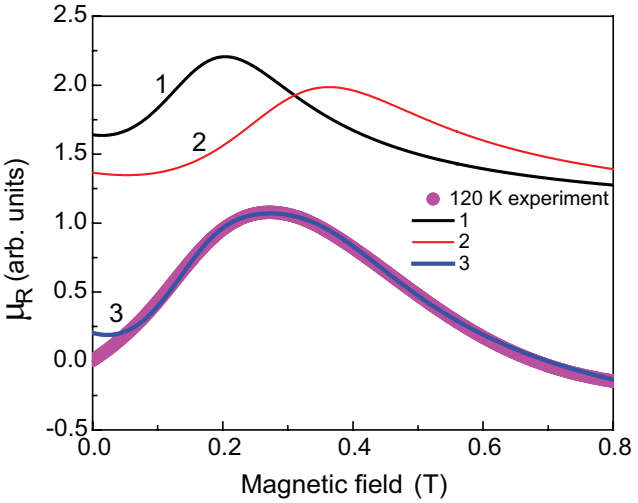

Fig. 1. Example of the experimental integrated X-band spectrum for the $Mn_{1-x}R_xSi$ sample with x = 0.8 (points) and simulation by the developed software (lines). 1, 2 – partial components, 3 – sum of the components 1 and 2.

Here M_0 is the oscillating magnetization in external steady field H_0 and ω denotes microwave frequency. Equations (2) may be used to find effective permeability μ_R and cavity losses $Q \sim (\mu_R R)^{1/2}$ for a metallic sample with the resistivity R. Details of the $\mu_R(H_0, \omega)$ calculation may be found elsewhere [3].

The above approach is applied for analysis of the X-band EPR spectra for novel ferromagnet with the Griffiths phase $Mn_{1-x}Rh_xSi$ [7]. The initial spectra were integrated numerically in the field range up to 1T using the trapezoid method due to its computational stability. The obtained experimental function was fitted by the model expression $\mu_R(H_0, \omega)$. The developed software allowed approximation consisting of several spectral components. For each EPR line forming a complicated spectrum, the full set of spectroscopic parameters, including hyromagnetic ratio (g-factor), relaxation parameter (line width) and oscillating magnetization, may be determined by optimization of the error functional. Special attention was paid to stability in the data distortion, which is critical for accurate determining of the fitting parameters. The initialization of the computation values may be done by approximate location of the peaks positions. An example of the $Mn_{1-x}Rh_xSi$ with x = 0.8 EPR spectrum decomposition into two lines in presented in Fig. 1. The developed method of data analysis is general and may be applied for various strongly correlated metallic systems. Support from RSF project 22-12-00008-П is acknowledged.

1. Feher G., Kip A.F.: Phys.Rev. **98**, 337–348 (1955)
2. Semeno A.V. et al. Phys.Rev. B **79**, 014423 (2009)
3. Demishev S.V.: Applied Magnetic Resonance **51**, 473–522 (2020)
4. Joshi J.P., Bhat S.V.: J. Magn. Res. **168**, 284–287 (2004)
5. Demishev S.V., Shestakov A.V., Yatsyk I.V. et al.: Solid State Commun. **385**, 11550 (2024)
6. Demishev S.V.: Applied Magnetic Resonance **55**, 1091–1114 (2024)
7. Demishev S.V. et al.: JETP Letters **121**, 111–118 (2025)

poster

Magnetic properties of polycrystalline $La_{0.83}Sr_{0.17}Mn_{0.9}Fe_{0.05}Zn_{0.05}O_3$ and $La_{0.83}Sr_{0.17}Mn_{0.9}Fe_{0.05}Mg_{0.05}O_3$

A.V. Shestakov[1], Z.Y. Seidov[2], M.A. Cherosov[3], I.V. Yatsyk[4], A.S. Ovchinnikov[5], F.G. Vagizov[3], V.A. Shustov[4], A.G. Badelin[6], V.K. Karpasyuk[6], M.J. Najafzade[2], I.N. Ibrahimov[2], H.-A. Krug von Nidda[7], R.M. Eremina[4]

[1] Prokhorov General Physics Institute of the RAS, Moscow, Russia
[2] Institute of Physics, Ministry of Science and Education, Baku, Azerbaijan
[3] Institute of Physics, Kazan Federal University, Kazan, Russia
[4] Zavoisky Physical-Technical Institute, FRC Kazan Scientific Center of RAS, Kazan, Russia
[5] Institute of Natural Sciences and Mathematics, Ural Federal University, Ekaterinburg, Russia
[6] Astrakhan State University, Astrakhan, Russia
[7] Experimental Physics V, Center for Electronic Correlations and Magnetism, Institute of Physics, University of Augsburg, Augsburg, Germany

Magnetic properties of polycrystalline $La_{0.83}Sr_{0.17}Mn_{0.9}Fe_{0.05}Zn_{0.05}O_3$ and $La_{0.83}Sr_{0.17}Mn_{0.9}Fe_{0.05}Mg_{0.05}O_3$ have been investigated by meanselectron spin resonance, magnetic susceptibility, and Mössbauer measurements, as a continuation of research

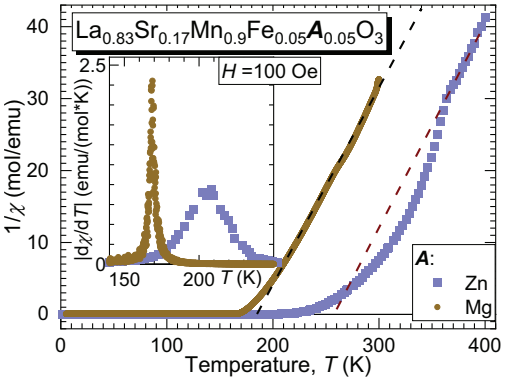

Fig. 1. Temperature dependence of dc inverse magnetic susceptibility at 100 Oe in $La_{0.83}Sr_{0.17}Mn_{0.9}Fe_{0.05}\boldsymbol{A}_{0.05}O_3$ with A=Zn and A=Mg. Inset: The derivative of magnetic susceptibility $d\chi/dT$ as a function of temperature.

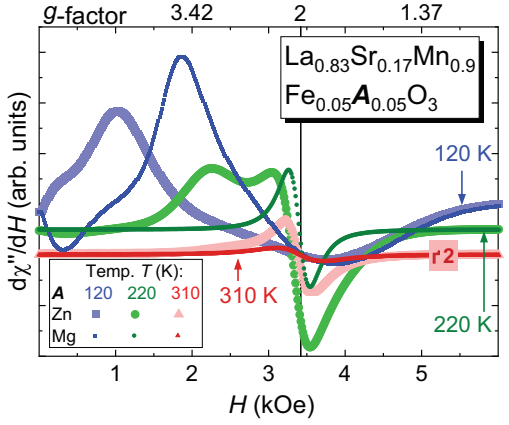

Fig. 2. Temperature evolution of the field dependence of the first derivative of the ESR absorption for the $La_{0.83}Sr_{0.17}Mn_{0.9}Fe_{0.05}\boldsymbol{A}_{0.05}O_3$ with A=Zn and A=Mg.

poster

on doped perovskite manganite systems [1]. Both samples exhibita clear ferromagnetic transition ($Zn_{0.05}$–T_C = 222 K; $Mg_{0.05}$–T_C = 168 K). The inverse susceptibility of the compounds with the Zn ion deviates from the Curie–Weiss law above T_C, indicating the presence of magnetic fluctuations near the ordering temperature, whereas for compounds with the Mg ion such a deviation is absent (Fig. 1). An anomalous downturn in the inverse susceptibility for $La_{0.83}Sr_{0.17}Mn_{0.9}Fe_{0.05}Zn_{0.05}O_3$ well above T_C along with the simultaneous observation of ferromagnetic resonance signals coexisting with paramagnetic resonance up to approximately room temperature suggests Griffiths-like behavior. This regime is characterized by the coexistence of ferromagnetic entities within the globally paramagnetic phase (Fig. 2).

Mössbauer studies indicate that Fe in both compounds is in the trivalent high-spin state. The temperature evolution of the Mössbauer spectra at $T < T_C$ is typical for ferromagnetic clusters with a wide distribution of size and magnetic correlation length.

Z. Seidov et al.: JMMM 552, 169190 (2022)

poster

Magnetic properties $Ca_{0.3}Sr_{0.3}La_{0.3}Mn_{0.5}Ti_{0.5}O_3$

I.V. Yatsyk[1], R.F. Likerov[1], R.M. Eremina[1], R.G. Batulin[2]

[1] Zavoisky Physical-Technical Institute, FRC Kazan Scientific Center of RAS, 420029, Kazan, Russia
[2] Institute of Physics, Kazan Federal University, 420008, Kazan, Russia

In recent years, scientists have shown great interest in high-entropy perovskite-type compounds, in which solid solutions are formed from five or more elements in relatively equal concentrations, since they can be stabilized by the high entropy of mixing. The properties of such materials strongly depend on the crystal structure. High-entropy compounds have a wide range of applications [1, 2], including sensors [3], catalysts [4], and some of them are potentially attractive for high-temperature applications in industries such as aerospace, energy production, automotive, turbine technology, etc., where the materials must withstand extremely high temperatures [5].

The first high-entropy materials to attract the attention of scientists were high-entropy alloys. Since 2015, high-entropy oxides have been produced [6], followed by high-entropy metallic diborides [7], carbides [8], fluorides [9], and sulfides [10].

The aim of this work is to study the magnetic properties of the high-entropy compound $Ca_{0.3}Sr_{0.3}La_{0.3}Mn_{0.5}Ti_{0.5}O_3$ using the electron spin resonance (ESR) and magnetometry methods, determine the phase transition temperatures, and construct phase diagrams.

The ESR method allows one to study the dynamics of magnetic properties of the studied compounds both in an ordered state and in the paramagnetic region.

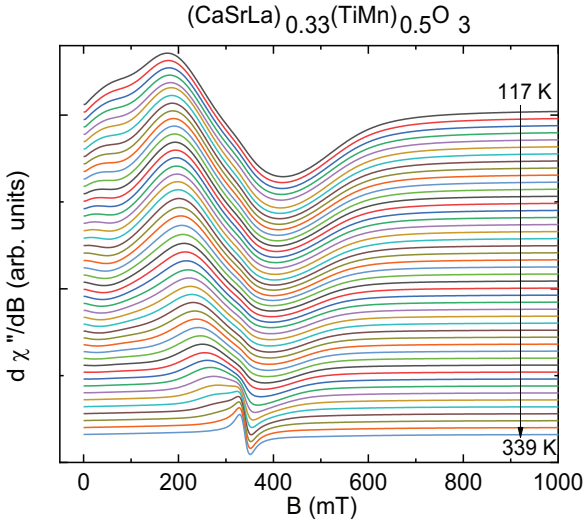

Fig. 1. Evolution of the electron spin resonance spectrum with temperature in the range from 117 to 339 K for $Ca_{0.3}Sr_{0.3}La_{0.3}Mn_{0.5}Ti_{0.5}O_3$.

poster

The synthesis of polycrystalline powder of $Ca_{0.3}Sr_{0.3}La_{0.3}Mn_{0.5}Ti_{0.5}O_3$ has been carried out via the solid-state route using precursor materials including $CaCO_3$ (≥99%), $SrCO_3$ (≥99%), $CaCO_3$ (≥99%), La_2O_3 (≥99%), TiO_2 (≥99%), and Mn_2O_3 (≥99%). Initially, the precursor powders have been mixed in a ball mill with zirconia balls in an ethanol medium. The resulting mixture is then dried overnight in a hot air oven. Subsequently, the dried powder underwent calcination at 1323 K for 10 hours under an air atmosphere. The calcined powder is then pressed into pellets using a hydraulic press and sintered at 1373 K for 6 hours under an air atmosphere. Detailed conditions for growing samples are given in [11].

EPR measurements were performed using a Bruker EMXplus (Xband) spectrometer, equipped with continuous-flow N2 cryostats. In these measurements we used the X-band with a frequency of 9.4 GHz, a temperature range of 117–339 K, and a magnetic-field range of 0–1.4 T. The ESR spectra are shown in Figure 1.

It can be seen that the shape of the magnetic resonance line from 117 K to 339 K changes greatly, which indicates a change in the magnetic phase. The phase transition temperature is near room temperature.

The work was carried out at the expense of a grant from the Academy of Sciences of the Republic of Tatarstan, provided to young candidates of science (postdoctoral students) for the purpose of defending a doctoral dissertation, carrying out research work, and also performing work functions in scientific and educational organizations of the Republic of Tatarstan within the framework of the State Program of the Republic of Tatarstan “Scientific and Technological Development of the Republic of Tatarstan.

1. Albedwawi S., AlJaberi A., Haidemenopoulos G., Polychronopoulou K.: Materials & Design. **202**, 109534 (2021)
2. Musicó B., Gilbert D., Ward T., Page K. et al.: APL Materials. **8**, 040912 (2020)
3. Zhang Y., Wang D., Wang S.: Small **18**, 2104339 (2021)
4. Li K., Chen W.: Materials Today Energy **20**, 100638 (2021)
5. P. Sathiyamoorthi, H. Kim.: Advanced Engineering Materials **20**, 1700645 (2017)
6. Sarkar A., Wang Q., Schiele A., Chellali M. et al.: Adv. Mater. **31**, 1806236 (2019)
7. Gild J., Zhang Y., Harrington T., Jiang S. et al.: Scientific Reports **6**, 37946 (2016)
8. Alvi S., Zhang H., Akhtar F.: High-Entropy Materials. IntechOpen 2019. – ISBN 978-1-78985-947-8
9. Chen X., Wu Y.: Journal of the American Ceramic Society **103**, 750–756 (2019)
10. Juan Kuang, Ping Zhang, Qianqian Wang, Zhenfeng Hu et. al.: Corrosion Science. **198**, 110134 (2022)
11. Tathagata Bhattacharya, Ritwik Banerjee and Tanmoy Maiti: Phys. Chem. Chem. Phys. **26**, 28874–28883 (2024).

poster

Analysis of temperature behavior of orientation dependent EMR signals in biological tissues

S.V. Yurtaeva[1], I.V. Yatsyk[1], V.N. Efimov[2], A.A. Rodionov[3]

[1] Zavoisky Physical-Technical Institute, FRC Kazan Scientific Center of RAS, Kazan, Russia
s.yurtaeva@kfti.knc.ru
[2] Kazan State Medical Univers ity, Kazan, Russia
[3] Institute of Physics, KFU, Kazan, Russia

Presently it is known that in various biological systems, electron magnetic resonance (EMR) signals that depend on the orientation of the magnetic field may be observed. The characteristics of these signals, ferrimagnetic in nature, differ essentially from any other EPR signals recorded in the samples of biological tissues, in particular from signals of paramagnetic centers associated with metal ions in proteins. The nature and source of these signals are still of the interest and are the subject of debate. The signals are characterized by a g-value > 2.1, non-monotonic temperature behavior of the resonance magnetic field (H_{res}), line width (ΔH), integrated intensity (I), asymmetric lineshape, and dependence of H_{res} on orientation. Such signals are detected in a number of biological objects: in brain tissue, tumors, pathological and healthy tissues of rats, DNA samples, organs of navigation and magnetoreseption in insects, birds, etc. However, they remain insufficiently studied. Previously, we registered this type of signals in tumors [1], pathological and healthy tissues of rats [2, 3], in dividing plant cells [4], and in the brain and heart of a snail.

In order to investigate the nature of these signals in this study, we analyzed the behavior of the following depending on temperature characteristics: temperature behavior of the resonant field, line width, lineshape and integrated intensity using for this purpose the previously published data [1–4]. Understanding the temperature behavior is the key to identifying the source of the signals. One of the important characteristics of these signals is the unusual nonmonotonic temperature behavior of H_{res}. When decreasing the temperature from room temperature to helium one H_{res} reaches its maximum value within the interval 110–125 K and further is substantially decreasing. At the same temperatures, a jump in linewidth is observed, and the integrated intensity reaches a maximum. Two temperature intervals with the phase transition (PT) at their boundary near a temperature of 120 K were found. An analysis of the literature showed that the shape of temperature dependence $H_{res}(T)$ coincides with the temperature dependence for magnetite (Fe_3O_4) powder with particle sizes of a hundred nm and more [5]. This fact confirms that EMR signals belong to nanocrystalline magnetite. It was determined that the anomaly in the vicinity 110–125 K is due to Verwey PT, character to magnetite crystals. At the temperatures above Verwey PT, the high correlation between temperature dependences of $H_{res}(T)$, $\Delta H(T)$ and temperature dependence of magnetite magnetocrystalline constant K_1 were detected [6]. The correlation coefficient was ~0.95–0.98.

It is known that in magnetite crystal structure above Verwey PT there are hopping electrons on iron cations. The shape of the temperature dependence above Verwey PT is due to hopping mechanism between of Fe^{2+} and Fe^{3+} cations. In the temperature interval below the Verwey PT, there is the fixation of electrons in definite position,

poster

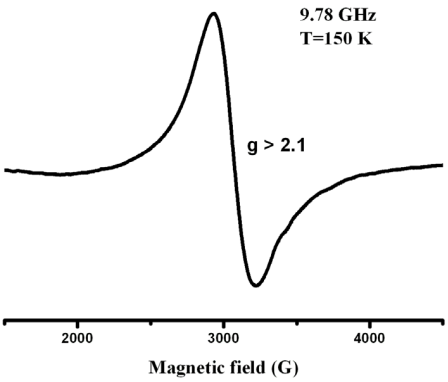

Fig. 1. Lineshape of EMR signal in biological tissue.

as a result the crystal structure of magnetite is transformed from cubic to monoclinic and magnetic moment is falling. In EPR spectra this is manifested in decreasing the integral intensity of signal and displacement of the signal to the lower fields below Verwey PT temperature. But H_{res} displacement with temperature is not so sharp as magnetocrystalline anisotropy of bulk magnetite. In biogenic magnetite, as experimental data show, Verwey PT is second order transition, while in bulk magnetite it is first order transition. This is explained by the nanosized nature of biogenic magnetite and the dispersion of nanoparticle sizes.

There was also observed the transformation of line shape from asymmetric Dyson-like shape confirming hopping conduction above the Verwey PT with an anisotropy parameter of ~0.25, to symmetric Lorentz one below PT, confirming the loss of mobility by electrons.

1. Yurtaeva S.V., Efimov V.N., Silkin N.I. et al.: Appl. Magn. Res. **42**, 299–311 (2012)
2. Yurtaeva S.V., Efimov V.N. et al.: Appl. Magn. Res. **47**, 555–565 (2016)
3. Yurtaeva S.V., Yafarova G.G. et al.: Russ. Phys. Bull. **89**, no. 10 (2025) (in press)
4. Yurtaeva S.V. Yatsyk I.V. et al.; Russ. Phys. Bull. **89**, no. 10 (2025) (in press)
5. Hagiwara M., Nagata K., Nagata K.: J. Phys. Soc. of Japan, **67,** no. 10, 3590–3600 (1998)
6. Bickford L.R., Brownlow J.M., Penoyer F.R.: Proc.IEEE **104,** 238–244 (1957)

SECTION 6

CHEMICAL AND BIOLOGICAL SYSTEMS

oral

Lipid-mediated effect of saponin β-escin on the localization of the transmembrane domain of E protein of SARS-COV-2

M.A. Arbuzova[1,2], O.Yu. Selyutina[1], N.E. Polyakov[1]

[1] Voevodsky Institute of Chemical Kinetics and Combustion of the Siberian Branch of the RAS, Novosibirsk, Russia
[2] Novosibirsk State University, Novosibirsk, Russia

β-Escin (Fig. 1) is the major saponin from the extract of chestnut seed of A. hippocastanum. Escin is known to exhibit antiviral activity, including against SARS-COV. The mechanism of antiviral action is considered to be inhibition of viral particle penetration into the host cell membrane. [1] SARS-CoV-2 is an enveloped virus. Envelope viruses are entering the host cell by fusion of the lipid envelope of the virus with the host cell membrane and subsequent release of the viral particle into the cell interior [1]. Envelope protein (E-protein) is a structure protein of SARS-CoV-2. It is assumed that the role of protein E is not in coordinating particle assembly, but in giving the viral particle envelope the necessary curvature. This protein is involved in many processes of the virus life cycle and plays a major role in pathogenesis. The E-protein, particularly its transmembrane domain (ETM), is highly conserved and evolves much more slowly than other proteins [2].

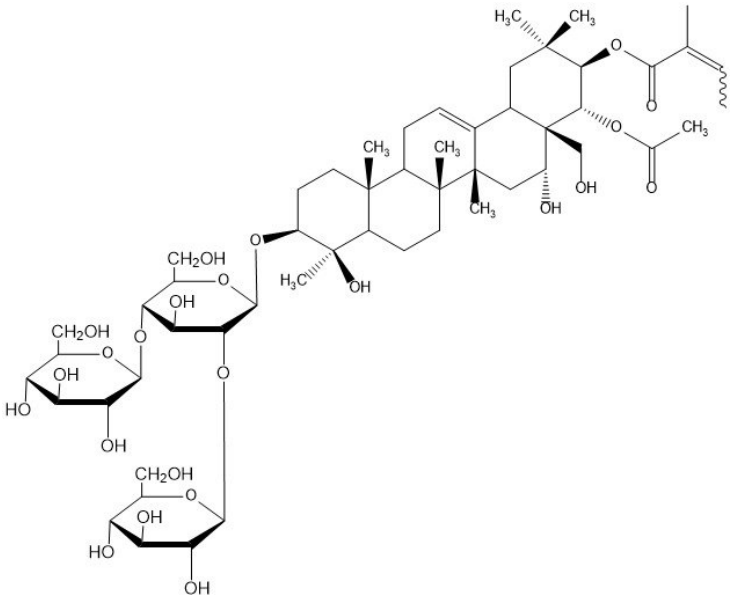

Fig. 1. Structure of β-Escin.

oral

The transmembrane domain of the E-protein of SARS-CoV-2 was used to study the lipid-mediated effect of escin on the envelope protein of coronavirus. Small isotropic lipid bicelles DHPC/DMPC were used as a lipid membrane model. The study was performed by Nuclear Overhauser Effect NMR spectroscopy (NOESY). It was found that escin and the transmembrane domain of E-protein are anchored in the lipid bilayer. The study was performed by Nuclear Overhauser Effect NMR spectroscopy (NOESY). It was found that Escin and the transmembrane domain of E-protein are anchored in the lipid bilayer. It is shown that the presence of Escin leads to a deeper immersion of the phenylalanine residue of ETM in the hydrophobic region. The effect of lipid composition (presence of cholesterol, charged lipids) on the localization of molecules was studied. The effect of escin on the localization of ETM in the presence of 1,2-dimyristoyl-sn-glycero-3-phospho-L-serine (DMPS) was also studied. In the presence of DMPS, escin changes its localization, its fragments can be located in both hydrophilic and hydrophobic regions. The ETM peptide in the presence of DMPS is localized predominantly in the hydrophilic region by its phenylalanine fragment. In the presence of escin, the peptide was localized by the phenylalanine residue in the hydrophilic and hydrophobic regions to the same extent. In addition, the interaction between escin and the transmembrane domain of E-protein was detected.

1. Mieres-Castro D., Mora-Poblete F.: “Saponins: Research Progress and Their Potential Role in the Post-COVID-19 Pandemic Era”, *MDPI*. Feb. 01, 2023
2. Kononova P.A., Selyutina O.Y., Fomenko V.V., Salakhutdinov N.F., Polyakov N.E.: “The mutual lipid-mediated effect of the transmembrane domain of SARS-CoV-2 E-protein and glycyrrhizin nicotinate derivatives on the localization in the lipid bilayer,” Arch. Biochem. Biophys. **758**, Aug. (2024)

oral

EPR spectroscopy for biostability assessment of metallodrug complexes

S.A. Dementev[1,2], R.A. Podarov[1,2], K.A. Koshenskova[3], I.L. Eremenko[3], I.A. Lutsenko[3,4], M.V. Fedin[1,2], O.A. Krumkacheva[1,2]

[1] International Tomography Center, SB RAS, Novosibirsk, Russia
[2] Novosibirsk State University, Novosibirsk, Russia
[3] N.S. Kurnakov Institute of General and Inorganic Chemistry, RAS, Moscow, Russia
[4] RUDN University, Moscow, Russia

Metal-coordinated organic complexes have emerged as potential therapeutic agents, offering unique structural and mechanistic opportunities through their distinctive coordination chemistry and redox properties [1]. Metallodrugs utilize metal ions as central elements for biological interactions, and are being investigated for antimicrobial, antibacterial, and anticancer applications, with copper complexes showing promise in preclinical studies as anticancer and antibacterial therapeutics [2]. Assessment of metallodrug stability in biological environments represents a critical challenge, with electron paramagnetic resonance (EPR) spectroscopy emerging as a powerful tool for investigating biostability of paramagnetic metal complexes. EPR spectroscopy provides detailed information about electronic structure, ligand coordination, and magnetic interactions, making it well-suited for characterizing ligand-exchange processes. Human serum albumin (HSA) binds metal ions with high affinity and can lead to dissociation of metal-containing complexes, making stability assessment in HSA presence critical. Our methodology employs continuous wave EPR spectroscopy in frozen water-glycerol solutions to monitor spectral changes upon HSA interaction, enabling quantitative analysis of complex speciation under physiologically relevant conditions.

Our EPR investigation of the anionic tetranuclear complex $[Cu_4(H_2O)_4(phen)_4(phyt)]\times 2Na^+\cdot 2NH^{4+}\cdot 32H_2O$ (Fig. 1) revealed distinct magnetic coupling patterns and demonstrated

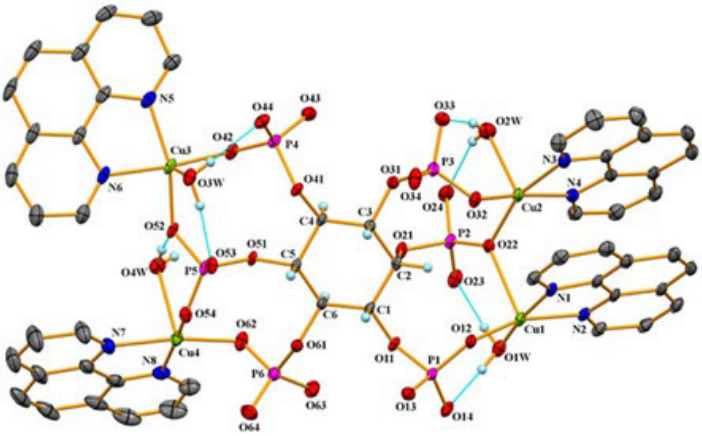

Fig. 1. The structure of anionic tetranuclear complex $[Cu_4(H_2O)_4(phen)_4(phyt)]\cdot 2Na^+\cdot 2NH_4^+\cdot 32H_2O$ [3].

oral

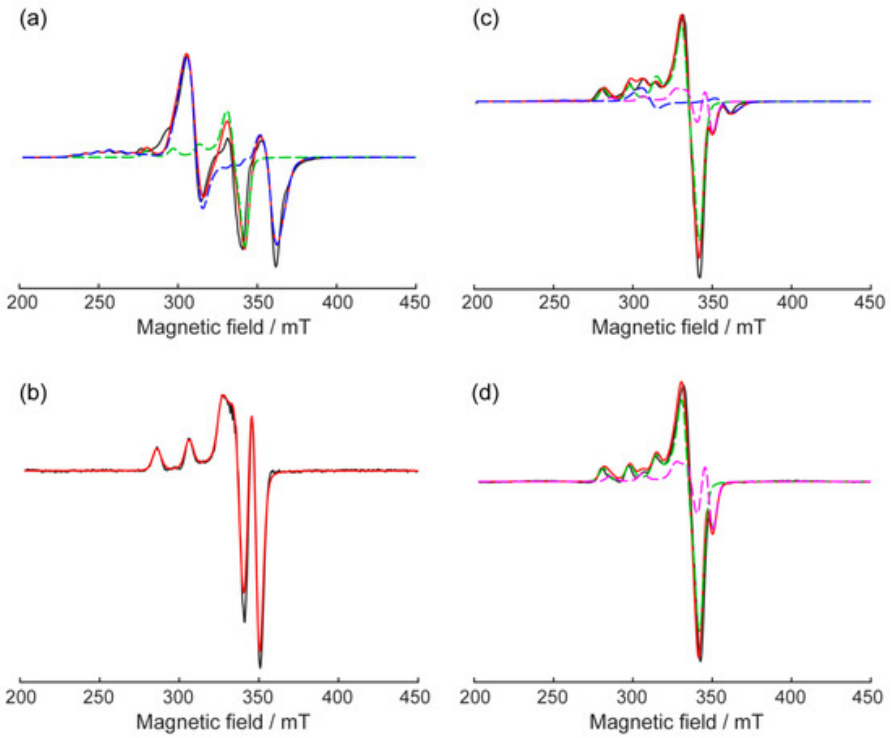

Fig. 2. X-band CW EPR spectra of samples recorded at 80 K in a 1:1 mixture of 10 mM PBS buffer and glycerol. Experimental spectra (black noisy lines) were simulated using EasySpin. Dashed colored lines represent simulated spectra for individual fractions; the red line is the final combined weighted simulation. (**a**) 1 mM 1: blue dashed line—tetrameric fraction; green dashed line—monomeric fraction. (**b**) Equimolar complex of 1 mM Cu^{2+} and 1 mM HSA. (**c**) Equimolar complex of 1 mM 1- and 1 mM HSA: blue dashed line-tetrameric fraction; green dashed line-monomeric fraction; magenta dashed line-Cu^{2+}-HSA complex. (**d**) 1:4 complex of 0.25 mM 1- and 1 mM HSA: green dashed line—monomeric fraction; magenta dashed line – Cu^{2+}-HSA complex.

significant structural changes upon HSA interaction [3]. The analysis identified two fractions within a compound: a dominant (tetrameric) fraction (70%) exhibiting exchange-coupled Cu(II) centers with zero-field splitting parameter $D = 1540$ MHz, and a secondary fraction (30%) showing monomeric copper behavior (Fig. 2a). Upon HSA interaction at equimolar ratios, the tetrameric fraction reduced from 70% to 20%, while new fractions emerged corresponding to Cu(II) bound to HSA (20%) and monomeric Cu(II) (60%) (Fig. 2b). At four-fold HSA excess, the tetrameric fraction completely disappeared, indicating partial dissociation while maintaining distinct coordination environments (Fig. 3d), demonstrating EPR spectroscopy's utility for quantitative metallodrug stability assessment.

1. Karges J., Stokes R.W., Cohen S.M.: Metal complexes for therapeutic applications. Trends in chemistry **3**, no. 7, 523–534 (2021)
2. Ferreira A.M.D.C. et al.: Molecular basis for anticancer and antiparasite activities of copper-based drugs // Redox-Active Therapeutics. P. 287–309 (2016)
3. Koshenskova K.A. et al.: «Green-Ligand» in Metallodrugs Design–Cu (II) Complex with Phytic Acid: Synthetic Approach, EPR-Spectroscopy, and Antimycobacterial Activity //Molecules **30**, no. 2, 313 (2025)

oral

Nanoscale structures in model phospholipid biomembranes probed by pulsed dipolar EPR spectroscopy

S.A. Dzuba

Voevodsky Institute of Chemical Kinetics and Combustion, Russian Academy of Sciences, Novosibirsk,630090, Russia, email: dzuba@kinetics.nsc.eu

Pulsed dipolar EPR spectroscopy (PDS) is widely used in various biophysical applications to study nanostructure of spin-labeled biomolecules. Among the various versions of PDS, the most commonly used is the double electron-electron resonance (DEER, also known as PELDOR). DEER is usually applied to double-spin labeled molecules. However, mono-spin labeled molecules can be used to study the nanostructure of biological membranes using the DEER method. In particular, this approach has revealed the self-organization of guest amphiphilic molecules in phospholipid bilayers, which can be described within the framework of the "chessbox" model [1].

It is widely accepted that the plasma membrane is largely divided into compartments in which lipids and proteins are organized into distinct nanoscale domains. More ordered domains are called lipid rafts; these domains are thought to compartmentalize membrane processes. Formation of lipid rafts is also known for the simpler model systems of cholesterol-containing lipid bilayers. In addition to the DEER experiment, we also used the two-pulse electron spin echo method, "cleaned" from the influence of thermal relaxation (2p ESE), to study raft-containing systems [2]. The combination of these two PDS methods for spin label nanoclusters allowed the classical DEER experiment to avoid the difficulties arising from the interference of different dipolar pathways. Using this combined approach – see Fig. 1 – we found that amphiphilic guest molecules in the raft-containing lipid bilayers form isolated clusters of about 4 nm in size, containing 6-8 molecules located at least 1.3 nm apart. This result can be explained by the direct interaction of amphiphilic guest molecules with lipid rafts.

This research was supported by the Russian Science Foundation, grant # 25-23-00061.

1. Kashnik A.S., Atnyukova A.N., Baranov D.S., Dzuba S.A.: Appl. Magn. Reson. **55**, 1145–157 (2024)
2. Golysheva E.A., Kashnik A.S., Baranov D.S., Dzuba S.A.: J. Phys. Chem. B **129**, 650–658 (2025)

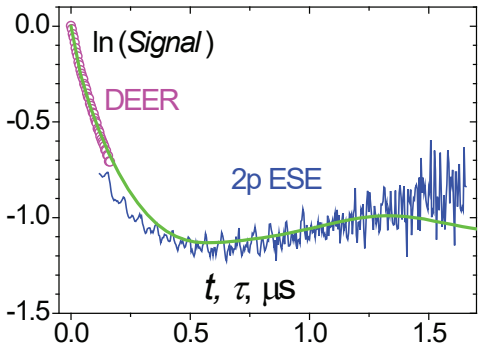

Fig. 1. Combined DEER and 2p ESE time traces obtained for spin-labeled ibuprofen drug in the raft-containing model phospholipid bilayer [2]. The smooth solid line is the simulation for the model of 6-membered nanocluster.

oral

EPR study of the content of nitric oxide and copper in the liver of rats after modeling combined brain and spinal cord injuries

Kh.L. Gainutdinov[1,2], V.V. Andrianov[1,2], L.V. Bazan[1], T.K. Bogodvid[2,3], I.B. Deryabina[2], G.G. Yafarova[2], A.I. Arslanov[1], T.S. Zharkova[2], R.V. Etkhemova[2], S.G. Pashkevich[4], T.A. Filipovich[4], V.A. Kulchitsky[4]

[1] Zavoisky Physical-Technical Institute, FRC Kazan Scientific Center of RAS, Kazan 420029, Russian Federation;
[2] Institute of Fundamental Medicine and Biology of Kazan Federal University, Kazan 420008, Russian Federation;
[3] Volga Region State University of Physical Culture, Sport and Tourism, Kazan 420010, Russian Federation;
[4] Institute of Physiology of Nat. Acad. of Sci. of Belarus, Minsk 220072, Belarus
kh_gainutdinov@mail.ru

The discovery of the ability of mammalian cells to synthesize nitric oxide (NO) has stimulated enormous research efforts to study the role of NO in all areas of chemistry, biology and medicine [1, 2]. NO, as a key signaling molecule, is involved in the regulation of many physiological functions of the body, including the nervous system [3]. NO is widely distributed in the nervous [4, 5], cardiovascular [6, 7] and other functional systems of the body [8]. Since NO is a chemically highly reactive free radical capable of acting as both an oxidizer and a reducer [1], an assumption arises about its diverse effects in biological tissues. Of great interest is the participation of NO in the mechanisms of development of various pathological conditions of the body [9]. One of the reasons for the involvement of NO in the pathological process is a long-term lack of oxygen, which leads to brain hypoxia [10, 11]. However, there are contradictions in the data on the role of NO in these processes, which allow us to state that at present there is no consensus on the role of endogenous NO in the processes occurring during damage to the nervous system [3, 10].

There are many methods for measuring NO production in biological systems. Accurately measuring both the constant concentration of NO and the rate of NO production in biological systems is challenging due to the low activity of NO synthases and its short half-life. In recent years, electron paramagnetic resonance (EPR) was proven as one of the most effective methods for the detection and quantification of nitric oxide in biological tissues [10, 12, 13]. According to this we tried to detail some of the biophysical patterns of nitrogen monoxide formation in combined trauma of the brain and spinal cord

EPR spectroscopy was used to study the dynamics of NO content in the brain of rats after modeling combined brain and spinal cord injuries. The intensity of NO production by EPR spectroscopy was measured using the spin trap method [10, 12], which is based on the reaction of NO with a spin trap. The complex of Fe^{2+} with diethyldithiocarbamate (DETC) was used for capture NO with generating a stable ternary complex $(DETC)_2$-Fe^{2+}-NO in animal tissue. These complexes are characterized by an easily recognizable EPR spectra with a *g*-factor value of $g = 2.035–2.040$ and a triplet hyperfine structure [1, 12, 13]. The measurements of spectra of complex of

biological samples $(DETC)_2$-Fe^{2+}-NO and Cu^{2+}-$(DETC)_2$ were made using a Bruker X-band (9.5320 GHz) EMX/plus spectrometer.

The intensity of NO production and copper content in the liver of rats after the formation of combined injury were studied using the EPR spectroscopy method. It was shown that 7 days after modeling combined injury of the brain and spinal cord, there was a significant (reliable) decrease in NO production in the liver by 2 times. Copper content in the liver also decreased, but not significantly.

The work was supported by the framework of a state assignment to Zavoisky Physical-Technical Institute of RAS and the Strategic Academic Leadership Program of Kazan Federal University (PRIORITY 2030).

1. Vanin A.F.: Nitric Oxide **54**, 15–29 (2016)
2. Ignarro L.J. et al.: J Cardiovasc Pharmacol. **34**(6), 879–886 (1999)
3. Lundberg J.O.; Weitzberg E.: Cell **185**, 2853–2878 (2022)
4. Steinert J.R. et al.: Neuroscientist **16**, 435–452 (2010)
5. Chachlaki K.; Prevot V.; British J. Pharmacol. **177** (24), 5437–5458 (2020)
6. Zaripova R.I. et al.: Zhurnal tekhnicheskoy fiziki **92**(7), 999–1003 (2022)
7. Lakomkin V.L. et al.: Nitric Oxide: Biology and Chemistry **16**(4), 413–418 2007
8. Boehning D.; Snyder S.H.: Annu. Rev. Neurosci. **26**, 105–131 (2003)
9. Pacher P. et al.: Physiol. Rev. **87**, 315–427 (2007)
10. Wierónska J.M. et al.: Biomolecules **11**, 1097 (2021)
11. Shlapakova T.I. et al.; Bioorganic Chemistry 46(5), 466–485 (2020)
12. Mikoyan V.D. et al.: Biochim. Biophys. Acta **1336**, No 2, 225–234 (1997)
13. Gainutdinov Kh.L. et al.: Technical Physics **65**(9), 1421–1426 (2020)

oral

Self-consistent relaxation theory of collective dynamics in Yukawa and Coulomb liquids

I.I. Fairushin, A.V. Mokshin

Kazan Federal University, Kazan, Russia

One of the key tasks of spectroscopy is the interpretation of experimental data on measuring the spectral densities of collective excitations of multiparticle systems. In this work, we develop a theoretical formalism that describes the collective dynamics of ions in systems such as Coulomb and Yukawa liquids. These systems are used as models when considering the physical properties of a large number of natural and laboratory objects. These include the dense astrophysical matter in white dwarfs and neutron stars, the working fluid of inertial fusion devices, ultracold plasmas, dusty plasmas, electrolytes and charged stabilized colloids and others. [1]. The proposed formalism is based on the self-consistent relaxation theory of collective dynamics of disordered systems [2, 3] and allows one to reproduce the dynamic structure factor spectra and the corresponding dispersion characteristics in agreement with molecular dynamics simulation data without using any fitting parameters [4, 5]. Note that the approach presented in our paper can be easily generalized to the cases of strongly coupled quantum electron liquids [6].

The work was carried out on the basis of the grant provided by the Academy of Sciences of the Republic of Tatarstan in 2024 for the implementation of fundamental and applied research work in scientific and educational organizations, enterprises and organizations of the real sector of the economy of the Republic of Tatarstan.

1. Fortov V.E., Ivlev A.V., Khrapak S.A., Khrapak A.G., Morphill G.E.: Phys. Rep. **421**, 1 (2005)
2. Mokshin A.V.: Theor. Math. Phys. **183**, 449 (2015)
3. Mokshin A.V., Galimzyanov B.N.: J. Phys.: Condens. Matter **30**, 085102 (2018)
4. Mokshin A.V., Fairushin I.I., Tkachenko I.M.: Phys. Rev. E **105**, 025204 (2022)
5. Fairushin I.I., Mokshin A.V.: Phys. Rev. E **108**, 015206 (2023)
6. Filinov A.V., Ara J., Tkachenko I.M.: Phys. Rev. B **107**, 195143 (2023)

oral

Spatial organization of polymer-metal coils in liquid solutions: "spin exchange titration"

A.I. Kokorin

N.N. Semenov FRC for Chemical Physics of RAS, Moscow, Russia

Spin Exchange Titration (SET) characterizes the efficiency of spin exchange in liquid solutions between paramagnetic metal ions coordinated by complex-forming polymers With Nitroxide spin probes of constant concentration [1, 2].

It is evident to all EPR spectroscopists that spin exchange reaction reflects not only kinetics of paramagnetic species (PS) collisions but also effects of the PS nature, spin-relaxation parameters, steric hindrances, Colomb charges, etc. The approach SET is an especially useful EPR technique characterizes ability of small molecules and ions in liquid solutions to penetrate inside the globe of metal-complexing polymers or ion exchangerts. That gives the important information about spatial organization of such polymer-metal complexs which is useful for catalytic systems.

Dependences presented in Fig. 1 can be easily explained. One can conclude analyzing these data that:

1) without complex-forming polymers (×), linear broadening of nitroxide spin probe lines ΔH is caused by usual spin exchange coupling between NSP and Cu(II) ions.

2) In the case of P4VP-M, β = 36% (○), the area of ΔH independence *vs*. [Cu(II)] in the range of 0 < [Cu] < ~0.02 mol/L exhibits that CuN_4 complexes formed with pyridine residues (Py) [1] are not available for collisions with small molecules (NSP). One can estimate a fraction of Py links the total amount of CuN_4 complexes in the polymer coil in H_2O+CH_3OH mixture at 298 K: 26±2% N atoms form $Cu(N)_4$ complexes, additional ~13% N form $Cu(N)_3$ and $Cu(N)_2$ structures [3, 4], while ~60% links are free pyridine residues i.e. are not involved into metal complex formation.

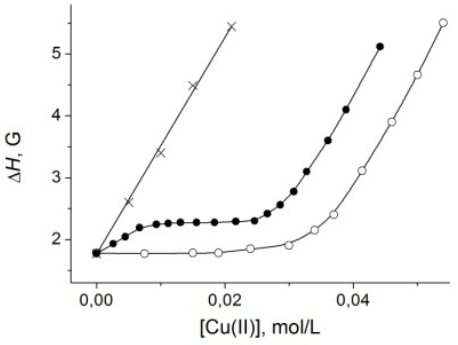

Fig. 1. Elfect of $Cu(NO_3)_2$ concentration on EPR line width ΔH in the absence (×) and presence of BPEI ([N] = 0.08 M) (●), and P4VP-E, β = 36%, ([N] = 0.36 M (○)) at 298 K.

oral

3) In the case of BPEI (●), approximately ~40% ethyleneimine links $–CH_2CH_2N–$ are involved in $Cu(N)_4$ complexes [5] and afterwards, up to ~90% N participate in "clusters" of $Cu(N)_4$ complexes self-organized in BPEI and LPEI coils [5, 6]. Indeed, at the first interval ($0 < [Cu(II)] < \sim 0.008$ M) a slope of ΔH dependence (Fig. 1) is approximately twice less than for spin exchange in the case without polymers (×). In this interval, only isolated $Cu(N)_4$ complexes do exist in PEI coils [6]. Afterwards, at $\sim 0.008 \text{ M} < [Cu(II)] < \sim 0.018$ M, $\Delta H \approx$ const, *i.e.*, new complexes forming in BPEI (as "clusters") are not available for collisions with NSP. At $[Cu(II)] > \sim 0.02$ M, newly added copper ions are actively involved into spin exchange.

We are thankful to Program of Fundamental Research of the Russian Federation (Reg. No: 125012200595-8).

1. Kokorin A.I.: Polymer Yearbook **13**, 141–161 (1996)
2. Kokorin A.I., Pridantscv A.A.: Russ. J. Phys. Chem. **71**, 1963–1968 (1997)
3. Kirsh Yu.E., Kovner V.Ya., Kokorin A.I., Zamaraev K.I., Chernyak V.Ya., Kabanov V.A.: Europ. Polymer J. **10**, 671–678 (1974)
4. Kokorin A.I., Zamaraev K.I., Kovner V.Y., Kirsh Yu.E., Kabanov V.A.: Europ. Polymer J. **11**, 719–722 (1975)
5. Kabanov N.M., Kokorin A.I., Rogacheva V.B., Zezin A.B.: Polym. Sci. USSR. **21**, 230–240 (1979)
6. Kokorin A.I., Shubin A.A.: Russ. J. Strukt. Khim. **30**, 106–112 (1989)

oral

Features of paramagnetic centers in nanosized porous aluminum oxide

E.A. Konstantinova[1], E.V. Kytina[1], Yu.V. Nazarkina[1,2]

[1] Physics Department, M.V. Lomonosov Moscow State University, Moscow, Russia
[2] National Research University of Electronic Technology – MIET, Zelenograd, Moscow, Russia

In recent years, interest in the study of porous anodic aluminum oxide (PAAO) has increased [1, 2]. This material is an array of ordered pores and is formed by a simple and accessible electrochemical method in electrolytes based on inorganic and organic acids. Interest in porous anodic aluminum oxide is primarily due to the large variability of its morphology (films on a substrate, free-standing films, powders, the pore range is from units to hundreds of nanometers). As a result, it can be used to create nanocomposites by filling the pores with another material, as a template for various nanostructures, as a sensor platform. The creation of a sensor platform based on porous anodic aluminum oxide for detecting biomarkers is the most urgent task at present in connection with the growth of infectious diseases in the world [3].

Aluminum foil (99.99% pure) was used for anodizing. Organic contaminants were removed from the surface by immersing the foil in acetone and placing it in an ultrasonic bath for 10 minutes. The surface roughness was reduced by polishing the aluminum substrates, which was carried out by electrochemical etching in a solution at a temperature of 5°C, containing 1:6 perchloric acid and ethyl alcohol, for 5 min at a voltage of 40 V, while stirring the electrolyte. After carrying out the described preliminary treatment of the surface of the aluminum substrates, they were thoroughly washed in deionized water and dried in air. Anodizing was carried out in a dilute solution of different acids (sulfuric, selenium, oxalic, etidronic) in the galvanostatic mode (in 1.5 M at a current density of 15 mA/cm^2 and at a different temperature of 5–55°C). To obtain an ordered porous structure of aluminum oxide, a two-stage anodization technique was used. The first stage was carried out for 30 min, after which the resulting sacrificial oxide layer was selectively removed for 15 min in an aqueous solution of 0.4 M phosphoric acid and 0.2 M chromic acid at a temperature of 80°C. The second stage was carried out with the same process parameters as the first, but for an hour. The dye rhodamine B was chosen as a model analyte, which was dissolved in deionized water to obtain a solution with a different concentration (10^{-5}–10^{-7}) M. The samples were immersed in the dye for 30 min at a temperature of 40°C, after which they were removed and dried in air.

The Helios NanoLab 650 scanning electron microscope (SEM) was used for study of sample structure. The pore diameters were studied using the FiJi software package. The electron paramagnetic resonance (EPR) studies were carried out in the EPR spectroscopy laboratory of the Collective Use Center of the Physics Faculty of Moscow State University using ELEXSYS-E500-10/12 equipment. The concentration of paramagnetic centers was estimated using a $CuCl_2 \cdot 2H_2O$ single crystal as a standard with a known number of spin centers.

oral

It was found that all samples contain oxygen vacancies with an unpaired electron (g = 2.0022 ± 0.0003); their concentration is maximum in the samples A2. In addition, O_2^- radicals (g_1 = 2.023±0.0003, g_2 = 2.008±0.0003, g_3 = 2.0035 ± 0.0003) were detected in samples A1 and A3. It was found that the photoluminescence intensity correlates with the concentration of oxygen vacancies. Therefore, it can be assumed that photoluminescence in auminium oxide nanotubes is due to radiative recombination of electrons and holes at oxygen vacancies.

The obtained PAAO samples are ordered arrays of pores with an average diameter of 10 nm when synthesized in an electrolyte at 5°C. Increasing the solution temperature to 25 °C leads to an increase in the average pore diameter to 14 nm, which indicates a significant increase in the chemical etching of the oxide walls. The surface of PAAO, synthesized at the electrolyte temperature 40 °C, consists of individual thread-like fibers. Oxygen vacancies (F^+ centers) were detected in all samples formed in sulfuric acid using the EPR method. In addition, in samples synthesized at 25°C, paramagnetic Al–SO_4 complexes were detected for the first time, which are incorporated into the structure of aluminum oxide from the electrolyte. It is assumed that Al–SO_4 complexes are localized on the surface and in the near-surface region of the pore walls, since their concentration decreases significantly in samples with etched pore walls (PAAO-40C).

The study was supported by the Russian Science Foundation grant No. 24-19-00402, https://rscf.ru/en/project/24-19-00402/.

1. Nikitin I.Yu., L. N. Borodina L.N., Boltenko A.V., Baranov M.A., Gladskikh I.A., Vartanyan T.A.: Optical Materials **160,** 116741 (2025)
2. Ku C.-A., Yu C.-Y., Hung C.-W., Chung C.-K.: Nanomaterials **13**, 2853 (2023)
3. Eessaa A.K., El-Shamy A.M.: Microelectron. Eng. **279**, 112061 (2023)

oral

Interaction of thiosemicarbazones with model lipid membranes: NMR and molecular dynamics simulations

V.E. Koshman, O.Yu. Selyutina, A.A. Dmitriev, N.E. Polyakov

Voevodsky Institute of Chemical Kinetics and Combustion of the Siberian Branch of the RAS, Novosibirsk, Russia

Thiosemicarbazones (TSC) are an important class of N-, S-donor compounds that exhibit a wide range of chemical and biological activity, including anticancer activity, and are of great interest to scientists from various fields of science.

NMR and molecular dynamics simulation methods revealed differences in the localization of new acridine-containing thiosemicarbazones: 2-benzoyl ((E)-N-(acridin-9-yl)-2-(phenyl(pyridin-2-yl)methylene)hydrazine-1-carbothioamide (AOBP) and 2-dipyridyl ((E)-N-(acridin-9-yl)-2-(di(pyridin-2-yl)methylene)hydrazine-1-carbothioamide (AODP) in a model lipid membrane.

Both thiosemicarbazones were shown to be able to penetrate into the lipid membrane. AOBP is able to penetrate into the center of the hydrophobic region of the lipid bilayer, while AODP is located closer to the surface and freely leaves the membrane, entering the aqueous environment. The result obtained using a combination of NMR and molecular dynamics modeling methods is in good agreement with the data in a recently published article [1], which, among other things, states that AOBP demonstrated greater antiproliferative activity against tumor cell lines BE(2)-C, KELLY, SH-SY5Y and SK-N-MC compared to AODP. This means that AOBP, penetrating deeper into the cell membrane, is more effective against tumor cells. In order to approximate more physiological conditions of the native cell lipid membrane, experiments were carried out with the addition of cholesterol, which is an important component of cell membranes, and its effect on the localization of AOBP and AODP molecules in the model lipid membrane was characterized. It was shown that the presence of cholesterol prevents the penetration of both thiosemicarbazones into the membrane.

Since the mechanism of anticancer activity of thiosemicarbazones is associated with their penetration into lysosomes, the obtained results are important for a better understanding of the mechanisms of activity of these compounds and the development of new drugs.

1. Kaya B. et al.: Innovative N-Acridine thiosemicarbazones and their Zn(II) complexes transmetallate with Cu(II): Redox activity and suppression of detrimental oxy-myoglobin oxidation // Inorg Chem. **63**, no. 43. 20840–20858 (2024)

oral

Effect of spin centers on photoluminescence in porous aluminum oxide synthesizing in organic acids

E.V. Kytina[1,2]

[1] Physics Department, M.V. Lomonosov Moscow State University, Moscow, Russia
[2] N.N. Semenov Federal Research Center for Chemical Physics, Russian Academy of Sciences, Moscow, Russia

.Currently, the urgent problem is the production, study of porous aluminum oxide and the creation of biosensors for biomarkers on its basis due to the constant growth of diseases of various natures throughout the world [1–3]. Spin centers (defects) play an important role in photoelectronic processes in porous aluminum oxide. It is important to know their nature and concentration. Therefore, the purpose of this work was to diagnose defects in porous aluminum oxide and identify their role in photoluminescence.

Aluminum foil (99.99% pure) was used for anodizing. Organic contaminants were removed from the surface by immersing the foil in acetone and placing it in an ultrasonic bath for 10 minutes. Anodizing was carried out in a dilute solution of oxalic acid (A-Ox samples) and etidronic acid (A-Et samples) in the galvanostatic mode (in 1.5 M at a current density of 15 mA/cm^2 and at a different temperature of 5–55°C). To obtain an ordered porous structure of aluminum oxide, a two-stage anodization technique was used.

The Helios NanoLab 650 scanning electron microscope (SEM) was used for study of sample structure. The electron paramagnetic resonance (EPR) studies were carried out in the EPR spectroscopy laboratory of the Collective Use Center of the Physics Faculty of Moscow State University using ELEXSYS-E500-10/12 equipment. The concentration of paramagnetic centers was estimated using a $CuCl_2$•$2H_2O$ single crystal as a standard with a known number of spin centers. Photoluminescence (PL) spectra were recorded on an LS-55 Perkin Elmer (USA) instrument (spectral range from 250 to 900 nm).

The obtained porous aluminum oxide samples are ordered arrays of pores with an average diameter of 25 nm when synthesized in an oxalic acid or 120 nm when synthesized in an etidronic acid at 5 °C.

The samples obtained in both oxalic and etidronic acids contain spin centers of only one type – oxygen vacancies (F^+ centers, g = 2.0022). Their concentration was 10^{15} g^{-1} и 10^{17} g^{-1} for A-Et and A-Ox samples synthesized at 5°C, respectively. Photoluminescence (PL) was maximal in A-Ox samples with maximal concentration of F^+ centers. Considering that PL excitation is less than the band gap, it can be assumed that PL has a defective nature and F^+ centers are responsible for it.

The concentration of F^+ centers in A-Et samples depends non-monotonically on synthesis temperature, reaching a maximum at approximately 10°C. In the PL spectra of A-Et samples synthesized at temperatures of 10–55°C, two PL bands are recorded: at 463 and 610 nm. The PL intensity changes non-monotonically with the synthesis temperature: the PL maximum at 463 nm occurs at 25°C, and the PL maximum at 610 nm occurs at 40°C. We found no relationship between the PL intensity and the

concentration of spin centers (F^+). Consequently, the PL in the samples is due to the radiative recombination of photoexcited charge carriers on nonparamagnetic defects. Since PL intensity has a maximum for the observed PL bands at different synthesis temperatures, it can be assumed that PL at 463 and 610 nm take place through radiative recombination of photoexcited electrons at various nonparamagnetic defects.

Thus, the nature of the luminescent centers in porous aluminum oxide synthesized in oxalic and etidronic acids is different. In A-Ox samples, PL occurs on spin centers, and in A-Et samples, PL occurs on non-paramagnetic centers.

The obtained results may be useful for the creation of optical sensor platforms based on porous alumina for the detection of biomarkers.

The study was supported by the Russian Science Foundation grant No. 24-19-00402, https://rscf.ru/en/project/24-19-00402/.

1. Ku C.-A., Yu C.-Y., Hung C.-W., Chung C.-K.: Nanomaterials **13**, 2853 (2023)
2. Eessaa A.K., El-Shamy A.M.: Microelectron. Eng. **279**, 112061 (2023)
3. Rajeev G., Prieto Simon B., Marsal L.F., Voelcker N.H.: Adv. Healthc. Mater. **7**, 1700904 (2018)

oral

Intramolecular distances and excluded volume: simultaneous analysis of deer traces in a model biradical

A.G. Matveeva[1], N.P. Isaev[1], I.A. Kirilyuk[2], Yu.S. Motygina[1]

[1] Voevodsky Institute of Chemical Kinetics and Combustion SB RAS, Novosibirsk, 630090, Russia, e-mail: y.motygina@g.nsu.ru
[2] N.N.Vorozhtsov Novosibirsk Institute of Organic Chemistry SB RAS, Novosibirsk, 630090, Russia

Double Electron-Electron Resonance (DEER) is a powerful tool for measuring distance distributions in nanoscale objects, which are often inaccessible to other methods. For example, it enables the analysis of distances between two spin labels during the functioning of protein molecules. Since the DEER signal arises from both intramolecular and intermolecular interactions, a key challenge is the accurate separation of these contributions. The standard approach accounts for the intermolecular contribution only under the assumption of zero molecular size. Such correction of DEER data focuses on studying intramolecular distance distributions and introduces errors in the interpretation of the intermolecular contribution.

In this work, we analyze the intermolecular part of the DEER signal using an approach that accounts for nonzero molecular sizes – the so-called excluded volume effect. This method allows for the simultaneous determination of intramolecular distances between paramagnetic centers with higher accuracy while also measuring the intrinsic molecular volume. We analyzed a DEER dataset of a model nitroxide biradical. Intramolecular distances between spin labels were compared with the excluded volume size. This work supported by RSF, project number 24-23-00484.

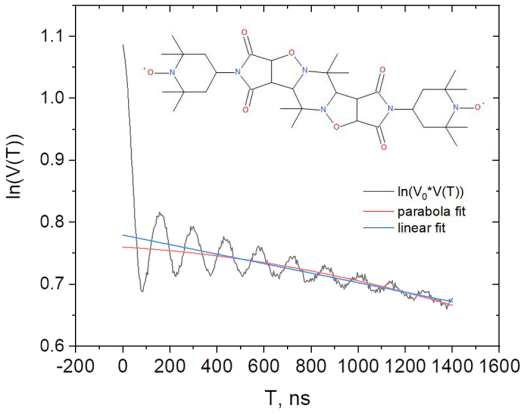

Fig. 1. DEER signal of the model biradical: experimental data (black), intermolecular parabolic fit (red), and a linear reference (blue) highlighting the deviation from pure distance-independent interactions.

oral

Water-soluble fullerenes as spin labels for dipolar EPR spectroscopy

R.A. Podarov[1,2], S.A. Dementev[1,2], P.A. Troshin[3], G.M. Fazleeva[4], M.V. Fedin[1,2], O.A. Krumkacheva[1,2]

[1] International Tomography Center, SB RAS, Novosibirsk, Russia
[2] Novosibirsk State University, Russia
[3] Skolkovo Institute of Science and Technology, Moscow, Russia
[4] Arbuzov Institute of Organic and Physical Chemistry, FRC Kazan Scientific Center of RAS, Kazan, Russia

Spin labels are paramagnetic molecules capable of selectively binding to studied objects, which are extensively investigated in the field of EPR spectroscopy methodology. An important goal is to develop an EPR methodology for spin labels based on photoinduced hyperpolarized triplet states, as well as to apply the developed approaches to studying biopolymers, including in cells. Such labels are distinguished by their non-equilibrium population, which allows achieving multiple signal enhancement, which is particularly relevant when studying biological objects at low concentrations [1]. Promising photoinducible spin labels are fullerenes and their modifications. However, their application in biology is often limited by minimal water solubility. In this regard, we faced the task of selecting conditions for maximum solubility of photoinduced spin labels based on fullerenes and their derivatives in order to obtain high-intensity echo-detected EPR spectra in X- and Q-bands.

Within the framework of this work, a series of water-soluble fullerene derivatives was investigated. From echo-detected EPR spectra, the degree of spin density delocalization in the triplet state was determined and compared with unmodified fullerene. The spin-

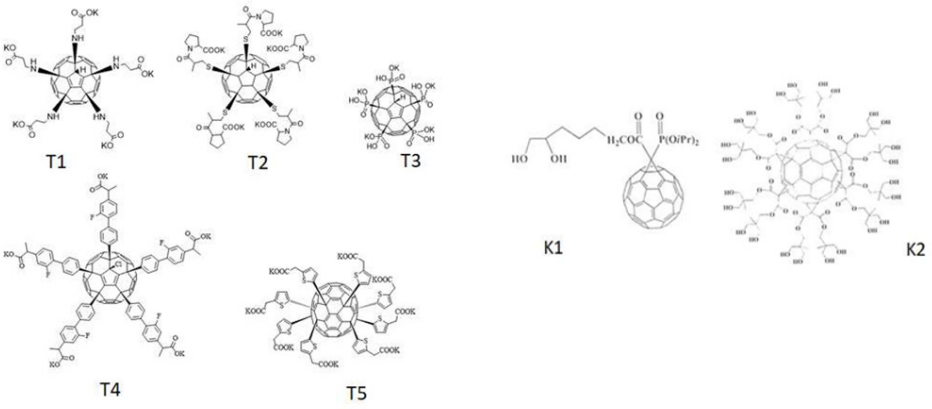

Fig. 1. Functionalized water-soluble fullerenes of the T and K series.

lattice and phase relaxation times of photoinducible fullerene-based labels measured in EPR experiments have similar relaxation times compared to standard trityl and nitroxide spin labels. A weak dependence of phase relaxation time on temperature was discovered, which is characteristic of cases where nuclear spin diffusion is the determining factor [2]. This served as the basis for comparing the behavior of spin echo of photoinduced labels in protonated and deuterated solvents, which showed an increase in phase relaxation time from 3 μs to 8 μs for the deuterated solvent. The obtained results are an important step toward the development of fullerene-based spin labels for EPR studies of biomolecules.

1. Kapsalis C., Wang B., El Mkami H., Pitt S.J., Schnell J.R., Smith T.K., ... & Pliotas C.: Allosteric activation of an ion channel triggered by modification of mechanosensitive nano-pockets. Nature Communications **10**(1), 4619 (2019)
2. Kuzin S., Syryamina V.N., Qi M., Fischer M., Hülsmann M., Godt A., ... & Yulikov M. ih-RIDME: A pulse EPR experiment to probe the heterogeneous nuclear environment. Magnetic Resonance Discussions, 1–31 (2024)

oral

Effect of rare earth dopants on the structural features of calcium phosphate-based materials by EPR spectroscopy

M.A. Sadovnikova[1], D.V. Shurtakova[1], G.V. Mamin[1], F.F. Murzakhanov[1], M.A. Goldberg[2], Yu.O. Zobkova[2], N.V. Petrakova[2], V.S. Komlev[2], M.R. Gafurov[1]

[1] Kazan Federal University, Kazan, Russia
[2] A.A. Baikov Institute of Metallurgy and Material Science, Russian Academy of Sciences, Moscow, Russia

The calcium phosphate (CaP) systems under investigation are widely used in biomedical applications, particularly in orthopaedics and maxillofacial surgery, as fillers for bone defects resulting from injuries or various diseases [1]. Incorporating rare earth (RE) elements – such as cerium (Ce^{3+}), neodymium (Nd^{3+}), europium (Eu^{2+}), gadolinium (Gd^{3+}), and erbium (Er^{3+}) – into the CaP crystal structure enables the development of bioimaging systems that enhance contrast for monitoring bone repair dynamics [2]. Modern diagnostics widely uses non-invasive imaging methods, including radiography, computed tomography (CT), single-photon emission computed tomography (SPECT), and magnetic resonance imaging (MRI). Ionizing radiation-based methods (radiography and CT), despite their high resolution and throughput, are associated with radiation risk and do not always provide sufficient contrast for accurate tissue differentiation. The search for new biocompatible and safe agents with more effective contrast enhancement is a popular area in practical diagnostics.

This study focuses on characterizing synthetic CaP doped with RE ions using continuous and pulsed electron paramagnetic resonance (EPR) techniques. The CaP-RE materials were synthesized via precipitation from aqueous salt solutions [3].

Samples of magnesium-calcium phosphate powders with gadolinium impurity centers were studied by EPR at a temperature of $T = 297$ K, since the Gd^{3+} ion with the electron configuration $4f^7$ ($^8S_{7/2}$ is the ground state) is the only trivalent RE element that can be observed at room conditions. The CaP crystal lattice without paramagnetic impurities does not contain ions with a non-zero electron spin, which leads to the absence of an EPR signal. The presence of a resonance low-intensity signal ($g \approx 2$) for a nominally pure sample (Fig. 1a, blue inset) indicates the presence of an uncontrolled impurity in the structure due to the reagents used, presumably indicating the presence of oxide groups or a free radical on the surface of magnesium-calcium phosphate powder nanoparticles. It is also worth noting that the broadening of the resonance absorption line is due to the fact that the Gd^{3+} ion is characterized by a strong spin-lattice interaction and due to extremely short longitudinal relaxation times ($T_1 \approx 1/T_n$ (K), where n is the exponent depending on the relaxation mechanisms). Based on the characteristic EPR signals with g-factors ($g_{eff} = 5.8$, $g_{eff} = 2.8$ and $g = 1.9$), we can unambiguously conclude that Gd^{3+} is embedded in the crystal lattice of the sample under study. Analysis of the intensities of the EPR spectra for two different concentrations of gadolinium (0.5% Gd and 1% Gd) indicates that the proposed synthesis method allows the introduction of the amount of impurity centers declared during chemical synthesis into the CaP structure (the integral intensity differs by a factor of 2).

oral

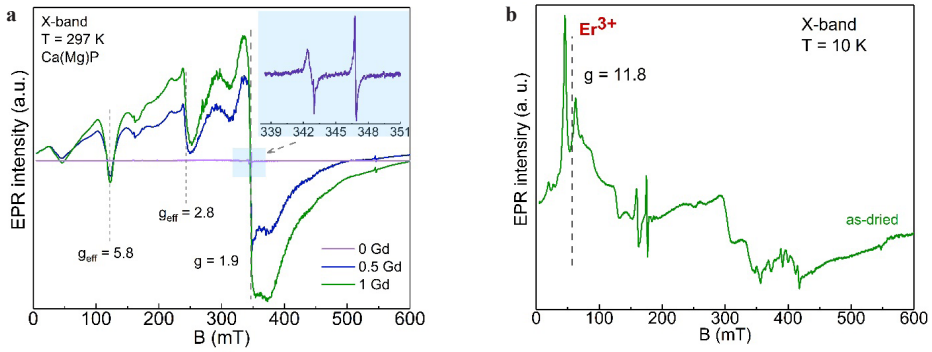

Fig. 1. a Concentration dependence of CW EPR spectra in the X-band for magnesium-calcium phosphate powders with Gd^{3+}; **b** EPR spectra recorded in CW mode in the X-band for hydroxyapatite with 0.25Er.

The typical detection range of the Er^{3+} signal is up to 20 K, at temperatures above 30 K the EPR signal is usually not observed, so the experiment was carried out at a sample temperature of 10 K (Fig. 1b). In polycrystalline systems, all crystal orientations are statistically equally probable. As a result, the EPR spectrum of the powder is the superposition of all nanocrystal orientations. Figure 1b shows the EPR spectra recorded at a sample temperature of 10 K. According to the literature data [4] the signal at the g-factor of 11.8 refers to the RE element Er^{3+}. The weak structural inflections detected in the spectrum (Fig. 1b) are possibly associated with the emergence of a hyperfine structure as a result of interaction with the ^{167}Er isotope with a nuclear spin of I = 7/2 (abundance of 23%). Also, the presence of low-intensity resonance curves can be caused by the presence of various uncontrolled impurities on the sample surface or in the interstitial sites of the crystal lattice. Thus, the obtained results indicate the introduction of Er^{3+} ions into the crystalline lattice of hydroxyapatite in the proposed synthesis method.

The results of this study demonstrate the potential of EPR spectroscopy as a powerful tool for investigating functional biomaterials doped with rare earth elements.

This research was funded by the RSF grant No 23-63-10056

1. Abdul Halim N.A., Hussein M.Z., Kandar M.K.: International Journal of Nanomedicine 6477–6496 (2021)
2. Mondal S., Park S., Choi J. et al.: Ceramics International **46** (18), 29249–29260 (2020)
3. Petrakova N.V., Zobkova Y.O., Komlev V.S. et al.: Ceramics International **50** (12), 20905–20916 (2024)
4. Gorni G., Serrano A., Bravo D. et al.: Journal of the American Ceramic Society **103** (7), 3930–3941 (2020)

oral

Inversion of electron spin polarization in organic chromophores. Time-resolved EPR study

A.A. Sukhanov[1], V.K. Voronkova[1], J. Zhao[2]

[1] Zavoisky Physical-Technical Institute, FRC Kazan Scientific Center of RAS, Kazan, Russia
[2] State Key Laboratory of Fine Chemicals, School of Chemical Engineering, Dalian University of Technology, Dalian 116024, P. R. China

As is known, the chromophore molecule can transition from the excited singlet state to the triplet state upon photoexcitation. The population of the sublevels of the triplet state occurs selectively. This nonequilibrium distribution of populations is known as the effect of the so-called chemically induced electron spin polarization (ESP). This effect of nonequilibrium ESP can be registered by the time-resolved EPR (TR EPR) method [1]. This method is based on direct detection of the EPR signal after the laser pulse. In TR EPR experiments we obtain both the time dependence of the EPR signal after the laser pulse and the dependence of the EPR signal on the magnetic field as for a CW EPR, but without magnetic field modulation.

Typically, the intensity of the triplet state TR EPR signal decreases with the observation time after the laser pulse. Therefore, the time dynamics of the EPR spectra are not analyzed. But there are examples where the ESP pattern changes dramatically. The ESP of the triplet TREPR spectra is inverted as the delay time after laser pulse. This change of ESP can be explained by the presence of strong anisotropy of the decay of the three sublevels of the triplet state. The nature of this anisotropy can be different.

We have studied various chromophores [2–4], including dyads in which we observe the ESP inversion. An analysis of the dynamics of EPR spectra is provided.

The study was supported by the government assignment for FRC Kazan Scientific Centre of RAS. A. A. S. acknowledges the grant of the Academy of Sciences of the Republic of Tatarstan, provided to young candidates of science (postdoctoral students) for the purpose of defending a doctoral dissertation, carrying out research work, and also performing work functions in scientific and educational organizations of the Republic of Tatarstan within the framework of the State Program of the Republic of Tatarstan “Scientific and Technological Development of the Republic of Tatarstan.

1. Weber S.: Transient epr. EPR Spectroscopy: Fundamentals and Methods. John Wiley & Sons Ltd (2008), p. 195.
2. Zhang Xue, Xu Ziqian, Sukhanov Andrey A., Yang Xichuan, Elmali Ayhan, Zhao Jianzhang, Dick, Ahmet Karatay Bernhard, Voronkova Violeta K.: Org. Chem. Front., **12**, 3344–3362 (2025)
3. Mambetov A., Sukhanov A., Zhang Xue, Zhao Jianzhang, Voronkova V.: Appl Magn Reson **55**, 1553–1567 (2024)
4. Wang Ruilei, Sukhanov Andrey A., He Yue, Mambetov Aidar E., Zhao Jianzhang, Escudero Daniel, Voronkova Violeta K., Donato Mariangela Di: J. Phys. Chem. B, **128**, 41, 10189–10199 (2024)

oral

Study of weak non-covalent interactions of quinone derivatives with GMP and oligonucleotides by NMR and CIDNP techniques

M. Ulyanova[1,2], O.Yu. Selyutina[1], N.E. Polyakov[1], O.A. Gulyaeva[3], E.V. Dmitrienko[3]

[1] Voevodsky Institute of Chemical Kinetics and Combustion of the Siberian Branch of the RAS, Novosibirsk, Russia
[2] Novosibirsk State University, Novosibirsk, Russia
[3] Institute of Chemical Biology and Fundamental Medicine of the Siberian Branch of the RAS, Novosibirsk, Russia

Various derivatives of 9,10-anthraquinone and 1,4-naphthoquinone are widely used in medicine, and possess chelating, redox, and intercalating properties due to their structural features. The ability to interact with DNA through intercalation constitutes the primary mechanism of quinones cytotoxicity. Additionally, quinones are considered as perspective agents in photodynamic therapy.

In the present work, quinone-DNA interactions were studied using NMR and CIDNP techniques. We have tested the interaction of two quinones, N-(2-chloro-1,4-naphthoquinonyl)-β-alanine (Nap) and 2-phenyl-4-(butylamino)-naphtholquinoline-7,12-dione (Q_1) with mono- and oligonucleotides 1G, 2G, 3G, 4G, where G denotes guanosine monophosphate (GMP).

It was found that both quinones form weak complexes with GMP, primarily through stacking interactions, but not with the oligonucleotides.

Another key aspect of our study involved investigation the interaction of these quinones with mono- and oligonucleotides under light exposure. Using chemically induced dynamic nuclear polarization (CIDNP), which arises upon irradiation, it was demonstrated that both Q_1 and Nap participate in photoinduced electron transfer reactions with GMP. It was found that in the Q_1-GMP and Nap-GMP systems, photoexcitation leads to quenching of triplet excited states of the quinones, resulting in the formation of quinone anion radicals ($Q_1^{\bullet-}$ and $Nap^{\bullet-}$) and GMP cation radicals ($GMP^{\bullet+}$), respectively.

Furthermore, the naphthoquinone Nap was shown to undergo electron transfer reactions with oligonucleotides 2G, 3G, and 4G, regardless of sequence length.

Since the cytotoxicity of quinones is linked to their ability to interact with DNA, these findings are crucial for understanding the mechanisms behind their therapeutic activity. The CIDNP data reveal the photochemical activity of the studied compounds.

This research was supported by grant from the Russian Science Foundation (№25-23-00243).

oral

Why, when there is oxygen in the tissues as a possible oxidizer of nitric oxide, the latter is preserved in the body of animals and humans, exercise a various physiological effect on it?

A.F. Vanin

Federal Research Center of Chemical Physics named after N.N. Semenov RAS Moscow

At present, it is assumed that the simultaneous functioning of oxygen as a universal oxidizer and nitric oxide as a universal regulator of biological processes in the organism of humans and animals occurs only because, at micromolar concentrations of NO in animal and human tissues, oxygen at millimolar concentrations in the same tissues is not capable of providing effective oxidation of NO to NO_2 to a level sufficient to suppress the physiological activity of NO. In this report, another explanation is proposed for the preservation of NO in the organism of animals and humans, which is achieved by the reversible incorporation of NO into dinitrosyl iron complexes (DNICs) with thiol-containing ligands that are preserved in animal and human tissues in the presence of oxygen. The formation of these complexes occurs as a result of disproportionation of NO molecules that bind pairwise in the presence of thiol-containing ligands to ferrous iron ions, i.e., in the reaction of NO dimers with these ions. As a result, the possibility of binding these dimers with oxygen and thus the oxidation of NO to NO_2 is excluded, since from the point of view of spin chemistry, only the reaction of O_2 with NO dimers can ensure the oxidation of this biologically important agent. As for DNIC with thiol-containing ligands, in animal tissues they are capable of acting not only as donors of NO molecules, as regulators of metabolic processes, but also as donors of nitrosonium cations (NO^+), as cytotoxic agents capable of suppressing the proliferation of tumor cells and the replication of respiratory viruses, such as SARS-CoV-2 in the body of animals.

oral

NMR of polymeric electrolytes for lithium batteries

N.A. Slesarenko[1], A.V. Chernyak[1,2], V.I. Volkov[1,3]

[1] Federal Research Center of Problems of Chemical Physics and Medicinal Chemistry, RAS, Chernogolovka, Russian
[2] Osipyan Institute of Solid State Physics, RAS, Chernogolovka, Russia
[3] Lomonosov Moscow State University, Moscow, Russia

Lithium power sources are used for autonomous power supply of a wide range of devices from portable electronics (laptops, cell phones, digital video cameras) to high-tech industries, including automotive, space and aviation technology, and shipbuilding.

Polymer electrolytes, including high-molecular networks, solvents and lithium salts, play a fundamental role in the creation of lithium batteries. Ionic liquids are often used as an important component especially for safety construction of devices. The targeted creation of highly effective materials requires a fundamental study of the mechanisms of ion and molecular transport. To date, extensive studies have been conducted on the macroscopic processes of electro- and mass transfer. However, to understand the mechanisms of selective transport, it is necessary to study the processes of diffusion of cations, anions and solvent molecules at the micro level. The more important characteristics are the residence time of the particle in a fixed state, time of the translational jump and the diffusion coefficients. These characteristics are determined by the structure of the solvate complexes and allow us to establish a connection between microscopic processes and macroscopic transport properties.

Such information can be provided by the NMR method, in particular, NMR-relaxation and pulsed field gradient NMR (PFG NMR) [1–4]. NMR-relaxation of ^{1}H, ^{7}Li, ^{19}F nuclei gives possibility to estimate a local mobility of solvent molecules as well as cations and anions. PFG NMR allows selective measurement of the self-diffusion coefficients of cations and anions, unlike electrochemical impedance spectroscopy, which characterizes the integrated ionic conductivity only.

The report presents the results of studies performed on ^{1}H, ^{7}Li, ^{11}B, ^{13}C, ^{19}F nuclei using NMR spectroscopy (including high resolution NMR, relaxation NMR and PFG NMR methods) in the NMR laboratory. Polymer electrolytes were synthesized in the laboratory of electrochemical dynamics and electrolyte systems (O.V. Yarmoolenko) based on polyethyleneglycol diacrylate polymer (PEGDA), with various solvents solvating the Li^{+} cation: 1,3-dioxolane (DOL), diglyme (G2), tetraglyme (G4) and ethylene carbonate (EC), with the addition of $LiBF_4$ salt, 1-ethyl-3-methylimidazolium tetrafluoroborate ($EMIBF_4$) ionic liquid (IL) and nanodispersed additives of SiO_2 and TiO_2 [5,6].

The structure of ionic complexes was obtained by comparing NMR spectroscopy data with quantum-chemical calculations. The detailed mechanism of ionic transport was studied, allowing the nature of ionic conductivity to be revealed on its basis. This allowed the optimal compositions of highly effective polymer electrolytes to be proposed.

oral

Acknowledgments: NMR measurements were performed using equipment of the Multi-User Analytical Center of the Institute of Problems of Chemical Physics RAS and Science Center in Chernogolovka RAS with the support of State Assignment of the Institute of Problems of Chemical Physics RAS (state registration number 124013000743-3 (FFSG-2024-0008).

1. Volkov V.I., Marinin A.A.: Russ. Chem. Rev. **82**, 248–272 (2013)
2. Volkov V.I., Yarmolenko O.V., Chernyak A.V., Slesarenko N.A., Avilova I.A., Baymuratova G.R., Yudina A.V.: Membranes **12**, 416 (2022)
3. Chernyak A.V., Slesarenko N.A., Slesarenko A.A., Baymuratova G.R., Tulibaeva G.Z., Yudina A.V., Volkov V.I., Shestakov A.F., Yarmolenko O.V.: Membranes. **12**, 1111–1126 (2022)
4. Volkov V.I., Chernyak A.V., Slesarenko N.A., Avilova I.A.: Int. J. Mol. Sci.. **23**, 5011 (2022)
5. Khatmullina K.G., Slesarenko N.A., Chernyak A.V., Baymuratova G.R., Yudina A.V., Berezin M.P., Tulibaeva G.Z., Slesarenko A.A., Shestakov A.F., Yarmolenko O.V.: Membranes. **13**, 548 (2023)
6. Slesarenko N.A., Chernyak A.V., Khatmullina K.G., Baymuratova G.R., Yudina A.V., Tulibaeva G.Z., Shestakov A.F., Volkov V.I., Yarmolenko O.V.: Membranes. **13**, 776 (2023)

oral

Changes of serum albumin function in cirrhotic patients studied by EPR

Mengqi Li[2], Wenyu Li[1], Qi Wang[2], Hong Zhao[2], Yidi Ge[2], Wenya Chen[2], Haijun Yang[1], Wen Xie[2]

[1] Chemistry Department, Tsinghua University, Beijing, China
[2] Center of Liver Diseases, Beijing Ditan Hospital, Capital Medical University, Beijing, China

Hepatitis B virus (HBV) infection remains one of the primary etiological factors leading to liver cirrhosis and hepatocellular carcinoma (HCC) in China. Patients with liver cirrhosis often exhibit reduced serum albumin levels and impaired albumin function. Currently, clinical assessment of disease severity largely depends on plasma albumin concentration, while effective methods for evaluating albumin functionality remain limited. Moreover, although albumin infusion is commonly employed in the management of cirrhosis, its clinical efficacy and treatment protocols remain controversial.

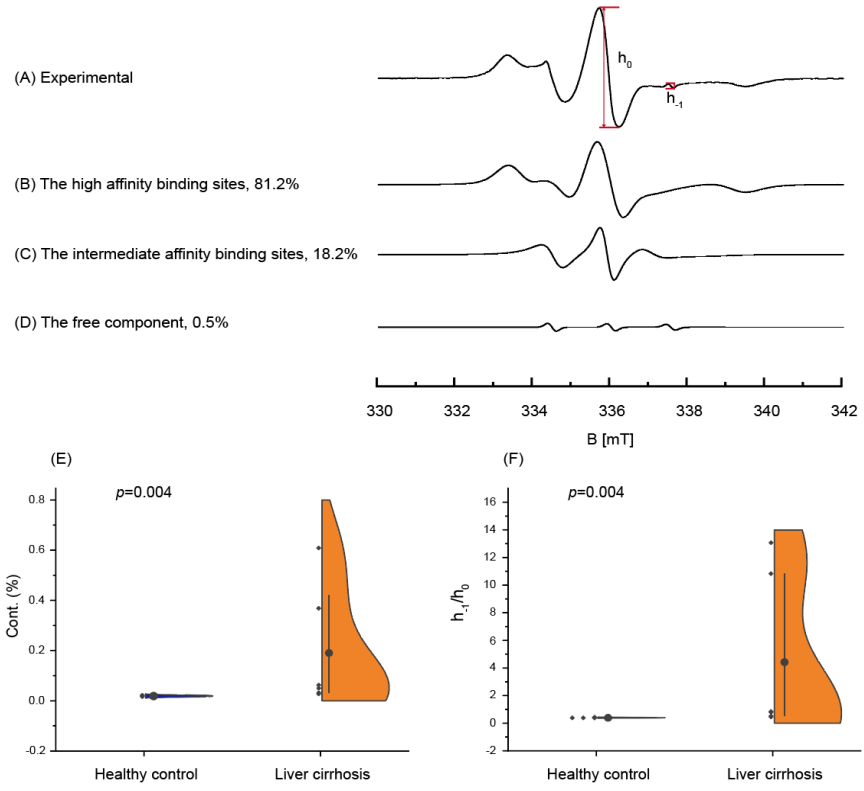

Fig. 1. (A) Experimental and simulated EPR spectra (B-D) of a healthy individual. (E-F) Comparison of the free component content obtained from simulation and h_{-1}/h_0 between healthy control and liver cirrhosis patient.

oral

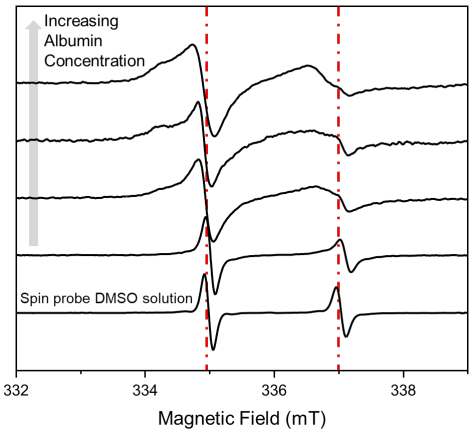

Fig. 2. Preliminary EPR results based on the ^{15}N-labelled spin probe.

This study aims to establish and optimize a method for assessing albumin function using electron paramagnetic resonance (EPR) spectroscopy [1], thereby providing a scientific basis for improving clinical treatment strategies. Utilizing 16-doxyl stearic acid (16-DSA) as a spin probe, we refined the EPR-based detection workflow by optimizing spectral analysis techniques, solvent selection, and the molar ratio of probe to albumin. The optimized method was applied to plasma samples from age- and sex-matched cohorts, including healthy controls, chronic hepatitis B patients, HBV-related cirrhosis patients, and those with HBV-related HCC, to evaluate changes in albumin functionality across disease stages and its correlations with clinical parameters (Fig. 1). In addition, we have successfully synthesized ^{15}N-labelled spin probe and obtained preliminary results (Fig. 2).

Results from a cohort of 120 samples demonstrated significantly reduced albumin-binding capacity in patients with HBV-related cirrhosis and HCC, with the most pronounced decline observed in patients with Child-Pugh class C cirrhosis. Furthermore, a strong positive correlation was identified between the directly measured h_{-1}/h_0 ratio and the free component proportion derived from spectral fitting, validating h_{-1}/h_0 as a reliable surrogate marker for albumin functionality. The h_{-1}/h_0 ratio was also found to be associated with various clinical indicators reflecting hepatic function, coagulation status, and inflammatory response.

1. Kazmierczak S., Gurachevsky A., Matthes G., Muravsky V.: Clinical Chemistry **52**, 2129–2134 (2006)

oral

Study of the triplet state of chromophores containing thionated carbonyl groups with time-resolved electron paramagnetic resonance spectra: large zero field splitting (ZFS)

Jianzhang Zhao[1], A.A. Sukhanov[2], V.K. Voronkova[2], I. Kurganskii[3], M.V. Fedin[3]

[1] State Key Laboratory of Fine Chemicals, School of Chemical Engineering, Dalian University of Technology, Dalian 116024, P. R. China. E-mail: zhaojzh@dlut.edu.cn
[2] Zavoisky Physical-Technical Institute, FRC Kazan Scientific Center of RAS, Kazan, Russia
[3] International Tomography Center SB RAS, Novosibirsk, 630090 Russia

Triplet excited states have been studied with the pulse laser excited time-resolved electron paramagnetic resonance (TREPR) spectroscopy for decades. With this spectroscopy, the selective population of the three sublevels of the T_1 state, i.e. T_x, T_y and T_z, can be probed, as well as the zero field splitting (ZFS) parameters. ZFS parameters can be used to characterize the spin dipolar interaction of the two electrons, and the spin orbit coupling (SOC) magnitude. Examples for former are well documented, however, molecular systems for the latter are rare.

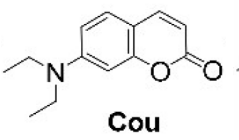

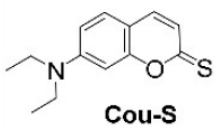

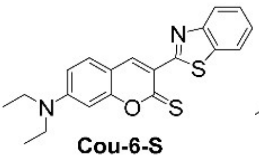

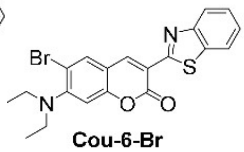

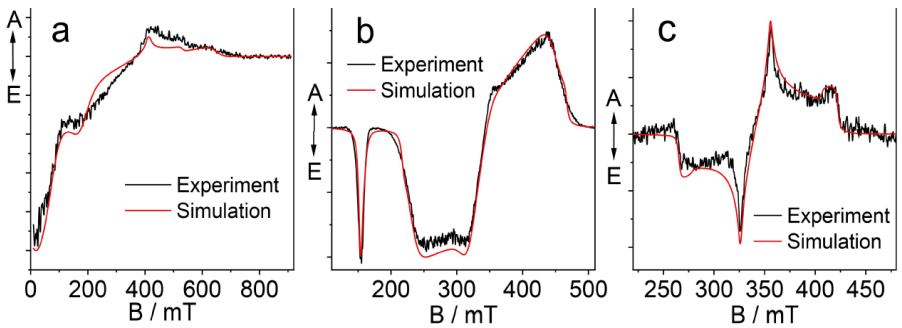

Fig. 1. TREPR spectra of (a) **Cou-S** (λ_{ex} = 440 nm), (b) **Cou-6-S** (λ_{ex} = 490 nm) and (c) **Cou-6-Br** (λ_{ex} = 415 nm) at the maximum of the kinetics with energy 1 mJ per pulse in TOL/2-MeTHF (1 : 3, v/v) at 80 K. Simulation (red curve) was performed with EasySpin package. $c = 1.0\times10^{-4}$ M.

oral

Recently, the intersystem crossing (ISC) of visible light-harvesting chromophores containing thionated carbonyl groups has attracted much attention, because this strategy represents a minimal variation of the molecular structure to achieving efficient ISC and it is a promising molecular structure design strategy for heavy atom-free triplet photosensitizers. However, the triplet state of this kind compounds has not studied with TREPR spectroscopy. We prepared a few model compounds based on the typical chromophore of coumarin and perylenebisimide (PBI), which contain thionated carbonyl groups [1, 2]. We found that the ZFS *D* parameters are unusually large for these organic molecules and it is correlated with the SOC matrix elements (SOCMEs) magnitudes, and the triplet state lifetimes are short. For some compounds, inversion of the electron spin polarization (ESP) of the triplet state TREPR spectra was observed.

1. Tang J., Sukhanov A.A., Zhao J., Dick B., Voronkova V.K., Li M.-D. et al.: Chem.-Eur. J. **31**, e202404589 (2025)
2. Chen X., Kurganskii I.V., Zhao J., Fedin M.V., Luo L., Escudero D., Dick B.: Angew. Chem. Int. Ed., **64**, e202500718 (2025).

oral

Modeling of CIDNP field dependence for molecular donor-acceptor compounds

I.V. Zhukov[1], N.N. Fishman[1], C. Lambert[2], G. Buntkowsky[3], N.N. Lukzen[1], A.V. Yurkovskaya[1]

[1] International Tomography Center SB RAS, Novosibirsk, Russia
[2] Institute of Organic Chemistry, University of Würzburg, Würzburg, Germany
[3] Institute of Physical Chemistry, Technical University Darmstadt, Darmstadt, Germany.

The study of magnetic and spin effects in a reversible photoinduced intramolecular electron transfer reaction establishes a connection between the exchange interaction and the spatial and electronic structure of the biradical. However, the interpretation of such experimental data is not necessarily straightforward. Careful modelling is required in order to obtain quantitative data on the exchange interaction and the biradical electronic structure. It creates a basis for the development of new approaches to the directed design of organic materials with specified electronic properties for practical applications in photovoltaics or spintronics.

In this presentation, we will examine the examples of numerical modeling of CIDNP field profiles derived from two distinct types of molecular donor-acceptor compounds (see Fig. 1): A rigid triad (D-Ir-A) has been utilized in the study of electron transfer, with D (triarylamine) serving as the e-donor, Ir (cyclometallated iridium complex) as the bridge, and A (naphthalene diimide) as the e-acceptor; the bridge complex Ir has been identified as a crucial component in this research [1]. A flexible tetrapeptide/photosensitizer conjugate, His-Gln(BP)-Tyr-Gly, with tyrosine or histidine residues serving

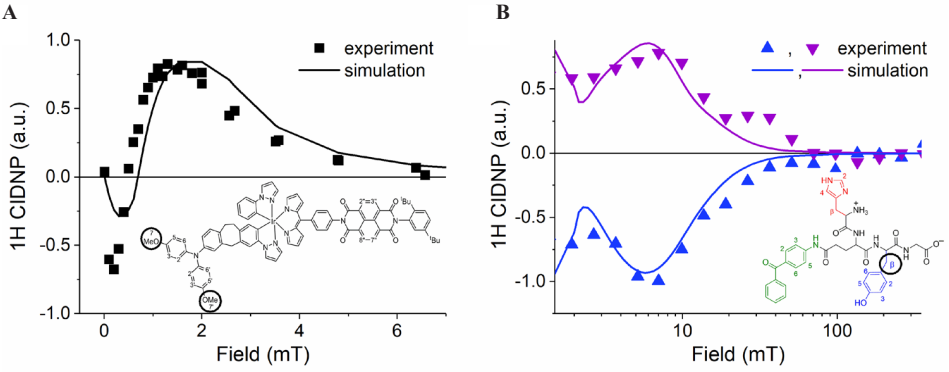

Fig. 1. Experimental (dots) and simulated (lines) 1H CIDNP field dependences of: A – six equivalent methyl protons of D–Ir–A; B – two β-protons of tyrosine residue of conjugate His-Gln(BP)-Tyr-Gly.

as the e-donor and 4-aminobenzophenone serving as the e-acceptor [2]. In both cases, the same numerical approach initially outlined in [1] was employed, with modifications described in [3] that significantly enhance the calculation speed and convenience of the simulation procedure.

This work was supported by Russian Science Foundation, grant No. 23-73-10103.

1. Lukzen N.N., Klein J.H., Lambert C., Steiner U.E.: Z. Phys. Chem. **231**, 197–223 (2017)
2. Fishman N.N., Herr K., Morozova O.B., Zhukov I.V., Geniman M.P., Brodrecht M., Wissel T., Buntkowsky G., Yurkovskaya A.V.: Sci. Rep. (in press, 2025)
3. Zhukov I.V., Fishman N.N., Lukzen N.N, Klein J., Steiner U. E., Lambert C., Yurkovskaya A.V.: J. Chem. Phys. **162**, 054116 (2025)

poster

Pulse EPR of radicals in mechanoactivated calcium gluconate

M.M. Akhmetov[1], G.G. Gumarov[1], R.B. Zaripov[1], G.N. Konygin[2], D.S. Rybin[2]

[1] FRC Kazan Scientific Center of RAS, Kazan, 420111, Russia, mansik86@mail.ru
[2] UdmFRC Ural Branch of RAS, Izhevsk, 426067, Russia, dsrybin@mail.ru

It was previously shown that the EPR spectrum in the X-band from mechanically activated calcium gluconate [1] is a narrow single line with a width of less than 10 Gs. However, in the W-band, it was found that the spectrum is multicomponent. The low-field part is well described by carbon radicals of the δ-gluconolactone molecule, formed as a result of the detachment of a proton from a carbon atom. However, identifying the high-field part turned out to be a non-trivial task. On the one hand, calculations using quantum chemistry methods indicate the possibility of localization of the spin density on the calcium ion. At the same time, according to the literature, this radical is short-lived and has so far been detected only in the gas phase. On the other hand, under strong energy impact on organic materials, the CO_2^- radical ion is often observed. In addition, it cannot be ruled out that the observed line is probably due to a contact ion pair consisting of the gluconate anion and calcium gluconate.

It has been shown [2] that the action of CO_2 on electron-rich MgO surfaces leads to the formation of paramagnetic species that have been unambiguously identified as adsorbed CO_2. The main attention is paid to the interaction of CO_2 molecules with (H+)(e-) centers, a recently discovered class of defects on the surface of ionic oxides. The action of H or H_2 atoms on MgO or CaO under UV-radiation leads to spontaneous ionization of H followed by stabilization of the electron on low-coordinated cation sites and the proton on the surface oxide anions. It is known that mechanical activation in a ball mill can activate carbon dioxide molecules. In addition, the CO_2 molecule can be activated by coordination with transition metal complexes or by interaction with solid surfaces [3].

As is known, CO_2^- radicals with low symmetry have a g-tensor with two higher and one lower eigenvalues than the g value of a free electron. In most solid matrices, the spectra have low symmetry, i.e. the three eigenvalues of the g-tensor differ from each other [4]. Axial symmetries with two equal eigenvalues are observed less frequently. The component with *g*-tensor values [2.0009 2.0009 2.0023] in a sample of mechanically activated calcium gluconate may correspond to two radicals at once, but this fact requires further studies (in particular, ENDOR).

1. Gumarov G.G., Petukhov V.Yu., Konygin G.N. et al.: J. Phys. Chem. **87**, 1 (2013) (in Russian)
2. Chiesa M., Giamello E.: Chem. Eur. J. **13**, 1261 (2007)
3. Freund H.J., Roberts M.W.: Surf. Sci. Rep. **25**, 225 (1996)
4. Angelov S., Stoyanova R., Dafinova R., Kabasanov K.: J. Phys. Chem. Solids **47**, 409 (1986)

poster

Effect of different anesthesia methods on NO detection in rat brain tissue by the spin trap method

V.V. Andrianov[1,2,3], I.B. Deryabina[2], A.I. Arslanov[1], L.V. Bazan[1,2], Kh.L. Gainutdinov[1,2]

[1] Zavoisky Physical-Technical Institute, FRC Kazan Scientific Center of RAS, Kazan, Russia, andrianov.neuro@yandex.ru
[2] Institute of Fundamental Medicine and Biology of Kazan Federal University, Kazan, 420008, Russia
[3] Federal Center of Brain Research and Neurotechnologies of the Federal Medical and Biological Agency of Russia, Moscow, 117513, Russia

Historically, nitric oxide (NO) in the body was discovered as a vasodilation factor associated with the endothelial mechanism of vascular relaxation [1, 2]. Nitric oxide is known as one of the most important signaling molecules regulating physiological functions of the body and cell metabolism [3, 4]. Studies of the role of NO in signal transmission in the nervous system began shortly after its discovery [5]. Since then, it has been demonstrated that NO is involved in various functions of the nervous and cardiovascular systems, and acts as a neurotransmitter and factor that ensures relaxation of smooth muscles [4, 6, 7].

The endothelial pathway of NO production is associated with endothelial NO synthase and is involved in the system of regulation of the tone of blood vessels by their muscle cells [4, 5]. At the same time, inducible NO synthase is also present in the smooth muscle cells of blood vessels, the activity of which is associated with expression in endothelial cells, as well as in macrophages, during pathological processes, including inflammation [8]. Relaxation of muscle tone during anesthesia with narcotic analgesics occurs through inhibition of centers in the nucleus of the brainstem and motor pathways of the spinal cord descending to the muscles. In this case, the use of narcotic drugs for pain relief and general anesthesia in surgical operations can be both general and selective, inhibiting nociceptive transmission, as well as local with inhibition of conduction at the level of peripheral nerves or the spinal cord [8, 9, 10]. In this case, muscle relaxants do not exert general central inhibition, but selective inhibition in signal transmission in the motor end plate, thereby achieving the shutdown of neuromuscular transmission. The particular importance of the use of muscle relaxants as a separate component of pharmacological anesthesia is associated with the possibility of significantly reducing the overall depth of anesthesia, and, thus, with the possibility of seriously reducing the likelihood of complications caused by the state of deep anesthesia.

The issue of quantitative determination of NO in living systems is relevant. Recently, one of the most effective methods for determining NO in biological tissues is the electron paramagnetic resonance (EPR) method [3, 10]. The spin capture method is based on the reaction of a radical (in this case, NO) with a spin trap. The complex

poster

(ДЭТК)2-Fe^{2+}-NO is characterized by an easily recognizable EPR spectrum with a *g*-factor value of $g = 2.035–2.040$ and a triplet hyperfine structure.

We used EPR spectroscopy to study the effect of some types of pharmacological anesthesia, mandatory for use in animal model studies, on the level of nitrogen monoxide production in body tissues. It was shown that the use of so-called muscle relaxants leads to a significant suppression of NO production when analyzing the NO content using a spin trap based on sodium diethyldithiocarbamate. At the same time, the isolated use of the general anesthesia drugs studied in the work did not lead to a noticeable difference in the amplitude of the EPR signals associated with NO in the complex $(DETC)_2$-Fe^{2+}-NO. The demonstrated direct relationship between the level of NO production and the use of drugs that have a selective muscle relaxant effect during anesthesia may be important and should be taken into account in preclinical studies when developing models of pathologies and various disorders of normal life in studies using animals.

The work was supported by the framework of a state assignment to Zavoisky Physical-Technical Institute of RAS and the Strategic Academic Leadership Program of Kazan Federal University (PRIORITY 2030).

1. Ignarro L.J. et al.: J Cardiovasc Pharmacol. **34**(6), 879–886 (1999)
2. Vanin A.F.: Nitric Oxide **54**, 15–29 (2016)
3. Vanin A., Poltorakov A.: Front. Biosci. **14**, 4427–4435 (2009)
4. Steinert J.R. et al.: Neuroscientist **16**(4), 435–452 (2010)
5. Boehning D., Snyder S.H.: Annu. Rev. Neurosci. **26**, 105–131 (2003)
6. Lundberg J.O.; Weitzberg E.: Cell **185**, 2853-2878 (2022)
7. Lakomkin V.L. et al.: Nitric Oxide: Biology and Chemistry. **16**(4), 413–418 (2007)
8. Lundberg J.O., Weitzberg E.: Cell **185**, 2853–2878 (2022)
9. Chachlaki K., Prevot V.: British J. Pharmacol. **177** (24), 5437–5458 (2020)
10. Wierónska J.M. et al.: Biomolecules **11**, 1097 (2021)

poster

Multifunctional heptanuclear iron complexes

E.E. Batueva[1,2], A.R. Sharipova[1], E.N. Frolova[1], A.A. Sukhanov[1], L.I. Savostina[1,2], O.A. Turanova[1], A.N. Turanov[1]

[1] Zavoisky Physical-Technical Institute, FRC Kazan Scientific Center of RAS, Kazan, Russia
[2] KFU Kazan (Volga region) Federal University, Kazan, Russia

Spin-crossover transition metal complexes represent a promising platform for creating materials with controllable properties. The ability of these complexes to switch their magnetic and optical characteristics under the influence of temperature, light, or pressure opens up prospects for the development of memory devices, sensors, state-memorizing systems, and, as demonstrated in this work, MRI contrast agents. In this study, heptanuclear iron complexes $[Fe(II)(CN)_6\{Fe(III)L\}_6]X_2$ (L = dianion N,N-bis(1-hydroxy-2-benzylidene)-1,7-diamino-4-azageptane, X^- = SCN, Cl) were investigated.

The Fe(II)-Fe(III) heptanuclear complex with the SCN anion was studied by time-resolved EPR spectroscopy in the X-band under pulsed laser irradiation (λ = 580 nm, ν = 100 Hz) within the temperature range of 25 to 80 K. A polarized signal from the low-spin state of the Fe(III) ion (S = 1/2) was observed at temperatures from 40 to 60 K. The origin of the spin polarization formation is discussed.

The structure of the complex with the Cl counterion was optimized in the ORCA program, and the spin density was analyzed at various multiplicities: **35** (Fe(II): S = 2, Fe(III): S = 5/2), **31** (Fe(II): S = 0, Fe(III): S = 5/2), **11** (Fe(II): S = 2, Fe(III): S = 1/2) and **7** (Fe(II): S = 0, Fe(III): S = 1/2).

The possibility of complexes application as a contrast agent for MRI in the future is being considered. For this purpose, the sample was dissolved in SDS micellar solutions (50 mmol SDS), and the relaxation times of water (T_1, T_2) were measured at complex concentrations of 11.35, 17.35, and 23.05 μmol/L by ^{1}H NMR spectroscopy (500 MHz, 303 K). The calculated relaxivity demonstrates a pronounced T_2 effect: r_2 = 118 ± 3 $mmol^{-1}\cdot s^{-1}$, r_1 = 2.4 ± 0.6 $mmol^{-1}\cdot s^{-1}$, and the ratio r_2/r_1 = 49.3. The obtained values, comparable to USPIO (ultra-small superparamagnetic iron oxide), confirm the prospects of the complex as a T_2-weighted (negative) MRI contrast agent.

poster

EPR method: methemoglobinemia in patients with connective tissue dysplasia

M.I. Ibragimova[1], A.I. Chushnikov[1], I.V. Yatsyk[1], D.Kh. Khaibullina[2], G.G. Gumarov[1]

[1] Zavoisky Physical-Technical Institute, FRC Kazan Scientific Center of RAS, Kazan, Russia
[2] Kazan State Medical Academy – Branch Campus of the FSBEIFPE RMACPE MOH, Russia

Hemoglobin (Hb) is a complex protein that is the main component of red blood cells. Hb consists of the protein globin and heme, a porphyrin core containing ferrous iron. Under the influence of a number of endogenous and exogenous factors (such as nitrogen oxides, chlorates, some toxic and pain-relieving drugs), oxidation of heme iron from Fe^{2+} (d^6) to Fe^{3+} (d^5, high-spin ferric state) can occur, that is, the formation of methemoglobin (MetHb). Normally, the concentration of MetHb should not exceed 2% of the total hemoglobin concentration. Since the iron in MetHb is in an oxidized state (Fe^{3+} instead of Fe^{2+}), this form of hemoglobin is not able to transport oxygen. This fact means that an increase in MetHb concentration can lead to methemoglobinemia, a condition in which oxygen transport to tissues is impaired.

One of the fairly common pathologies is connective tissue dysplasia (CTD) – a multi-organ and multi-system pathology with progressive clinical course. There are several aspects that may link methemoglobin and CTD, although these connections are currently hypothetical. In essence, this is an increased risk of developing methemoglobinemia due to oxidative stress, which disrupts the structure and function of connective tissue. Moreover, elevated methemoglobin levels can aggravate tissue hypoxia, which negatively affects the condition of connective tissue.

In this work, blood samples of patients with connective tissue dysplasia associated with back pain were studied using the X-band EPR in the temperature range of 5–80 K.

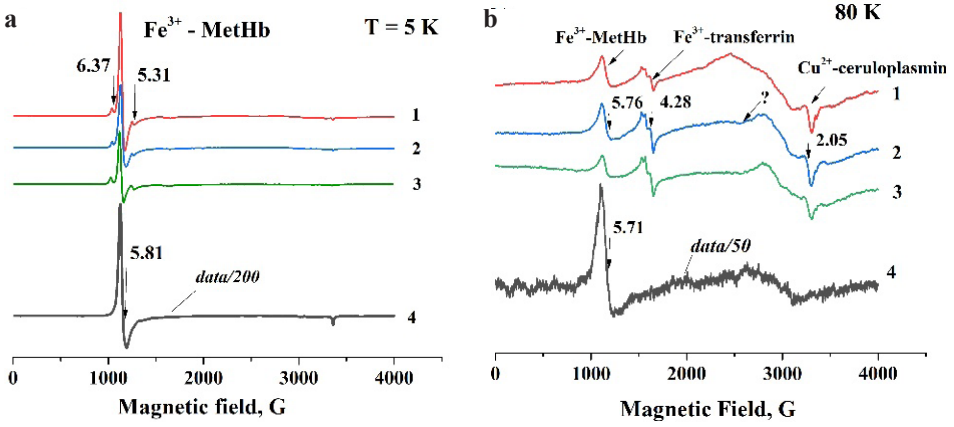

Fig. 1. X-band EPR spectra blood recorded at 5 K (**a**) and 80 K (**b**).

poster

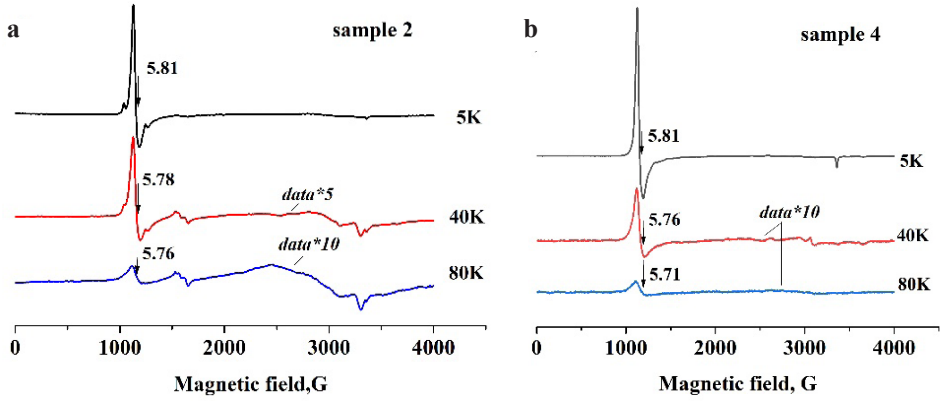

Fig. 2. X-band EPR spectra of blood recorded in the temperature range from 5 to 80 K.

EPR spectra were recorded using the spectrometer "Bruker Plus" at a frequency of ~9.38 GHz with a modulation frequency of 100 kHz, modulation amplitude of 5 G and microwave power of 20 mW from blood samples of equal volume (0.15 ml).

Fig. 1a, b show the EPR spectra of blood recorded at 5 and 80K, respectively. As can be seen from Fig.1a, at a temperature of 5 K the absorption line from Fe^{3+}-MetHb with g = 5.81 dominates. Along with the signal from ferric heme, two more (but not intensive) absorption lines with g-factors of 6.37 and 5.31 are visible in the three spectra, having non-equivalence of the EPR absorption along the x and y-directions in the heme's plane. This signal is attributed to the high spin ferric heme state of erythrocyte catalase [1]. As can be seen from Fig. 1, the amplitude of the signal (peak-to-peak) from Fe^{3+}-MetHb in spectra 1–3 at both 5 K and 80 K, although different, is more than two orders of magnitude smaller than the signal from ferric heme in spectrum 4.

Temperature dependences of the EPR spectra of blood for samples 2 and 4 are shown in Fig. 2. Firstly, it was found that with an increase in temperature from 5 to 80 K, the intensity of the signal from Fe^{3+}-MetHb decreases significantly. At the same time, even at 80 K, the signal from Fe^{3+}-MetHb dominates in the EPR spectrum of sample 4 (see Fig. 1b and 2b). Secondly, with an increase in temperature, the line width from Fe^{3+}-MetHb increases. It was found that both the absolute value of the line width and the nature of its change (Δ) in the temperature range of 5–80 K are different for samples 2 and 4. At 5 K, the line width is 105 and 130 G in spectra 2 and 4, respectively. The increase in line width in the range from 5 to 80 K is $\Delta \sim$ 45 G for sample 2 and $\Delta \sim$ 65 G for sample 4. Note that the blood serum spectrum from sample 4 does not have any anomalies and is similar to all the samples tested.

Such a significant difference in the concentration of Fe^{3+}-MetHb in sample 4 relative to samples 1–3 is due, in our opinion, to the severity of CTD. Sample 4 is the blood of a patient with the third (maximum) degree of CTD (male, 17 years old). Against the background of all the main factors causing CTD, such a high degree of methemoglobinemia, apparently, significantly affects the condition of the connective tissue due to hypoxia.

It should be noted that even with a less pronounced degree of severity of CDT (spectra 1–3), the concentration of Fe^{3+}-MetHb is quite high and even with one degree of CDT it can differ by more than 2 times at a temperature of 5 K.

We think that in the pathogenesis of connective tissue dysplasia, the role of MetHb can be significant, especially in severe CTD. Moreover, the mechanism leading to the formation of methemoglobin, especially in the context of oxidative stress, may be different at different degrees of CTD. Obtained data will certainly be of interest and require further research.

1. Svistunenko D.A.: J. Biomed Res. **35**, 294 (2021)

poster

Investigation of the origin of the radiation-induced paramagnetic centers in melanin by EPR spectroscopy

I.S. Ivanova[1], D.R. Bajtimirov[1], S.V. Konev[1], D.V. Ivanov[1,2], A.P. Podshivalov[1]

[1] Ural Federal University, Yekaterinburg, Russia
[2] M.N. Mikheev Institute of Metal Physics, Ural Branch of the Russian Academy of Sciences, Ekaterinburg, Russia

The work is devoted to the study of radiation-induced centers (RIC) by the EPR method – free radicals arising in human hair samples under the influence of ionizing radiation.

It was previously shown that human hair can be used as an object for dosimetric measurements, since it is sensitive to ionizing radiation and is characterized by high RIS stability.

At the same time, human hair normally has a paramagnetic response with a complex EPR signal containing two main components – a wide one associated with the protein (keratin) structure of the hair and a narrow one corresponding to the pigment melanin, which gives color and intensity of hair coloring depending on the combination of its two types – eu- and pheomelanin. As a result, it turns out that the narrow component, in the case of using hair as an object of dosimetry, is a background signal.. The melanin content in hair of different colors varies significantly, because of that dosimetry on them will always have a systematic error. Thus, it is advisable to correct this error considering the color of a specific hair sample. In the course of the presented work, EPR signals were measured for more than 30 hair samples of different pigmentation, divided into five color groups – black, red, gray, light brown, dark brown – before and after irradiation with a dose of 10 kGy, created by a linear electron accelerator of the UELR-10-10S2 model. All samples have a characteristic EPR signal shape (Fig. 1), apparently associated with the molecular structure of the corresponding type of melanin.

The study showed that the shape and characteristics of the RIS depend on the type and intensity of melanin pigmentation, according to the division of samples into corresponding groups, while the sensitivity of samples to IR increases with a decrease in the degree and type of sample pigmentation (Fig. 2).

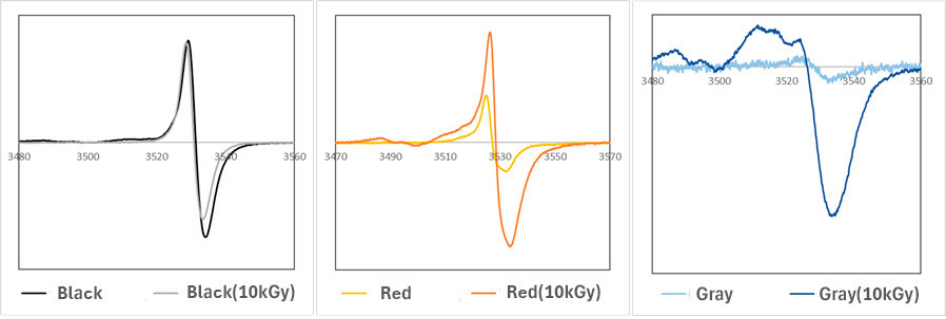

Fig. 1. Examples of EPR signals of hair of variable color before and after irradiation.

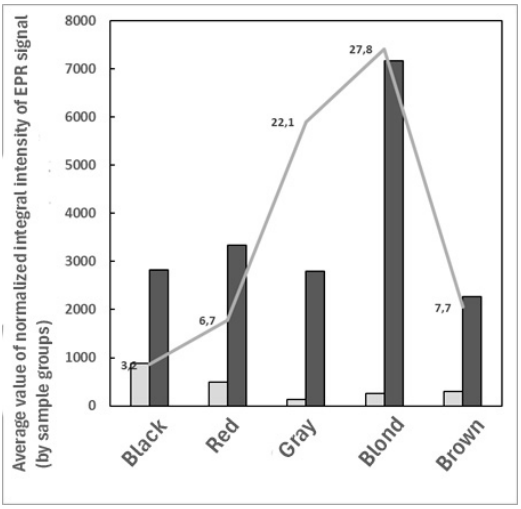

Fig. 2. Average values of mass-normalized intensity of melanin EPR signals before (Ibackground, gray column) and after irradiation with a dose of 10 kGy (Iirradiation, black column), characterizing the corresponding groups of samples. The gray line shows the dependence of the Iirradiation / Ibackground ratio.

This behavior may indicate the radioprotective properties of eumelanin, which is predominant in black hair samples, which binds free radicals formed during irradiation. In samples of light and gray hair, a significant increase in the intensity of the EPR signal after irradiation may be associated not only with radiation-induced centers localized in pheomelanin granules, but also with radicals that arise during the destruction of the protein structure of the hair.

poster

Study of the influence of hydroxyapatite synthesis conditions on its dosimetric properties using the EPR method

A.P. Podshivalov[1], D.R. Bajtimirov[1], D.V. Ivanov[1,2], S.F. Konev[1], G.P. Slesarev[1]

[1] Ural Federa University, Ekaterinburg, Russia
[2] M.N. Mikheev Institute of Metal Physics, Ural Branch of the Russian Academy of Sciences, Ekaterinburg, Russia

In this paper we summarize the intermediate results of our study of the influence of hydroxyapatite synthesis conditions on its dosimetric properties using the EPR method. Namely, the influence of the pH of the synthesis medium, CO_2 bubbling, annealing and centrifugation.

At the first stage of the study, the effect of pH of the synthesis medium was studied.

The samples demonstrated sensitivity to ionizing radiation in the absence of EPR signal saturation in the dose range of up to 30 kGy. At the same time, the sample with the maximum amplitude of the radiation-induced EPR signal (pH = 8.6) demonstrated sensitivity to ionizing radiation only four times lower than natural hydroxyapatite of tooth enamel. In addition, it was found that the pH parameter affects the shape of the radiation-induced signal – the magnitude of the EPR line splitting decreases linearly with increasing pH.

Also at this stage, the effect of annealing the samples at a temperature of 700°C on their sensitivity to ionizing radiation was recorded. As can be seen from the figure, calcining the sample at a temperature of 700°C leads to an increase in the number of radiation-induced paramagnetic centers by about 1.5–2 times in the entire dose range from 10 to 40 kGy.

At the next stage, the effect of CO_2 bubbling during synthesis was studied

In these samples, the EPR spectra contained two groups of lines with a complex hyperfine structure, characteristic of manganese oxide. This structure arose due to contamination of the reagents with Mn ions and their "capture" of oxygen during CO_2 bubbling.

The nature of the dependence of the RIS amplitude on the dose has a clear correlation with the pH value. For samples with a pH value > 6.5, rapid saturation of the radiation-induced EPR signal is characteristic already at 10 kGy. Bubbling with carbon dioxide leads to an increase in the magnitude of the paramagnetic response to sample irradiation compared to samples synthesized in the absence of bubbling. The RIS amplitude at pH > 6 is only 3 times smaller than the amplitude of tooth enamel.

These samples were also calcined at a temperature of 900 °C for 30 minutes. Annealing of the samples leads to a significant increase in the concentration of paramagnetic centers of manganese. Both hyperfine structure signals and a radiation-induced signal are observed in the obtained spectra.

The value of the RIS amplitude for almost all samples does not depend on the IR dose, which indicates a rapid saturation of the EPR signal. Only for samples with pH = 6 is a slight increase within 15% up to 30 kGy followed by a sharp decline. At the same time, it should be noted that the magnitude of the radiation-induced signal

of the annealed samples has an inverse dependence on the pH value in comparison with the samples of irradiated artificial hydroxyapatite that were not subjected to heat treatment. For annealed samples with pH < 6.5, the RIS value is three to four times greater than the RIS value of samples with pH > 6.5. Thus, annealing of the bubbled samples at a temperature of 900°C for 30 minutes leads to a decrease in the concentration of paramagnetic centers responsible for the radiation-induced signal, relative to the samples that were not annealed.

X-ray diffraction analysis showed that the concentration of HA in the samples during bubbling was about 17–30%. To increase the concentration of HA, it was decided to use centrifugation (test 4 minutes).

After centrifugation, the samples were divided into three parts – upper, central and lower. All parts of the same samples follow the same trajectory with small deviations. This may indicate the similarity of the structure of the samples. At the same time, the deviations in the lower part of the sample are greater than in the others.

The amplitudes of the lower parts of the samples behave basically the same, when the other parts are less correlated with each other. But none of the samples behaved in a similar way. On average, after centrifugation, the concentration of HA in the samples increased by 5–10%.

In general, the experimental data confirm the possibility of using synthetic hydroxyapatite in EPR dosimetry. However, to achieve sensitivity parameters comparable to the natural material, further optimization of the synthesis conditions is required.

Currently, the most effective synthesis conditions include:

- The pH value of the synthesis medium is 8.6;
- Annealing the sample at a temperature of 700 °C;
- Centrifugation of the precipitate and collection of the lower part to increase the concentration of the material.

The work was partially supported by the Ministry of Science and Higher Education of the Russian Federation (through the basic part of the government mandate, project No. FEUZ-2023-0013 and State task «Spin» #122021000036-3).

poster

Exchange and spin dipolar interactions in perylenebisimide-tempo dyads

A.A. Sukhanov[1], V.K. Voronkova[1], Zh. Li[2], Xi Chen[2], J. Zhao[2]

[1] Zavoisky Physical-Technical Institute, FRC Kazan Scientific Center of RAS, Kazan, Russia
[2] State Key Laboratory of Fine Chemicals, School of Chemical Engineering, Dalian University of Technology, Dalian 116024, P. R. China

Triplet photosensitizers (PSs) are versatile compounds having strong visible light absorption, efficient intersystem crossing (ISC) and long-lived triplet states as result of which they are widely used. It is crucial to develop new structures of heavy-atom-free organic chromophores showing predetermined efficient ISC. Stable radicals attached to an organic chromophore can greatly enhance the ISC efficiency because in the presence of the radical, the spin-forbidden $S_1 \rightarrow T_1$ transition is converted to a spin-allowed ^{2}[R–S] (sing-doublet state) $\rightarrow$ ^{2}[R–T] (trip-doublet state) process due to the electron spin-spin exchange between the radical and the photoexcited chromophore

TEMPO radical was linked to perylene-3,4:9,10-bis(dicarboximide) (PBI) at varying distances and orientations to study the effect of the distance and orientation between radicals and chromophore on the sign and magnitude of spin exchange interaction J_{TR} between the triplet state of chromophore and stable radical.

Time-resolved electron paramagnetic resonance (TREPR) spectroscopy demonstrates different electron exchange interactions (J_{TR}) in the dyads, varying from ferromagnetic interaction corresponding to strong exchange regime to weak antiferromagnetic exchange interaction with increasing the distance between PBI and TEMPO units. Transient-nutation experiments further clarify the TREPR signals.

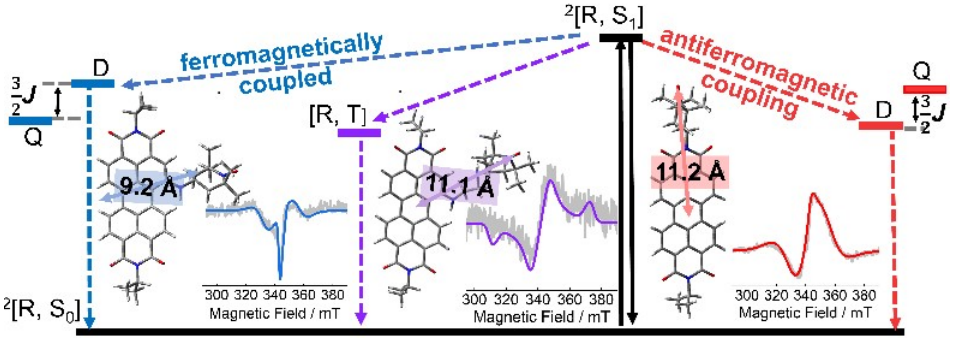

Fig. 1. Effect of linker length and orientation on REISC.

poster

Influence of solvents on β-enaminon spectral characteristics and dynamics by NMR, UV-visible spectroscopy and DFT data

A.F. Shaidullina[1], L.I. Savostina[1,2], A.R. Sharipova[2], M.Yu. Volkov[2], O.A. Turanova[2], A.N. Turanov[2]

[1] Kazan Federal University, Kazan, Russia
[2] Zavoisky Physical-Technical Institute, FRC Kazan Scientific Center of RAS, Kazan, Russia

The effect of solvents on the physicochemical properties of β-enaminones is an important aspect of their reactivity, spectral characteristics, and structural dynamics. The effect may be due to the polarity of the solvents, the ability to form hydrogen bonds or steric factors.

In this work, we study the effect of different solvents on molecules of 1-phenyl-3-(quinolin-8-ylamino)prop-2-en-1-one (β-enaminone) by NMR and UV-*vis* spectroscopy and DFT modeling. One-dimensional and two-dimensional NMR spectra of β-enaminone in deuterated acetone, carbon tetrachloride, and DMSO solvents at room temperature were recorded on a Bruker spectrometer at 400 MHz. It has been established that the chemical shifts of the protons of the molecule vary significantly depending on the nature of the solvent (Fig. 1). However, the spin-spin splitting constants for the ^{1}H NMR signals remain practically unchanged or very close in all solvents studied. The analysis of UV-*vis* spectroscopy data showed a pronounced bathochromic shift depending on the value of the dielectric constant.

These experimental results are in agreement with quantum-chemical calculations by the DFT method.

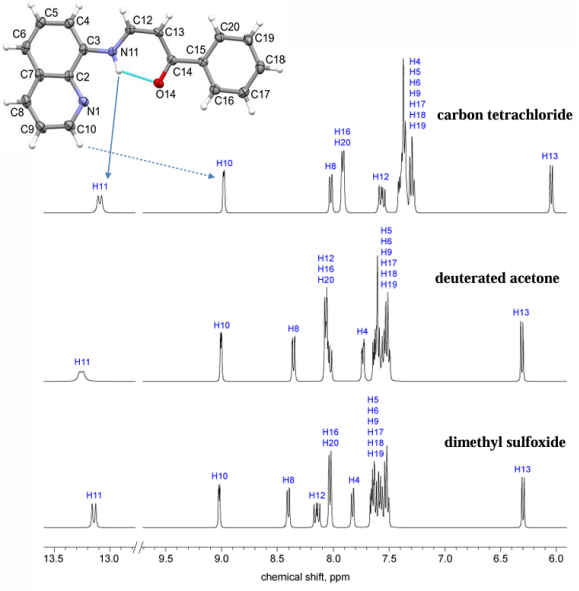

Fig. 1. ^{1}H NMR spectra of 1-phenyl-3-(quinolin-8-ylamino)prop-2-en-1-one in different solvents.

poster

Proton exchange in water-ethanol mixture. NMR

E.K. Shamsutdinova[1], A.N. Turanov[2]

[1] Institute of Physics, Kazan Federal University, Kazan, Russia
[2] Zavoisky Physical-Technical Institute, FRC Kazan Scientific Center of RAS, Kazan, Russia

Proton exchange plays a key role in the energy supply of cellular organisms. The application of water-alcohol mixtures in pharmacology, the food industry, and various technological processes provides study relevance of molecular associates formed due to hydrogen bonds and proton exchange in such systems.

The presented work describes the results of the study of ethanol-distilled water-deuterated water solution by high-resolution ^{1}H NMR spectroscopy as well as by an inversion-recovery pulse sequence with a selective 180° pulse. All measurements performed on a Bruker AVANCE II TM 500 NMR spectrometer at +25°C.

The spectrum contains three signals from CH_3-, -CH_2-, and -OH groups of ethanol, as well as a proton signal in HOD. The inversion-recovery pulse sequence is usually used to study longitudinal relaxation in systems with no exchange. It is more efficient to use a selective inverse 180° pulse to study exchange processes: spin, chemical, in this case proton exchange. Exchange between -OH and HOD has an influence on the recovery of signals, especially noticeable at the initial stage. The approximation and analysis of the dependence of -OH and HOD signals intensity vs. the delay time between pulses allowed to characterize both longitudinal relaxation and exchange processes between the mentioned structural-molecular groups.

It is planned to study the dependence of exchange processes in such systems on temperature, acidity of the solution and other factors, as well as modeling of NMR spectra of solutions under the influence of pulse sequences with different pulse parameters.

It is planned to study the influence of temperature, acidity of the solution, and other factors on exchange processes in such systems, as well as modeling of NMR spectra of solutions at different pulse sequence parameters.

poster

Potential control of magnetic properties of a new Fe(III) complex by means of synthesis methods

A.R. Sharipova, E.N. Frolova, O.A. Turanova, L.V. Bazan, A.N. Turanov

Zavoisky Physical-Technical Institute, FRC Kazan Scientific Center of RAS, Kazan, Russia

For the complex $[Fe(L)_2]BS$ (here L is anion of 1-phenyl-3-(quinolin-8-ylamino)prop-2-en-1-onato, BS is the anion of benzosulfonic acid), a significant dependence of magnetic properties on the method of sample synthesis was found.

For the synthesis of sample 1, a methanol solution containing the sodium salt of benzosulfonic acid and iron (III) chloride was added to a solution of the ligand in dichloromethane. Samples 2–4 were obtained by mixing solutions of $[Fe(L)_2Cl]$ complex and sodium salt of benzosulfonic acid. Synthesis 2 was carried out in methanol with the addition of diethyl ether to precipitate the sample. Sample 3 was obtained in aqueous medium by heating. The synthesis of sample 4 was carried out in ethanol. The composition and structure of all the obtained compounds were characterised by elemental analysis and UV spectroscopy.

It was shown by EPR method that complex 1 exhibits a bistable state in which the relative amounts of LS (S = 1/2) and HS (S = 5/2) centres do not change in the temperature range of 4–340 K (Fig. 1). In sample 2, the LS state was predominant, and an incomplete spin cross-over (SCO) was registered on its background. For sample 3, an almost complete SCO was realised. In sample 4, the HS state was predominant, and significant exchange interactions between Fe(III) centres are observed.

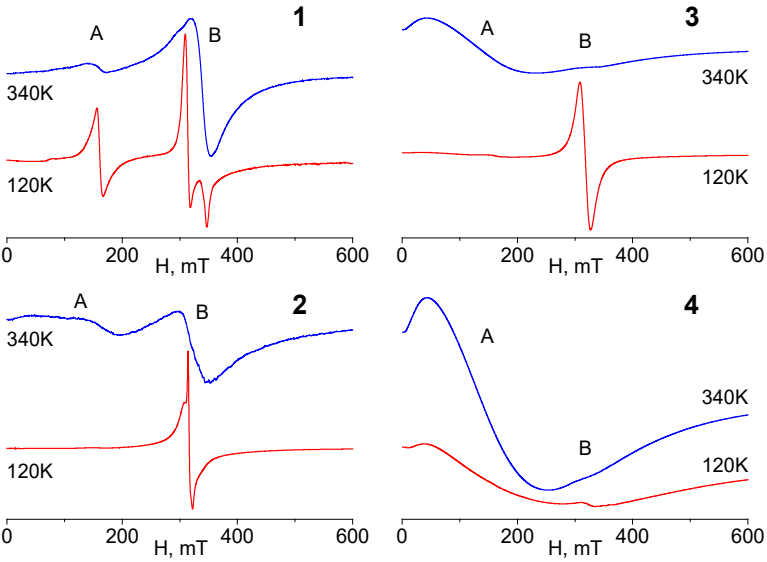

Fig. 1. EPR spectra of samples **1**–**4** at 120 and 340 K. A and B indicate the position of lines for HS and LS complexes Fe(III), respectively.

poster

Study of 1-[4-(4-pentylcyclohexyl)-phenyl]-3-(quinolin-8-ylamino)-prop-2-en-1-one by NMR and UV spectroscopy

M.Yu. Volkov, A.R. Sharipova, O.A. Turanova

Zavoisky Physical-Technical Institute, FRC Kazan Scientific Center of RAS, Kazan, Russia

Enaminones can be used as convenient building blocks in the production of photosensitive substance. Enaminones are irreplaceable reagents for the synthesis of N-heterocycles. Some enaminones are biologically active substances. Because β-enaminone molecules contain nitrogen and oxygen atoms as well as have a chelate structure, they are promising ligands for the synthesis of metal complexes. The study of the tautomerism of the enaminone molecules and the determination of their conformations is important because the various conformations of the enaminones have different reactivity in the synthesis of metal complexes. Also, the presence of double bonds in the molecules of enaminons determines the possibility of their E-Z photoisomerization.

In this work 1-[4-(4-pentylcyclohexyl)-phenyl]-3-(quinolin-8-ylamino)prop-2-en-1-one was first synthesized and studied by NMR and UV spectroscopy (Fig. 1). There are four possible isomers of the molecule of this β-enaminone: ketoimine, enolimine, and also the cis- and trans- forms of enaminoketone.

The electronic spectra and NMR spectra of this substance were recorded in solutions by a Varian Cary 100 spectrophotometer and a Bruker Avance 400 NMR spectrometer. UV irradiation of the solutions was carried out by a Vilber Lourmat lamp with λ = 365 nm.

^{1}H and ^{13}C NMR spectra of the substance demonstrate certain sets of signals both in the downfield region and in the upfield region. The UV spectra of the compound before UV irradiation shows the intense absorption band with λ_{max} = 398 nm in the chloroform solution and with λ_{max} = 392 nm in the acetone solution. This band is attributed to the π-π* transition. NMR spectroscopy allowed us to establish that the molecules of this substance both in polar acetone and in weakly polar chloroform exist in the cis-form of enaminoketone. Irradiation of the solution of the substance in acetone with UV light results in a decomposition of the dissolved molecules, while the same irradiation of the solution in chloroform leads to reversible cis-trans isomerization of the dissolved molecules.

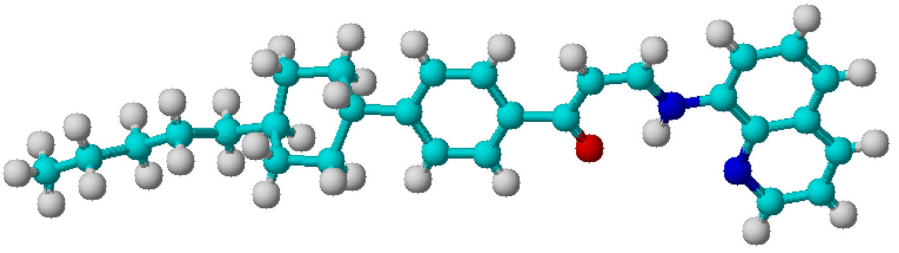

Fig. 1. The possible view of the molecule of 1-phenyl-3-(quinolin-8-ylamino)prop-2-en-1-one.

SECTION 7

DEFECTS AND SPIN QUBITS

oral

Orientation and host dependence of spin-lattice relaxation times for oxo-vanadium porphyrins

S.S. Eaton, G.R. Eaton

Department of Chemistry and Biochemistry, University of Denver, Denver, CO 80210 USA

Opportunities for using molecules as qubits are driving studies to understand properties that contribute to long electron spin lattice relaxation times. Vanadyl porphyrins are of particular interest as qubits because of their relatively long electron spin relaxation times. Spin-lattice relaxation was measured by inversion recovery EPR as a function of temperature and of position in the spectrum for vanadyl tetraphenylporphyrin (VOTPP) in titanyl tetraphenylporphyin (TiOTPP) and zinc tetraphenylporphyrin (ZnTPP) hosts [1]. T_1 also was measured for the vanadyl complexes of octaethylporphyrin (OEP) and tetratolylporphyrin (TTP) in ZnOEP or ZnTTP, respectively. Doping levels were 0.05% to 0.5%. T_1 anisotropy is defined as the ratio of T_1 when the magnetic field is along the VO bond (the z axis) to T_1 when the magnetic field is in the porphyrin plane. For these vanadyl porphyrins T_1 anisotropy increases rapidly between about 60 and 140 K and is strongly dependent on the host lattice, ranging from the unusually large maxima of 36 for VOTPP in TiOTPP to 3.8 for VOTPP in ZnTPP and 3.3 for VOOEP in ZnOEP. Characterizing processes that enhance relaxation in the perpendicular plane are key to understanding relaxation. Empirical modeling of the temperature dependence of T_1 showed that phonons with energies of 190 to 225 cm^{-1} make substantially larger contributions to relaxation in the perpendicular plane than along the z axis and that the magnitudes of these contributions were strongly dependent on the host lattice. X-ray crystallography has shown that TiOTPP and VOTPP are isostructural, which means that there is a closer match of structures between the dopant and the host than for the Zn porphyrins, which may enhance energy transfer. These results demonstrate that optimizing molecules as qubits requires consideration of interaction with the host lattice in addition to molecular properties [2].

1. These samples were provided by Prof. Masahiro Yamashita, Tohoku University, Japan and Prof. Yoji Horii, Nara Women's University, Japan.
2. Eaton S.S., Yamabayashi T., Horii Y., Yamashita M., Eaton G.R.: J. Amer. Chem. Soc. **147**.

oral

Lindblad dephasing relaxation and quantum entanglement in two-spin systems

S.G. Vasil'ev[1], E.I. Kuznetsova[1], E.I. Shipulya[1,2], E.B. Fel'dman[1], A.I. Zenchuk[1]

[1] Federal Research Center of Problems of Chemical Physics and Medicinal Chemistry RAS, Chernogolovka, Moscow region, 142432, Russia
[2] Moscow State University, Moscow, 119991 Russia

Multiple quantum (MQ) NMR spectroscopy is a valuable tool in the investigation of quantum many-body dynamics, specifically the manifestation of irreversible quantum dynamics [1]. The time-consuming excitation of MQ coherences is accompanied by the loss of the detectable signal caused by not only the experimental imperfections, but also substantially by the interactions within the spin system [2, 3]. To get insight into the observed process we investigate the simplest systems, suitable for MQ excitation, consisting of two dipolar coupled spins-1/2 weakly interacting with surrounding spins. The interactions with surrounding in our analytical treatment are taken into account by the Lindblad equation [4], which plays an important role in the problems associated with the dynamics of open quantum systems.

We consider the Lindblad equation under the conditions of MQ experiment [5] with dephasing relaxation. The equation for the density matrix for this case reads

$$\frac{d\rho(t)}{dt}=\frac{Di}{2}\left[I_1^+I_2^++I_1^-I_2^-,\rho(t)\right]+g\sum_{k=1}^{2}\left\{I_{zk}\rho(t)I_{zk}-\frac{1}{2}I_{zk}^2\rho(t)-\frac{1}{2}\rho(t)I_{zk}^2\right\}, \quad (1)$$

where D is the dipolar coupling constant, $I_{\alpha k}$ (k=1,2) is the spin angular momentum projection operator on the α axis (α = x,y,z), I_k^+, I_k^- (k=1,2) are the raising and lowering operators and g is the rate of the dephasing relaxation. It is possible to simplify Eq.(1) for spins ½ noting that I_{zk}^2 =1/4 and performing the transformation

$$\rho(t)=e^{-\frac{1}{2}gt}\bar{\rho}(t) \quad (2)$$

Then we can rewrite Eq. (1) in the following form

$$\frac{d\bar{\rho}(t)}{dt}=\frac{Di}{2}\left[I_1^+I_2^++I_1^-I_2^-,\bar{\rho}(t)\right]+g\sum_{k=1}^{2}I_{zk}\bar{\rho}(t)I_{zk} \quad (3)$$

At t=0, the system is in the thermodynamic equilibrium state and its density matrix is

$$\bar{\rho}(0)=\frac{e^{\beta I_z}}{Z},\quad Z=Tr\left\{e^{\beta I_z}\right\}. \quad (4)$$

where β is proportional to inverse temperature. It is possible to obtain an analytical solution of Eq.(3) with the initial state (4). As a result, the density matrix has the X-form [5] and can be represented as

$$\bar{\rho}(t)=\begin{pmatrix}a_{11}&0&0&a_{14}\\0&a_{22}&0&0\\0&0&a_{33}&0\\a_{41}&0&0&a_{44}\end{pmatrix}, \quad (5)$$

oral

where the matrix elements a_{11}, a_{14}, a_{22} , a_{33} , a_{41} , a_{44} are

$$a_{11} = \frac{e^{\frac{gt}{2}}\cosh\beta}{4\cosh^2\frac{\beta}{2}} + \frac{1}{2}\tanh\frac{\beta}{2}\cos\sqrt{D^2 - \frac{g^2}{4}}t + \frac{g}{4}\frac{\tanh\frac{\beta}{2}}{\sqrt{D^2 - g^2/4}}\sin\sqrt{D^2 - g^2/4}t,$$

$$a_{14} = a_{41}^* = \frac{1}{2i}\tanh\frac{\beta}{2}\frac{D}{\sqrt{D^2 - g^2/4}}\sin\sqrt{D^2 - \frac{g^2}{4}}t,$$

$$a_{22} = a_{33} = \frac{e^{\frac{gt}{2}}}{4\cosh^2\frac{\beta}{2}}, \qquad (6)$$

$$a_{44} = \frac{e^{\frac{gt}{2}}\cosh\beta}{4\cosh^2\frac{\beta}{2}} - \frac{1}{2}\tanh\frac{\beta}{2}\cos\sqrt{D^2 - \frac{g^2}{4}}t - \frac{g}{4}\frac{\tanh\frac{\beta}{2}}{\sqrt{D^2 - g^2/4}}\sin\sqrt{D^2 - \frac{g^2}{4}}t.$$

The density matrix of Eq.(5) allows us to obtain the intensities of MQ NMR coherences. The intensity of the MQ NMR coherence of the zeroth order is

$$J_0(t) = \tanh\frac{\beta}{2}\left(\cos\sqrt{D^2 - \frac{g^2}{4}}t + \frac{g}{2\sqrt{D^2 - g^2/4}}\sin\sqrt{D^2 - \frac{g^2}{4}}t\right)^2 e^{-gt}. \quad (7)$$

The intensities of the MQ NMR coherences of the plus/minus second order are

$$J_{\pm 2}(t) = \frac{1}{2}\tanh\left(\frac{\beta}{2}\right)\frac{D^2 e^{-gt}}{D^2 - g^2/4}\sin^2\sqrt{D^2 - \frac{g^2}{4}}t \qquad (8)$$

It is interesting to notice that the oscillations of MQ NMR coherences are determined by $\sqrt{D^2 - g^2/4}$ rather than D as in the case without relaxation. The decreasing of the oscillation frequency as compared with D was observed experimentally in [2,3]. Another direction of our work was an investigation of quantum correlations in the system under the conditions of MQ NMR. Quantum correlations (quantum entanglement) [6] has been investigated at different values of the rate of dephasing relaxation. It is shown that the dependence of the intensity of the second-order MQ coherence on the excitation time coincides with that dependence for the quantum entanglement when relaxation is absent. The increase of the dephasing relaxation rate results in the decrease of quantum correlations.

The work was performed as a part of the state task, the state registration number N. 124013000760-0.

1. Bengs C., Zhang C., Ajoy A: J. Chem. Phys. **162** (21), 214108 (2025)
2. Fel'dman E.B., Kuznetsova E.I., Panicheva, Vasil'ev S.G., Zenchuk A.I.: J. Magn. Reson. **363**, 107706 (2024)
3. Fel'dman E.B., Kuznetsova E.I., Fedorova A.V. et al.: Bull. Russ. Acad. Sci. Phys. **88**, 1099–1106 (2024)
4. Manzano D.: AIP Advances **10**, 025106 (2020)
5. Fel'dman E.B., Kuznetsova E.I., Shipulya E.I. et al.: (in press) Appl. Magn. Reson. (2025)
6. Wootters W.K.: Phys. Rev. Lett. **80**, 2245 (1998)

poster

Hyperfine and quadrupole coupling in hexagonal boron nitride

E.V. Dmitrieva[1], G.V. Mamin[1], F.F. Murzakhanov[1], I.N. Gracheva[1], M.R. Gafurov[1], V.A. Soltamov[2]

[1] Institute of Physics, Kazan Federal University, Kazan, Russia
[2] The Ioffe Physical-Technical Institute of the Russian Academy of Sciences, St. Petersburg, Russia

Hexagonal boron nitride (hBN) has emerged as a prospective platform for quantum technologies owing to unique spin, optical and coherent properties. hBN offers a significant advantage for quantum applications by enabling the initialization, manipulation, and readout of spin states at room temperature – unlike superconducting qubits, which require cryogenic temperature [1–2]. Additionally, the hyperfine and quadrupole interactions between the electron spin of vacancies and nearby nuclei (^{10}B, ^{11}B and ^{14}N), allow the utilization of nuclear qubits as long-lived quantum memory units. This is critical for quantum devices, as nuclear spins exhibit millisecond-scale coherence times, ensuring robust information storage, while electron spins facilitate fast control and readout [3–4]. Therefore, boron vacancy centers in hBN, coupled with surrounding nuclear spins enable coherent multiqubit operations and quantum sensing applications. Understanding hyperfine (HFI) and quadrupole interactions (QI) in these systems crucial for advancing quantum computing and sensing protocols.

A high-purity hBN crystal (0.90 × 0.54 × 0.05 mm^3) was irradiated with 2 MeV electrons to create boron vacancies. Electron paramagnetic resonance (EPR) measurements were performed at 94 GHz (W-band) using a Bruker Elexsys E680 spectrometer under optical excitation (λ = 532 nm). Pulsed electron-nuclear double resonance (ENDOR) at T = 25 K was employed to obtain signals arising from electron-nuclear interactions.

The boron vacancy spin system (S = 1) exhibited a zero-field splitting parameter D = 3550 MHz (T = 25 K) and g-factor = 2.004. For nitrogen nuclei ^{14}N (I = 1, 99.6 %) located closest to the spin defect were determined the HFI tensor components as A_{xx} = 46.5 MHz, A_{yy} = 45.0 MHz, A_{zz} = 87 MHz, with a quadrupole coupling constant C_q = 1.96 MHz and asymmetry parameter η = −0.07. The following parameters for ^{11}B nuclei (I = 3/2, 80.1%) in the second coordination sphere were also established: the hyperfine interaction tensor component A_{xx} = −3.80 MHz and the quadrupole coupling constant C_q = 2.7 MHz.

This work provides insights into the nuclear spin environment surrounding boron vacancies, specifying key parameters for optimizing quantum memory protocols and multi-qubit operations. The HFI and QI parameters determined in this work enable implementation of highly selective resonant transitions for pre-selected nuclei within the coordination sphere through narrow-band excitation pulses. Our findings directly contribute to the development of practical quantum computing architectures with application the unique advantages of two-dimensional materials for scalable quantum information processing.

This research was funded by the RSF grant № 24-12-00151.

1. Gottscholl A., Kianinia M., Soltamov V., Orlinskii S., Mamin G., Bradac C., Kasper C., Krambrock K., Sperlich A., Toth M., Aharonovich I., Dyakonov V.: Nat. Mater. **19**, 540–545 (2020)
2. Gottscholl A., Diez M., Soltamov V., Kasper C., Sperlich A., Kianinia M., Bradac C., Aharonovich I., Dyakonov V.: Sci. Adv. **7**, eabf3630 (2021)
3. Wolfowicz G., Heremans F.J., Anderson C.P., Kanai S., Seo H., Gali A., Galli G., Awschalom D.D.: Nat. Rev. Mater. **6**, 906–925 (2021)
4. Murzakhanov F.F., Mamin G.V., Orlinskii S.B., Gerstmann U., Schmidt W.G., Biktagirov T., Aharonovich I., Gottscholl A., Sperlich A., Dyakonov V., Soltamov V.A.: Nano Letters **22**, 2718–2724 (2022)

poster

Temperature stability of spin defects in ^{6}H-SiC studied by EPR and luminescence spectroscopy

Y.E. Ermakova[1], I.N. Gracheva[1], F.F. Murzakhanov[1], A.N. Smirnov[2], I.A. Eliseyev[2], O.P. Kazarova[2], G.V. Mamin[1], M.R. Gafurov[1]

[1] Institute of Physics, Kazan Federal University, Kazan, 420008 Russia
[2] Ioffe Institute, St. Petersburg, 194021 Russia

Among the silicon carbide (SiC) polytypes 3*C*, 4*H* and 6*H* are particularly promising for qubit applications [1]. These polytypes can host defects with properties similar to those of nitrogen-vacancy (NV) centers in diamond [1]. In silicon carbide, an NV defect forms when a nitrogen (N) atom substitutes a carbon (C) atom, accompanied by an adjacent silicon vacancy. A divacancy defect, in contrast, consists of a pair of adjacent carbon and silicon vacancies. Under optical excitation, NV defects emit in the near-infrared range, which coincides with the low-loss transmission window of optical fibers. These defects also exhibit some of the longest coherence times among solid-state qubits. Moreover, color centers in silicon carbide are promising candidates for use as quantum single-photon sources. This study focuses on investigating the parameters and dynamic characteristics of spin defects in the 6*H*-SiC polytype.

Using electron paramagnetic resonance (EPR) and electron-nuclear double resonance (ENDOR) spectroscopy, we characterized the hyperfine and quadrupole interaction parameters of NV-type defects in 6*H*-SiC. Analysis of pulsed EPR spectra (Fig. 1) revealed that the signal intensity of the NV center decreases at lower temperatures, whereas

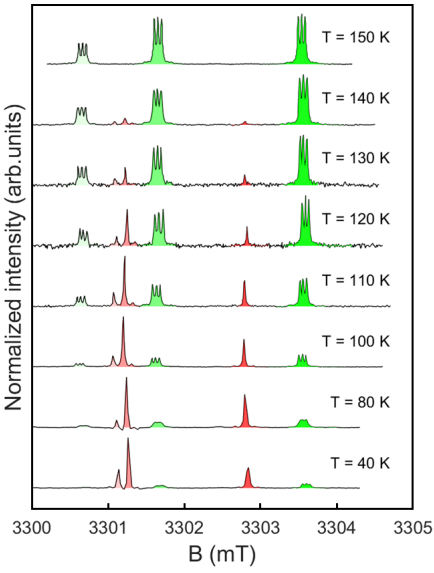

Fig. 1. Normalized photoinduced pulsed EPR spectra of 6H-SiC recorded between 40–150 K ($B_0 \| c$). The observed high-frequency spin transitions correspond to low-field resonant absorption of microwave quanta.

poster

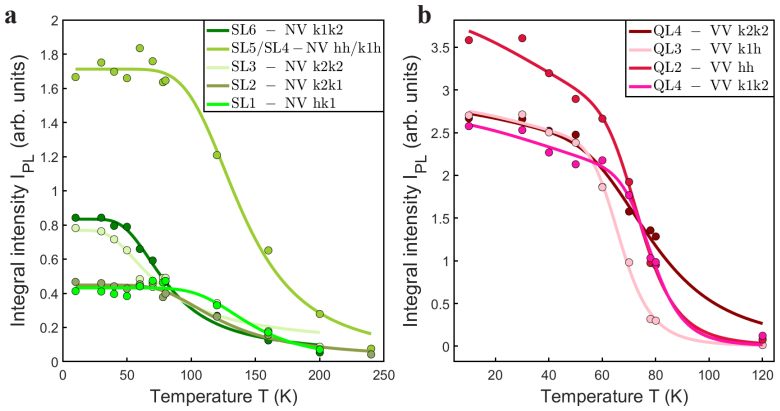

Fig. 2. Temperature dependence of integrated photoluminescence intensity for different spin defect configurations in 6H-SiC (left: NV centers, right: VV centers) over the 10-240 K range. Experimental data are shown as points, while the solid line represents the model curve describing the thermal quenching mechanism of defect luminescence.

the signals from divacancy (VV) centers increase suggesting temperature-dependent charge redistribution between these defects. At elevated temperatures, VV centers exhibit rapid spin relaxation. However, as the temperature decreases, their relaxation processes slow significantly, enhancing both the stability of the VV signals and their contribution to the EPR spectrum. Analysis of the angular dependence of NV center resonant frequencies in ENDOR spectra revealed that the components of the hyperfine interaction tensor, $A_{\parallel}$ and $A_{\perp}$, are nearly identical. This suggests a highly symmetric crystalline environment around the defect and a uniform distribution of spin density. Temperature-dependent relaxation times were also measured. Fitting of the T_1 relaxation data showed that, within the 50–275 K range, longitudinal relaxation is dominated by a thermally activated process, with a minor temperature-independent contribution. At low temperatures, spectral diffusion of electrons begins to influence the transverse relaxation time T_2. The characteristic parameters of this process were determined.

To investigate the optical properties and thermal stability of defect centers in 6*H*-SiC, luminescence spectra were measured over a temperature range of 10–280 K. The temperature-dependent integrated luminescence intensity was analyzed for different defect configurations in silicon carbide. Analysis of the temperature-dependent luminescence (Fig. 2) profiles revealed distinct emission mechanisms for divacancies and NV centers. NV centers exhibit significantly higher luminescence quenching temperatures compared to divacancies, demonstrating superior thermal stability across a broad temperature range. While both defect types show comparable activation energies, divacancies display lower quenching temperatures due to the dominance of non-radiative processes in their emission mechanism, which limits their suitability for high-temperature quantum applications. Among the investigated spin defects in 6*H*-SiC, the NV hh/k1h, NV k2k1, and NV hk1 centers exhibited exceptional thermal stability, making them particularly promising candidates for quantum technologies.

The study was funded by the subsidy allocated to Kazan Federal University for the state assignment in the sphere of scientific activities (Project No. FZSM-2024-0010).

1. Khazen Kh., von Bardeleben H.J., Zargaleh S.A., Cantin J.L., Zhao M., Gao W., Biktagirov T., Gerstmann U.: Physical Review B. **100**, 205202 (2019)

poster

Research a relaxation processes of E' centers in pure quartz fibers by electron paramagnetic resonance method

L.V. Nikiforov[1], D.V. Dmitrieva[1], D.S. Dmitrieva[1], V.V. Davydov[2,3]

[1] St. Petersburg State University of Telecommunications named after Prof. M.A. Bonch-Bruevich, Saint-Petersburg, Russia
[2] Peter the Great St.Petersburg Polytechnic University, Saint-Petersburg, Russia
[3] Saint-Petersburg Electrotechnical University "LETI", Saint-Petersburg, Russia

In the modern world there is a constant increase in radiation background, as well as factors and materials that create additional γ-radiation to the existing natural level [1]. Optical systems are the most sensitive to γ-radiation, especially under prolonged exposure. Under the action of γ-radiation in the optical material coloration centers are formed, which deteriorate its optical characteristics [2]. Optical fibers, especially on trunk lines and in communication and equipment control systems (e.g., at nuclear power plants and others) are subjected to various effects of γ-radiation. Various defects are formed in the fiber, which create great problems in the transmission of information or control and monitoring commands.

The most complex both in structure and relaxation processes are defects that belong to E' centers. These defects form dark-colored (opaque to radiation) points in the fiber structure with the size from 200 to 230 nm depending on the type of the optical fiber material structure [3]. At their large accumulation in the fiber core the laser radiation is completely attenuated and the transmitted information is lost. The developed method of optical fiber cleaning from coloration centers using ultraviolet laser radiation [4] has a number of limitations in its application. The most significant limitation is related to the distance (optical fiber length) of its application. The optical signal attenuation coefficient (scattering loss) of laser radiation at λ = 216 nm for dif-

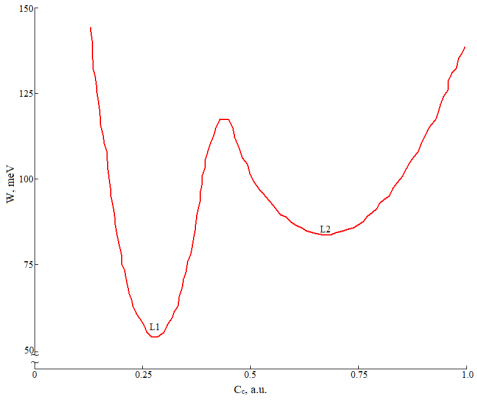

Fig. 1. Total energy for the structural configurations of the E' centers associated with the experimental L1 and L2 line shapes.

poster

ferent types of optical fibers is more than 8.2 dB/km. For this reason, the efficiency of its application at distances greater than 3000 m is zero. Other methods to clear the fiber from the coloration centers are currently not available. For this reason, numerous studies are aimed at developing technologies to reduce the influence of γ-radiation on the rate of formation of dye centers, especially E' centers. Different concepts to reduce this influence are proposed.

In our work we consider a concept related to the increase in the resistance of optical fiber to the formation of E' centers. Exposure of optical fibers to γ-radiation leads to two radiation effects: displacement and ionization. Displacement is associated with the shift of atoms from a stationary state in the crystal lattice to a more unstable state. This defect mainly applies to germanium oxide doped fibers. Numerous experiments have shown that the most radiation-resistant fibers are those with a core of pure quartz [2–4]. They are characterized by a defect associated with ionization, as a result of which electron-ion pairs are formed. The high-energy electron knocks out oxygen from the OH compound and takes its place in the crystal lattice. Our research will be aimed at determining the conditions in the technology of manufacturing optical fibers from pure quartz (first of all, the freezing temperature) and processing of quartz after manufacturing, which will make changes in the structure of the crystal lattice, changes the coordinate configuration Cc and make the fiber more resistant to the effects of γ-radiation (the process of formation of E' centers will begin at higher doses of absorption). Studies of various pure quartz samples irradiated with different doses of γ-radiation absorption were realized on Bruker EMX EPR spectrometer operating at 9.8 GHz. The studies were carried out at a modulating magnetic field frequency of 100 kHz, modulation amplitude of 0.01 mTL and microwave power of 800 nW. Fig. 1 shows for example the result of the variation of the energy of states from the configuration coordinate for two line shapes L1 and L2 obtained at low and high dose of ionization irradiation.

The axial form of the L1 line is observed after irradiation with low doses and may be associated with those centers of formation in which electron substitution is energetically favorable. As the irradiation dose increases, other centers are formed in the state of metastable configuration associated with the orthorhombic form of the L2 line. The transformation from L2 to L1 is induced by heating and can be explained by considering that part of the energy of thermal fluctuations is used in the structural transformation in which the metastable centers change to more stable ones. Typologies of E' centers in SiO_2 have been established, which are distinguished by small variations in the shape of the EPR line, which can be related to different atomic compositions of the vicinity of the unpaired electron. Moreover, it is for the E' center that the evolution of the line shape after thermal treatment at a temperature of $T \sim 500$ K was found, which indicates the existence of unexplained degrees of structural freedom of the defect that further affect the attenuation of the optical signal in the fiber.

1. Rana S., Subbaraman H., Fleming A., Kandadai N.: Sensors **21**, 4111–4122 (2021)
2. Girard S., Alessi A., Richard N.: Reviews in Physics **4**, 100032 (2019)
3. Girard S., Kuhnhenn J., Gusarov A., Brichard B., Van Uffelen M., Ouerdane Y. IEEE Transactions on nuclear science **60(3)**, 2015–2036 (2013)
4. Dmitrieva D.S., Pilipova V.M., Dudkin V.I., Davydov R.V., Davydov V.V. Lecture Notes in Computer Science (including subseries Lecture Notes in Artificial Intelligence and Lecture Notes in Bioinformatics). **13158 LNCS**, 230–239 (2022)

poster

Modeling the dynamics of spin qubits in the presence of stochastic impact of lattice in the semiclassical approximation

A.Yu. Oshchepkov

Perm State University, Perm, Russia

The isotropic interaction of two nuclear spins ½ (A and B) under the influence of the environment (lattice) is considered. The lattice motions leading to dissipative and decoherentizing processes are described by random local magnetic fields, which in the proposed model are generated using the original method of a virtual paramagnetic particle.

The resonant frequencies of the spins in a constant magnetic field that forms the energy levels of the qubits are equal to ω_A and ω_B. The interaction energy of the spins in frequency units is equal to Ω. In the first order of perturbation theory in parameter $\varepsilon = \Omega / \omega_A$, a closed system of evolutionary equations is obtained for the polarization vectors of individual spins m_A and m_B [1]:

$$\dot{\vec{m}}_A = \omega_A \vec{m}_A \times \left(\vec{B}_A + \varepsilon \vec{m}_B \right);$$

$$\dot{\vec{m}}_B = \omega_A \vec{m}_B \times \left(\beta \vec{B}_B + \varepsilon \vec{m}_A \right); \beta = \frac{\omega_B}{\omega_A}.$$

Magnetic fields $\vec{B}_A, \vec{B}_B$ contain both external components acting on both spins: a constant magnetic field; control radio pulses at resonant frequencies, the duration of which is specified by the corresponding cyclogram; a stabilizing field that counteracts dissipative processes, in the form of continuous pulses directed perpendicular to the quantization axis [2, 3], – as well as local disturbances, individual for each spin.

Based on the evolution equations, a computer model was created in Simulink. The block diagram of the model is shown in Fig. 1. In the absence of coupling between spins, the model allows one to study the dynamics of individual qubits and single-qubit

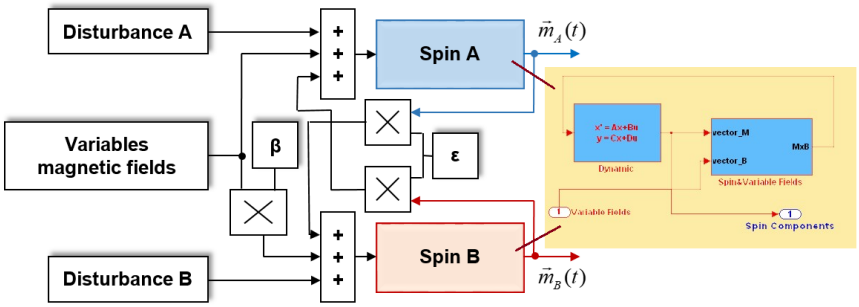

Fig. 1. Block diagram of the model of two interacting spins 1/2.

poster

operations. When modeling a two-qubit CNOT operation, spin A is the control spin, and spin B is the target spin.

The numerical experiments showed that the created computer model adequately describes the dynamics of single-qubit and two-qubit operations, allows to estimate the values of errors in quantum calculations caused by lattice movements. It is shown that the stabilizing impact in the form of magnetic field pulses in the direction orthogonal to the constant field is effective both in storing data before and after quantum computing operations are completed.

1. Oshchepkov A.Yu.: Evolutionary equations for studying the dynamics of qubits in variable magnetic fields. Bulletin of Perm University. Physics, no. 2, 5–18 (2024) (In Russian).
2. Oshchepkov A.Yu.: Stabilization of a qubit in the presense of inphase noise. In Vest. Perm. un-ta, sir. Information systems and technologies. **2011**, pp. 55–62. (In Russian).
3. Oshchepkov A.Yu.: Robust stabilization system of qubit based on spin 1/2 in a magnetic field // Proceedings of the 9th International Scientific Conference on Physics and Control – Moscow: LLC “Publishing House “Pero”, 2019, P. 194–199.

poster

Hyperfine structure of EPR spectra of Cr-53 impurity ions in synthetic forsterite

A.A. Sukhanov[1], V.F. Tarasov[1], Ya.S. Didenko[2], K.A. Subbotin[3], E.V. Zharikov[2]

[1] Zavoisky Physical-Technical Institute, FRC Kazan Scientific Center of RAS, Kazan, Russia
[2] Prokhorov General Physics Institute of the Russian Academy of Sciences, Moscow, Russia

Single crystals of synthetic forsterite (Mg_2SiO_4) doped with chromium ions are known as effective laser media for generation of femtosecond pulses in the range of 1230-1580 nm. The active laser centers are Cr^{4+} ions substituting Si^{4+} ions in tetrahedral positions. At the same time, Cr^{2+} and Cr^{3+} ions can substitute Mg^{2+} in the forsterite crystal lattice.

In this work we studied hyperfine structure (HFS) of continuous wave EPR spectra of Cr^{2+} and Cr^{3+} ions substituting Mg^{2+} ions in two structurally nonequivalent octahedral positions M1 and M2. Crystal was grown from the melt with 0.14 wt.% Cr by the Czochralski technique in slightly oxidizing atmosphere. The ^{53}Cr isotope content was 0.977%. Measurements were carried out in X-band at temperatures of 80 and 300 K on Bruker ELEXSYS E680 spectrometer.

Two different types of HFS were detected. The HFS of a single $^{53}Cr^{3+}$ ion, shown in Fig. 1a, consists of 4 lines corresponding to allowed transitions between nuclear levels of the ^{53}Cr with nuclear spin $I = 3/2$. A weak signal from even chromium isotopes is observed in the center of the spectrum. In addition to these spectra, spectra with a more complex HFS were detected. An example of such a spectrum is presented in Fig. 1b. We believe that this spectrum is due to a $^{53}Cr^{3+}$-$^{53}Cr^{3+}$ dimer associate. In general, the HFS of this associate should consist of 16 allowed transitions, however, some lines overlap each other. Therefore, the HFS represents 7 lines corresponding to the total nuclear spin $I_{dim} = 3$ with a ratio of intensities of 1:2:3:4:3:2:1.

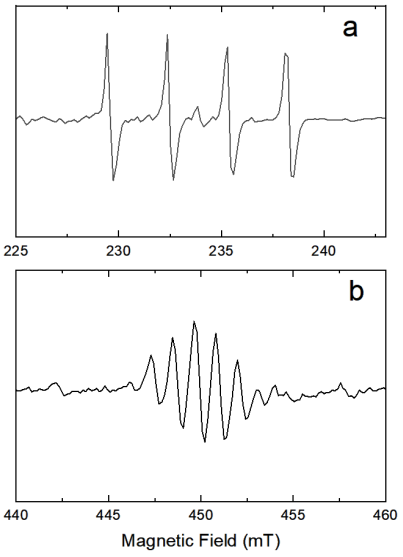

Fig. 1. Spectra of $^{53}Cr^{3+}$ ions in Mg_2SiO_4. **a** single Cr^{3+} ion; **b** Cr^{3+}-Cr^{3+} dimer associate.

poster

EPR study of [Mn^{2+}-Ag^{2+}] exchange coupled pairs synthesized in BaF_2 single crystal

R.B. Zaripov[1], V.A. Ulanov[1,2], R.R. Zainullin[2]

[1] Zavoisky Physical-Technical Institute, FRC Kazan Scientific Center of RAS, Kazan, Russia
[2] Kazan State Power Engineering University, Kazan, Russia

The alkaline-earth fluorides (MeF_2) are important models for understanding the solid-state chemistry of point defects in insulating crystals. The extensive experimental and theoretical investigation of these systems has resulted in a detailed microscopic picture on physical-chemical reactions between native and impurity defects.

Our investigations of the solid-state reactions between defects of impurity Jahn-Teller d-ions reveal a possibility to synthesize paramagnetic impurity clusters of two [1] or three [2] similar Jahn-Teller d-ions. It was found that each of these ions substitutes for a lattice cation and find itself in the center of an anionic cube formed by eight fluorine ions. Stability of such clusters realizes by interaction of impurity d-ions via a field of the Jahn-Teller deformations.

Another mechanism of cluster formation is an electronic exchange between the impurity ions.

The present work was devoted to impurity pairs of non-similar d-ions. The first object of the present investigation was BaF_2 crystal doped by manganese and silver impurities. The samples under investigation were grown by Bridgman method. The EPR method was used to study the magnetic properties, molecular structure and relative concentration of Mn-Ag pairs. The anisotropic EPR spectra with nicely resolved fine, hyperfine and superhyperfine structures were observed in the samples under investigation. These spectra contain very reach information on the molecular structure and magnetic properties of the pairs under study. It was found that the magnetic symmetry of the Mn-Ag pairs was tetragonal. In each impurity pair, the Mn^{2+} and Ag^{2+} ions were shifted towards each other. As it turned out, the observed spectra contain two groups of lines with different integral intensities. The angular dependences of the positions of the spectral lines of the first group were described by the spin Hamiltonian corresponding to the spin momentum $S = 2$. It is assumed that the group of less intense lines belongs to another type of (Mn^{2+}-Ag^{2+}) pairs. The noted facts clearly indicate the presence in the crustal under study of two types of manganese and silver pairs, in which Mn^{2+} and Ag^{2+} ions are linked by antiferromagnetic exchange interaction.

1. Fazlizhanov I.I., Ulanov V.A., Zaripov M.M.: Fizika Tverdogo Tela **44**, 1483 (2002)
2. Ulanov V.A., Zaripov M.M., Fazlizhanov I.I.: Fizika Tverdogo Tela **47**, 1596 (2005)

SECTION 8

MAGNETIC RESONANCE IMAGING AND APPLICATIONS IN MEDICAL PHYSICS SYSTEMS

oral

Magnetic resonance imaging of laboratory animals lungs using hyperpolarized ^{129}Xe

Ya.V. Fattakhov[1], A.R. Fakhrutdinov[1], D.A. Konovalov[1], V.L. Odivanov[1], V.A. Shagalov[1], A.A. Bayazitov[1], F.V. Bashirov[2], V.A. Markosyan[2], V.M. Vodovozov[3], A.V. Pavlenko[3], R.F. Kurunov[3], V.M. Baev[3], M.V. Kuleshov[3], V.V. Eremkin[3], A.A. Baturina[3], M.S. Sirko[3]

[1] Zavoisky Physical-Technical Institute, FRC Kazan Scientific Center of RAS, Kazan, Russia
[2] Federal State Budgetary Educational Institution of Higher Education Kazan State Medical University of the Ministry of Health of the Russian Federation, 420012, Kazan, Russia
[3] Joint-Stock Company "D.V. Efremov Scientific Research Institute of Electrophysical Equipment", 196641, Saint Petersburg, Russia

The purpose of this work was to develop a technique for obtaining NMR images of plants and laboratory animals using hyperpolarized (HP) ^{129}Xe. An HP ^{129}Xe production facility was created [1], and the MRI system [2] was modified to run on xenon atoms. A device for monitoring the respiration of laboratory animals has also been developed and manufactured, which allows periodic switching of the supply of a breathing mixture or xenon gas, as well as ensuring respiratory retention during measurement. The technology of tracheostomy of laboratory animals has been developed to ensure their respiration during lung scanning. To obtain images on samples with hyperpolarized gas, the pulse program "Fast gradient Echo" was developed, based on the use of exciting pulses with small rotation angles of the magnetization vector (in our case ~9°), which allows performing a full image scanning cycle with one portion of gas. An experiment was conducted to obtain images of laboratory animals' lungs using HP ^{129}Xe.

1. Vodovozov V.M., Pavlenko A.V., Kurunov R.F., Baev V.M., Kuleshov M.V., Chumichev V.A., Eremkin V.V., Baturina A.A.: An experimental sample of a laser installation for the development of hyperpolarized ^{129}Xe. International conference "XXV Kharitonov thematic scientific readings. Modern Laser Technologies", Sarov, March 25–29, 2024, FSUE RFNC-VNIIEF, Abstracts. In Russian.
2. Fattakhov Ya.V., Anikin A.N., Bayazitov A.A., Fakhrutdinov A.R., Khabipov R.Sh., Odivanov V.L., Salikhov K.M., Shagalov V.A., Reshetnikov N.M., Abdulganieva D.I., Mikhailov M.K., Ryzhkin S.A., Anisimov V.I. The first results of using a specialized MRI system with magnetic field of 0.4 T // Modern Development of Magnetic Resonance, Kazan, September 28–October 2, 2020. Book of Abstracts, P. 184.

oral

Recent technical advances in EPR spectroscopic mapping for mouse tumor models

H. Hirata

Division of Bioengineering and Bioinformatics, Hokkaido University, Sapporo, Japan

EPR spectroscopy is a powerful analytical method for obtaining molecular information from EPR spectra. In biomedical applications, such as cancer studies, oxygenation, extracellular acidification, and reduction/oxidation (redox) status in the tumor microenvironment are essential parameters for understanding tumor pathophysiology. Those spatial distributions in solid tumors can be mapped using EPR [1–3]. Several technical challenges in low-field EPR imaging need to be addressed to achieve high-precision mapping of these parameters.

In this presentation, recent progress in EPR imaging will be reported. The first method is for mapping the partial pressure of oxygen (pO_2) using nitroxyl radical agents. Nitroxyl radicals have been used for continuous-wave EPR-based pO_2 mapping; however, the concentration of the imaging agent affects the linewidth of the EPR absorption spectrum, leading to errors in the pO_2 estimation [4]. Using ^{14}N- and ^{15}N-labelled nitroxyl radicals [5], the influence of the agent concentration can be reduced by solving the numerical model of the linewidths for two nitroxyl radical agents. The second technique is an image reconstruction method that uses randomly sampled spectral projections [6]. CW-EPR imaging is generally based on the acquisition of spectral projections under magnetic field gradients. To accelerate the image acquisition, the number of spectral projections being acquired can be reduced. However, it leads to a degradation of the image quality. To address this technical problem, a method of randomly selecting the direction of the magnetic field gradient helps improve image quality. Examples of image reconstruction using this approach are presented, including a solution sample and a mouse tumor model.

This work was supported by the Japan Society for the Promotion of Science (JSPS) KAKENHI grants JP22H00200 and JP1K18165.

1. Nakaoka R. et al.: Anal. Chem. **95**, 3940–3950 (2023)
2. Sato-Akaba H. et al.: Magn. Reson. Med. **94**, 424–435 (2025)
3. Li T. et al.: Mol. Imaging Biol. **26**, 448–458 (2024)
4. Halpern H.J. et al.: Proc. Natl. Acad. Sci. USA **91**, 13047–13051 (1994)
5. Yokoyama T. et al.: J. Magn. Reson. **305**, 122–130 (2019)
6. Oba M. et al.: Mol. Imaging Biol. **26**, 459–472 (2024)

poster

Study of the efficiency of helium-3 nuclear polarization in magnetized plasma under various RF pumping conditions

A.S. Makarchenko, V.V. Kuzmin

Kazan Federal University, Kazan 420008, Russia

Hyperpolarized noble gases (helium-3 and xenon-129) serve as probes for studying porous media using nuclear magnetic resonance (NMR) techniques. Their principal advantage lies in the substantial enhancement of detection sensitivity. The most widely employed methods for producing hyperpolarized gases are optical techniques: spin-exchange optical pumping (SEOP) and metastability exchange optical pumping (MEOP), with the latter being exclusively applicable for the hyperpolarization of helium-3 nuclear spins. In 2018, a new polarization method for hyperpolarizing helium-3 nuclei in plasma was discovered and called PAMP (polarization atoms in a magnetized plasma) [1].

To achieve polarization via PAMP method, helium-3 plasma must be subjected to a strong magnetic field while maintaining the following conditions: high-purity helium-3 (with impurity levels of ~1 ppm) and a gas pressure of approximately 10 mbar. The PAMP method offers a distinct advantage over alternative approaches through its relative implementation simplicity, as it eliminates the need for complex laser systems.

For the investigation of helium-3 nuclear spin polarization dynamics using the PAMP technique, we assembled a specialized experimental setup comprising: a high-purity helium-3 gas purification system with polarization cells, NMR signal detection apparatus specifically designed for helium-3, and an RF excitation system for plasma generation in helium-3 [2].

Subsequent experimental studies focused on evaluating the efficiency of PAMP-induced polarization under various conditions. We systematically examined the dependence of polarization magnitude on temperature in the range 300–520 K and RF power for creating plasma revealing a pronounced correlation between polarization and these parameters [3]. The maximum achieved polarization magnitude in our experiments reached 8%.

In this work, we investigated the dependence of both polarization magnitude and rate on the power and frequency of RF excitation. Detailed measurements of the polarization kinetics demonstrated that the process occurs with remarkable rapidity, exhibiting a time constant of approximately 1 second at high RF power levels. The RF excitation power (W_{eff}) was varied across a broad range from several watts up to ~60 watts, while the excitation frequency was varied between 12 and 55 MHz. These studies provided comprehensive characterization of the polarization dynamics under different excitation conditions. Experimental data show that increasing the pumping frequency enhances the polarization rate at constant power.

This work was financially supported by the Russian Science Foundation (project no. 25-22-00389).

1. Maul A., Blümler P., Nacher P.J., Otten E., Tastevin G., Heil W.: Nuclear hyperpolarization of ^{3}He by magnetized plasmas. Physical Review A **98**(6), 063405 (2018)
2. Makarchenko A.S., Kuzmin V.V., Safiullin K.R., Kan D.V., Tagirov M.S.: Cryogenic Purification of Helium and its Use for Preparing Polarization Cells and Carrying Out Non-Optical Polarization of ^{3}He Nuclei. Instruments and Experimental Techniques, 64, 911-916.
3. Makarchenko A., Kuzmin V., Safiullin K., Tagirov M. Temperature-related effects in the polarization of atoms in a magnetized plasma as a promising feature towards high ^{3}He nuclear polarization. Physical Review A **106**(2), 023101 (2022)

poster

Application of convolutional neural network to improve the efficiency of tumor segmentation in prostate MRI

N.A. Nefediev[1], N.E. Staroverov[2], R.V. Davydov[3]

[1] Department of Bioinformatics and Mathematical Biology, Alferov University, St. Petersburg, Russia
[2] Department of Electronic Instruments and Devices, Saint Petersburg Electrotechnical University "LETI", Saint Petersburg, Russia
[3] Institute of Cybersecurity and Computer Science, Peter the Great St. Petersburg Polytechnic University, St. Petersburg, Russia

Prostate cancer is one of the leading causes of death among the male population from oncological diseases. One of the reasons for high mortality is the difficulty of diagnosing the disease in the early stages of tumor development. The classic method of cancer detection is monitoring prostate-specific antigen (PSA). One of the options for helping in the analysis of MRI studies is the development of technological solutions based on Artificial Intelligence (AI) algorithms [1, 2].

Among the AI methods for detecting neoplasms on prostate MRI, semantic segmentation is the most suitable, as it allows pixel-by-pixel division of images (MRI slice) into neoplasm and healthy tissue. For most tasks, it is sufficient to use one neural network architecture, but complex problems may require using complex approaches, including several neural networks. Our work is aimed at finding and describing the optimal method for detecting prostate cancer in pelvic MRI studies. The main task is to obtain segmentation of the prostate and cancer. The work used anonymized data from a closed dataset of 400 studies. Based on our research and the results obtained, we can divide the course of the study into three stages – preliminary, main, and final.

The preliminary stage includes the use of a neural network for prostate cancer segmentation, as well as an approach with the preliminary use of a classifier trained to divide slices into two classes: "with cancer" and "without cancer". In the first case, we used two approaches to cancer segmentation – segmentation of 2D data, and segmentation of 3D data. In the second case, we formed a new dataset, leaving only those slices that were marked by the classifier as containing cancer. Then the new dataset was used to train neural networks for 2D and 3D segmentations. It is worth noting that here and below, when choosing neural networks to train, we focused on architectures that showed excellent results in medical problems close or adjacent to ours. The standard segmentation metric, the dice metric, was used as a training quality metric.

The main stage of the research in our work was based on the allocation of the prostate area and took place in three stages. At the first stage, we checked the quality of the neural networks of segmentation for the allocation of the prostate on 2D and 3D data.

To improve the results, we decided to try the idea from the preliminary stage, namely, to transfer to the segmentation network only those sections that contained the prostate. To do this, we trained the neural network for binary classification (presence/absence of the prostate on the slice). Then we formed a new dataset. However, at this stage, we made adjustments to the rule for forming the new dataset, namely, now we left only sections in the range from the smallest to the largest section number. This

poster

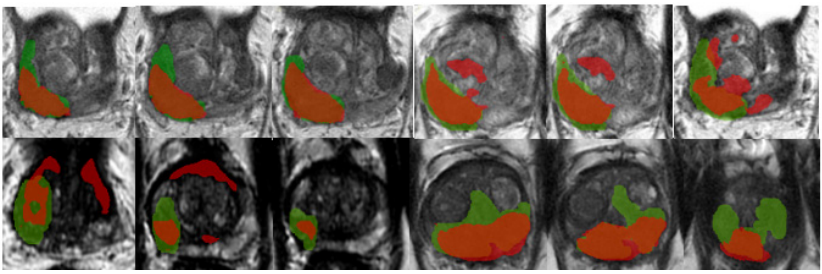

Fig. 1. Сегментация рака итоговой моделью 3D сегментации. Зелёный цвет соответствует истинной маске.

approach is justified by the fact that the prostate is a solid continuous organ, and thus we exclude a possible classifier error in the middle section.

To improve the results, we decided to try the idea from the preliminary stage, namely, to transfer to the segmentation network only those sections that contained the prostate. To do this, we trained the neural network for binary classification (presence/absence of the prostate on the section). Then we formed a new dataset. However, at this stage, we made adjustments to the rule for forming the new dataset, namely, now we left only sections in the range from the smallest to the largest section number. This approach is justified by the fact that the prostate is a solid continuous organ, and thus we exclude a possible classifier error in the middle section.

The final stage involved using the best prostate segmentation method to generate a modified dataset and training networks for 2D and 3D cancer segmentation with the best performance from the preliminary stage.

As a result, at the final stage, we trained two networks for cancer segmentation on the modified dataset. The SwinUNETR architecture network showed the best results in 3D segmentation. The results of cancer segmentation by the best method are shown in Fig. 1.

1. Sung H., Ferlay J., Siegel RL.: Global cancer statistics 2020: GLOBOCAN estimates of incidence and mortality worldwide for 36 cancers in 185 countries. CA Cancer J Clin. **71**(3), 209–249 (2021)
2. Turkbey B., Rosenkrantz AB., Haider MA.: Prostate imaging reporting and data system version 2.1: 2019 update of prostate imaging reporting and data system version 2. Eur Urol. **76**(3), 340–351 (2019)
3. Rodrigues NM., Silva S., Vanneschi L.: A Comparative study of automated deep learning segmentation models for prostate MRI. Cancers (Basel) **15**(5):1467 (2023)

SECTION 9

RELATED PHENOMENA

poster

Magnetocaloric effect and the hysteresis properties of $LiDyF_4$

G.Iu. Andreev, E.I. Baibekov, I.V. Romanova

Kazan Federal University, Kazan, Russia

The rare-earth double fluorides $LiRF_4$ (R = Gd-Yb) have gained attention as model objects for the physics of dipolar magnetism. $LiDyF_4$ is a dipolar antiferromagnet, the magnetic moments of Dy^{3+} ions are ordered in the (001) plane, T_N = 610(15) mK; the crystal structure belongs to the symmetry group of $I4_1/a$ [1, 2].

Previously, a magnetic hysteresis effect in the temperature range of 2–10 K was detected in crystalline samples (both a micro-sized powder and a single crystal: see example at Fig. 1) [3]. In this work, an attempt is made to explain this phenomenon by using the magnetocaloric approach (described in [4] for $DyScO_3$ Ising magnetic), including *ab initio* calculations of the phonon characteristics of the $LiDyF_4$ crystal in the framework of density functional theory.

Authors are grateful to Prof. Boris Malkin for fruitful discussions.

This work was supported by RSF grant #22-12-00259-П.

1. Aminov L.K., Malkin B.Z., Teplov M.A.: Handbook on the Physics and Chemistry of Rare Earths. **22**, 296–506 (1996)
2. Mennenga G., de Jongh L.J., Huiskamp W.J., Laursen I.: J. Mag. Mag. Mat. **44**, 1-2, 48–58 (1984)
3. Andreev, G.Iu. et al.: Mat. Res. Bull. **156**, 112002 (2022)
4. Andriushin, N.D., Nikitin S.E., Ehlers G., Podlesnyak A.: Phys. Rev. B. **106**, 104427 (2022)

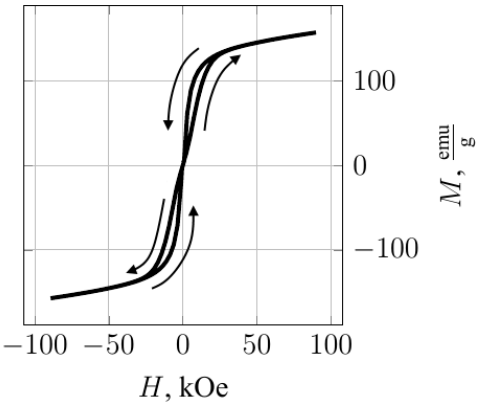

Fig. 1. Measured magnetic hysteresis of the microsized powder sample of $LiDyF_4$ at the temperature of 2 K. Arrows denote the data at increasing/decreasing magnetic field.

poster

The realisation of solitary superconductivity in a superconducting spin valve

D. Arbuzov[1,2], A. Kamashev[1], N. Garif'yanov[1]

[1] Zavoisky Physical-Technical Institute, FRC Kazan Scientific Center of RAS, Kazan, Russia
[2] Kazan Federal University, Russia

We report about probably observation of a solitary superconductivity in a F1/F2/S ($Co_2Cr_{1-x}Fe_xAl/Co_2Cr_{1-x}Fe_xAl/Pb$) spin-valve structure, where superconductivity is realized only in the antiparallel (AP) magnetization configuration of the ferromagnetic layers. By optimizing the thicknesses of the superconducting Pb layer and the ferromagnetic layers, we achieve a complete suppression of superconductivity in the parallel (P) while maintaining a finite transition temperature in the AP configuration. in the limit, the magnitude of the effect reaches $\Delta T_c = T_c^{AP} - T_c^{P} = 1.6$ K in a magnetic field of 1 kOe, significantly exceeding previously reported values for conventional F1/F2/S systems. This behavior is explained by the compensation of exchange fields in the AP state, which weakens the pair-breaking effect and allows the emergence of superconductivity.

The interaction features of superconductors (S) and ferromagnets (F) have found important application in superconducting current control devices. Thus, models of a superconducting spin valve (SSV) based on F1/F2/S structures were proposed [1]. The superconductivity in the SSV is controlled by changing the mutual orientation of the magnetization of the F-layers using an external magnetic field. As a rule, with the parallel (P) orientation of the magnetizations F1 and F2, the critical transition temperature T_c^{P} is lower than in the case of their antiparallel (AP) orientation T_c^{AP}.

The so-called state of solitary superconductivity has great prospects in this field [2]. In this state, the transition to the superconducting state is possible only with AP orientation for certain thicknesses of the F2 layer. In this case, the main characteristic of

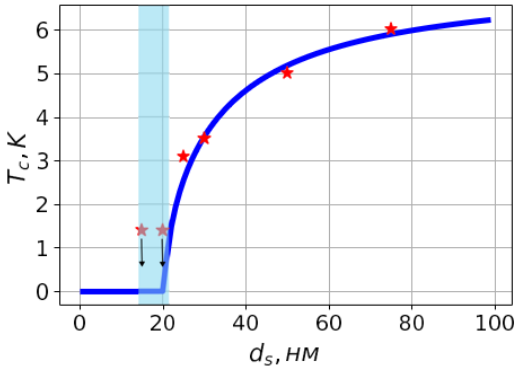

Fig. 1. The dependence of the critical temperature HA(12 nm)/Cu(1.5 nm)/Pb on the thickness of the superconducting layer d_S. The arrows mark the points lying below T_{lim} = 1.4K. The selected area corresponds to thicknesses for which T_c is close to zero.

poster

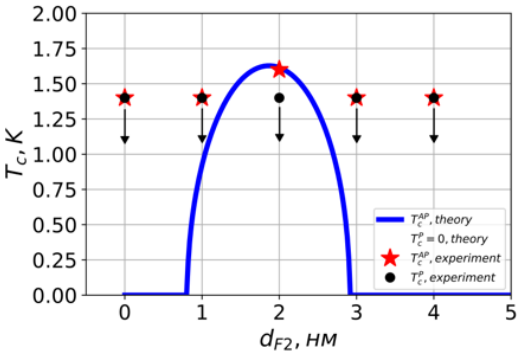

Fig. 2. T_c of HA(5 nm)/Cu(1.2nm)/HA(dF 2)/Cu(1.5nm)/Pb(17.5nm) from the thickness of the ferromagnetic layer d_{F2}. The arrows mark the points below T_{lim} = 1.4 K.

SSV $\Delta T_c = T_c^{AP} - T_c^{P} = T_c^{AP}$ is determined by only one critical temperature. However, due to the difficulty of precisely selecting the thicknesses of the layers, in which the transition will be possible only in one of the orientations, solitary superconductivity has not yet been experimentally detected.

At the first stage, the thickness of the F-layer was fixed in the HA/Pb (HA = $Co_2Cr_{1-x}Fe_xAl$) system and the thickness of the S-layer dS was varied in search of the value at which Tc is maximally suppressed. The found value of ds must be used in the manufacture of SSV in the future. From Fig. 1 it can be seen that Tc decreases with decreasing dS and reaches zero in the region of $d_S \sim$ 20nm. Thus, the working area for the occurrence of solitary superconductivity is the range d_S = [15 ÷ 22]nm. Under this condition, the SSV superconductivity in the P orientation will remain completely suppressed ($T_c^P = 0$). At the same time, in the AP orientation, the weakening of the magnetic part of the system will be sufficient to transition to the superconducting state. It should be noted that our measuring system has a temperature limit of $T_{lim} \approx$ 1.4 K, which can be cooled to, and some of the samples have Tc below this limit value, or they do not enter the superconducting state at all (see Fig. 1).

The final stage of the research was the implementation of a superconducting spin valve in the solitary superconductivity mode based on the data obtained (Fig. 2). For this purpose, the thicknesses of the HA1 and Pb layers were recorded in the HA1/HA2/Pb system and the dependence of the magnitude of the ΔT_c effect on the thickness of the HA2 layer was investigated. Shown in Fig. 2 experimental data obtained with a gradual decrease in the thickness of the S-layer (in the range ds dim 20nm) demonstrate the existence of an interval d_{F2} = [0.8 ÷ 2.9] nm in the phase diagram, which may correspond to the desired state. Of particular interest is a sample with an F2 layer thickness of 2 nm, for which the transition temperature in the AP orientation is $T_c^{AP} \approx$ 1.6 K, but no superconductivity was detected in parallel. In this case, the value $\Delta T_c >$ 0.2 K turns out to be unusually large for the ”classical” SSV in the form of the F1/F2/S structure and reaches a huge limit for such systems of values ΔT_c = 1.6 K.

1. Tagirov L.R.: Low-field superconducting spin switch based on a superconductor/ferromagnet multilayer. Phys. Rev. Lett. **83**, 2058 (1999)
2. Avdeev M.V., Proshin Y.N: Solitary superconductivity in a ferromagnet–superconductor heterostructure. Jetp. Lett. **102**, 96–99 (2015)

poster

Investigation of features of magnetic properties of oxidized layers in superconducting spin valve structures CO/PB/CO

A.A. Kamashev, N.N. Garifyanov, A.A. Validov, D.A. Arbuzov, I.A. Garifullin

Zavoisky Physical-Technical Institute, FRC Kazan Scientific Center of RAS, Kazan, Russia

Superconducting spin valves (SSVs) of the CoO_x/Co/Pb/Co design, featuring oxidized superconductor/ferromagnetic interfaces, are promising systems for superconductivity control. The superconductor/ferromagnetic (Pb/Co) interface plays a key role in such structures. Oxidation of this interface, as demonstrated in previous experiments, does not preclude observation of the classical SSV effect, characterized by a critical temperature shift $\Delta T_c \approx 0.2$ K. It is important to note that the full spin valve effect was confirmed in the studied structures, as the observed ΔT_c exceeded the superconducting transition width δT_c.

Direct estimation of the oxide layer thickness within the complete SSV heterostructure during fabrication is technologically challenging. To address this limitation, a calibration technique was developed. A series of single-layer cobalt films with varying thicknesses were fabricated and oxidized under strictly controlled conditions identical to those used for interface oxidation in the full SSV structures. Ferromagnetic resonance (FMR) spectroscopy – a highly sensitive method for probing the magnetic properties of thin films and surfaces – was employed to estimate the thickness of the oxide layer formed on the Co films. Based on FMR data, the thickness of the oxide layer formed on the cobalt films under relevant conditions was less than 0.5 nm.

poster

High-entropy perovskite-like oxide $(BaCaSrLaNa)_{0.2}FeO_3$: Synthesis and EPR measurements

R.F. Likerov, I.V. Yatsyk, R.M. Eremina

Zavoisky Physical-Technical Institute, FRC Kazan Scientific Center of RAS, Kazan, Russia

High-entropy oxides (HEO) are considered suitable for thermoelectric applications [1] and outperform traditional thermoelectric materials, such as Bi_3Te_2 in case of high working temperatures. The following characteristics of HEO are important: thermal conductivity κ, electrical conductivity σ, Seebeck coefficient S.

In this work, we report the synthesis and EPR study of $Ba_{0.2}Ca_{0.2}Sr_{0.2}La_{0.2}Na_{0.2}FeO_3$ HEO with perovskite-like structure. This compound was synthesized by solid-state reaction method. We used analytical grade reagents such as $BaCO_3$, $CaCO_3$, $SrCO_3$, Na_2CO_3, La_2O_3 and Fe_2O_3 (all are >99% purity), which was mixed in planetary ball mill at 300 rpm for 3 hours. Then we calcined mixed powders in air for 6 hours at T = 1050°C and pressed calcined powders with P = 470 MPa for pellet sintering at T = 1100°C for 6 hours.

Room temperature CW EPR measurements at X-band showed magnetic phase stabilization for $Ba_{0.2}Ca_{0.2}Sr_{0.2}La_{0.2}Na_{0.2}FeO_3$ sintered pellet in comparison with calcined powders (Fig. 1).

1. Bhattacharya T., Banerjee R., Maiti T.: Phys. Chem. Chem. Phys. **26**, 28874–28883 (2024)

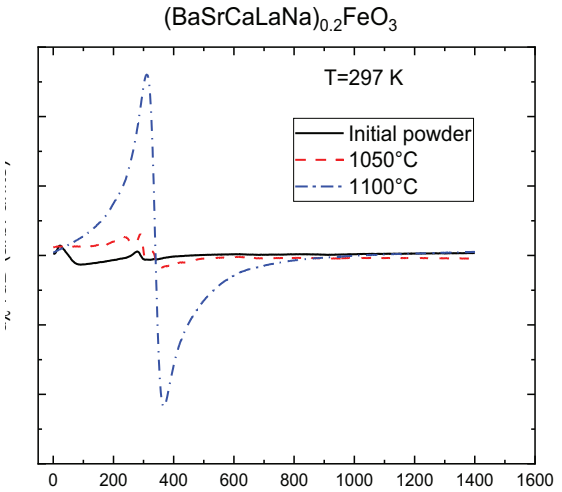

Fig. 1. Room temperature EPR spectra of initial precursor powders (black line), calcined powders (red dash line) and sintered pellet formed by pressurizing the calcined powders (blue dash-dot line).

poster

Measuring magnetostriction using capacitive dilatometer

M.E. Menshikov, A.V. Dooglav, R.G. Batulin, S.L. Korableva, O.A. Morozov, I.V. Romanova

Kazan Federal University, Kazan 420008, Russia

In this paper, we present the construction of capacitive dilatometer and the results of measuring the magnetostriction of the Van Vleck dielectric single crystal of lithium-thulium double fluorides $LiTmF_4$ along the [100] crystallographic axis. The capacitive dilatometer was designed and assembled according to the design proposed by G. M. Schmiedeshof et al [1] and was used with a PPMS system and a capacitive bridge [2].

The $LiTmF_4$ single crystal was grown by S.L. Korableva using the Bridgman-Stockbarger method. After evaluating the single crystallinity and axis orientation, two parallel planes perpendicular to the crystallographic axis [100] were selected and polished using a brass mandrel and water-based abrasives.

Using a capacitive dilatometer, the magnetostriction of the $LiTmF_4$ single crystal was obtained at a temperature of T = 5 K. A single crystal $LiTmF_4$ was selected as a reference sample for the study. Our data are consistent with previous studies by Altshuller and Krotov in 1980 up to 3 T [3] and also qualitatively consistent with preliminary calculation in a single crystal up to 3.5 T.

This work was supported by RSF grant #22-12-00259-П

1. Schmiedeshoff G. et al.: Rev. of Sci. Instrum 77.12 (2006)
2. Model 2550A digital capacitance bridge manufactured by Andeen-Hagerling, Inc.
3. Al'tshuler S., Krotov V., Malkin B.: JETP Lett. **32**(3), 232–235 (1980)

poster

Investigation of spin-current conversion in Py/$Bi_{1.08}Sn_{0.02}Sb_{0.9}Te_2S$ heterostructure

V.O. Sakhin[1], B.F. Gabbasov[2], D.G. Zverev[2], E.F. Kukovitsky[1], N.N. Garifyanov[1], A.A. Kamashev[1]

[1] Zavoisky Physical-Technical Institute, FRC Kazan Scientific Center of RAS, Kazan, Russia
[2] Institute of Physics, Kazan Federal University, Kazan, Russia

Topological insulators (TIs) are promising materials for numerous applications in spintronics. They are narrow-gap semiconductors in the bulk, but possess conductive Dirac surface states. Strong spin–orbit coupling (SOC) in bismuth chalcogenide-based TIs leads to the so-called spin-momentum locking at these surface states. This makes TIs natural candidates platform to observe the inverse spin Hall effect (ISHE) [1,2]. ISHE is essentially a conversion of spin current into charge current in systems with strong SOC [3]. In TIs the conversion is expected to occur at the topological surface states, potentially leading to higher efficiency [2]. Investigating ISHE in such systems is not only of fundamental interest but also could be useful for engineering spintronic devices based on spin currents in topologically protected states.

Traditionally, ISHE is studied in ferromagnet/heavy metal bilayer systems [4,5]. In the current study, we have fabricated such heterostructures using permalloy as the ferromagnet layer and $Bi_{1.08}Sn_{0.02}Sb_{0.9}Te_2S$ (BSSTS) as the conductive substrate with strong SOC. Permalloy is a classic ferromagnetic material that was found to have good adhesion to the BSSTS surface and have been previously used in ISHE studies [6]. The advantage of using a complex compound like $Bi_{1.08}Sn_{0.02}Sb_{0.9}Te_2S$ is its low bulk carrier concentration, which ensures that at low temperatures surface states dominate the conductivity in the TI [7]. Single crystals of BSSTS were mechanically cleaved to obtain macroscopic flakes, onto which Py was deposited using a magnetron sputtering technique. The prepared heterostructure was placed on a specially designed circuit to detect emerging voltage and avoid additional magnetogalvanic effects.

Simultaneous measurements of ferromagnetic resonance (FMR) in the Py layer and voltage in the BSSTS layer were carried out using an electron paramagnetic resonance spectrometer. FMR conditions are necessary to induce spin pumping from the ferromagnetic layer with strong SOC. In the presence of in-plane magnetic field spin current is expected to be converted into a charge current, which is detected via a lock-in amplifier at the spectrometer's modulation frequency.

The work was partially supported by RSF project № 21-72-20153-p and partially by the government assignment for FRC Kazan Scientific Center of RAS.

1. Jamali M., Lee J.S., Wang J.-P.: Nano Lett. **15**, 10, 7126–7132 (2015)
2. Khang N., Ueda Y., Hai P.N.: Nature Mater **17**, 808–813 (2018)
3. Wang X.: Commun Phys **4**, 55 (2021)
4. Ando K., Takhashi A. et al.: J. Appl. Phys. **109**, 103913 (2011)
5. Kadikova A., Gabbasov B., Yanilkin I. et al.: Bull. Russ. Acad. Sci. Phys. **88**, 1094–1098 (2024)
6. Tsukahara A., Ando Y. et al.: Phys. Rev. B **89**, 235317 (2014)
7. Sakhin V., Kukovitsky E., Talanov Y. et al.: Jetp Lett. 115, 239–244 (2022)

Ответственный редактор Т. П. Гаврилова; редактор В. К. Воронкова;
технический редактор О. Б. Яндуганова. Издательство ФИЦ КазНЦ РАН,
420029, Казань, Сибирский тракт, 10/7, лицензия № 0325 от 07.12.2000.